Enhancing the persistence and memory of CAR T cells

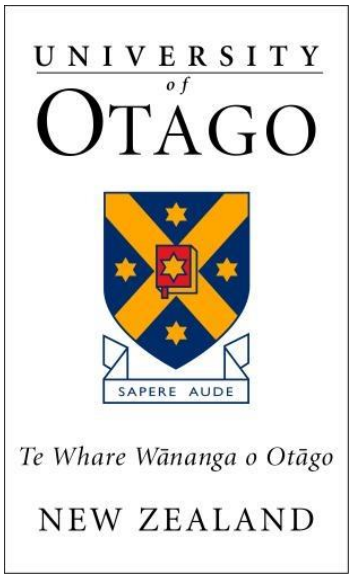

Ali Hosseini Rad SM

University of Otago

Department of Microbiology & Immunology

September 2020

A thesis submitted in fulfillment of the degree of Doctorate of Philosophy

Acknowledgments

I would like to express my deep, sincere and gratitude to my supervisor Professor Alexander McLellan for the continuous support and guidance throughout my PhD. His guidance helped me all the time in the research and writing of this thesis.

I thank my friends Aarati Poudel and Grace Min Yi Tan for always being good friends and for all their help, support and all the fun we have had in the last four years. I also wanted to thank all my fellow labmates, especially Dr Sarah Saunderson, for her help and support during my thesis. I would like to thank the Russell laboratory, Dr Bruce Russell, Dr Remy Muhsin, and Peter Christensen for being good friends.

Last but not least, I would like to have a special thank you to my family and my wife Chayapa and my son Aran for being patient and giving me confidence always. I love you.

I dedicate this thesis to
my family, my wife Chayapa, and my son Aran
for their constant support and unconditional love.
I love you all dearly.

Abstract

CAR T cell therapy has revolutionized cancer treatment, but has also provided an opportunity for treating chronic viral infections such as HIV, HBV, and HCV. Despite the profound outcomes in the treatment of hematological malignancies, CAR T cell therapy for solid tumours has not been almost invariably unsuccessful in the clinic. Hostile conditions of TME, low tumour infiltration, lack of persistence, and absence of memory CAR T cell formation are the main obstacles ahead of CAR T cell therapy for solid tumours. This study aimed to improve Her2-CAR T cell persistence and T_M (T memory) development.

T_M cells have distinct mitochondria morphology and metabolism. T_M cells have larger mitochondria (fusion) and rely on OXPHOS metabolism. In order to achieve the aim of this study, we selected Mcl-1 and miR429 as genes to overexpress in CAR T cells. Recently, several studies suggested that AICD (activation-induced cell death) induced by the CD95 pathway is the one of the main causes of low CAR T cell persistence *in vivo*. Mcl-1 is also well characterised for its role in OXPHOS metabolism, mitochondrial energetics and mitochondrial fusion. To complement this approach, the miRNA429 was selected as a means to enhance CAR T cell function through the suppression of genes that negatively affect T cell function, T_M development, and mitochondrial fusion such as TCAIM, MFF, and TET-2.

The first aim of this study was to upregulate the endogenous level of Mcl-1. We tested eight small activating RNA (saRNA) targeting different regions of the Mcl-1 promoter, but none of them was able to induce Mcl-1. Further promoter analysis led to the identification and characterisation of the first antisense transcript (named mcl1-AS1) that modulate Mcl-1 expression. However, due to the late manifestation of gene regulation (at 48 - 72 hours) that was seen following mcl1-AS1 inhibition, it was not applicable for us to use this strategy to increase Mcl-1 expression (Chapter II).

The next strategy to control expression of Mcl-1 was using the Tet-On system. We used several approaches to improve the Tet-On system, including gene replacement, codon-optimisation of rt-TA, using G72V-rtTA, removing cryptic splice sites within rt-TA, creating an autoregulatory Tet-On system, and manipulating regulatory elements in TCE minimal promoter. Our final optimised construct showed high inducibility and a very low background expression compared to the original construct (Chapter III). However, due to the low transfection efficiency of SB system in primary T cells and lack of artificial antigen presenting cell (aAPC) at the time for expansion of T cells, we decided to create an inducible LV system. The lack of inducibility in

low doxycycline concentration and low transduction efficiency made our inducible LV system not suitable for our study. Therefore, we decided to use a constitutive system to see the effects of Mcl-1 and miR429 overexpression in CAR T cells.

In order to express Mcl-1 and miR429 in a constitutive LV system, we examined the strength of four commonly used promoters, EF-1, CMV, RPBSA, and hPGK, in running short and long transcripts. EF-1 showed to be the best promoter in running short and long RNA in T cells (Chapter IV). As a result, we chose EF-1 to run the GFP-P2A-Her2CAR and hPGK to transcribe Mcl-1 or miR429.

For the first time, we showed that TCAIM, MFF, and TET-2 are direct targets of miR429. Overexpression of miR429 in CAR T cells slightly increased the number of T_{SCM} and T_{CM} in $CD4^+$CAR T cells, while the number of T_{reg} and T_{EMRA} cells was marginally decreased. Upregulating Mcl-1 in CAR T cells promoted the T_{SCM} and T_{CM} development in both $CD4^+$ and $CD8^+$ CAR T cells, whereas the frequency of T_{reg} and T_{EMRA} cells declined. Mcl-1 overexpression also protected CAR T cells from CD95L-induced AICD. Although our study cannot provide a mechanism for the Mcl-1 role in memory CAR T cell development, an increase in mitochondrial mass and mtDNA suggest that Mcl-1 likely enhances mitochondrial energetics and fusion (Chapter V).

Lastly given lack of access to the laboratory dues to the SARS-CoV-2 pandemic, the effect of recurrent mutations on viral RNA secondary structure and host miRNA interaction was investigated remotely. From an evolutionary point of view, mutations that arise several times independently (homoplasies) and lead to clade expansion are highly likely to increase viral fitness. The emergence of several mutations has resulted in the emergence of a G-clade responsible for 97% of cases around the globe. This clade consists of four mutations, two cause amino changes (C14408U and A23403G), while others (C241U, C3037U) are silent and are currently of unknown impact on viral fitness. Based on our bioinformatics survey, the C3037U mutation destroys the miR-197-5p binding site. Interestingly, miR-197-5p is highly expressed in SARS-CoV-2 target cells and has been reported to be upregulated in patients with cardiovascular disease. Interestingly, this miRNA also acts as defence against variety of viral infections such as HBV, HCV, HAV, Enterovirus 71, Ebola and H7N9. Further *in vitro* work is underway to test the significance of the C3037U mutation on miRNA inhibition in a SARS-2 pseudovirus and live virus assays.

Table of contents

List of abbreviations

NK cells	Natural killer cells
TME	Tumour microenvironment
IL	Interleukin
TGF-β	Transforming growth factor-β
T_{reg}	Regulatory T cells
MHC	Major histocompatibility complex
TAA	Tumour-associated antigen
mAbs	Monoclonal antibodies
ACT	Adoptive cell therapy
IFN-α	Interferon-alpha
TNF-α	Tumour necrosis factor-α
GM-CSF	Granulocyte-macrophage colony-stimulating factor
DC	Dendritic cell
TSA	Tumour specific antigens
FDA	Food and Drug Administration
PD-1	Programmed cell death-1
CTLA-4	Cytotoxic T-lymphocyte-associated antigen-4
TIM-3	T-cell immunoglobulin and mucin-domain containing-3
LAG-3	Lymphocyte-activation gene-3
TILs	Tumour-infiltrating lymphocytes
TCR	T-cell receptor
CAR	Chimeric antigen receptor
TM	Transmembrane

scFVs	Single-chain variable fragments
VL	Variable light chain
VH	Variable heavy chain
ITAMs	Immunoreceptor tyrosine-based activation motifs
T_{EFF}	Effector T cells
T_M	Memory T cells
T_N	Naïve T cells
IL-2Rβ	IL-2 receptor β-chain
TF	Transcription factor
EGFRVIII	EGFR variant III
Her2	Human epidermal growth factor receptor 2
AICD	Activation-induced cell death
TNF	Tumour necrosis factor
MMP	Matrix metalloproteases
DISC	Death-inducing signalling complex
FADD	Fas-associated with a death domain
tBid	Truncated Bid
T_{SCM}	T memory stem cells
lz-CD95L	Leucine zipper CD95L
ATP	Adenosine triphosphate
TCA	Tricarboxylic acid cycle
OXPHOS	Oxidative phosphorylation
Ac-CoA	Acetyl-CoA
FAO	Fatty acid oxidation

NADH	Nicotinamide adenine dinucleotide
FADH	Flavin adenine dinucleotide
ETC	Electron transport chain
MFN1	Mitofusin 1
OPA1	Optic atrophy 1
HR2	Heptad repeat region
CL	Cardiolipin
Drp1	Dynamin-related protein 1
Mid49	Mitochondrial dynamics proteins of 49 kDa
MFF	Mitochondrial fission factor
Mcl-1S	Mcl-1 short variant
Mcl-1L	Mcl-1 long variant
BH	BCL-2 homology
PEST	Proline, glutamic acid, serine and threonine
Mcl-1ES	Mcl-1 extra short variant
Mcl-1JAM	Just another Mcl1
OCR	Oxygen consumption rate
mtDNA	Mitochondrial DNA
TCAIM	T cell activation inhibitor, mitochondrial
TOAG-1	Tolerance-associated gene
ΔΨm	Mitochondrial membrane potential
UTR	Untranslated region
pri-miRNA	Primary miRNA

List of publications

1. McLellan AD and Hosseini Rad SM. Chimeric antigen receptor T cell persistence and memory cell formation. Immunology and Cell Biology 2019.

2. Hosseini Rad SM, Grace Min Yi Tan, Aarati Poudel, Kevin He and Alexander D McLellan. Regulation of Human Mcl-1 by a Divergently-Expressed Antisense Transcript. Gene 2020.

3. Hosseini Rad SM, Poudel A, Tan GMY, and McLellan AD. Optimisation of Tet-On inducible systems for Sleeping Beauty-based chimeric antigen receptor (CAR) applications. Scientific Reports 2020.

4. Hosseini Rad SM, Poudel A, Tan GMY, and McLellan AD. Promoter choice: who should drive the CAR in T Cells? PLoS One 2020.

5. Hosseini Rad SM and McLellan AD. Implications of SARS-CoV-2 mutations for genomic RNA structure and host microRNA targeting. International Journal of Medical Science 2020.

Chapter I:

Introduction

1.1 Cancer immunotherapy

In the last decades, there has been extensive progress regarding our understanding of the human immune system and its interaction with cancer. The first theory that there is a host immune system reaction against tumour cells proposed in 1909 by Paul Ehrlich, the time that his theory was not backed up by experimental data due to lack of tools (1). He wrote: “in the enormously complicated course of fetal and post-fetal development, aberrant cells become unusually common. Fortunately, in the majority of people, they remain completely latent thanks to the organism's positive mechanisms” (1). Later, an immunological surveillance mechanism was suggested in which the immune system is capable of recognising specific neo-antigens on tumour cells and subsequently destroying them (2, 3). Eventually, Burnet formulated the immune surveillance theory against tumour cells. He stated that: “It is by no means inconceivable that small accumulation of tumour cells may develop and because of their possession of new antigenic potentialities provoke an effective immunological reaction with regression of the tumour and no clinical hint of its existence” (4).

Although now we know immune surveillance occurs against cancer by T cells and natural killer cells (NK cells), unfortunately, the immune system fails to eliminate the established tumours. Several mechanisms are involved such immune evasion and immune tolerance. For example, the immunosuppressive nature of the tumour microenvironment (TME) is enriched in suppressive cytokines such as interleukin (IL)-10 and transforming growth factor-β (TGF-β) that induces T cell exhaustion and regulatory T cells (T_{reg}) differentiation leading to immune tolerance (5). Besides, tumour cells can escape from recognition by immune cells through downregulation of the major histocompatibility complex (MHC) molecules or tumour-associated antigens (TAAs) (6, 7). The mechanisms are described in detail by Hanahan and Weinberg as hallmarks of cancers (8).

In general, immunotherapy refers to therapeutic approaches that use or enhance the immune system to fight cancers. Immunotherapy falls into five main categories: immune system modulators, cancer vaccines, monoclonal antibodies (mAbs), immune checkpoints (ICPs) blockage and adoptive cell therapy (ACT) (9).

1.1.1 Immune system modulators

Immune system modulators comprise a range of treatments (e.g., cytokines and growth factors) that enhance the immune system's ability to destroy cancer cells. Developed cancers have limited ability to trigger an effective immune response. This low immunogenicity of tumour cells due to the weak expression of MHC and adhesion molecules as well as downregulation of costimulatory signals, does not allow T cells to be completely activated. In this case, cytokines such as IL-2 (10, 11), interferon-alpha (IFN-α) (10, 12, 13) and tumour necrosis factor-α (TNF-α) (14) have been used to boost immune system function in clinical trials. Hematopoietic growth factors (also known as hematopoietic cytokines) such as granulocyte-macrophage colony-stimulating factor (GM-CSF) have been used in several clinical trials (15, 16). GM-CSF enhances tumour antigen presentation to CD4 and CD8 T cells by recruited dendritic cells (DC) and macrophages (17). IL-2 was approved by FDA for treatment of metastatic melanoma 1998.

1.1.2 Therapeutic cancer vaccines

Therapeutic cancer vaccines, as opposed to traditional vaccines which are preventive, are designed to magnify and improve the quality of the existent response against TAA (18). Therapeutic cancer vaccines are administered as peptides, proteins, or tumour-antigen-pulsed DCs with adjuvants. Since many of therapeutic cancer vaccines were not associated with clinical benefits, their position in cancer therapy remains limited (19). Most of these vaccines are designed to boost the immune responses against TAA, which are generally not immunogenic such as viral antigens or tumour specific antigens (TSA). TAA are expressed in normal tissues at a low level; hence specific mechanisms of tolerance may occur for them.

1.1.3 Monoclonal antibodies (mAbs)

Since 1997, several mAbs have been approved for use in oncology. Most anti-cancer mAbs bind to TAA and provoke direct or indirect immune responses to destroy the tumour cells (20-22). The mechanism of tumour cell killing mediated by mAbs

consists of blocking tumour cell survival signalling pathways (Pertuzumab), hindering tumour growth by inhibiting angiogenesis (Bevacizumab), triggering an immune-mediated cytotoxic response and inducing apoptosis (Rituximab and Trastuzumab) (20-22). The Fc region of mAbs are important for their functions in killing of cancer cells such as activation of antibody-dependent cell-mediated cytotoxicity (ADCC) or complement-dependent cytotoxicity (CDC) (22). A recently updated list of mAbs approved by the Food and Drug Administration (FDA) is provided by Bayer *et al.* (20).

1.1.4 Immune checkpoint (ICP) blockade

ICPs are co-inhibitory molecules mainly expressed on T cells. The primary role of ICPs in normal physiological conditions is to maintain the self-tolerance, prevent autoimmunity and protect tissues from damages during inflammatory responses against pathogens (23, 24). However, cancer cells can hijack this mechanism and by overexpressing ICPs translate it to an immune resistance mechanism. Examples of ICPs and their corresponding blockages are as follow; Programmed cell death-1 (PD-1, Nivolumab), Cytotoxic T-lymphocyte-associated antigen-4 (CTLA-4, Ipilimumab), T-cell immunoglobulin and mucin-domain containing-3 (TIM-3, MBG453) and Lymphocyte-activation gene-3 (LAG-3, IMP321) (23, 24).

1.1.5 Adoptive cell therapy (ACT)

Tumour-infiltrating lymphocytes (TIL) are all lymphocytic cells (mainly T cells) that enter the tumour tissues. Several studies show that T cells are associated with tumour regression, and T cells have a prominent role in adoptive cell therapy (ACT) . However, the clinical benefits of ACT are still limited due to short response duration and TIL disappearance (25). Further studies revealed that lymphodepletion using a nonmyeloablative chemotherapy regimen before ACT can enhance tumour regression and TIL persistence in patients (26).

Although tumour-specific lymphocytes can be expanded *in vitro* from different cancers, ACT using TILs seems to be mainly effective in melanoma (25). Weak antigenicity, less-accessible tumour sites and inadequate number of TILs due to

technical complications are the major limitations of ACT (27). With advances in gene transfer technology, T cells were genetically engineered to express T cell receptor (TCR) or a chimeric antigen receptor (CAR) specific for a TAA (25, 28). This allowed ACT technology to expand to the other cancer types.

In TCR-mediated therapy TIL with high TCR affinity for tumour antigens are isolated. Then, genes encoding the selected clones of TCR alpha and beta chains are transduced into primary T cells. After an in vitro expansion, TCR transduced T cells are reinfused back to the patient (Figure 1.1) (28). Successful TCR therapy is limited due to inconsistent TCR expression, low persistency of T cells, inability to confer an immunologic memory (28-30) and increased risk of autoimmunity (28).

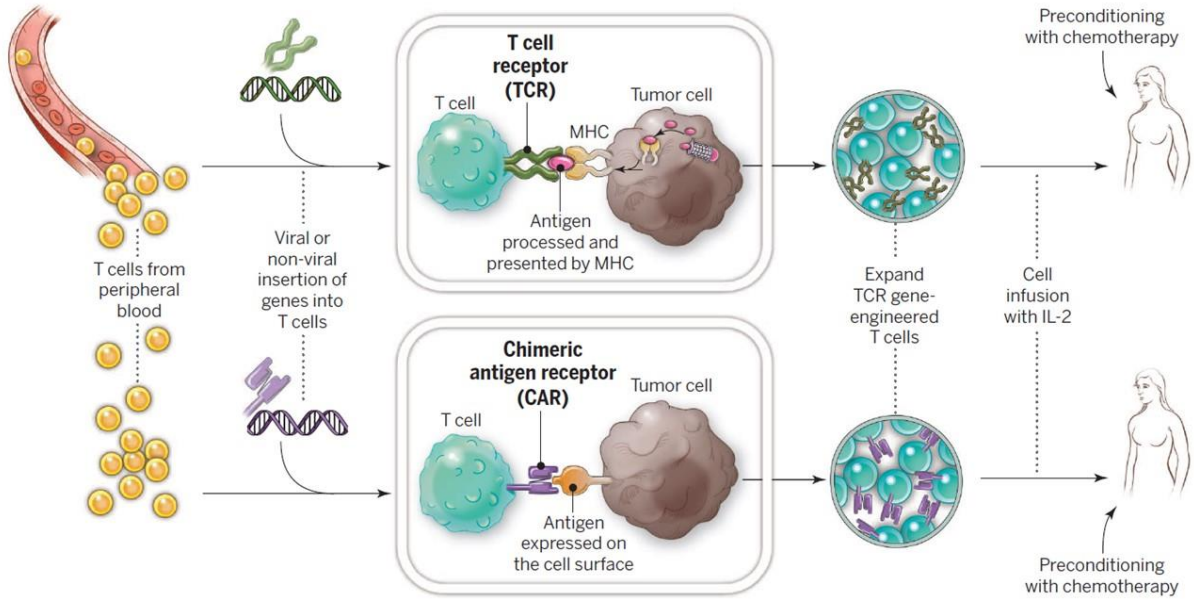

Figure 1.1. An overview of genetically engineered T cells in the ACT. T cells obtained from patients can be transduced with alpha and beta chains of TCR with high affinity for tumour antigens or a chimeric antigen receptor specific for an antigen. After an in vitro expansion, TCR transduced T cells are reinfused back to the patient. Figure was from Rosenberg *et al*. (25).

1.1.5.1 Chimeric antigen receptor (CAR) T cell therapy

Generally, a CAR is composed of both components of antibody and TCR that can recognise TAA in an MHC-independent manner. Indeed, this is the most significant advantage of CAR T cells over TILs and TCR therapy, mostly when tumour cells lose or downregulate MHC expression. A CAR made of three central parts: extracellular domain (antigen recognition domain and hinge), a transmembrane (TM) domain and intracellular domain(s). The antigen recognition domain is a single-chain variable fragment (scFV) consist of variable light (VL) and heavy (VH) chain regions of a mAb. A flexible linker, usually made of glycine and serine repeats, separates the VL and VH. The hinge and TM are commonly derived from CD28, CD8α or IgG (31, 32).

The first CAR T cell was developed by Kuwana *et al*. in 1987 (33), and is known as a "first-generation" type". This CAR uses a CD3ζ signalling domain as the sole intracellular signalling domain. Upon binding of scFv to antigen, intracellular domain clusters and undergoes conformational changes, ZAP-70 and immunoreceptor tyrosine-based activation motifs (ITAMs) become phosphorylated (31, 32). This leads to signal transduction, which results in T cell activation. This design has undergone a subsequent stepwise evolution as our knowledge about T cell activation and development increased. The first change was replacing CD3γ with CD3ζ (34, 35). However, the first-generation CAR was not able to optimally activate T cells and had low persistence and antitumor efficacy *in vivo* (35, 36).

Identification of costimulatory molecules and their function in T cells resulted in designs of second and third-generations of CAR T cells (Figure 1.2) (37-40). The second-generation CARs use one costimulatory domain which is either CD28, CD137 (4-1BB) or CD134 (OX40) linked in tandem with either CD3-ζ or FcRγ chains (31). The second-generation CAR T cells are the most widely utilised CAR T cells in clinical trials. The CD28 costimulatory domain has several vital roles in T cell function. This signalling is critical for sufficient IL-2 production and Bcl2-xL upregulation. Both of these proteins are essential for T cell survival and proliferation (41). Also, CD28 stimulation promotes the glycolysis pathway in T cells to support the energy demand and providing precursors necessary for cell division (see T cell

metabolism section) (42). CD28 is needed for the establishment of memory T cells (T_M) and effector T cells (T_{EFF}) from Naïve T cells (T_N) (31, 43). Furthermore, CD28 is believed to be dispensable for cytotoxicity and sustained response of T cells (31).

CD137 sustains the proliferation and IL-2 production in T cells (37) through the initiation of signalling pathways important for survival and memory T cell development (37). The advantages of using CD137 over CD28 in the second-generation CAR T cells is that CD137- CD3ζ-CAR T cells have higher persistence (44). However, CD137- CD3ζ-CAR T cells may still result in early exhaustion in CAR T cells (45). CD28- CD3ζ -CAR T cells are more potent in tumour clearance, and may enable the tonic signalling through clustering of intracellular domains in which enhance the proliferation of CAR T cells (46). More studies are needed to compare the

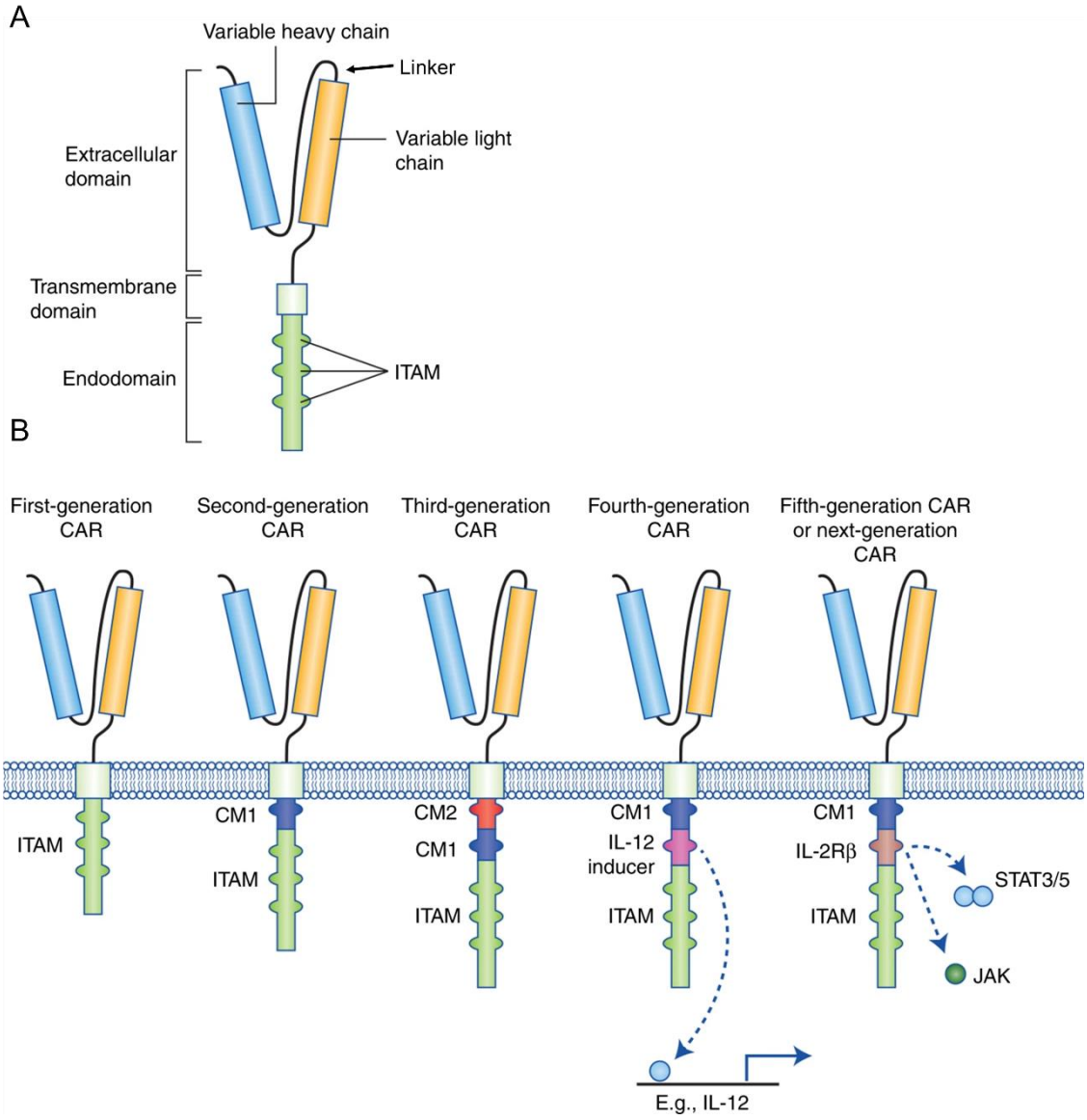

ability of CD28- CD3ζ -CAR T cells versus CD137- CD3ζ -CAR T cells in different cancer types in clinical trials.

Figure 1.2. Structure of a chimeric antigen receptor (CAR) and five different CAR generations. **(A)** A CAR is composed of an extracellular domain, a transmembrane domain and intracellular domain(s). The extracellular domain is composed of a single-chain variable fragment (scFV) responsible for antigen recognition, a transmembrane (TM) domain and intracellular domain. Based on the composition of costimulatory domains in the intracellular part of CARs, they fall into five categories. The first-generation CAR have only CD3 as intracellular domain, second-generation has one of CD28/CD134/CD137 while, third-generation has CD3/CD28 along with either CD134 or CD137. Fourth and fifth-generation CARs overexpress IL-2 or activate JAK–STAT3/5 signalling, respectively, to enhance the cytotoxicity of CAR T cells. CM; costimulatory molecule. Figure was from Tokarew *et al*. (32).

Third-generation CARs are based on second-generation CD28-CD3ζ along with either CD134 (CD28-CD134-CD3ζ) or CD137 (CD28-CD137-CD3ζ). Therefore, the third-generation CARs have the advantages of two co-stimulatory domains. Third-generations CAR T cells have shown enhanced immune activities such as cytokine production and killing ability (47). However, the third-generation CD20 and Her2 CAR T cells did not show improvement compared to the second-generation CAR T cells (48, 49). Further clinical trials are needed to properly evaluate the efficacy and safety of the third-generation CAR T cells.

Fourth and fifth generations are based on second-generation CARs. Fourth-generation uses constitutive or inducible overexpression of IL-12 to increase synergistic signals that lead to higher cytokine production and killing abilities (31). Fifth-generation has a truncated cytoplasmic IL-2 receptor β-chain (IL-2Rβ) domain with a binding site for the transcription factor (TF) STAT3. Upon antigen binding, a physiologically fully activated T cell similar to TCR activation happens by activation of CD3ζ, CD28 and JAK–STAT3/5 signalling at the same time (32).

CAR T cell therapy has profound therapeutic capacity against haematological malignancies. For instance, patients suffering from acute B-cell lymphoblastic leukaemia have shown 81% of 75% complete remission when they are treated with

CD19-CAR T cells (50, 51). However, due to the immunosuppressive nature of TME, successful CAR T cell therapy for solid tumours has been a challenge.

1.1.5.2 Barriers ahead of successful CAR T cell therapy in solid tumours

1.1.5.2.1 Target antigen

The ideal target for a CAR T cell therapy is an antigen that is expressed on all tumour cells but not normal tissue. However, since tumour cells derived from normal cells, they share the same antigens with normal tissue but at a different level. Therefore, an ideal target for CAR T cell therapy against tumour cells should at least meet two criteria; first, a TAA overexpressed in all tumour cells at a high level. Second, TAA should be expressed at low level on normal tissue CD19-CAR T cells, and its expression should not be on vital organs such as heart, liver, brain and lungs whereas its expression is necessary for tumour growth. One of the reasons CD19 CAR have shown such a success in the clinic is due to the fact this TAA meets both criteria.

To date, almost 30 TAAs have been evaluated as targets for CAR T cell therapy (52). These TAAs can be classified into three groups: neoantigens, oncofetal antigens and tumour-selective antigens. Neoantigens are the result of mutations in coding genes. Epidermal growth factor receptor (EGFR) rearrangements in glioblastoma are one of the most attractive neoantigens for CAR T cell therapy. EGFR variant III (EGFRVIII), which is the result of the exons 2–7 deletion, is the most commonly detected variant in glioblastoma cells (53). Other examples of neoantigens are mostly posttranslational modifications. For instance, abnormal glycosylation of extracellular domain of MUC1 can induce tumour specific responses (54). Both EGFRVIII- and MUC1 CAR T cells have shown promising outcome (54, 55).

Oncofetal antigens are usually proteins that express during development and sometimes on normal adult stem cells. These stem cell genes again re-express in tumour cells. Oncofetal antigens are attractive targets since their expression is limited to cancer cells (56). Examples of oncofetal antigens that have been used in CAR T cell therapies are Alpha-Fetoprotein (57), carcinoembryonic antigen (58) and 5T4 trophoblast glycoprotein (59).

Tumour-selective antigens express at a high level on transformed cells and low basal level on normal tissue. For example, mesothelin is overexpressed in mesothelioma, ovarian and pancreatic carcinomas while it presents at a low level on peritoneal, pleural, and pericardial surfaces (60). Several CAR T cell therapies for mesothelin are undergoing (60). Human epidermal growth factor receptor 2 (Her2) overexpresses 20-100 fold more in 20% of breast cancers, making it a suitable target for CAR T cell therapy (61). The Her2 CAR T cell is the most studied CAR for solid tumours in clinical trials.

1.1.5.2.2 Trafficking

Successful migration of CAR T cells to tumour sites depends on the expression of adhesion molecules on both T cells and the tumour endothelium as well as, a match between the chemokine receptors on the CAR T cells such as CXCR3 and CCR5 and the chemokines secreted by the tumour cells. However, tumour cells downregulate the suitable ligand for T cell chemokine receptors in order to reduce T cell infiltration in the TME. An approach to facilitate the trafficking of T cells into tumour sites is an exogenous expression of chemokines on CAR T cells. For example, expression of CCR2b in CAR T cells enhanced intratumoral migration of CAR T cells to tumours expressing CCL2 (62, 63). Other chemokine receptors that have been used to improve the trafficking are CCR2 (64), CCR4 (65), CCR7 (66), CXCR2 (67) and CXCR4 (68).

1.1.5.2.3 The hostile TME

Beside anatomical barriers, TME contains factors that can abolish the effector function of CAR T cells (69). These factors include adenosine, lactate, acidosis, vascular endothelial growth factor, phosphatidylserine, high extracellular K^+ levels, hypoxia, cytokines and ICPs that have immunosuppressive functions (70). Coexpressing a CAR and an accessory gene have been shown to enhance CAR T cell function. For example, inhibition of protein kinase A localisation signalling using a decoy protein in Mesothelin-CAR promoted the migration and killing ability of CAR T cells *in vivo*

(71). Moreover, TME is enriched in T_{reg}, myeloid-derived suppressor cells, tumour-associated macrophages and tumour-associated neutrophils creating an extremely immunosuppressive environment by secreting TGF-β, IL-10, nitric acid, and indoleamine dioxygenase 2–3 (69-71). Redirecting CAR T cells to recognize soluble TGF-β not only covert the immunosuppressive effect of TGF-β to an activatory signal, but can also protect neighbouring immune cells against TGF-β–induced Treg differentiation (72).

1.1.5.2.4 Low persistence and survival

Successful CAR T cell therapy ideally accomplishes long-term complete remission. The extent of T cell expansion and persistence in patients receiving the CAR T cells determine the outcome of therapy (73). Adequate expansion and persistence are required in order for CAR T cells reach a sufficient number necessary to eliminate tumour cells. 'Expansion of T cells depends on their proliferation capacity while they receive survival signals. Fundamentally, T cells require three signals to drive proliferation and survival; TCR engagement, costimulatory signalling and cytokine signalling (32, 74). Adding costimulatory domains such as CD28 and CD137 in the second and third-generation CARs or expressing IL-12 in fourth and fifth-generation CAR T cells, are the strategies to overcome insufficient CAR T cell expansion *in vivo* (73).

Durable tumour remission will be achieved if CAR T cells overcome the following barriers (73); (i) immunosuppressive nature of TME, (ii) tolerance induced by continuous exposure to antigen, (iii) exhaustion mediated by tonic/chronic CAR, (iv) inhibitory cytokines and ICPs, (v) contraction after the majority of tumour cells are dead, and CAR T cells do not receive enough signalling due to lack of antigen, (vi) activation-induced cell death (AICD) mediated by CD95:CD95L interaction (vii) lack of memory T cell differentiation. More information is provided about CAR T cell persistence and memory on our review article provided at the end of this chapter (73). In the next sections, I will focus on topics related to my project, namely AICD induced by CD95 pathway and the role of mitochondria in T cell persistence and memory development.

1.1.5.2.5 CD95:CD95L pathway in T cell persistence and survival

CD95 (Fas/APO-1/TNFRSF6) belongs to the tumour necrosis factor (TNF) receptor family and induces apoptosis when bound to its ligand, CD95L (FasL/CD178/TNFSF6) or stimulated with antibodies (75). CD95L expresses in activated T cells, NK cells and tissues of immune-privilege (e.g. testis and eye) (75). There are two forms of CD95L, transmembrane (m-CD95L) and soluble (s-CD95L) forms. Membrane CD95L exists in a multi-aggregated homotrimer and induces cell death on cells that express the CD95 receptor (76). On the other hand, s-CD95L is the result of matrix metalloproteases (MMP) cleavage of m-CD95L (MMP3, MMP7, MMP9, and ADAM10) and has a nonapoptotic role, namely in activating NF-κB and PI3K pathways (77). It's worth to mention each of the MMPs create a unique type of s-CD95L and s-CD95L cleaved by MMP7 can induce apoptosis (78). Here, I focus on m-CD95L (mentioned in the text as CD95L) and its role in T cell persistence and memory.

Upon binding of CD95L to CD95, assembling of the death-inducing signalling complex (DISC) initiate the cascade. DISC consist of CD95, Fas-associated with a death domain (FADD), procaspase-8, procaspase-10, and the caspase-8/10 regulator c-FLIP (75). Following the formation of DISC complex, oligomerisation of procaspase-8 results in its activation, autoproteolytic processing, and release of an active heterotetrameric caspase-8 (79). Based on the apoptosis downstream pathway, cells divide into two types; type I cells are independent of mitochondria in CD95-induced apoptosis, whereas type II need mitochondria involvement to induce apoptosis via CD95 pathway (80). In the type I cells, the amount of activated caspase-8 is enough to activate caspase-3 and downstream cascade result in apoptosis. In contrast, in type II cells, the cleavage of the BH3-only protein Bid via caspase-8 create truncated Bid (tBid) which leads to dimerization of Bax and Bak complexes on MOM, mitochondria depolarization and release of cytochrome C into cytosol (75, 79, 81). Both type I and type II activate the mitochondrion-dependent apoptotic pathway (Figure 1.3) (81).

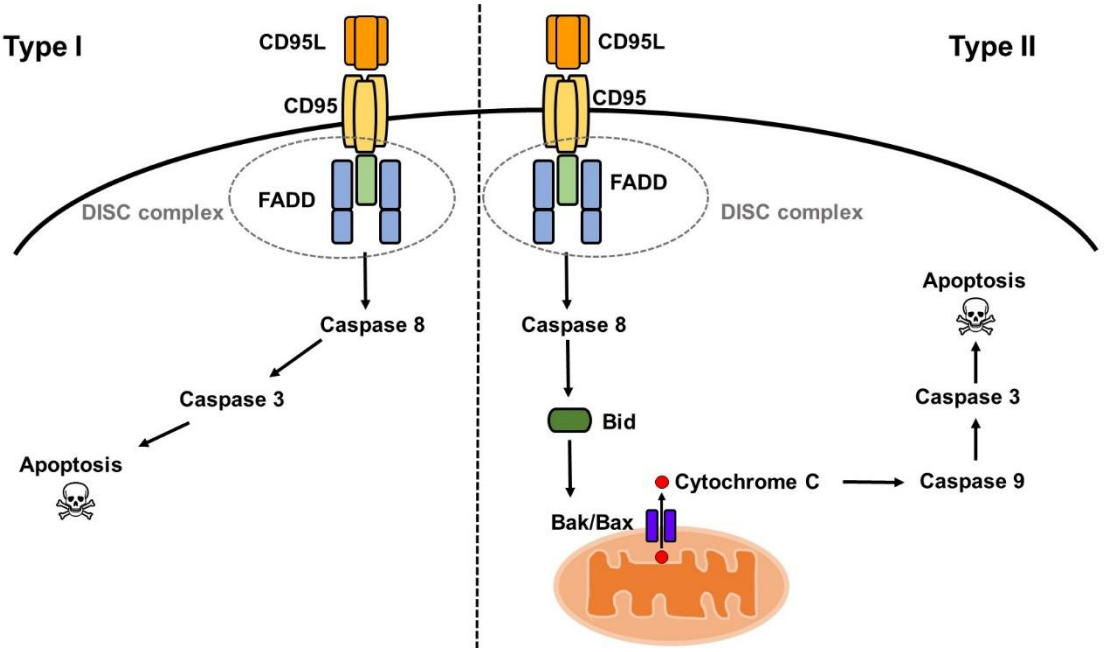

Figure 1.3. Schematic illustration of CD95-induced apoptosis in type I and II cells. Activation of CD95 upon binding to CD95L result in the formation of death-inducing signalling complex (DISC). Activation of caspase-8, in type I cells leads to direct activation of caspase-3 and then induction of apoptosis independent of mitochondria. In type II cells, caspase-8 cleaves the Bid proapoptotic protein to make truncated tBid. Next, tBid promote the oligomerisation of Bak/Bax complexes to form pores in the mitochondria outer membrane. Releasing cytochrome C in cytosol activates caspase-9, which in turn activates caspase-3 and then apoptosis.

CD95-induced apoptosis is one of the main ways that both CD4 and CD8 cytolytic T_{EFF} use to kill transformed and virally infected cells (75). Almost all human tumours express CD95 and CD95L on their cell surface (81). Upregulation of CD95L along with downregulation of CD95 promote tumour progression. In the "tumour counterattack" theory, high level of CD95L on the tumour cell surface, activate AICD in TILs (75). This theory is supported by the data gained from *in vitro* studies that have shown activated T cells are susceptible to AICD triggered by CD95L on tumour cells. The lack of *in vivo* studies is due to failure in the establishment of mouse models (75, 82). Tumour cells expressing a high level of CD95L often get rejected after injection into mice due to rapid infiltration of neutrophils and other granulocytes (81).

Several studies have shown that endothelial cells of patients with solid tumours overexpress CD95L on their surface (82). The expression of CD95L on endothelial cells reduced the number of TILs in the ovarian cancer mouse model, and mAb against CD95L could reverse the effect (82).

Tumour cells also benefit from nonapoptotic functions of CD95 signalling. Cancer cells upregulating CD95/CD95L also express chemotactic factors such as IL-8 and MCP1. Chemotactic proteins increase the recruitment of proinflammatory cells and create an inflammatory environment supporting cancer growth (81, 83). Activation of CD95 in apoptosis-resistant tumour cells results in the induction of pathways or set of genes with a variety roles in tumour progression. For instance, activation of CD95 is an inducer for NF-κB and all three major MAPK pathways: ERK1/2, p38, and JNK1/2 (84). The implications of these pathways are in growth, invasion, metastasis, resistance to apoptosis and cell cycle progression (8). Moreover, the vast majority of reports have shown that upregulation of CD95L by cancer cells is a negative prognostic marker for many solid tumours (75), and the elimination of CD95 or CD95L in cancer cells induces "death induced by CD95 or CD95L" (85).

Recently, several studies suggested that AICD induced by CD95 pathway is the main reason for CAR T cell low persistence *in vivo* (86-89). Blockage of CD95:CD95L pathway showed to enhances the CAR T cell therapy *in vivo*. For example, inhibition of CD95 or CD95L translation via siRNA increases the CD171-CAR T cells persistence (87). Blockade of CD95:CD95L either with a dominant-negative form of FADD or mAb, increases the number of CAR T cells without causing autoimmunity (86, 88, 89).

CAR T cells also use CD95L to lysis CD95 positive target cells. Hong *et al.* showed that CD30-CAR T cells killed their $CD30^+$ target cells as well as $CD30^-$ surrounding cells via a cell-cell contact-dependent CD95:CD95L interaction (90). In addition, it is well-known that memory T cells express CD95 as their marker, and overexpression of CD95 has been shown in a memory T cell subset known as "T memory stem cells (T_{SCM})" (91). In another study, Klebanoff *et al.* showed that stimulating CD95 signalling using leucine zipper CD95L (lz-CD95L) elevated memory CAR T cell

differentiation (92). Due to the dual role of CD95 pathway in AICD and T_M development, careful considerations are needed.

1.2. Mitochondrial dynamic in T cells

1.2.1 Overview of mitochondrial functions in T cells

Mitochondria dynamics in the T cells involves alterations of size, shape, cellular localisation and a variety of oxidative and metabolic-related functions. In T cells, mitochondria have at least seven functions, which I will discuss briefly (Figure 1.4) (93). Mitochondrial localisation is necessary for polarization and migration of T cells. Generally, mitochondria tend to accumulate where the highest amount of ATP and calcium demand is needed (93, 94). Mitochondrial position and producing ATP at the posterior trailing edge (known as uropod) is crucial during T cell migration and blocking mitochondria to locate in uropod inhibit T cell migration (95). During the T cell activation, mitochondria absorb calcium and release it later at the end of the calcium transient peak during T cell activation. Mitochondria and endoplasmic reticulum are responsible for regulating the calcium homeostasis during T cell activation and resting condition (96).

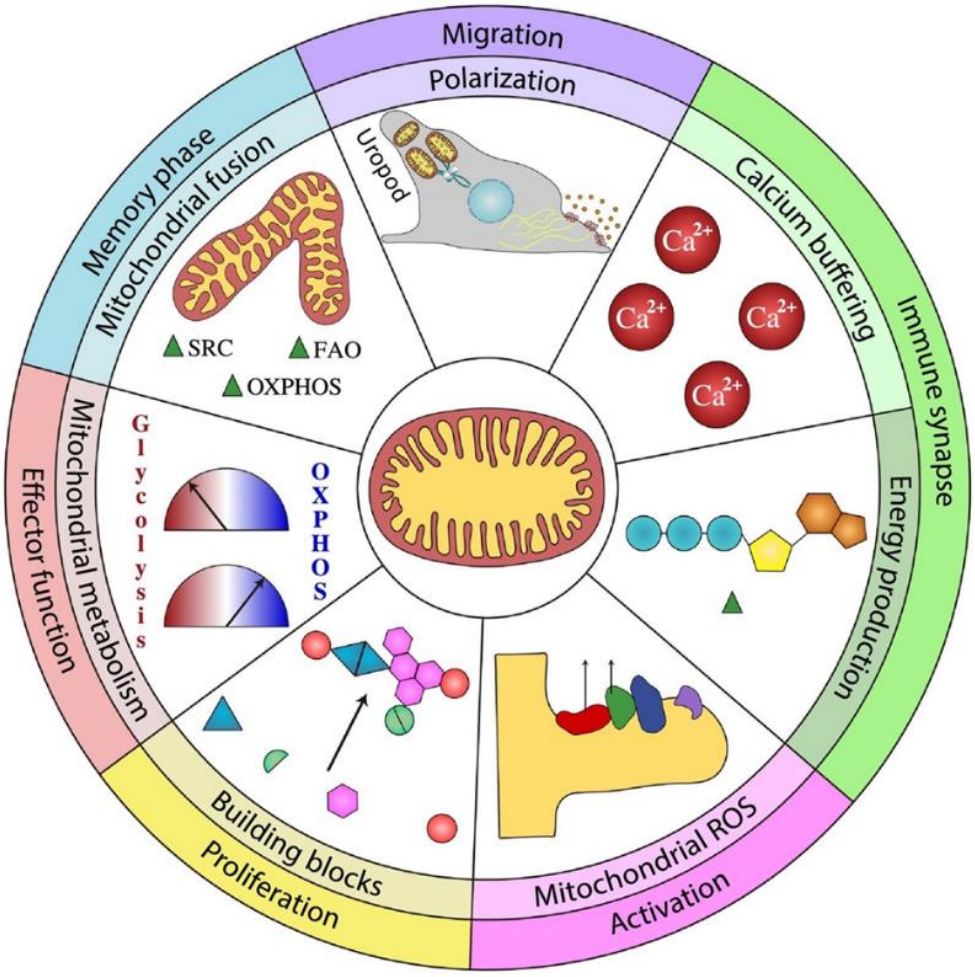

Figure 1.4. Mitochondrial functions in T cells. When T cells detect the chemotactic factors, mitochondria accumulate at the uropod to support the energy demand during T cell migration. Mitochondria take up calcium during stimulation and have a role in the calcium homeostasis. Besides, mitochondria by anabolic metabolism provide ATP and energy for T cells, while by catabolic metabolism providing building blocks for cell proliferation. Figure was from Desdín-Micó *et al*. (93).

1.2.2 Catabolism and anabolism pathways

Adenosine triphosphate (ATP) is the energy in cells and cells use three macromolecules to produce ATP, carbohydrates (e.g. glucose), fatty acids and amino

acids (e.g. glutamine). Glucose catabolism starts with glycolysis, a process to generate two ATP and pyruvate as the final product. In the resting cells, pyruvate enters the tricarboxylic acid cycle (TCA) and oxidative phosphorylation (OXPHOS) in the mitochondria. Fatty acids enter the TCA after they convert to acetyl-CoA (Ac-CoA) via a process known as fatty acid oxidation (FAO) in mitochondria. Amino acids join the TCA after being metabolised into 3-, 4-, and 5-carbon substrates. TCA cycle is a series of an enzymatic reaction that converts citrate to oxaloacetate resulting in the production of NADH (reduced nicotinamide adenine dinucleotide) and FADH2 (reduced flavin adenine dinucleotide). NADH and FADH2 generate thirty-four ATPs by passing through the electron transport chain (ETC). The process that macromolecules being broken down to generate energy called catabolic metabolism. Stem cells, T_N, T_M and T_{reg} use this pathway to generate maximum ATP (Figure 1.4A) (122, 127).

Rapidly proliferating cells such as T_{EFF} cells use anabolic metabolism, a process to manufacture new molecules. Every time a cell divides, they need to synthesis new DNA molecules and lipid for the cell membrane. Lactate dehydrogenase converts pyruvate to lactate, which is used to regenerate NAD. NAD is required for enzymatic reactions that lead to *de novo* synthesises of purine and pyrimidine bases. Lipids are made from citrate by ATP citrate lyase (Figure 1.4B) (122, 127).

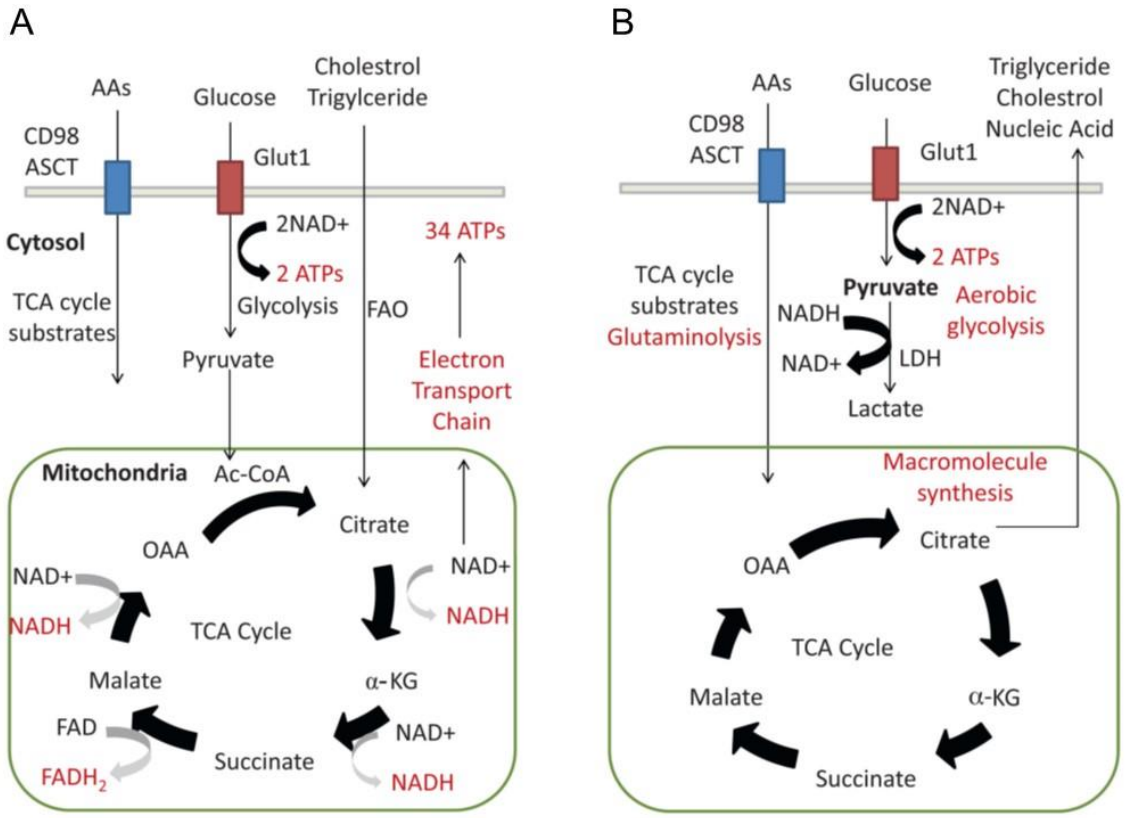

Figure 1.4. Catabolic and anabolic metabolisms. **(A)** Stem cells, T_N, T_M, T_{reg} cells use the catabolic pathway to break down the carbohydrates (e.g. glucose), fatty acids and amino acids (e.g. glutamine). In mitochondria, a series of enzymatic reactions called the TCA cycle produces NADH and FADH2. Next, TCA products enter the respiration process by passing through the electron transport chain located in the mitochondria matrix to produce 34 ATP in exchange for each glucose molecule. (B) Rapid proliferative cells such as T_{EFF} cells and cancer cells, use anabolic metabolism. This pathway only produces two ATP in exchange for one glucose through the glycolysis. Pyruvate converts to lactate and enters the TCA cycle as substrates for the synthesis of membrane lipids and purine and pyrimidine bases. AA; amino acids, FAO; fatty acid oxidation, Ac-CoA; acetyl coenzyme A, OAA; oxaloacetate, α-KG; α-ketogluterate, FAD; flavin adenine dinucleo-tide, NAD; nicotinamide adenine dinucleotide, ATP; adenosine triphosphate, TCA cycle; tricarboxylic acid cycle. Figure was from Park *et al*. (97).

1.2.3 Metabolic changes during T cell activation

Mitochondria has two shapes with distinct functions and bioenergetics capacity in T cells (126). The mitochondrial dynamic is controlled by external (e.g. the growth factors and nutrient) and internal factors (e.g. TFs and reactive oxygen species). T cells are mobile; they need to adapt their metabolism to the new environment. T_N cells rely on catabolic metabolism through the TCA cycle coupled with OXPHOS to maximise the ATP production (98). Upon activation, T_N cells undergo metabolic reprograming to switch to anabolic metabolism and aerobic glycolysis (98, 99). As mentioned above, the anabolic pathway provides the building blocks such as lipids and DNA molecules to support T_{EFF} expansion. Intrinsic and extrinsic factors coordinate to initiate the metabolism reprogramming. IL-2 and activation of CD28 enhance the glycolysis by inducing expression of the nutrient transporters, activation of anabolic regulators such as mTOR and Akt (100). C-Myc, estrogen-related receptor α (ERRα), and hypoxia inducible factor-1α (HIF-1α) are main the TFs in this metabolic remodelling (99, 100).

After antigen clearance, most of T_{EFF} cells undergo apoptosis (contraction), while a small number of T cells differentiate to long-lived T_M cells. Activation of FAO metabolic program is necessary for T_M differentiation, long-term survival and enhanced response to the second antigen encounter. It has been shown that the enhanced response in T_M cells compared to T_{EFF} cells is linked to the mitochondria mass, upregulation of genes involved in FAO and their higher spare respiratory capacity (SRC) (101, 102).

1.2.4 Mitochondria fusion and fission

In T cells, mitochondria have two morphologies, short (fission) or long (fusion) tubules. During the fission and fusion transition, the mitochondrial OMM, IMM and matrix undergo changes that will determine the mitochondrial function (103). The exact mechanism of fusion and fission transition in mammalian is poorly known. Three GTPases proteins are known to be critical for fusion; Mitofusin 1 and 2 (Mfn1 and Mfn2) and optic atrophy 1 (OPA1). MFN1 and MFN2 are localised at OMM and form

complexes between two adjacent mitochondria during fusion (Figure 5). C-terminal region of Mfn1/2 contains a hydrophobic heptad repeat region (HR2). The HR2 region dimerized with other Mfn on other ends of adjacent mitochondria to bring both mitochondria close in order to initiate fusion. OPA1 and cardiolipin (CL) localise within the mitochondrial intermembrane space, and both are responsible for the IMM fusion (Figure 1.5) (104).

Mitochondrial fission initiate by recruiting the dynamin-related protein 1 (Drp1), a GTPase protein, to mitochondrial fission sites at the OMM. Mitochondrial dynamics proteins of 49 and 51 kDa (Mid49 and Mid51) and mitochondrial fission factor (MFF) are responsible for Drp1 recruitment. Next, Drp1 oligomerises to form a belt around mitochondria, then GTP hydrolysis by Drp1 constrict the mitochondria to split both inner and outer membranes (Figure 1.5) (105).

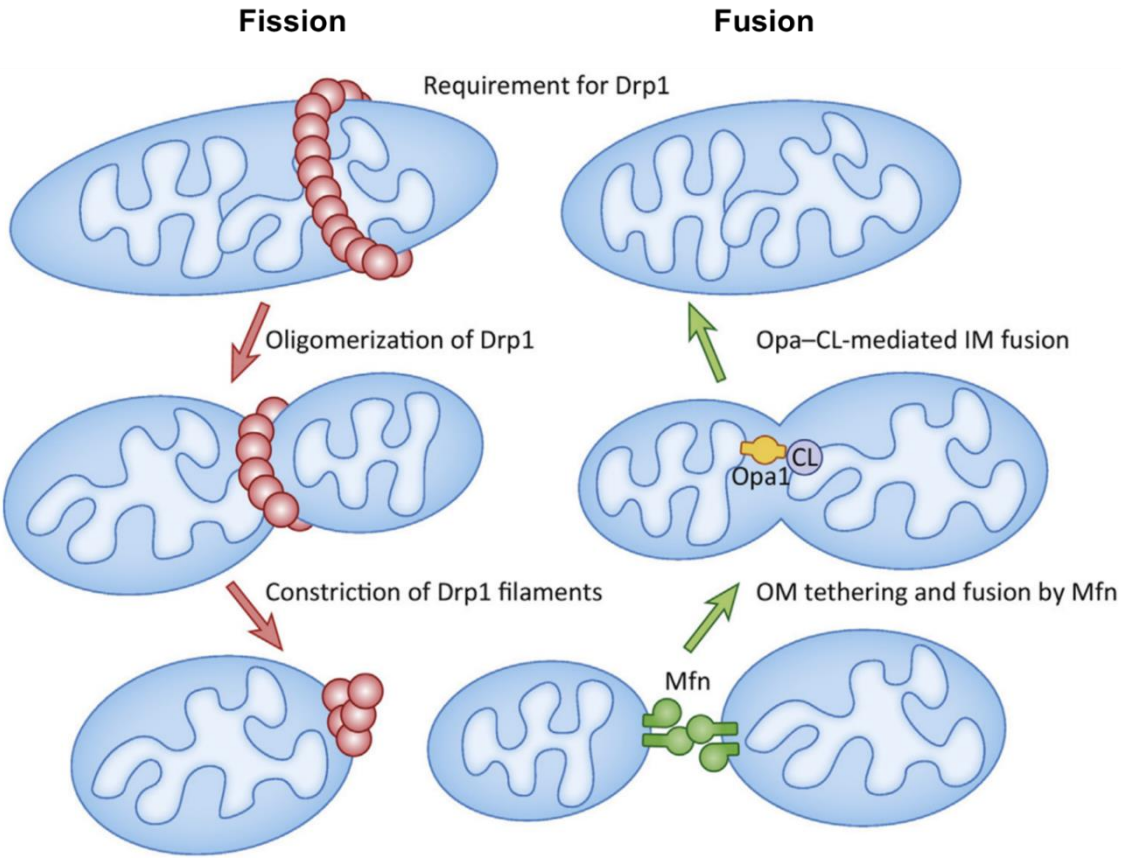

Figure 1.5. Mitochondria fusion and fission. During fission, Mid49, Mid51 and MFF recruit Drp1 to mitochondrial fission sites at the OMM. Then, Drp1 oligomerises to form a spiral around the mitochondria. GTP hydrolysis by Drp1 drives the compression of Drp1 spiral and dividing the mitochondria in two. Mitochondrial fusion starts by tethering MFN1 and MFN2 proteins and fusing OMM of two mitochondria. Interaction between OPA1 and cardiolipin (CL) leads to IMM fusion. Figure was from Kameoka *et al*. (106).

T_N and T_M cells have fusion mitochondria, while T_{EFF} cells have fission mitochondria. It has been shown that T cell fate can be modulated by altering mitochondria fusion and fission (107). Enforcing fission and aerobic glycolysis impairs the T_M cell development in activated T cells. On the other hand, enhancing mitochondria fusion, promoting OXPHOS and FAO in T_{EFF} T cells resulted in increasing T_M phenotypes (45, 93, 97-99, 103). For instance, treating T cells with IL-15 promote T_M cell development by enhancing mitochondria fusion and FAO metabolism (108).

1.3 Role of the Mcl-1 gene in T cells

Myeloid Cell Leukemia-1 (Mcl-1) is an antiapoptotic member of the Bcl-2 protein family. The Bcl-2 proteins family is divided into two groups based on inhibiting or promoting apoptosis. Proapoptotic members are Bax, Bak, Bok, Bid, Bim, Noxa, Puma and Mcl-1 short variant (Mcl-1S). Antiapoptotic members are Bcl-2, Bcl-xL, Bcl-w and Mcl-1 long variant (Mcl-1L) (109). All antiapoptotic members of Bcl-2, enhance cell survival and inhibit apoptosis (110).

Upon activation of proapoptotic members, Bak and Bax become activated. Then, Bak and Bax oligomerise on the OMM to create pores that result in the release of cytochrome C into the cytosol. Cytochrome C activates the caspase 9, which activates caspase 3 leading to nuclear fragmentation and apoptotic body formation, and cell death. Mcl1-L blocks this pathway by binding and sequestering Bak and Bax (111).

Mcl-1 protein is the largest protein in the Bcl-2 family and composed of 350 amino acids. At the C-terminal (residues 170-300) of Mcl-1 shows high similarity to other antiapoptotic members such as Bcl-xL. This region contains three putative the BCL-2

homology (BH) 1, BH2, BH3, responsible for binding to proapoptotic members of the family. Two weak PEST (proline, glutamic acid, serine and threonine), as well as two strong PEST domains, are located in the N-terminal region (Figure 1.6). These motifs regulate the Mcl-1 turnover, localisation and phosphorylation. The PEST sequences are common among labile proteins (protein with short half-life); however, the Mcl-1 half-life depends on cellular conditions and cell type (110, 111).

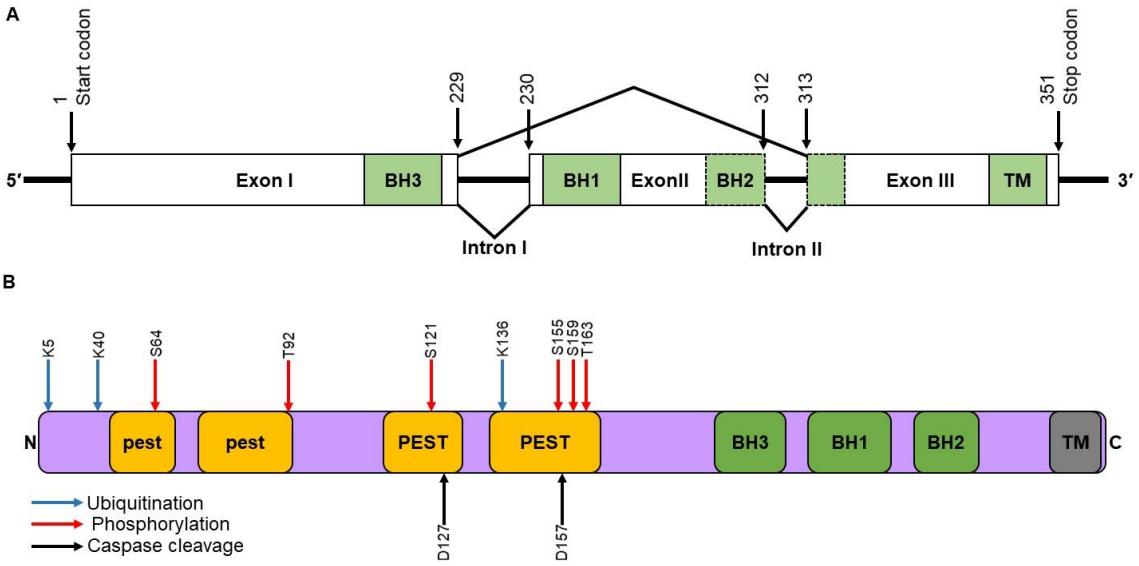

Figure 1.6 Schematic representation of the Mcl-1 **(A)** gene and **(B)** protein. **(A)** Alternative splicing between exon I and exon III result in Mcl-1S isoform while Mcl-1L contains all three exons. **(B)** The relative positions of post-translational modifications including ubiquitination, phosphorylation and caspase cleavage sites are shown with blue, red and black arrows, respectively. Mcl-1 N-terminal contains two weak (lower case) and two strong (upper case) PEST sites. At the -terminal, Mcl-1 has three the Bcl-2 homology domains (BH1, 2 & 3) and a transmembrane (TM) domain.

It has been shown that several other variants of Mcl-1 present in a tiny fraction along with Mcl-1L. For instance, an extra short variant (Mcl-1ES), contains truncated exon 1 (lacks PEST motifs) but have motifs at C-terminal region (BH1, BH2, BH3 and TM). The Mcl-1ES has 197 amino acids, bears three mutations probably introduced at post-transcriptional level and similar to Mcl1-S is proapoptotic (112). Another Mcl-1 splice

variant carries a 45 bp deletion in the Mcl-1L named Mcl-1_{JAM} (Just Another Mcl1) (113). Due to the lack of Gly158 to Asp172, Mcl-1_{JAM} is very unstable protein. Overexpression of Mcl-1_{JAM} protects cells against apoptosis by sequestrating proapoptotic Bim. However, in contrast to antiapoptotic Mcl-1L, Mcl-1_{JAM} does not bind to proapoptotic Noxa (113).

Mcl-1L and Mcl-1S are the dominant forms of Mcl-1 (114, 115). Mcl-1S (271 amino acids) is either result of proteolytic cleavage of Mcl-1L by caspase 3/8 (116), or product of alternative splicing by skipping the second exon (117). However, recent studies have confirmed that proteolytic cleavage of Mcl-1L is probably the primary mechanism for Mcl1-S generation. Indeed, the overexpression of a codon-optimised intronless (used in this study) of Mcl-1L leads to producing both Mcl-1L and Mcl-1S.

Mcl-1 is unique among Bcl-2 family protein due to its expression in a wide range of cells. Mcl-1 expresses from the early stage of embryonic development to many differentiated cells (118). Mcl-1 is crucial for haematopoiesis and expressed in all blood cells except monocyte (Figure 1.7) (118, 119).

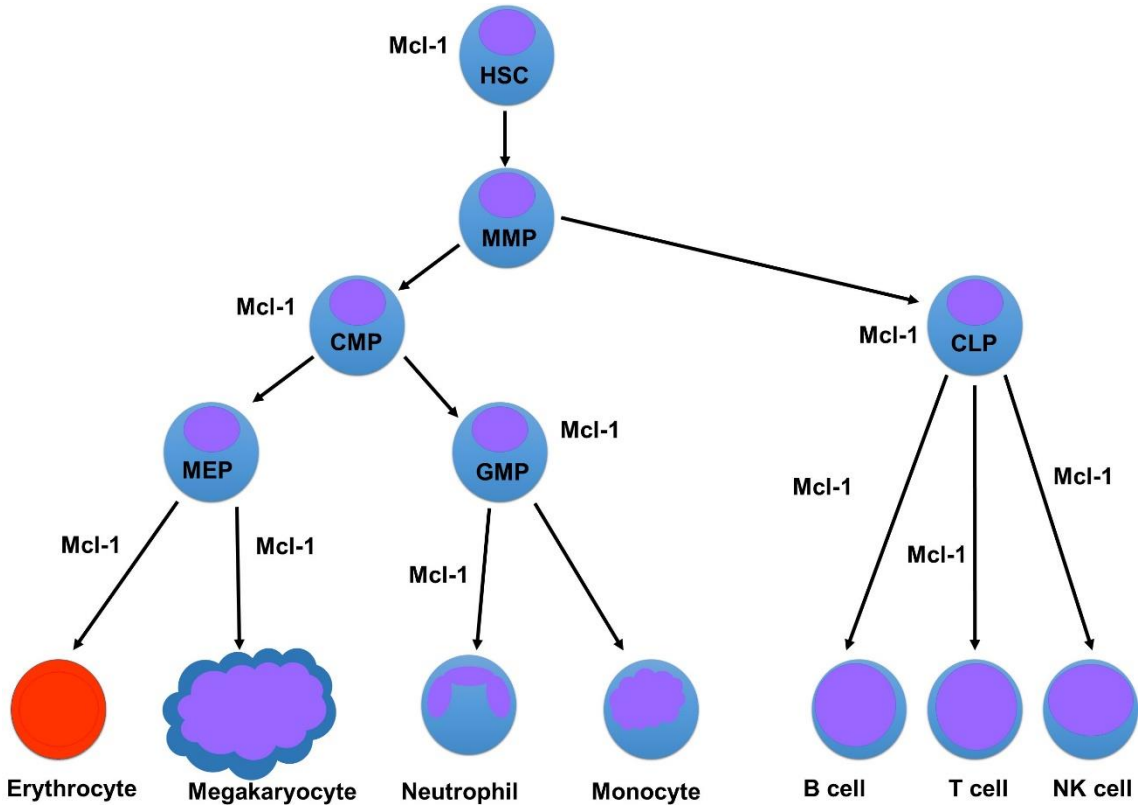

Figure 1.7. Expression of Mcl-1 in haematopoiesis. Hematopoietic stem cells (HSCs) are multipotent stem cells with self-renewal capability. During haematopoiesis, HSCs produces multipotent progenitors (MPPs) which have lower self-renewal capacity. Next MPPs give rise to two progenitor cells, common myeloid progenitors (CMPs) and common lymphoid progenitors (CLPs). CLPs differentiates to the lymphoid lineages including B cells, T cells and natural killer (NK) cells. CMPs give rise to two other unipotent progenitor cells, megakaryocyte erythroid progenitor (MEP) and granulocyte monocyte progenitor (GMP), which finally differentiate to the other blood cells. Mcl-1 expresses in all blood cell types except monocytes.

In a normal condition, Mcl-1 localises in various part of cells including mitochondria, nucleus and cytoplasm (111). In the nucleus, Mcl-1 interacts with cyclin-dependent kinase 1 (CDK-1) and proliferating cell nuclear antigen (PCNA), and regulate cell cycle (111). Mcl-1L and Mcl-1S exhibit different mitochondrial sub localisation (114, 116, 117). Mcl-1L enriches at OMM where it stops the formation of Bak and Bax complex. On the other hand, Mcl1-S only localise at IMM and matrix, where it enhances mitochondria homeostasis, fusion and respiratory function (Figure 1.8) (114).

Still much to discover about the nonapoptotic functions of Mcl-1. Recent studies have shown that Mcl-1S is required for the formation of normal IMM structure, mitochondrial fusion, as well as OXPHOS (109, 114). Cells lacking Mcl-1S have impaired oxygen consumption rates (OCRs) and elevated mitochondrial superoxide levels (114). Interestingly, Mcl-1S deletion did not alter the expression of nuclear-encoded ETC complexes (I, II and III), but mitochondrial -encoded subunits of complex IV (Cox 1 and Cox 2) showed lower expression. Further experiments confirmed that deletion of Mcl-1S leads to decreases of mitochondrial DNA (mtDNA). Furthermore, lack of Mcl1-S impairs the assembly of F1F0-ATP synthase oligomers and organisation of cristae membranes (114). Mcl-1 can also promote FAO metabolism by direct interaction of its BH3 motif to very long-chain Ac-CoA dehydrogenase (VLCAD), a key enzyme in this pathway (120).

One of the newly discovered roles of Mcl-1 is its involvement in mitochondria fusion and fission. The first 50 aa of Mcl-1 N-terminal carries a mitochondrial targeting

sequence (MTS), which is cleaved by an unknown mitochondrial protease in IMM (114). Mcl-1 can interact with the Drp1 at OMM, and reverse the Drp1-mediated mitochondria fission (109). In addition, Mcl-1 interaction with MFF seems to be a part of the mechanism that Mcl-1 inhibits the mitochondrial fission (121). Later Rasmussen *et al*. showed that Mcl-1 could also binds to fusion promoting factors OPA1, MFN1 and MFN2 at IMM and increases their stability and promote the fusion (122).

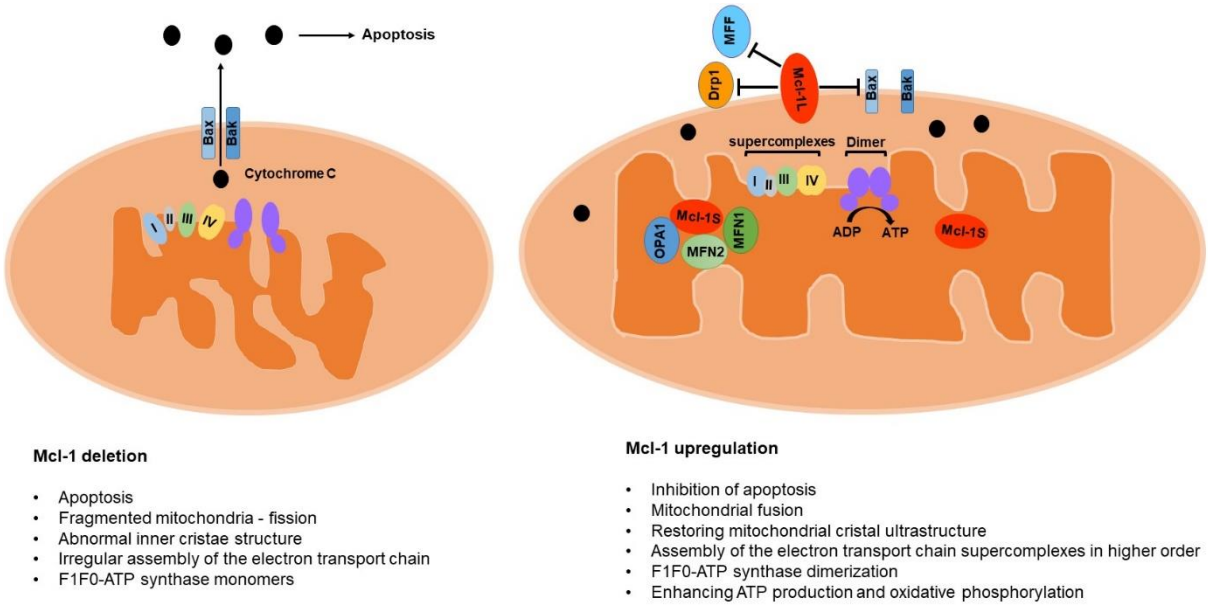

Figure 1.8. The localisation of Mcl1-L and Mcl-1S at the outer mitochondrial membrane (OMM) and inner mitochondrial membrane (IMM), respectively. Mcl-1L stops the formation of the pore by Bak and Bax complex, whereas Mcl-1S enhances mitochondrial functions. Mcl-1 can bind to fission promoting factors Drp1 and MFF and stop the mitochondrial fission. In addition, Mcl-1S binds to fusion promoting factors such as OPA1, MFN1 and MFN2 and enhance mitochondrial fusion.

1.4 T cell activation inhibitor, mitochondrial (TCAIM)

TCAIM (also known as tolerance-associated gene (TOAG-1) positioned at the long arm of chromosome 12 with 71983 bp length (NC_000003.12). The TCAIM protein localises exclusively to mitochondria, and only a few studies have carried out on the TCAIM gene or protein. TCAIM protein has not been fully annotated, and only a

mitochondrial leader sequence at N-terminal and a J-domain at its C-terminal have been annotated so far (123, 124). TCAIM is highly expressed in T_N, T_{reg} and $CD11c^+$ DCs, but its expression is downregulated upon T cell activation (125). Knock-in TCAIM mice have reduced T_M cells; higher T_{reg} cells and reject the allogeneic skin grafts (126). DCs in TCAIM knock-in mice, produce less proinflammatory cytokines and have a lessened capacity of priming both $CD4^+$ and $CD8^+$ T cells (123, 127).

Human T cells upregulating TCAIM have decreased proliferation, lower mitochondrial membrane potential ($\Delta\Psi m$) and are more susceptible to apoptosis (124). Similar to mice studies, overexpression of TCAIM in human T cells leads to a reduction in T_N and T_M phenotypes (124). TCAIM is a newly identified protein, and the functions in T cell is unknown.

1.5. Hsa-microRNA-429 (miR429)

MicroRNAs (also known miRNAs or miRs) are small non-coding RNAs, negatively regulate gene expression at post-transcriptional level by binding to 5′ untranslated region (UTR), coding and 3′ UTR of all mRNAs (128). The miRNA biogenesis is described in details in Figure 1.9.

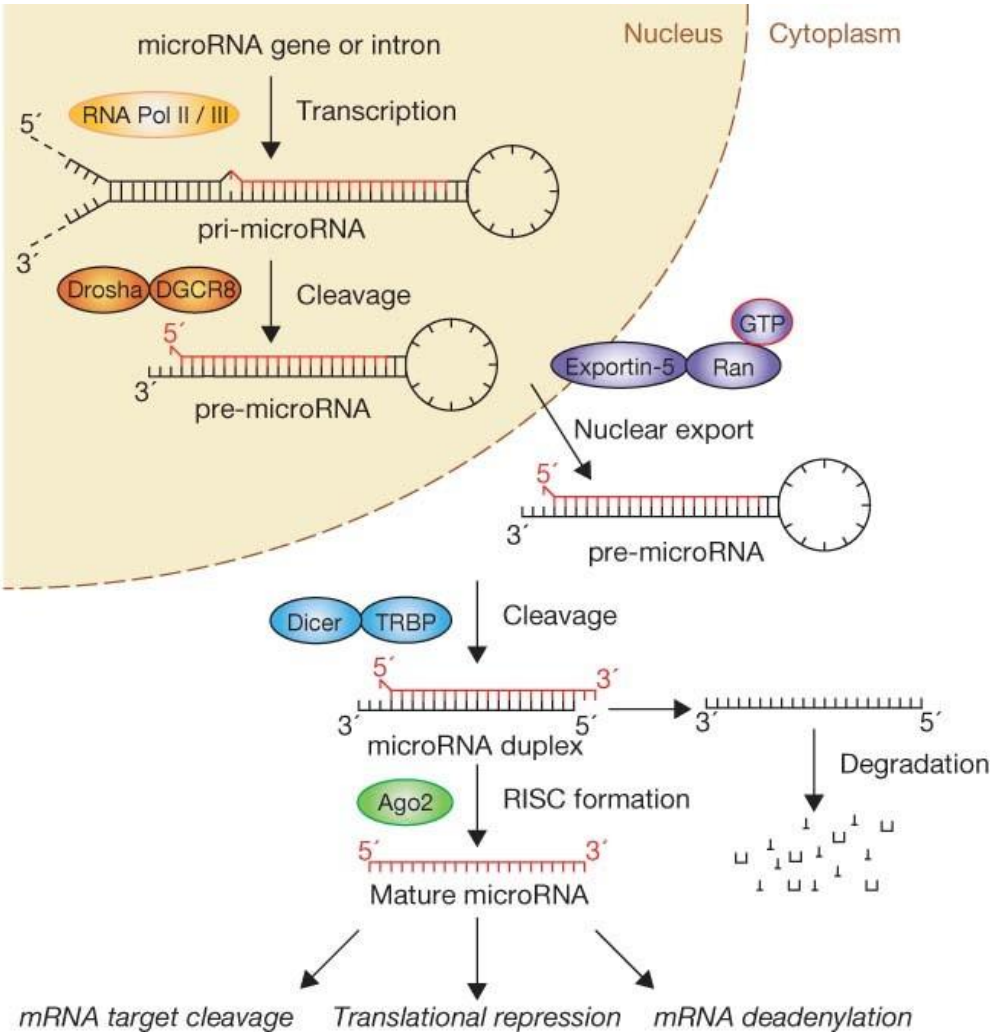

Figure 9. miRNA biogenesis. MiRNAs are initially transcribed into primary miRNA (pri-miRNA) by RNA polymerase II, and similar to the coding mRNAs, they have a 5′ cap (7-methylguanosine) and a polyA tail at their 3′ ends. Pri-miRNAs undergo cleavage by Drosha/DGCR8 complex to produce a ~70 bp precursor miRNA (pre-miRNA). Next, pre-miRNA export to the cytoplasm by cellular exportin-5, where the loop region is cleaved by Dicer to form miRNA duplex. Depending on which strand loads into the RNA induced silencing complex (RISC); one duplex miRNA can result in two functional miR-5p (if the sense strand is loaded) or miR-3p (if the antisense strand is loaded). Then RISC complex scans the mRNAs; perfect matches result in mRNA degradation, while imperfect matches result in translational interference. It is well known that one miRNA can target a set of genes or modulate a cascade (129, 130). Figure was from Winter *et al.* (130).

miR429 belongs to the miR200 (consist of miR200a, b, c, miR141 and miR429) family and its functional form is miR429-3p (Figure 1.10) (131). MiR429 is a tumour suppressor-miRNA and targets a variety of oncogenes such as ZEB1, ZEB2, several genes in Notch1 signalling pathway (131, 132).

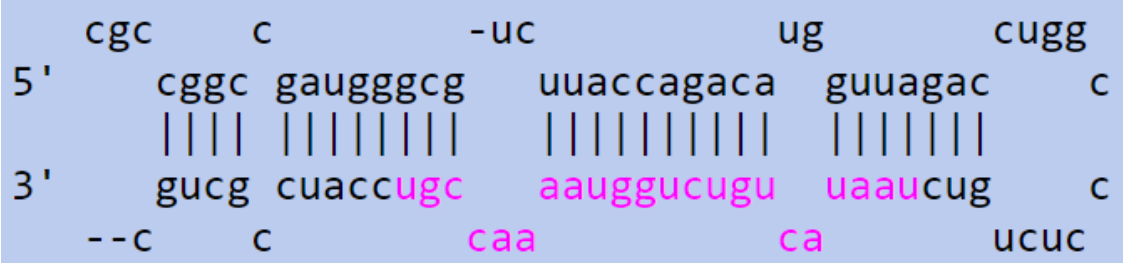

Figure 1.10. The pre-miR429 structure obtained from miRBase database. The mature sequence of miR429 is shown in purple.

miR429 target genes in T cells are still unknown. Guan *et al.* showed miR429 downregulates ZEB2 but not ZEB1 in T cells (133). This finding is interesting because ZEB2 cooperate with T-bet to switch on a terminal differentiation program while the repressing genes necessary for T_M development (134). The miR429 highly expresses in T_N cells, downregulates in T_{EFF} cells and then again upregulates in T_M cells during viral infection (133).

In our recently published review article (73) (provided at the end of this chapter), we explain memory T cell subsets, their characteristic and their potential usages in CAR T cell therapy. We also reviewed the potential strategies to enhance CAR T cell persistence and memory developments. Finally, we proposed a mechanism for TEFF to TM development.

1.6. Scope and aims of the study

This thesis is presented as six chapters and includes five publications with self-supporting materials and method provided within the manuscripts and supplementary materials. The main aim of this study is to enhance the persistence and memory development of the Her2-CAR T cell. Mitochondrial status is the organelle in resistant

to the AICD (as the primary reason for CAR T cell lost) and memory T cell development. We hypothesised by overexpression or downregulation of genes involved in the mitochondrial dynamic we can increase memory T cell development. We chose Mcl-1 to upregulate and TCAIM to downregulate via overexpressing miR429 as a TCAIM negative regulator.

The aims of this study are listed below and shown as four main chapters. As I was finalising my thesis, a pandemic happened. During the NZ lockdown period, I characterised mutations in genome and their implications in genome structure and host miRNA targeting and the viral life cycle. The findings were published the International Journal of Molecular Science (IJMS) and included as the sixth chapter of this thesis.

- Strategies to elevate the endogenous level of Mcl-1
- Inducible overexpression of Mcl-1 using a Tet-on system
- Strategies for constitutive overexpression of Mcl-1
- The role of Mcl-1 and miR429 overexpression in human Her2-CAR T cells
- Implications of SARS-CoV-2 Mutations for Genomic RNA Structure and Host microRNA Targeting

References

1. Ehrlich P. Ueber den jetzigen Stand der Karzinomforschung1908.
2. Burnet M. Cancer—a biological approach: I. The processes of control. II. The significance of somatic mutation. British medical journal. 1957;1(5022):779.
3. Thomas L, Lawrence H. Cellular and humoral aspects of the hypersensitive states. New York: Hoeber-Harper. 1959:529-32.
4. Burnet M. Immunological surveillance: Elsevier; 2014.
5. Anderson MS, Su MA. AIRE expands: new roles in immune tolerance and beyond. Nature Reviews Immunology. 2016;16(4):247-58.
6. Marincola FM, Shamamian P, Alexander RB, Gnarra JR, Turetskaya RL, Nedospasov SA, et al. Loss of HLA haplotype and B locus down-regulation in melanoma cell lines. The journal of Immunology. 1994;153(3):1225-37.
7. Cabrera T, Fernandez MA, Sierra A, Garrido A, Herruzo A, Escobedo A, et al. High frequency of altered HLA class I phenotypes in invasive breast carcinomas. Human immunology. 1996;50(2):127-34.
8. Hanahan D, Weinberg RA. Hallmarks of cancer: the next generation. cell. 2011;144(5):646-74.
9. McCune J. Immunotherapy to treat cancer. Clinical Pharmacology & Therapeutics. 2016;100(3):198-203.
10. Atzpodien J, Kirchner H, Hänninen EL, Deckert M, Fenner M, Poliwoda H. Interleukin-2 in combination with interferon-α and 5-fluorouracil for metastatic renal cell cancer. European Journal of Cancer. 1993;29:S6-S8.
11. Margolin KA, editor Interleukin-2 in the treatment of renal cancer. Seminars in oncology; 2000.
12. Edwards B, Merritt J, Fuhlbrigge R, Borden E. Low doses of interferon alpha result in more effective clinical natural killer cell activation. The Journal of clinical investigation. 1985;75(6):1908-13.
13. Borden EC, Lindner D, Dreicer R, Hussein M, Peereboom D, editors. Second-generation interferons for cancer: clinical targets. Seminars in cancer biology; 2000: Elsevier.

14. van Horssen R, ten Hagen TL, Eggermont AM. TNF-α in cancer treatment: molecular insights, antitumor effects, and clinical utility. The oncologist. 2006;11(4):397-408.
15. Simmons S, Tjoa B, Rogers M, Elgamal A, Kenny G, Ragde H, et al. GM-CSF as a systemic adjuvant in a phase II prostate cancer vaccine trial. The Prostate. 1999;39(4):291-7.
16. Dai S, Wei D, Wu Z, Zhou X, Wei X, Huang H, et al. Phase I clinical trial of autologous ascites-derived exosomes combined with GM-CSF for colorectal cancer. Molecular therapy. 2008;16(4):782-90.
17. Dranoff G. GM-CSF-based cancer vaccines. Immunological reviews. 2002;188(1):147-54.
18. Berzofsky JA, Terabe M, Wood LV, editors. Strategies to use immune modulators in therapeutic vaccines against cancer. Seminars in oncology; 2012: Elsevier.
19. Tran T, Blanc C, Granier C, Saldmann A, Tanchot C, Tartour E, editors. Therapeutic cancer vaccine: building the future from lessons of the past. Seminars in immunopathology; 2019: Springer.
20. Bayer V, editor An Overview of Monoclonal Antibodies. Seminars in oncology nursing; 2019: Elsevier.
21. Luo J, Nishikawa G, Prasad V. A systematic review of head-to-head trials of approved monoclonal antibodies used in cancer: an overview of the clinical trials agenda. Journal of Cancer Research and Clinical Oncology. 2019;145(9):2303-11.
22. Scott AM, Allison JP, Wolchok JD. Monoclonal antibodies in cancer therapy. Cancer Immunity Archive. 2012;12(1):14.
23. Jafari S, Molavi O, Kahroba H, Hejazi MS, Maleki-Dizaji N, Barghi S, et al. Clinical application of immune checkpoints in targeted immunotherapy of prostate cancer. Cellular and Molecular Life Sciences. 2020:1-18.
24. Pardoll DM. The blockade of immune checkpoints in cancer immunotherapy. Nature Reviews Cancer. 2012;12(4):252-64.
25. Rosenberg SA, Restifo NP. Adoptive cell transfer as personalized immunotherapy for human cancer. Science. 2015;348(6230):62-8.

26. Dudley ME, Wunderlich JR, Robbins PF, Yang JC, Hwu P, Schwartzentruber DJ, et al. Cancer regression and autoimmunity in patients after clonal repopulation with antitumor lymphocytes. Science. 2002;298(5594):850-4.
27. Bonini C, Mondino A. Adoptive T-cell therapy for cancer: The era of engineered T cells. European journal of immunology. 2015;45(9):2457-69.
28. Schmitt TM, Ragnarsson GB, Greenberg PD. T cell receptor gene therapy for cancer. Human gene therapy. 2009;20(11):1240-8.
29. Cooper LJ, Kalos M, Lewinsohn DA, Riddell SR, Greenberg PD. Transfer of specificity for human immunodeficiency virus type 1 into primary human T lymphocytes by introduction of T-cell receptor genes. Journal of virology. 2000;74(17):8207-12.
30. Dossett ML, Teague RM, Schmitt TM, Tan X, Cooper LJ, Pinzon C, et al. Adoptive immunotherapy of disseminated leukemia with TCR-transduced, CD8+ T cells expressing a known endogenous TCR. Molecular Therapy. 2009;17(4):742-9.
31. Zhang C, Liu J, Zhong JF, Zhang X. Engineering car-t cells. Biomarker research. 2017;5(1):22.
32. Tokarew N, Ogonek J, Endres S, von Bergwelt-Baildon M, Kobold S. Teaching an old dog new tricks: next-generation CAR T cells. British journal of cancer. 2019;120(1):26-37.
33. Kuwana Y, Asakura Y, Utsunomiya N, Nakanishi M, Arata Y, Itoh S, et al. Expression of chimeric receptor composed of immunoglobulin-derived V resions and T-cell receptor-derived C regions. Biochemical and biophysical research communications. 1987;149(3):960-8.
34. Gross G, Waks T, Eshhar Z. Expression of immunoglobulin-T-cell receptor chimeric molecules as functional receptors with antibody-type specificity. Proceedings of the National Academy of Sciences. 1989;86(24):10024-8.
35. Eshhar Z, Waks T, Gross G, Schindler DG. Specific activation and targeting of cytotoxic lymphocytes through chimeric single chains consisting of antibody-binding domains and the gamma or zeta subunits of the immunoglobulin and T-cell receptors. Proceedings of the National Academy of Sciences. 1993;90(2):720-4.

36. Brocker T, Karjalainen K. Signals through T cell receptor-zeta chain alone are insufficient to prime resting T lymphocytes. The Journal of experimental medicine. 1995;181(5):1653-9.
37. Finney HM, Akbar AN, Lawson AD. Activation of resting human primary T cells with chimeric receptors: costimulation from CD28, inducible costimulator, CD134, and CD137 in series with signals from the TCRζ chain. The Journal of Immunology. 2004;172(1):104-13.
38. Imai C, Mihara K, Andreansky M, Nicholson I, Pui C, Geiger T, et al. Chimeric receptors with 4-1BB signaling capacity provoke potent cytotoxicity against acute lymphoblastic leukemia. Leukemia. 2004;18(4):676-84.
39. Pulè MA, Straathof KC, Dotti G, Heslop HE, Rooney CM, Brenner MK. A chimeric T cell antigen receptor that augments cytokine release and supports clonal expansion of primary human T cells. Molecular Therapy. 2005;12(5):933-41.
40. Wang J, Jensen M, Lin Y, Sui X, Chen E, Lindgren CG, et al. Optimizing adoptive polyclonal T cell immunotherapy of lymphomas, using a chimeric T cell receptor possessing CD28 and CD137 costimulatory domains. Human gene therapy. 2007;18(8):712-25.
41. Watts TH. Staying alive: T cell costimulation, CD28, and Bcl-xL. The Journal of Immunology. 2010;185(7):3785-7.
42. Frauwirth KA, Riley JL, Harris MH, Parry RV, Rathmell JC, Plas DR, et al. The CD28 signaling pathway regulates glucose metabolism. Immunity. 2002;16(6):769-77.
43. Suresh M, Whitmire JK, Harrington LE, Larsen CP, Pearson TC, Altman JD, et al. Role of CD28-B7 interactions in generation and maintenance of CD8 T cell memory. The Journal of Immunology. 2001;167(10):5565-73.
44. Porter DL, Hwang W-T, Frey NV, Lacey SF, Shaw PA, Loren AW, et al. Chimeric antigen receptor T cells persist and induce sustained remissions in relapsed refractory chronic lymphocytic leukemia. Science translational medicine. 2015;7(303):303ra139-303ra139.
45. Long AH, Haso WM, Shern JF, Wanhainen KM, Murgai M, Ingaramo M, et al. 4-1BB costimulation ameliorates T cell exhaustion induced by tonic signaling of chimeric antigen receptors. Nature medicine. 2015;21(6):581-90.

46. Yang L, Tarun S, Chien CD, Kohler ME, Qin H, Fry TJ. Analysis of CAR 41-BB versus CD28 co-stimulatory domains exposes emergence of extramedullary disease in acute myeloid leukemia. AACR; 2018.
47. Marin V, Pizzitola I, Agostoni V, Attianese GMPG, Finney H, Lawson A, et al. Cytokine-induced killer cells for cell therapy of acute myeloid leukemia: improvement of their immune activity by expression of CD33-specific chimeric receptors. Haematologica. 2010;95(12):2144-52.
48. Morgan RA, Yang JC, Kitano M, Dudley ME, Laurencot CM, Rosenberg SA. Case report of a serious adverse event following the administration of T cells transduced with a chimeric antigen receptor recognizing ERBB2. Molecular Therapy. 2010;18(4):843-51.
49. Till BG, Jensen MC, Wang J, Qian X, Gopal AK, Maloney DG, et al. CD20-specific adoptive immunotherapy for lymphoma using a chimeric antigen receptor with both CD28 and 4-1BB domains: pilot clinical trial results. Blood, The Journal of the American Society of Hematology. 2012;119(17):3940-50.
50. Maude SL, Laetsch TW, Buechner J, Rives S, Boyer M, Bittencourt H, et al. Tisagenlecleucel in children and young adults with B-cell lymphoblastic leukemia. New England Journal of Medicine. 2018;378(5):439-48.
51. Turtle CJ, Hanafi L-A, Berger C, Gooley TA, Cherian S, Hudecek M, et al. CD19 CAR–T cells of defined CD4+: CD8+ composition in adult B cell ALL patients. The Journal of clinical investigation. 2016;126(6):2123-38.
52. Gill S, Maus MV, Porter DL. Chimeric antigen receptor T cell therapy: 25 years in the making. Blood reviews. 2016;30(3):157-67.
53. Rutkowska A, Stoczyńska-Fidelus E, Janik K, Włodarczyk A, Rieske P. EGFRvIII: An Oncogene with Ambiguous Role. Journal of Oncology. 2019;2019.
54. Wilkie S, Picco G, Foster J, Davies DM, Julien S, Cooper L, et al. Retargeting of human T cells to tumor-associated MUC1: the evolution of a chimeric antigen receptor. The Journal of Immunology. 2008;180(7):4901-9.
55. Johnson LA, Scholler J, Ohkuri T, Kosaka A, Patel PR, McGettigan SE, et al. Rational development and characterization of humanized anti–EGFR variant III chimeric antigen receptor T cells for glioblastoma. Science translational medicine. 2015;7(275):275ra22-ra22.

56. Tan HL, Yong C, Tan BZ, Fong WJ, Padmanabhan J, Chin A, et al. Conservation of oncofetal antigens on human embryonic stem cells enables discovery of monoclonal antibodies against cancer. Scientific reports. 2018;8(1):1-11.
57. Liu H, Xu Y, Xiang J, Long L, Green S, Yang Z, et al. Targeting alpha-fetoprotein (AFP)–MHC complex with CAR T-cell therapy for liver cancer. Clinical cancer research. 2017;23(2):478-88.
58. Burga RA, Thorn M, Point GR, Guha P, Nguyen CT, Licata LA, et al. Liver myeloid-derived suppressor cells expand in response to liver metastases in mice and inhibit the anti-tumor efficacy of anti-CEA CAR-T. Cancer Immunology, Immunotherapy. 2015;64(7):817-29.
59. Owens GL, Sheard VE, Kalaitsidou M, Blount D, Lad Y, Cheadle EJ, et al. Preclinical assessment of CAR T-cell therapy targeting the tumor antigen 5T4 in ovarian cancer. Journal of immunotherapy (Hagerstown, Md: 1997). 2018;41(3):130.
60. Morello A, Sadelain M, Adusumilli PS. Mesothelin-targeted CARs: driving T cells to solid tumors. Cancer discovery. 2016;6(2):133-46.
61. Gutierrez C, Schiff R. HER2: biology, detection, and clinical implications. Archives of pathology & laboratory medicine. 2011;135(1):55-62.
62. Craddock JA, Lu A, Bear A, Pule M, Brenner MK, Rooney CM, et al. Enhanced tumor trafficking of GD2 chimeric antigen receptor T cells by expression of the chemokine receptor CCR2b. Journal of immunotherapy (Hagerstown, Md: 1997). 2010;33(8):780.
63. Moon EK, Carpenito C, Sun J, Wang L-CS, Kapoor V, Predina J, et al. Expression of a functional CCR2 receptor enhances tumor localization and tumor eradication by retargeted human T cells expressing a mesothelin-specific chimeric antibody receptor. Clinical cancer research. 2011;17(14):4719-30.
64. Brown CE, Vishwanath RP, Aguilar B, Starr R, Najbauer J, Aboody KS, et al. Tumor-derived chemokine MCP-1/CCL2 is sufficient for mediating tumor tropism of adoptively transferred T cells. The Journal of Immunology. 2007;179(5):3332-41.
65. Di Stasi A, De Angelis B, Rooney CM, Zhang L, Mahendravada A, Foster AE, et al. T lymphocytes coexpressing CCR4 and a chimeric antigen receptor targeting

CD30 have improved homing and antitumor activity in a Hodgkin tumor model. Blood, The Journal of the American Society of Hematology. 2009;113(25):6392-402.

66. Carlsten M, Levy E, Karambelkar A, Li L, Reger R, Berg M, et al. Efficient mRNA-based genetic engineering of human NK cells with high-affinity CD16 and CCR7 augments rituximab-induced ADCC against lymphoma and targets NK cell migration toward the lymph node-associated chemokine CCL19. Frontiers in immunology. 2016;7:105.
67. Kershaw MH, Wang G, Westwood JA, Pachynski RK, Tiffany HL, Marincola FM, et al. Redirecting migration of T cells to chemokine secreted from tumors by genetic modification with CXCR2. Human gene therapy. 2002;13(16):1971-80.
68. Hillerdal V, Essand M. Chimeric antigen receptor-engineered T cells for the treatment of metastatic prostate cancer. BioDrugs. 2015;29(2):75-89.
69. Newick K, Moon E, Albelda SM. Chimeric antigen receptor T-cell therapy for solid tumors. Molecular Therapy-Oncolytics. 2016;3:16006.
70. Vaupel P, Multhoff G. Accomplices of the hypoxic tumor microenvironment compromising antitumor immunity: adenosine, lactate, acidosis, vascular endothelial growth factor, potassium ions, and phosphatidylserine. Frontiers in immunology. 2017;8:1887.
71. Newick K, O'Brien S, Sun J, Kapoor V, Maceyko S, Lo A, et al. Augmentation of CAR T-cell trafficking and antitumor efficacy by blocking protein kinase A localization. Cancer immunology research. 2016;4(6):541-51.
72. Hou AJ, Chang ZL, Lorenzini MH, Zah E, Chen YY. TGF-β–responsive CAR-T cells promote anti-tumor immune function. Bioengineering & translational medicine. 2018;3(2):75-86.
73. McLellan AD, Ali Hosseini Rad SM. Chimeric antigen receptor T cell persistence and memory cell formation. Immunology and cell biology. 2019;97(7):664-74.
74. Melero I, Rouzaut A, Motz GT, Coukos G. T-cell and NK-cell infiltration into solid tumors: a key limiting factor for efficacious cancer immunotherapy. Cancer discovery. 2014;4(5):522-6.

75. Peter ME, Hadji A, Murmann AE, Brockway S, Putzbach W, Pattanayak A, et al. The role of CD95 and CD95 ligand in cancer. Cell death & differentiation. 2015;22(4):549-59.
76. O'Reilly LA, Tai L, Lee L, Kruse EA, Grabow S, Fairlie WD, et al. Membrane-bound Fas ligand only is essential for Fas-induced apoptosis. Nature. 2009;461(7264):659-63.
77. Tauzin S, Chaigne-Delalande B, Selva E, Khadra N, Daburon S, Contin-Bordes C, et al. The naturally processed CD95L elicits a c-yes/calcium/PI3K-driven cell migration pathway. PLoS biology. 2011;9(6).
78. Vargo-Gogola T, Crawford HC, Fingleton B, Matrisian LM. Identification of novel matrix metalloproteinase-7 (matrilysin) cleavage sites in murine and human Fas ligand. Archives of biochemistry and biophysics. 2002;408(2):155-61.
79. Le Gallo M, Poissonnier A, Blanco P, Legembre P. CD95/Fas, non-apoptotic signaling pathways, and kinases. Frontiers in immunology. 2017;8:1216.
80. Özören N, El-Deiry WS. Defining characteristics of Types I and II apoptotic cells in response to TRAIL. Neoplasia. 2002;4(6):551-7.
81. Peter ME, Budd RC, Desbarats J, Hedrick SM, Hueber A-O, Newell MK, et al. The CD95 receptor: apoptosis revisited. Cell. 2007;129(3):447-50.
82. Motz GT, Santoro SP, Wang L-P, Garrabrant T, Lastra RR, Hagemann IS, et al. Tumor endothelium FasL establishes a selective immune barrier promoting tolerance in tumors. Nature medicine. 2014;20(6):607.
83. Matsumoto N, Imamura R, Suda T. Caspase-8-and JNK-dependent AP-1 activation is required for Fas ligand-induced IL-8 production. The FEBS journal. 2007;274(9):2376-84.
84. Barnhart BC, Legembre P, Pietras E, Bubici C, Franzoso G, Peter ME. CD95 ligand induces motility and invasiveness of apoptosis-resistant tumor cells. The EMBO journal. 2004;23(15):3175-85.
85. Hadji A, Ceppi P, Murmann AE, Brockway S, Pattanayak A, Bhinder B, et al. Death induced by CD95 or CD95 ligand elimination. Cell reports. 2014;7(1):208-22.
86. Yamamoto TN, Lee P-H, Vodnala SK, Gurusamy D, Kishton RJ, Yu Z, et al. T cells genetically engineered to overcome death signaling enhance adoptive cancer immunotherapy. The Journal of clinical investigation. 2019;129(4).

87. Künkele A, Johnson AJ, Rolczynski LS, Chang CA, Hoglund V, Kelly-Spratt KS, et al. Functional tuning of CARs reveals signaling threshold above which CD8+ CTL antitumor potency is attenuated due to cell Fas–FasL-dependent AICD. Cancer immunology research. 2015;3(4):368-79.
88. Tschumi BO, Dumauthioz N, Marti B, Zhang L, Schneider P, Mach J-P, et al. CART cells are prone to Fas-and DR5-mediated cell death. Journal for immunotherapy of cancer. 2018;6(1):71.
89. He B, Wang L, Neuber B, Schmitt A, Kneisel N, Hoeger T, et al. Blockade of CD95/CD95L Death Signaling Enhances CAR T Cell Persistence and Antitumor Efficacy. American Society of Hematology Washington, DC; 2019.
90. Hong LK, Chen Y, Smith CC, Montgomery SA, Vincent BG, Dotti G, et al. CD30-Redirected chimeric antigen receptor T cells target CD30+ and CD30− embryonal Carcinoma via antigen-Dependent and Fas/FasL interactions. Cancer immunology research. 2018.
91. Gattinoni L, Lugli E, Ji Y, Pos Z, Paulos CM, Quigley MF, et al. A human memory T cell subset with stem cell–like properties. Nature medicine. 2011;17(10):1290.
92. Klebanoff CA, Scott CD, Leonardi AJ, Yamamoto TN, Cruz AC, Ouyang C, et al. Memory T cell–driven differentiation of naive cells impairs adoptive immunotherapy. The Journal of clinical investigation. 2016;126(1):318-34.
93. Desdín-Micó G, Soto-Heredero G, Mittelbrunn M. Mitochondrial activity in T cells. Mitochondrion. 2018;41:51-7.
94. Morlino G, Barreiro O, Baixauli F, Robles-Valero J, González-Granado JM, Villa-Bellosta R, et al. Miro-1 links mitochondria and microtubule Dynein motors to control lymphocyte migration and polarity. Molecular and cellular biology. 2014;34(8):1412-26.
95. Sánchez-Madrid F, Serrador JM. Bringing up the rear: defining the roles of the uropod. Nature reviews Molecular cell biology. 2009;10(5):353-9.
96. La Rovere RM, Roest G, Bultynck G, Parys JB. Intracellular Ca2+ signaling and Ca2+ microdomains in the control of cell survival, apoptosis and autophagy. Cell calcium. 2016;60(2):74-87.
97. Park BV, Pan F. Metabolic regulation of T cell differentiation and function. Molecular immunology. 2015;68(2):497-506.

98. Buck MD, O'sullivan D, Pearce EL. T cell metabolism drives immunity. Journal of Experimental Medicine. 2015;212(9):1345-60.
99. Buck MD, Sowell RT, Kaech SM, Pearce EL. Metabolic instruction of immunity. Cell. 2017;169(4):570-86.
100. Klein Geltink RI, Kyle RL, Pearce EL. Unraveling the complex interplay between T cell metabolism and function. Annual review of immunology. 2018;36:461-88.
101. Nicholls DG. Spare respiratory capacity, oxidative stress and excitotoxicity. Portland Press Ltd.; 2009.
102. van der Windt GJ, O'Sullivan D, Everts B, Huang SC-C, Buck MD, Curtis JD, et al. CD8 memory T cells have a bioenergetic advantage that underlies their rapid recall ability. Proceedings of the National Academy of Sciences. 2013;110(35):14336-41.
103. Chao T, Wang H, Ho P-C. Mitochondrial control and guidance of cellular activities of T cells. Frontiers in immunology. 2017;8:473.
104. Chan DC. Mitochondrial fusion and fission in mammals. Annu Rev Cell Dev Biol. 2006;22:79-99.
105. Youle RJ, Van Der Bliek AM. Mitochondrial fission, fusion, and stress. Science. 2012;337(6098):1062-5.
106. Kameoka S, Adachi Y, Okamoto K, Iijima M, Sesaki H. Phosphatidic acid and cardiolipin coordinate mitochondrial dynamics. Trends in cell biology. 2018;28(1):67-76.
107. Buck MD, O'Sullivan D, Geltink RIK, Curtis JD, Chang C-H, Sanin DE, et al. Mitochondrial dynamics controls T cell fate through metabolic programming. Cell. 2016;166(1):63-76.
108. Bordon Y. IL-15 provides breathing space for memory. Nature Reviews Immunology. 2012;12(2):77-.
109. Morciano G, Giorgi C, Balestra D, Marchi S, Perrone D, Pinotti M, et al. Mcl-1 involvement in mitochondrial dynamics is associated with apoptotic cell death. Molecular biology of the cell. 2016;27(1):20-34.
110. Senichkin VV, Streletskaia AY, Gorbunova AS, Zhivotovsky B, Kopeina GS. Saga of Mcl-1: regulation from transcription to degradation. Cell Death & Differentiation. 2020:1-15.

111. Thomas LW, Lam C, Edwards SW. Mcl-1; the molecular regulation of protein function. FEBS letters. 2010;584(14):2981-9.
112. Kim J-H, Sim S-H, Ha H-J, Ko J-J, Lee K, Bae J. MCL-1ES, a novel variant of MCL-1, associates with MCL-1L and induces mitochondrial cell death. FEBS letters. 2009;583(17):2758-64.
113. Hagenbuchner J, Kiechl-Kohlendorfer U, Obexer P, Ausserlechner MJ. A novel Mcl1 variant inhibits apoptosis via increased Bim sequestration. Oncotarget. 2013;4(8):1241.
114. Perciavalle RM, Stewart DP, Koss B, Lynch J, Milasta S, Bathina M, et al. Anti-apoptotic MCL-1 localizes to the mitochondrial matrix and couples mitochondrial fusion to respiration. Nature cell biology. 2012;14(6):575-83.
115. Shore GC, Warr MR. Unique biology of Mcl-1: therapeutic opportunities in cancer. Current molecular medicine. 2008;8(2):138-47.
116. Weng C, Li Y, Xu D, Shi Y, Tang H. Specific cleavage of Mcl-1 by caspase-3 in tumor necrosis factor-related apoptosis-inducing ligand (TRAIL)-induced apoptosis in Jurkat leukemia T cells. Journal of Biological Chemistry. 2005;280(11):10491-500.
117. Bae J, Leo CP, Hsu SY, Hsueh AJ. MCL-1S, a splicing variant of the antiapoptotic BCL-2 family member MCL-1, encodes a proapoptotic protein possessing only the BH3 domain. Journal of Biological Chemistry. 2000;275(33):25255-61.
118. Perciavalle RM, Opferman JT. Delving deeper: MCL-1's contributions to normal and cancer biology. Trends in cell biology. 2013;23(1):22-9.
119. Viant C, Guia S, Hennessy RJ, Rautela J, Pham K, Bernat C, et al. Cell cycle progression dictates the requirement for BCL2 in natural killer cell survival. Journal of Experimental Medicine. 2017;214(2):491-510.
120. Escudero S, Zaganjor E, Lee S, Mill CP, Morgan AM, Crawford EB, et al. Dynamic regulation of long-chain fatty acid oxidation by a noncanonical interaction between the MCL-1 BH3 helix and VLCAD. Molecular cell. 2018;69(5):729-43. e7.
121. Liu Y, Ma Y, Tu Z, Zhang C, Du M, Wang Y, et al. Mcl-1 inhibits Mff-mediated mitochondrial fragmentation and apoptosis. Biochemical and Biophysical Research Communications. 2020;523(3):620-6.

122. Rasmussen ML, Kline LA, Park KP, Ortolano NA, Romero-Morales AI, Anthony CC, et al. A non-apoptotic function of MCL-1 in promoting pluripotency and modulating mitochondrial dynamics in stem cells. Stem cell reports. 2018;10(3):684-92.
123. Vogel SZ, Schlickeiser S, Jürchott K, Akyuez L, Schumann J, Appelt C, et al. TCAIM decreases T cell priming capacity of dendritic cells by inhibiting TLR-induced Ca2+ influx and IL-2 production. The Journal of Immunology. 2015;194(7):3136-46.
124. Keeren K, Friedrich M, Gebuhr I, Philipp S, Sabat R, Sterry W, et al. Expression of tolerance associated gene-1, a mitochondrial protein inhibiting T cell activation, can be used to predict response to immune modulating therapies. The Journal of Immunology. 2009;183(6):4077-87.
125. Sawitzki B, Bushell A, Steger U, Jones N, Risch K, Siepert A, et al. Identification of gene markers for the prediction of allograft rejection or permanent acceptance. American Journal of Transplantation. 2007;7(5):1091-102.
126. Schumann J, Stanko K, Woertge S, Appelt C, Schumann M, Kühl A, et al. The mitochondrial protein TCAIM regulates activation of T cells and thereby promotes tolerance induction of allogeneic transplants. American Journal of Transplantation. 2014;14(12):2723-35.
127. Panov I, Schlickeiser S, Vogel S, Schumann J, Schliesser U, Gossen M, et al. Transcriptional control of tolerance associated gene TCAIM is CREB, NFATc1 and C/EBPβ dependent resulting in generation of tolerogenic dendritic cells (P2152). Am Assoc Immnol; 2013.
128. Lee I, Ajay SS, Yook JI, Kim HS, Hong SH, Kim NH, et al. New class of microRNA targets containing simultaneous 5′-UTR and 3′-UTR interaction sites. Genome research. 2009;19(7):1175-83.
129. O'Brien J, Hayder H, Zayed Y, Peng C. Overview of microRNA biogenesis, mechanisms of actions, and circulation. Frontiers in endocrinology. 2018;9:402.
130. Winter J, Jung S, Keller S, Gregory RI, Diederichs S. Many roads to maturity: microRNA biogenesis pathways and their regulation. Nature cell biology. 2009;11(3):228-34.

131. Humphries B, Yang C. The microRNA-200 family: small molecules with novel roles in cancer development, progression and therapy. Oncotarget. 2015;6(9):6472.
132. Muralidhar GG, Barbolina MV. The miR-200 family: versatile players in epithelial ovarian cancer. International journal of molecular sciences. 2015;16(8):16833-47.
133. Guan T, Dominguez CX, Amezquita RA, Laidlaw BJ, Cheng J, Henao-Mejia J, et al. ZEB1, ZEB2, and the miR-200 family form a counterregulatory network to regulate CD8+ T cell fates. Journal of Experimental Medicine. 2018;215(4):1153-68.
134. Dominguez CX, Amezquita RA, Guan T, Marshall HD, Joshi NS, Kleinstein SH, et al. The transcription factors ZEB2 and T-bet cooperate to program cytotoxic T cell terminal differentiation in response to LCMV viral infection. Journal of Experimental Medicine. 2015;212(12):2041-56.

Immunology & Cell Biology 2019; **97**: 664–674
www.wileyonlinelibrary.com/journal/icb

SPECIAL FEATURE REVIEW

Chimeric antigen receptor T cell persistence and memory cell formation

Alexander D McLellan & Seyed M Ali Hosseini Rad

Department of Microbiology and Immunology, University of Otago, Dunedin 9054, New Zealand

Keywords
adaptive immunity, cancer, CAR T cells, cellular immunity, immunological memory, immunology, innate immune cells, persistence

Correspondence
Alexander D McLellan, Department of Microbiology and Immunology, University of Otago, Dunedin 9054, New Zealand.
E-mail: alex.mclellan@otago.ac.nz

Received 22 January 2019; Revised 17 April 2019; Accepted 17 April 2019

doi: 10.1111/imcb.12254

Immunology & Cell Biology 2019; **97**: 664–674

Abstract

It is now becoming clear that less differentiated naive and memory T cells are superior to effector T cells in the transfer of immunity for adoptive cell therapy. This review will outline the challenges faced by chimeric antigen receptor (CAR) T cell therapy in the generation of persistence and memory for CAR T cells, and summarize recent strategies to improve CAR T cell persistence, with a focus on memory cell formation. The relevance of enhancing persistence in more differentiated effector T cells is also covered, because genetic and pharmacological interventions may prolong effector T cell activity and lifespan, thereby improving anti-cancer activity. In particular, it may be possible to enforce epigenetic changes in differentiated T cells to enhance memory CAR T cell formation. Optimizing the generation of self-renewing T cell populations (e.g. memory cells), while maintaining differentiated effector T cells through epigenome modification, will help overcome barriers to T cell expansion and survival, thereby improving clinical outcomes in CAR T cell therapy.

INTRODUCTION

Chimeric antigen receptor T cell therapy

Chimeric antigen receptor (CAR) T cell therapy has now emerged as a clinically tested and effective treatment for CD19-positive lymphoma and leukemia. CARs are comprised of an anti-cancer monoclonal antibody, spliced to intracellular T cell receptor (TCR) signaling domains. CAR T cells expanded *in vitro* are adoptively transferred back into the patient to destroy cancer cells when triggered by tumor antigen.[1-7] In CAR T cell therapy of B-cell malignancies, expansion and persistence of adoptively transferred T cell populations is considered a critical requirement for long-term tumor immunity without relapse.[1-5,8,9] This may be especially true for B-cell acute lymphoblastic leukemia which typically requires prolonged conventional treatment timelines. In contrast, for certain B-cell non-Hodgkin's lymphoma subtypes that often respond to shorter, intensive courses of chemotherapy, as evidenced by the recovery of normal B cells in CAR T cell–treated lymphoma patients in remission, long-term CAR T cell persistence may be of lesser importance.[10] Anti-CD19 CAR T cells may persist for months to years in the blood of lymphoma patients, with the longevity of CAR T cells likely influenced by costimulator domain of the CAR, as well as the disease subtype.[1-3,9]

In contrast to physiological T cell responses, CAR T cell expansions differ in several ways, as summarized in Figure 1. First, CAR transduction occurs *ex vivo* within a polyclonal population, that can then be expanded relatively independently of endogenous TCR expression. Second, CAR T cell expansion *ex vivo* involves exposure to elements not encountered by *in vivo* expanded T cells; for example, transducing virus exposure and infection (most frequently gamma-retroviral or lentiviral particles) and CD3/CD28 stimulation in the presence of recombinant cytokines. Preconditioning of patients encourages lymphopenic expansion of the CAR product. Predictably, the final expanded CAR T cell population will be polyclonal with respect to TCR (but not CAR) specificity, and will likely possess a diversity of activation/differentiation states among individual CAR T cells.

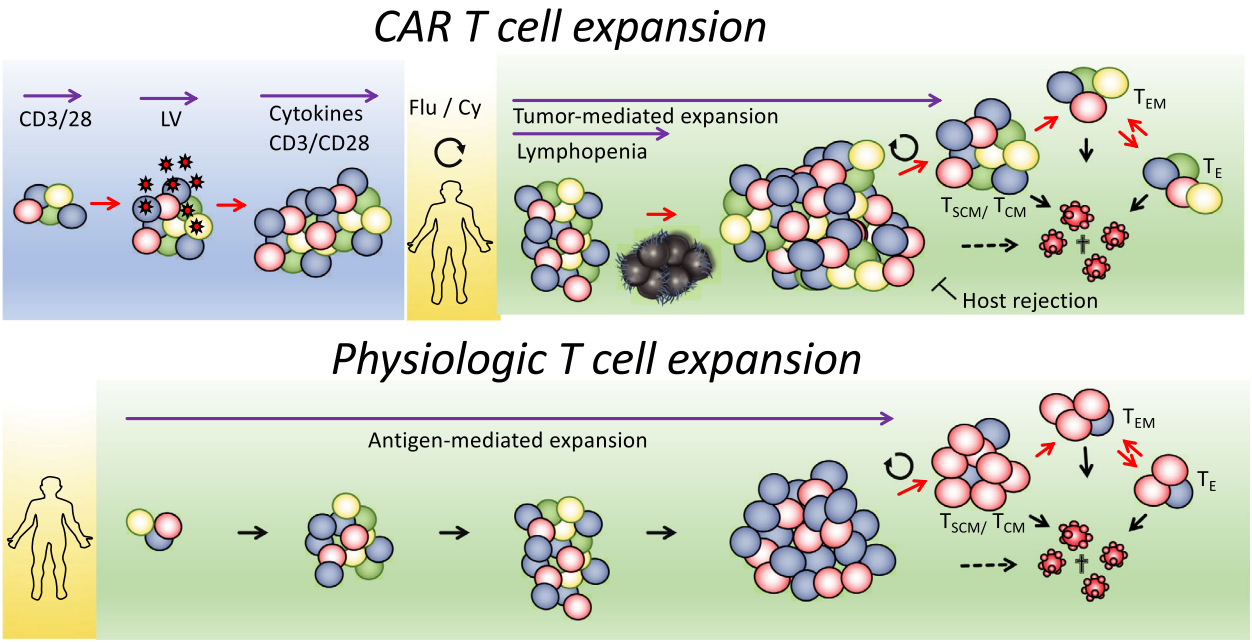

Figure 1. Contrasting chimeric antigen receptor (CAR) T cell and physiogical processes for T cell expansion and memory cell development. Top panel: The generation of CAR T cells requires *ex vivo* stimulation of patient T cells with CD3/CD28, lentiviral (LV), retroviral or transposon mediated gene transfer, followed by additional culture in a selection of cytokines that stimulated via the common gamma chain. Patients are preconditioned with lymphodepleting regimes (fludarabine/cyclophosphamide; Flu-Cy). Following adoptive transfer, CAR T cells undergo further activation and expansion in response to lymphopenic environment and tumour antigen. Bottom panel: Physiologic activation of T cells proceeds strictly *in vivo* in response to antigen and does not involve lymphopenic expansion. Physiologically activated T cells will be expected have a lower endogenous T cell receptor (TCR) diversity, compared to CAR T cells that are produced from a nonselected, polyclonal repertoire. [The color version of this figure can be viewed at www.wileyonlinelibrary.com/journal/icb]

Barriers to CAR T cell persistence

The maintenance of functional anti-cancer CAR T cell therapy could be hampered by the following: (1) insufficient expansion of the initial T cell product, (2) recognition of immunogenic CAR sequences and rejection by the host immune system, (3) tumor immune-suppression, (4) tolerance induced by normal B cells expressing tumour-associated antigen (TAA) (5) activation-induced cell death (AICD), (6) exhaustion that follows tonic/chronic CAR or TCR triggering and (7) contraction that occurs when antigen is no longer available at sufficient levels to maintaining the dividing pool of T cells. These factors may translate into inefficient tumor killing and poorer patient outcomes. The subject of barriers to CAR T cell therapy topic has been dealt with in recent reviews,[11,12] and due to space limitations, only exhaustion, AICD and contraction will be discussed further (see below). Instead, this review will outline the contribution of memory and persistence to CAR T cell therapy, as well as relevant strategies to improve clinical outcomes.

Exhaustion, AICD and lymphocyte contraction

Exhaustion describes the onset of often irreversible epigenetic changes in terminally differentiated T cells.[13-16] The evolutionary advantage of exhaustion is that T cells that are repeatedly stimulated by self-peptide/major histocompatibility complex (MHC) are inactivated. However, in many cancers, antigen may persist for extended periods of time and despite initial effective anti-cancer cell responses, T cells can become exhausted and susceptible to AICD.[13,14,17] Following chronic repetitive antigen stimulation, the antigen T cell–specific T cell pool may contract, or become effete in terms of cytokine secretion and cytolytic potential.[13,17]

Although CAR T cells have been shown to undergo AICD via CD95:CD95L,[14] T cell contraction can occur in the absence of CD95, CD95L and TNF signaling, suggesting that cell-intrinsic mechanisms may play out during lymphocyte contraction. For example, replicative senescence and growth factor withdrawal are possible mechanisms, in addition to cell-intrinsic onset of terminal exhaustion.[13,17] In infection settings, lymphocyte contraction occurs following the peak immune response, yet memory cell formation is the usual outcome.[17,18]

Given that withdrawal of antigen signaling can enhance memory cell formation,[18] it is not clear why CAR T cells are lost, even in patients with complete responses, but is likely the result of the combination of the factors discussed above.[2,3] It is also possible that the sensitivity of polymerase

chain reaction (PCR) used to detect CAR T cells may not be consistent across different studies. Therefore, PCR-based CAR detection may miss trace populations of persisting CAR T cells at numbers below the limit of detection, or fail to detect CAR T cells that infiltrate the spleen, lungs, lymph node or bone marrow.[6] Surprisingly, the lack of long-term persistence of CAR T cells is in some cases unrelated to positive clinical outcomes, particularly in non-Hodgkin's lymphoma (NHL). This is demonstrated by relapse-free survival observed well after CAR T cells have dropped below the limit of detection, and non-malignant B cells have rebounded.[10]

Persistence and memory

Are persistence and memory one and the same? Although the terms of T cell memory and persistence may sometimes be used interchangeably, a working definition of memory T cell function must include longevity and self-renewal.[19,20] In terms of persistence, functionally active anti-cancer T cells, without typical memory features, may persist in favorable conditions in the host, particularly when the manifestation of exhaustion-related and AICD is minimized.[21-26] Strategies to prolong the lifespan and activity of non-memory T cells may still contribute markedly to the anti-tumor response. Moreover, appropriately primed effector T cells (T_E) can provide a source of memory cells,[21-30] although T_E to T memory cell transformation has yet to be demonstrated in adoptive CAR T cell therapy. Despite possessing limited capacity for self-renewal, improving T_E longevity would be expected to improve anti-cancer immunity.[13,31]

SUBSETS OF MEMORY CELLS

The development of naive T cells into memory and effector cell populations follows progressive epigenetic changes that impart unique gene expression profiles and functions.[15,19,20,32] It has been proposed that considerable artificial complexity exists in memory T cell subset definitions, and that such stringent categorization may not accurately reflect the true phenotypic and functional gradients existing in nature.[32] In this review, we will only briefly cover the definitions of memory cells in order to illustrate how *in vitro* culture and clinical interventions could contribute to enhancing CAR T cell memory and persistence. For more extensive discussion on T cell memory subsets, the reader is referred to three excellent and recent reviews.[19,20,32]

Naive T cells reflect the most immature T cell, and by classic definition have not been antigen-triggered. Upon interaction via the native TCR or CAR, naive T cells proliferate and differentiate to form T_E and/or memory cells. Central memory T cells (T_{CM}) circulate throughout the body and provide rapid cytokine production upon stimulation, but are poorly cytotoxic. The adoptive transfer of a single T_{CM} clone is sufficient to confer self-renewal of memory cells, while allowing the differentiation of effector cells for the appropriate immune response.[33] T_{CM} cell division forms T_E, more daughter T_{CM}, or effector memory T cells (T_{EM}).[19,20,34] T_{CM} to T_{EM} transition results in the downregulation of CCR7 and CD62L, and a loss in homing ability to lymphoid tissues, although T_{EM} exhibit the highest level of cytotoxicity of all the memory cell subtypes.[19,20,34]

Stem cell memory T cells (T_{SCM}) appear to be a subset of T_{CM} that display a more extensive capacity for self-renewal.[19,20,34] Despite their maturity, as determined by TCR excision circle dilution, T_{SCM} share transcription factor profiles, as well as self-renewing characteristic with classic stem cells.[19,20]

In adoptive cell immunotherapy, naive, T_{SCM} or T_{CM} subsets outperform T_E and T_{EM}, in spite of the enhanced cytotoxic and cytokine-releasing potential of effector T cell subsets.[8,20,25,33,35] Since T_E display superior tumor killing capacity *in vitro*, as compared to naive or memory T cells, the results might be explained by the low-level self-renewal capacity of effector cells. However, it is also possible that effector cells are inefficiently transferred to the host by the adoptive transfer procedure and have limited niche homing and survival, compared to their less differentiated counterparts. For example, lung or splenic trapping may render adoptive transfer of activated lymphocytes for niche formation less efficient. In a recent clinical trial, CAR T cells predominantly homed to the lungs and spleen, possibly as a result of the enhanced integrin expression on effector CAR T cells, leading to trapping in highly vascular organs.[6] In contrast to the limited ability of effector cells to survive following adoptive transfer, strategies to establish populations of memory cells within the host will give rise to populations of both T_E, as well as self-renewing memory cells (Figure 1).

Tissue resident memory T cells (T_{RM}) resemble T_{EM} in that they home to nonlymphoid tissue, but T_{RM} express CD103 and CD69, do not recirculate, and are self-renewing *in situ*.[19,36] The degree of infiltration of solid tumors by T_{RM} may be a useful indicator of anti-cancer responses, including the success of immune checkpoint inhibition.[36] T_{RM} appear to possess direct cytotoxicity, which is dependent on CD103 interactions.[36] Due to their ability to infiltrate solid tumors and immediate cytotoxicity, T_{RM} hold potential as ideal CAR T cells for the therapy of solid tumors. Furthermore, the ability of anti-PD1 reagents to reverse T_{RM} suppression, points to further control measures that

may be used to enhance to the activity of transferred CAR T cells[36] (see Figures 2 and 3).

Virus-specific T cells represent a convenient source of memory cells in peripheral blood that can be expanded with antigen-presenting cells pulsed with peptide pools, for example, to Epstein–Barr virus or varicella zoster. Repeated stimulation for expansion via the native (virus-specific) TCR was best achieved using CD28 endodomains, demonstrating that the choice of costimulator domains is critical for maintaining CAR T cell proliferation via the endogenous TCR.[9,37] However, 41BB-based CAR gave superior *in vivo* anti-tumor responses, as compared to CD28-based CAR.[37]

Virtual memory T (T_{VM}) cells are memory T cells differentiated from naive T cells via interactions with MHC: self-peptide. This self-recognition upregulates the IL-15-receptor, which in turn provides signals from endogenous IL-15 for memory cell development.[38] Despite their selection by self-recognition, T_{VM} cells do not appear to contribute to pathological autoimmune reactions.[39] T_{VM} make up 15–20% of $CD8^+$ memory cells in a naive murine host and their presence in humans is inferred by the presence of a similar population of $CD45RA^+$/$Eomes^+$/KIR^+/$NKG2A^+$ T cells representing 5% of $CD45RA^+$ T cells in adult blood.[38] Therefore, T_{VM} are likely to have been inadvertently included in CAR transduction protocols, using either unselected or selected memory cell populations. Although their potential role in CAR T cell activity has not been investigated, T_{VM} produce IFN-γ in an infection model and provide a level of protection superior to naive counterparts, but similar to T_{CM}.[39] Despite the potential for auto-reaction from including T_{VM} in CAR T cell product, CAR T cell trials have shown minimal evidence for autoantigen-specific reactions.[1-7] Therefore, T_{VM} remain an attractive subset for further investigation in CAR T cell therapy.

Ex vivo and *in vivo* expansion, and memory cell formation

Because the epigenetic status of memory T cells reflects that of undifferentiated T cells, one of the major challenges is the generation of CAR T memory in the face of the potent *ex vivo* stimuli necessary for optimal CAR T cell transduction and expansion (see Figure 1). In comparison to physiological expansion of antigen reactive lymphocytes, CAR T cells undergo *in vitro* CD3/CD28 stimulation, transduction, further CD3/CD28 stimulation, followed by expansion in recombinant cytokines in the weeks prior to adoptive transfer (Figure 1).[14-28] Given that all T cells present in the *ex vivo* culture preparation will have been triggered via CD3 and CD28, by definition the product lacks strictly "naive" T cells. *In vivo*, naive T

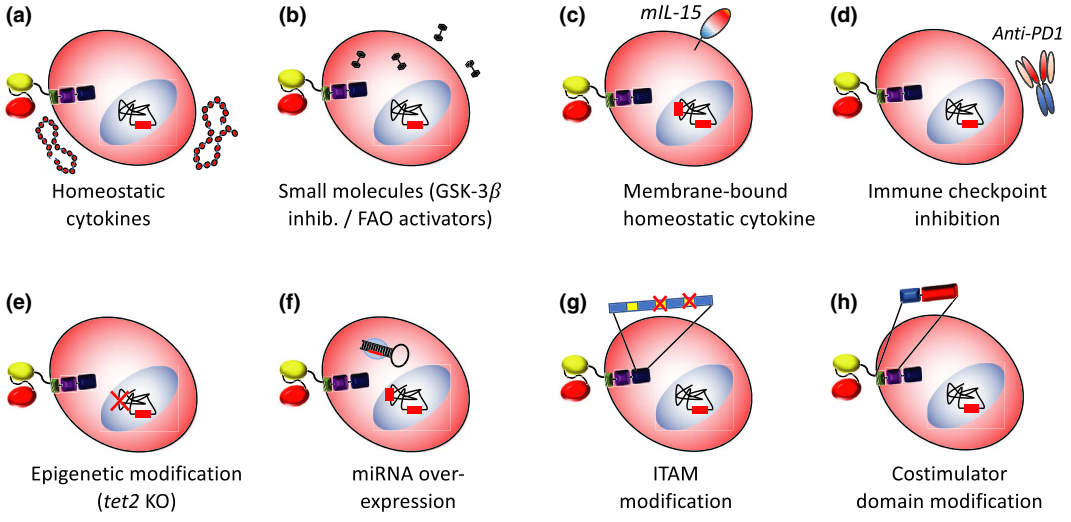

Figure 2. Summary of strategies employed in CAR T cell therapy to enhance persistence and memory cell formation. Strategies to enhance CAR T cell persistence, memory or effector cell activity, as discussed in this review: **(a)** Cytokine stimulation during *ex vivo* CAR T cell generation; **(b)** small molecule inhibitors that activate transcription or metabolic transformation;[50,52,54] **(c)** membrane expression of homeostatic cytokines, for example, mIL-15;[60] **(d)** immune checkpoint blockade (e.g. with anti-PD1 mAb);[15,36,66,67] **(e)** knockout of pro-exhaustion demethylase *tet2*;[64] **(f)** enforced expression of microRNA to enhance persistence and anti-tumor activity, for example, miR-155[61] or miR-143;[62] **(g)** detuning CD3ζ activation by reducing ITAM number;[55] or **(h)** choice of costimulator domain to enhance memory or persistence appropriate to the subtype of cancer.[9] [The color version of this figure can be viewed at www.wileyonlinelibrary.com/journal/icb]

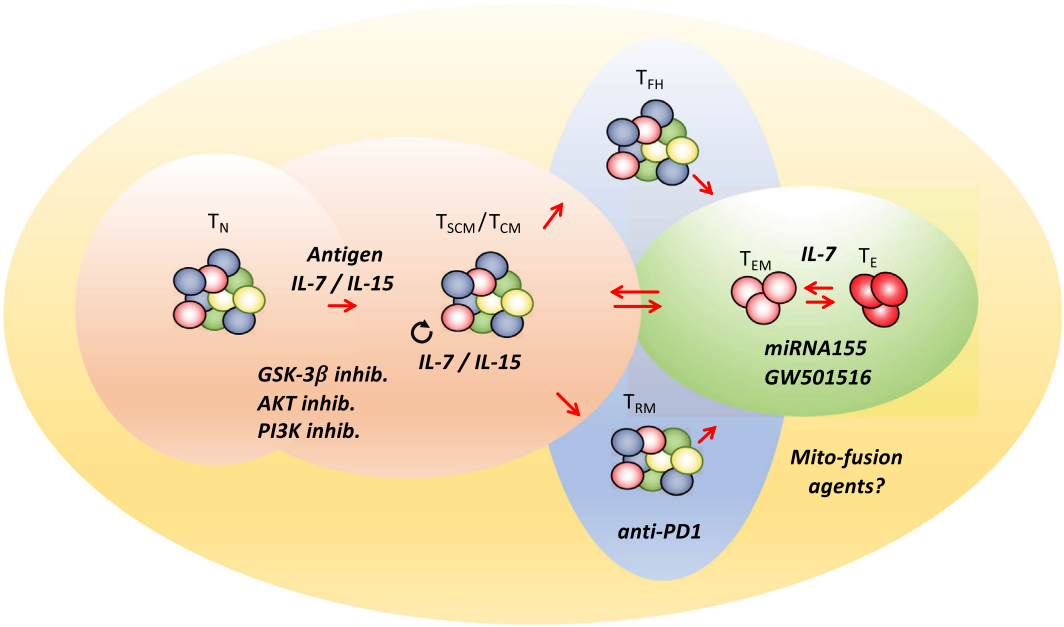

Figure 3. Manipulating persistence and memory cell development at different points of CAR T cell differentiation. Illustration of the approximated points of interactions of different interventions with T cell differentiation state. [The color version of this figure can be viewed at www.wileyonlinelibrary.com/journal/icb]

cells may divide once every 3–6 years;[34] however, a typical CAR T cell stimulation protocol with CD3/CD28 pushes naive cell division to occur every few hours.[40,41] Following CAR transduction and *ex vivo* expansion, only a minor proportion of naive T cells maintain expression of CD27, CCR7, CD62L and CD45RA.[4,40] Memory or effector lineage commitment may occur as early as the first cell division.[32] Therefore, strategies to increase the generation and maintenance of self-renewing memory CAR T cells *ex vivo* must operate in the presence of potent differentiating factors during the *ex vivo* CAR T cell culture. Furthermore, to improve the *in vivo* expansion of adoptively transferred CAR T cells, recipients are preconditioned using chemotherapeutic drugs which destroy host lymphocytes to increase the levels of the homeostatic cytokines IL-7 and IL-15.[19,20] Increased availability of niche and resources to the adoptively transferred CAR T cells allows rapid, lymphopenic expansion of adoptively transferred T cells further driving T cell differentiation to establish pools of effector and memory CAR T cells. Therefore, unlike physiological T cell expansion, CAR T cells expand under the aegis of both lymphopenia and CAR-triggering by tumor antigen (Figure 1).[34] Such expansion is critical to efficacy: the most important predictor of CAR T cell response in lymphoma patients is CAR T cell expansion: responders to treatment were reported to have area under the plasma concentration *versus* time curve from 0 to 28 days that is 5.4 times higher than nonresponders.[42] The abundance of tumor antigen can increase the magnitude of peak expansion,[1] as well as persistence of CAR T cells, therefore antigen availability plays an important role in expanding and maintaining CAR T cell populations.[7]

STRATEGIES TO ENHANCE CAR T CELL PERSISTENCE AND MEMORY

Composition of the blood product

Despite the proven synergistic effects of including antigen-specific CD4 and CD8 in adoptive cell therapy for tumor models,[4] a challenge with treatment of lymphoma patients is the highly variable numbers and ratios of $CD4^+$ and $CD8^+$ T cells, and in the depletion of naive or memory T cell subsets—a situation exacerbated by prior chemotherapy.[4,5,7] For example, B-cell lymphoma patients have an increased percentage of $CD8^+$ T cells and T_{EM} cells, but depressed numbers of naive CD4 and CD8 cells.[4] Normalizing CD4: CD8 ratios, or using defined naive or memory cell subsets, improves engraftment in preclinical models, which may improve clinical outcomes. In particular, co-infusion of naive $CD4^+$ T cells provides optimized help for $CD8^+$ T_{CM} activation, proliferation and cytotoxicity.[4,5,7] It is possible that transfer of defined $CD4^+$ and $CD8^+$ ratios enhances the generation of CAR T cell memory for naive cells; however, this has not been extensively investigated.[4,5,7]

Adoptive transfer of defined CD4 and CD8 ratios undoubtedly shows clear benefits. However, costs and processing time may be increased by the cell selection and *ex vivo* expansion procedures, with an overall lowered CAR T cell product yield due to the extensive cell selection procedures.

The presence of memory cells in unselected populations of CAR T cells can result in a deleterious conversion of naive T cells into a more differentiated state that performs poorly in adoptive therapy.[43] Dubbed a type of "quorum sensing," the conversion mechanism occurs via a non-apoptotic CD95 signaling in responding naive T cells.[43] Therefore, despite the well-researched benefit of including memory T cells in CAR product,[4,8,20,25,33,35] this may negatively impact on the anti-tumor effects of adoptively transferred naive T cells.

In general, naive T cells, or T_{SCM}/T_{CM} cells, induce potent anti-tumor responses in adoptive cell therapy.[5,8,43,44] In a NHL phase I trial, safety was demonstrated using CAR T cells with a memory phenotype generated using IL-2 and IL-15, followed by bead-selection for CD3, CD45RO and CD62L.[45] Although feasible in generating product for infusion for this patient cohort, it is likely that not all lymphoma patients will possess sufficient existing memory subsets for expansion.[5] Moreover, T_{CM} generation *ex vivo* required longer expansion times (24 days), compared with 10–15 days for standard CAR T cell generation from peripherla blood mononuclear cells (PBMC).[45] *In vivo* persistence of CAR T cell product enriched for memory cells was similar to that obtained using standard CAR T cell treatment.[45] In a more recent study, patients with relapsed/refractory B-cell malignancies were treated with CD19.28.ζ CAR T cells. The frequency of $CD8^+$ $CD45RA^+$ $CCR7^+$ T_{SCM}-like CAR T cells, was the only identified factor that correlated with *in vivo* CAR T cell expansion in the first 6 weeks.[44] In additional preclinical studies, Xu *et al.* further showed that IL-7 and IL-15 preferentially increased the frequency of $CD8^+$ CD45 RA^+ $CCR7^+$ CAR T cells with superior *in vivo* anti-tumor responses.[44]

A recent landmark study identified factors associated with CAR T cell responses in B-cell chronic lymphocytic leukemia, where the response rate to CAR T cell therapy is much lower than that of B-cell acute lymphoblastic leukemia. Differences in response rates were not explained by patient and disease characteristics. Instead, the presence of T memory populations with the appropriate gene expression profile impacted significantly on the clinical response. Patients that responded well demonstrated a gene-set signature of IL-6/phosphorylated STAT3 in pre-infusion CAR T cells. CAR T cell product containing higher numbers of memory-like $CD27^+$/$CD45RO^-$/$CD8^+$/$TCF7^+$/$LEF1^+$ T cells was associated with clinical remission.[5]

Metabolism

The transition from quiescent naive T cells to proliferating T_E utilizes the aerobic glycolysis pathway, but entry to the memory pool requires metabolic reprogramming toward fatty acid oxidation. This was first demonstrated by pioneering studies showing that inhibition of the mammalian target of rapamycin (mTOR) pathway and enhancement of fatty acid oxidation induced an increase in the differentiation rate of memory $CD8^+$ T cells.[46-48] The production of metabolically "fit" memory cells appears to be promoted by mitochondrial remodeling, including networks of fused mitochondria, with recent findings showing that CD28 co-stimulation drives that process.[49,50] T_{CM} either synthesize their own fatty acids in order to drive fatty acid oxidation, or in the case of skin T_{RM}, use the more direct pathway of free fatty acid uptake (involving the fatty acid-binding proteins Fabp4 and Fabp5) to satisfy their fatty acid oxidation needs.[32] Pearce and colleagues reported enhanced memory cell formation following treatment of T cells with the mitochondria "fusion promoter" M1 and the "fission inhibitor" Mdivi-1. Moreover, T_E treated with fusion enforcers performed better in adoptive cell therapy (ACT) setting, with superior anti-tumor responses as compared to untreated T cells.[50] Fusion-promoted T_E cells underwent subtle shifts toward a surface memory cell phenotype, and maintained proliferative and cytolytic capacities, with enhanced cytokine production. However, it was not clear whether drug-treated T_E gained additional memory cell function (e.g. self-renewal). Other strategies to boost T cell memory through metabolic shifting include the use of GW501516. GW501516 activates the peroxisome proliferator-activated receptors alpha and delta to boost T cell memory-related fatty acid oxidation. Despite the high expression of T-bet, GW501516-treated cells displayed enhanced persistence *in vivo*, and improved activity in adoptive cell therapy.[51]

Small molecule inhibitors

Activating Wnt signaling arrests the development of effector cell populations and induces self-renewing $CD8^+$ T_{SCM} with enhanced proliferation and better antitumor activity compared to T_{CM} and T_{EM} subsets.[52] While several small molecules identified to date can preferentially arrest T cells at the T_{CM} stage, they can reduce cell yield, putting their widespread use in *in vitro* CAR T cell expansion in doubt.[20] In contrast, inhibition of Akt may promote "memory-naive" phenotype by downregulating perforin and IFN-γ synthesis, and enhancing CD27, IL-6 and IL-7 expression.[53] Recently, an *ex vivo* protocol was optimized for the use of highly selective Akt inhibitors for generation of memory T cells.[54]

Modulating CAR signal strength

Tonic CAR signaling in the absence of antigen-specific stimulation, or hyperstimulation during TAA-recognition could impact on T cell survival and persistence. A recent study carried out a systematic mutation of each of three immunoreceptor tyrosine-based activation motif (ITAMs) of CD3ζ in a CD28-based CAR. T cells possessing only the first (membrane proximal) ITAM displayed superior tumor killing *in vivo* and persistence, compared to the original CD28.CD3ζ CAR. CARs with an intact distal ITAM more efficiently generated a central and effector memory cell phenotype, distal ITAM CARs lacked anti-tumor activity.[55] However, a single distal ITAM increased CAR T cell persistence and the generation of central memory cells. Recently, switchable CAR systems that allow *in vivo* rest and restimulation cycles, were reported to improve CAR T cell memory.[56] Therefore, signal strength tuning of CAR signaling is critical to balance the outcomes of effector and memory cell development.

Cytokine selection

The preferential *in vitro* expansion of memory cells with stem cell like properties can be facilitated using gamma-chain cytokines present during antigen-stimulation of naive $CD8^+$ T cells.[57,58] In addition, pre-formed memory cells undergo homeostatic proliferation in response to IL-7 and IL-15, even in the absence of antigen triggering (see Figure 3).[20] IL-7 and IL-15 increase resistance to AICD and maintain normal lymphocyte migration within secondary lymphoid tissues.[19,20,44] The use of 1L-7 and IL-15 is therefore widespread in CAR T cell protocols that intend to generate, or enrich for T memory cells. Common γ-chain cytokines may appear redundant, but differ in their ability to support persistence and the type of memory cell formation.[19,20] IL-21 was reported to induce the formation of memory cells and improve adoptive cell therapy,[59] but its use in CAR T cell protocols appears less common compared to IL-7/IL-15. Another approach is the expression of membrane IL-15, tethered in the context of the natural IL-15Rα receptor.[60] Dual CAR and membrane-bound IL-15 resulted in increased rates of T_{SCM} generation, superior CAR T cell persistence, with enhanced anti-tumor responses.[60]

micro RNA

Micro RNA (miR) are 20–23-base-pair-long noncoding RNAs involved in RNA silencing and translational regulation of gene expression. The discrete expression of different miRNA subsets in different memory and effector T cell subsets imparts critical control over natural gene sets involved in the broad function of each subset. miR-155 is expressed in T_{EM} and T_E and controls multiple points of protein expression to enhance Th1 and Th17 inflammation.[20,31] An attractive proposition in adoptive cell therapy is the avoidance of preconditioning with lymphodepletion regimes that may cause adverse events, mostly related to toxicity and immunosuppression. However, lymphodepletion reduces competition for endogenous host common γ-chain cytokines required for the proliferation and maintenance of adoptively transferred lymphocytes. Strikingly, the overexpression of miRNA-155 in adoptively transferred T cells produced equivalent anti-tumor responses in both lymphodepleted and nonlymphodepleted recipients. In contrast, control transduced T cells were only effective in lymphodepleted hosts.[61] Enforced miR-155 expression induced cytokine polyfunctionality, persistence and enhanced effector cell activity.[61] Modulation of T cells with miR-155 carried a theoretical risk due to the association of miR-155 with B-cell lymphomas. However, mice engrafted with miR-155-transduced lymphocytes followed for up to >700 days showed no increase in cellular transformation, as compared with control cells.[61] The main pathway of activation was through src homology 2 (SH2) – containing inositol 5-phosphatase (SHIP) inhibition which increased STAT5a activation, T cell persistence, and enhanced T cell activation via Akt. Similarly, overexpression of miR-143 enhanced central memory T cell development, decreased apoptosis and potentiated proinflammatory cytokine secretion and anti-tumor cytotoxicity of HER2-CAR T cells.[62]

Costimulator domains

While inclusion of the CD28 in the CAR structure appeared to generate effector memory cells with an enhanced reliance on glycolysis, 4-1BB-based CARs elaborated T_{CM} with enhanced mitochondrial biogenesis and fatty acid oxidation.[63] The inclusion of the 4-1BB-domain in clinically applied CARs appears to enable long-term T cell persistence.[9] Similarly, inducible T cell costimulator (ICOS) and CD27 costimulator molecules have been reported to enhance the persistence of CAR T cells.[9] ICOS stimulation results in the formation of $CD4^+$ Th17 cells, which may represent a less differentiated form of CD4 with possible multipotency.[20] Th17 expresses high levels of the Tcf7 and β-catenin memory cell markers, and appears to possess multipotency similar to their $CD8^+$ T_{CM} counterparts.[20] Although 4-1BB CAR T cells may persist longer than CD28-based CAR T cells, the long-term response rates in B-cell Non Hodgkin Lymphoma, appear to be similar with both CAR subtypes.[9] Due to space limitations for this section, the reader is referred to our recent review on the impact of CAR costimulator domains on CAR activity.[9]

Epigenetic modification

Exhaustion is a progressive degradation of differentiation potential mediated by epigenetic changes that erode memory and persistence. Because immune checkpoint inhibition does not prevent the suppressive imprinting of exhaustion,[15] cell intrinsic strategies appear to be the most likely way to prevent and reverse exhaustion-related epigenetic changes. The Ten Eleven Translocation (TET2) family of methylcytosine dioxygenases catalyzes DNA methylation through oxidation of 5-methylcytosine to 5-hydroxymethylcytosine—an intermediate step in DNA demethylation. Methylation of DNA can alter the transcription levels of a variety of immune-associated genes, resulting in changes in T cell differentiation and activity. Disruption of the *tet2* gene improves T cell proliferation and memory differentiation.[16,64] In particular, a recent study found that in one CLL patient in remission, CAR T cells had preferentially expanded from a single clone that harbored one allele with an inborn loss of *tet2* function, while the second allele had been mutated by the transgene insertion.[64] The conclusion being that *tet2* mutations not only conferred a cell division survival advantage, but also enabled potent anti-tumor activity.[64] T cell suppression by *tet2* may be explained by a loss of DNA methylation at the PD-1 promotor region.[15]

In contrast to the key role of TET2 in demethylation, DNMT3a is a DNA methylase.[15,16] However, similar to TET2, DNMT3a activity drives T cell suppression and exhaustion, presumably by enabling epigenetic changes at loci distinct from *tet2*.[15,16] *De novo* methylation driven by DNMT3a increases dramatically during late effector cell generation and DNMT3a inhibits T cell lineage plasticity and selectively downregulates the expression of factors, such as TCF7 and CCR7, involved in memory cell formation.[15,16] Therefore, DNMT3a inhibits the differentiation of early effector cells into memory precursor cells.[16] Similar to TET2, reducing DNMTA3a activity during critical events in T cell differentiation offers a promising avenue of research.

Immune checkpoint blockade

Combining CAR T cell therapy with immune checkpoint blockade may be a useful strategy to enhance the persistence and memory cell formation in CAR T therapy. In a study utilizing CAR T cells to treat $Her2^+$ tumors, John *et al.* were able to improve CAR T cell activity by PD-1 blockade, which also decreased the numbers of tumor-associated $Gr1^+/CD11b^+$ myeloid-derived suppressor cells.[64] PD-1-mediated expansion of T cells appear to act on $CXCR5^+/TIM3^-$ T cells, as well as tissue and tumor-resident memory T cells.[36,66] However, it does not appear to reverse exhaustion in majority of T cells.[15,67] It was recently demonstrated that a proportion of supposedly "exhausted" tumor-infiltrating T cells that express TCF1 (see below) preferentially respond to anti-PD1 treatment and could transform into self-renewing memory cells.[26]

Enabling effector cell to memory cell transformation

Data from adoptive cell therapy of six melanoma patients demonstrated that terminally differentiated CD8 effector cells acquire T_{EM}-like phenotypes ($CD28^+$ $CD27^+$ $IL7R\alpha^+$ $CD62L^-$ $CCR7^-$), and that these cells were detected in patient blood for more than 6 months and able to eliminate tumors.[22] This study is in line with the finding that T_E with high-level common-γ-chain receptor expression are possible precursors of memory T cells, with enhanced persistence through Bcl-2 expression.[23,25] In a macaque model, Berger *et al.* were able to show that T_E derived from T_{CM} but not T_{EM} were able to undergo rescue *in vivo* with γ-chain cytokines, particularly IL-15 and form both T_{CM} and T_{EM}.[24,25]

The transformation of T_E to memory T cells occurs via the appearance of a transient population of memory precursor effector cells. These precursors have arrested cell cycle and do not proliferate upon Ag or cytokine exposure.[27] The fully transcriptional network responsible for transition from precursor to mature memory cells is poorly known, but it appears that transcription factors such as TCF-1 and FoxO1 play a crucial role.[26,27,30] Re-entry into the cell cycle activation may be critical for effector cell to memory cell transformation—similar to the model somatic cell reprogramming to induced pluripotent stem cells through enforced expression of oct-4, sox2, klf4 and c-myc.[28] We hypothesize that in effector to memory T cell transition, c-myc activates the cell cycle, which in turn induces DNA replication, reducing repressive heterochromatin conformation (see Figure 4). Memory cell-related transcription factors can then gain access to newly exposed regulatory regions to initiate the necessary transcriptional changes.[29] Thus, T effector cells that express c-myc and IL7Rα or IL15Rα are able to enter cell cycle and acquire a memory phenotype.[21,24,25]

CONCLUSIONS AND FUTURE DIRECTIONS

T cell–mediated immunotherapy requires the establishment of long-term memory, together with the generation of anti-cancer effector cells. Our review has summarized the contribution of expansion, persistence and memory to CAR T cell therapy. Although stem cell-like memory T cells are required to establish immunity in an adoptive cell therapy, downstream effector cell generation is required for cancer cell destruction. Interventions that increase effector cell lifespan and activity may act

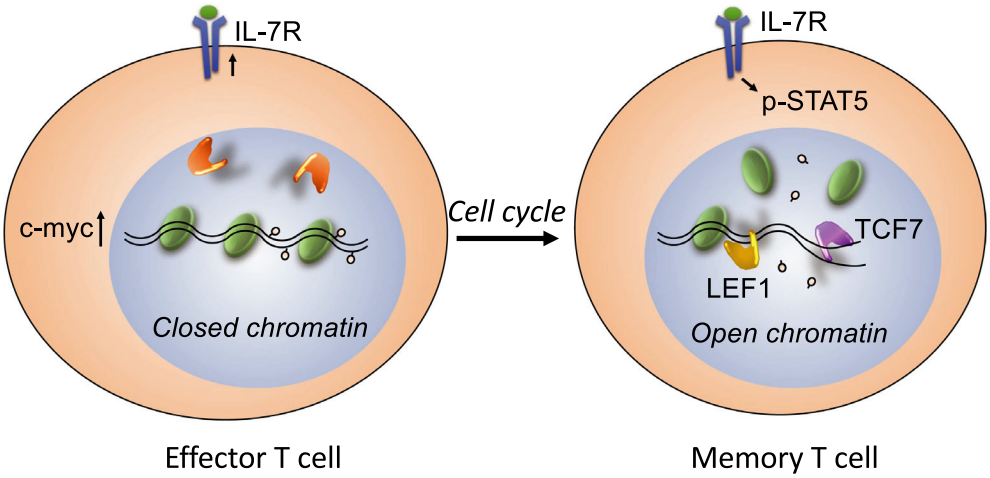

Figure 4. Mechanisms of inducing effector to memory CAR T cell transition. A proportion of T_E cells that express IL7Rα and c-myc are able to re-enter the cell cycle. The onset of DNA synthesis erases epigenetic histone marks (e.g. H3K27me3 and H3K9me3) on the newly synthesised DNA strand, enabling the binding of memory T cell–associated transcription factors (e.g. TCF7 and LEF1) that reprogramme the T cell into more memory cell-like state.[21-23,26,27] [The color version of this figure can be viewed at www.wileyonlinelibrary.com/journal/icb]

independent of memory cell development, yet still enhance anti-tumor activity. Although current efforts are mainly focused on the generation and expansion of memory cells, new knowledge of epigenetic modification opens up the possibility of strategies to enhance effector cell activity and their possible differentiation into true memory cells.

ACKNOWLEDGMENTS

We thank Drs Robert Weinkove and Philip George for critical comments. The authors apologize to scientific colleagues who could not be cited due to reference limitations.

CONFLICT OF INTEREST

None.

REFERENCES

1. Gardner RA, Finney O, Annesley C, *et al.* Intent-to-treat leukemia remission by CD19 CAR T cells of defined formulation and dose in children and young adults. *Blood* 2017; **129**: 3322–3331.
2. Kochenderfer JN, Dudley ME, Feldman SA, *et al.* B-cell depletion and remissions of malignancy along with cytokine-associated toxicity in a clinical trial of anti-CD19 chimeric-antigen-receptor-transduced T cells. *Blood* 2012; **119**: 2709–2720.
3. Turtle CJ, Hanafi LA, Berger C, *et al.* Immunotherapy of non-Hodgkin's lymphoma with a defined ratio of $CD8^+$ and $CD4^+$ CD19-specific chimeric antigen receptor-modified T cells. *Sci Transl Med* 2016; **8**: 355ra116.
4. Sommermeyer D, Hudecek M, Kosasih PL, *et al.* Chimeric antigen receptor-modified T cells derived from defined $CD8^+$ and $CD4^+$ subsets confer superior antitumor reactivity *in vivo*. *Leukemia* 2016; **30**: 492–500.
5. Fraietta JA, Lacey SF, Orlando EJ, *et al.* Determinants of response and resistance to CD19 chimeric antigen receptor (CAR) T cell therapy of chronic lymphocytic leukemia. *Nat Med* 2018; **24**: 563–571.
6. Ritchie DS, Neeson PJ, Khot A, *et al.* Persistence and efficacy of second generation CAR T cell against the LeY antigen in acute myeloid leukemia. *Mol Ther* 2013; **21**: 2122–2129.
7. Turtle CJ, Hanafi LA, Berger C, *et al.* CD19 CAR-T cells of defined $CD4^+$:$CD8^+$ composition in adult B cell ALL patients. *J Clin Invest* 2016; **126**: 2123–2138.
8. Gattinoni L, Klebanoff CA, Palmer DC, *et al.* Acquisition of full effector function *in vitro* paradoxically impairs the *in vivo* antitumor efficacy of adoptively transferred $CD8^+$ T cells. *J Clin Invest* 2005; **115**: 1616–1626.
9. Weinkove R, George P, Dasyam N, McLellan AD. Selecting costimulatory domains for CARs: functional and clinical considerations. *Clin Transl Immunol* 2019; **8**: e1049.
10. Kochenderfer JN, Somerville RPT, Lu T, *et al.* Long-duration complete remissions of diffuse large B cell lymphoma after anti-CD19 chimeric antigen receptor T cell therapy. *Mol Ther* 2017; **25**: 2245–2253.
11. Shah NN, Fry TJ. Mechanisms of resistance to CAR T cell therapy. *Nat Rev Clin Oncol* 2019. https://doi.org/10.1038/s41571-019-0184-6
12. Lim WA, June CH. The principles of engineering immune cells to treat cancer. *Cell* 2017; **168**: 724–740.
13. Wherry EJ, Kurachi M. Molecular and cellular insights into T cell exhaustion. *Nat Rev Immunol* 2015; **15**: 486–499.
14. Kunkele A, Johnson AJ, Rolczynski LS, *et al.* Functional tuning of CARs reveals signaling threshold above which $CD8^+$ CTL antitumor potency is attenuated due to cell Fas-FasL-dependent AICD. *Cancer Immunol Res* 2015; **3**: 368–379.

15. Ghoneim HE, Fan Y, Moustaki A, *et al. De novo* epigenetic programs inhibit PD-1 blockade-mediated T cell rejuvenation. *Cell* 2017; **170**: 142–157.e19.
16. Ladle BH, Li KP, Phillips MJ, *et al. De novo* DNA methylation by DNA methyltransferase 3a controls early effector $CD8^+$ T cell fate decisions following activation. *Proc Natl Acad Sci USA* 2016; **113**: 10631–10636.
17. Marrack P, Scott-Browne J, MacLeod MK. Terminating the immune response. *Immunol Rev* 2010; **236**: 5–10.
18. Rolle CE, Carrio R, Malek TR. Modeling the $CD8^+$ T effector to memory transition in adoptive T cell antitumor immunotherapy. *Cancer Res* 2008; **68**: 2984–2992.
19. Busch DH, Frassle SP, Sommermeyer D, Buchholz VR, Riddell SR. Role of memory T cell subsets for adoptive immunotherapy. *Semin Immunol* 2016; **28**: 28–34.
20. Gattinoni L, Klebanoff CA, Restifo NP. Paths to stemness: building the ultimate antitumour T cell. *Nat Rev Cancer* 2012; **12**: 671–684.
21. Chandran SS, Paria BC, Srivastava AK, Rothermel LD, Stephens DJ, Kammula US. Tumor-specific effector $CD8^+$ T cells that can establish immunological memory in humans after adoptive transfer are marked by expression of IL7 receptor and c-myc. *Cancer Res* 2015; **75**: 3216–3226.
22. Powell DJ, Dudley ME, Robbins PF, Rosenberg SAJB. Transition of late-stage effector T cells to $CD27^+$ $CD28^+$ tumor-reactive effector memory T cells in humans after adoptive cell transfer therapy. *Blood* 2005; **105**: 241–250.
23. Kaech SM, Tan JT, Wherry EJ, Konieczny BT, Surh CD, Ahmed RJ. Selective expression of the interleukin 7 receptor identifies effector CD8 T cells that give rise to long-lived memory cells. *Nat Immunol* 2003; **4**: 1191–1198.
24. Haque M, Song J, Fino K, *et al.* C-Myc regulation by costimulatory signals modulates the generation of $CD8^+$ memory T cells during viral infection. *Open Biol* 2016; **6**: 150208.
25. Berger C, Jensen MC, Lansdorp PM, Gough M, Elliott C, Riddell SR. Adoptive transfer of effector $CD8^+$ T cells derived from central memory cells establishes persistent T cell memory in primates. *J Clin Invest* 2008; **118**: 294–305.
26. Siddiqui I, Schaeuble K, Chennupati V, *et al.* Intratumoral $Tcf1^+PD\text{-}1^+CD8^+$ T cells with stem-like properties promote tumor control in response to vaccination and checkpoint blockade immunotherapy. *Immunity* 2019; **50**: 195–211.
27. Tejera MM, Kim EH, Sullivan JA, Plisch EH, Suresh M. FoxO1 controls effector-to-memory transition and maintenance of functional CD8 T cell memory. *J Immunol* 2013; **191**: 187–199.
28. Saito H, Okita K, Chang AE, Ito F. Adoptive transfer of $CD8^+$ T cells generated from induced pluripotent stem cells triggers regressions of large tumors along with immunological memory. *Cancer Res* 2016; **76**: 3473–3483.
29. Hanna J, Markoulaki S, Schorderet P, *et al.* Direct reprogramming of terminally differentiated mature B lymphocytes to pluripotency. *Cell* 2008; **133**: 250–264.
30. Kratchmarov R, Magun AM, Reiner SL. TCF1 expression marks self-renewing human $CD8^+$ T cells. *Blood Adv* 2018; **2**: 1685–1690.
31. Stelekati E, Chen Z, Manne S, *et al.* Long-term persistence of exhausted CD8 T cells in chronic infection is regulated by MicroRNA-155. *Cell Rep* 2018; **23**: 2142–2156.
32. Jameson SC, Masopust DJI. Understanding subset diversity in T cell memory. *Immunity* 2018; **48**: 214–226.
33. Graef P, Buchholz VR, Stemberger C, *et al.* Serial transfer of single-cell-derived immunocompetence reveals stemness of $CD8^+$ central memory T cells. *Immunity* 2014; **41**: 116–126.
34. van den Broek T, Borghans JAM, van Wijk F. The full spectrum of human naive T cells. *Nat Rev Immunol* 2018; **18**: 363–373.
35. Hinrichs CS, Borman ZA, Gattinoni L, *et al.* Human effector $CD8^+$ T cells derived from naive rather than memory subsets possess superior traits for adoptive immunotherapy. *Blood* 2011; **117**: 808–814.
36. Corgnac S, Boutet M, Kfoury M, Naltet C, Mami-Chouaib F. The emerging role of $CD8^+$ tissue resident memory T (TRM) cells in antitumor immunity: a unique functional contribution of the CD103 integrin. *Front Immunol* 2018; **9**: 1904.
37. Omer B, Castillo PA, Tashiro H, *et al.* Chimeric antigen receptor signaling domains differentially regulate proliferation and native T cell receptor function in virus-specific T cells. *Front Med* 2018; **5**: 343.
38. White JT, Cross EW, Burchill MA, *et al.* Virtual memory T cells develop and mediate bystander protective immunity in an IL-15-dependent manner. *Nat Commun* 2016; **7**: 11291.
39. Drobek A, Moudra A, Mueller D, *et al.* Strong homeostatic TCR signals induce formation of self-tolerant virtual memory CD8 T cells. *EMBO J* 2018; **37**: e98518.
40. Li Y, Kurlander RJ. Comparison of anti-CD3 and anti-CD28-coated beads with soluble anti-CD3 for expanding human T cells: differing impact on CD8 T cell phenotype and responsiveness to restimulation. *J Transl Med* 2010; **8**: 104.
41. Petersen CT, Hassan M, Morris AB, *et al.* Improving T cell expansion and function for adoptive T cell therapy using *ex vivo* treatment with PI3Kδ inhibitors and VIP antagonists. *Blood Adv* 2018; **2**: 210–223.
42. Neelapu SS, Locke FL, Bartlett NL, *et al.* Axicabtagene ciloleucel CAR T cell therapy in refractory large B-cell lymphoma. *N Engl J Med* 2017; **377**: 2531–2544.
43. Klebanoff CA, Scott CD, Leonardi AJ, *et al.* Memory T cell-driven differentiation of naive cells impairs adoptive immunotherapy. *J Clin Invest* 2016; **126**: 318–334.
44. Xu Y, Zhang M, Ramos CA, *et al.* Closely related T-memory stem cells correlate with *in vivo* expansion of CAR.CD19-T cells and are preserved by IL-7 and IL-15. *Blood* 2014; **123**: 3750–3759.
45. Wang X, Popplewell LL, Wagner JR, *et al.* Phase 1 studies of central memory-derived CD19 CAR T cell therapy following autologous HSCT in patients with B-cell NHL. *Blood* 2016; **127**: 2980–2990.
46. Pearce EL, Walsh MC, Cejas PJ, *et al.* Enhancing CD8 T cell memory by modulating fatty acid metabolism. *Nature* 2009; **460**: 103–107.

47. Araki K, Turner AP, Shaffer VO, *et al.* mTOR regulates memory CD8 T cell differentiation. *J Immunol* 2009; **460**: 108.
48. Rao RR, Li Q, Odunsi K, Shrikant PAJI. The mTOR kinase determines effector versus memory $CD8^+$ T cell fate by regulating the expression of transcription factors T-bet and Eomesodermin. *Immunity* 2010; **32**: 67–78.
49. Geltink RIK, O'Sullivan D, Corrado M, *et al.* Mitochondrial priming by CD28. *Cell* 2017; **171**: 385–397.e11.
50. Buck MD, O'Sullivan D, Klein Geltink RI, *et al.* Mitochondrial dynamics controls T cell fate through metabolic programming. *Cell* 2016; **166**: 63–76.
51. Saibil SD, Paul MS, Laister RC, *et al.* Activation of peroxisome proliferator-activated receptors α and δ synergizes with inflammatory signals to enhance adoptive cell therapy. *Cancer Res* 2018; **79**: 445–451.
52. Gattinoni L, Zhong XS, Palmer DC, *et al.* Wnt signaling arrests effector T cell differentiation and generates $CD8^+$ memory stem cells. *Nat Med* 2009; **15**: 808–813.
53. Macintyre AN, Finlay D, Preston G, *et al.* Protein kinase B controls transcriptional programs that direct cytotoxic T cell fate but is dispensable for T cell metabolism. *Immunity* 2011; **34**: 224–236.
54. Mousset CM, Hobo W, Ji Y, *et al. Ex vivo* AKT-inhibition facilitates generation of polyfunctional stem cell memory-like $CD8^+$ T cells for adoptive immunotherapy. *Oncoimmunology* 2018; **7**: e1488565.
55. Feucht J, Sun J, Eyquem J, *et al.* Calibration of CAR activation potential directs alternative T cell fates and therapeutic potency. *Nat Med* 2019; **25**: 82–88.
56. Viaud S, Ma JSY, Hardy IR, et al. Switchable control over in vivo CAR T expansion, B cell depletion, and induction of memory. *Proc Natl Acad Sci USA* 2018; **115**: e10898–e10906.
57. Lugli E, Gattinoni L, Roberto A, *et al.* Identification, isolation and *in vitro* expansion of human and nonhuman primate T stem cell memory cells. *Nat Protoc* 2013; **8**: 33–42.
58. Wolfl M, Greenberg PD. Antigen-specific activation and cytokine-facilitated expansion of naive, human $CD8^+$ T cells. *Nat Protoc* 2014; **9**: 950–966.
59. Singh H, Figliola MJ, Dawson MJ, *et al.* Reprogramming CD19-specific T cells with IL-21 signaling can improve adoptive immunotherapy of B-lineage malignancies. *Cancer Res* 2011; **71**: 3516–3527.
60. Hurton LV, Singh H, Najjar AM, *et al.* Tethered IL-15 augments antitumor activity and promotes a stem-cell memory subset in tumor-specific T cells. *Proc Natl Acad Sci USA* 2016; **113**: E7788–E7797.
61. Ji Y, Wrzesinski C, Yu Z, *et al.* miR-155 augments $CD8^+$ T cell antitumor activity in lymphoreplete hosts by enhancing responsiveness to homeostatic gammac cytokines. *Proc Natl Acad Sci USA* 2015; **112**: 476–481.
62. Zhang T, Zhang Z, Li F, *et al.* miR-143 regulates memory T cell differentiation by reprogramming T cell metabolism. *J Immunol* 2018; **201**: 2165–2175.
63. Kawalekar OU, O'Connor RS, Fraietta JA, *et al.* Distinct signaling of coreceptors regulates specific metabolism pathways and impacts memory development in CAR T cells. *Immunity* 2016; **44**: 380–390.
64. Fraietta JA, Nobles CL, Sammons MA, *et al.* Disruption of TET2 promotes the therapeutic efficacy of CD19-targeted T cells. *Nature* 2018; **558**: 307–312.
65. John LB, Devaud C, Duong CP, *et al.* Anti-PD-1 antibody therapy potently enhances the eradication of established tumors by gene-modified T cells. *Clin Cancer Res* 2013; **19**: 5636–5646.
66. Ribas A, Shin DS, Zaretsky J, *et al.* PD-1 blockade expands intratumoral memory T cells. *Cancer Immunol Res* 2016; **4**: 194–203.
67. Im SJ, Hashimoto M, Gerner MY, *et al.* Defining $CD8^+$ T cells that provide the proliferative burst after PD-1 therapy. *Nature* 2016; **537**: 417–421.

Chapter II

Endogenous upregulation of Mcl-1

The aim of this chapter was to induce the endogenous level of Bcl2-family member Mcl-1 for possible application in CAR T cell therapy. We tested eight small activating RNA (saRNA) targeting different regions of the Mcl-1 promoter. However, none of the overexpressed saRNA were able to induce Mcl-1 above endogenous levels. During this work we identified an uncharacterized lncRNA (LOC107985203) transcribed from the opposite direction of the Mcl-1 promoter. Using gain-of-function and loss-of-function experiments, we verified LOC107985203 lncRNA (named mcl1-AS1) expresses from Mcl-1 promoter and negatively modulates Mcl-1 expression.

Author contributions:

AR and AM wrote the paper and supervised the study. AR performed experimental data in all figures, prepared the tables and performed the bioinformatics analysis. GT and AP contributed to viability and flow cytometry experiments and edited the first draft of manuscript. KH produced the dual reporter pSB-GFP-RFP plasmid backbone.

Gene 762 (2020) 145016

Contents lists available at ScienceDirect

Gene

journal homepage: www.elsevier.com/locate/gene

Research paper

Regulation of human Mcl-1 by a divergently-expressed antisense transcript

S.M. Ali Hosseini Rad*, Grace Min Yi Tan[1], Aarati Poudel[1], Kevin He, Alexander D. McLellan*

Department of Microbiology and Immunology, University of Otago, Dunedin 9010, Otago, New Zealand

ARTICLE INFO

Keywords:
Long non-coding RNA
LOC107985203
Mcl-1
Antisense transcript

ABSTRACT

Mcl-1 is a member of the Bcl-2 anti-apoptotic protein family with important roles in the development, lifespan and metabolism of lymphocytes, as well as oncogenesis. Mcl-1 displays the shortest half-life of all Bcl-2 family members, with miRNA interference and proteasomal degradation being major pathways for Mcl-1 down-regulation. In this study, we have identified a previously undescribed control mechanism active at the RNA level. A divergently transcribed lncRNA LOC107985203 (named here mcl1-AS1) negatively modulated Mcl-1 expression resulting in downregulation of Mcl-1 at both mRNA and protein level in a time-dependent manner. Using reporter assays, we confirmed that the mcl1-AS1 lncRNA promoter was located within Mcl-1 coding region. We next placed mcl1-AS1 under tetracycline-inducible control and demonstrated decreased viability in HEK293 cells upon doxycycline induction. Inhibition of mcl1-AS1 with shRNA reversed drug sensitivity. Bioinformatics surveys predicted direct mcl1-AS1 lncRNA binding to Mcl-1 transcripts, suggesting its mechanism in Mcl-1 expression is at the transcriptional level, consistent with a common role for anti-sense transcripts. The identification of a bi-directional promoter and lncRNA controlling Mcl-1 expression will have implications for controlling Mcl-1 activity in cancer cells, or for the purpose of enhancing the lifespan and quality of anti-cancer T lymphocytes.

1. Introduction

Myeloid cell leukemia factor 1 (Mcl-1) belongs to the Bcl-2 anti-apoptotic family which inhibit apoptosis by binding and interrupting the formation of Bak / Bax dimers on the mitochondrial outer membrane (Thomas et al., 2010). Mcl-1 has tissue specific expression and apart from other Bcl-2 family members has a unique roles in physiological and pathological conditions (Thomas et al., 2010). Mcl-1 deregulation has been reported in both hematological (Gouill et al., 2004) and solid cancers (Fleischer et al., 2006) and its overexpression is associated with chemotherapy resistance (Song et al., 2005). In the immune system, Mcl-1 contributes to T lymphocyte viability, respiration and memory cell formation (Kim et al., 2016; Morciano et al., 2016). Due to the potential importance of control of Mcl-1 to activity and lifespan of chimeric antigen receptor (CAR) T cells, we investigated mechanisms of Mcl-1 control with a view to modulating these for enhanced anti-cancer responses.

Mcl-1 expression in lymphocytes is rapidly induced by T cell receptor signaling and during peak cell expansion (Wensveen et al., 2010; Tripathi et al., 2013). However, Mcl-1 displays the lowest stability of all Bcl-2 family members with a half-life of < 1 h (Liu et al., 2005; Senichkin et al., 2020). Mcl-1 expression is controlled by a number of non-coding RNA (Senichkin et al., 2020). In addition, post-translational control is mediated by caspases and Mcl-1 PEST domains that undergo phosphorylation to induce proteasomal degradation (Senichkin et al., 2019).

lncRNAs are a heterogeneous class of non-coding RNAs (ncRNAs) classified as ≥ 200 bp in length to distinguish them from small ncRNAs (e.g. rRNAs, tRNAs, microRNAs (Mercer et al., 2009). lncRNAs are normally expressed in a time and tissue-specific manner, and display a greater tissue-specificity than mRNAs (Rutenberg-Schoenberg et al., 2016). lncRNAs are implicated in pathological and biological processes such as cancer, development, proliferation and immunity (Chen et al., 2017; Rad et al., 2017; Kopp and Mendell, 2018). For example, lncRNA MALAT1 plays an important role in normal biological and physiological process such as RNA splicing, transcriptional regulation of genes, neural development as well as its oncogenic role in development of various cancers (Zhang et al., 2017).

Abbreviations: Mcl-1, Myeloid cell leukemia factor 1; CAR, Chimeric antigen receptor; ncRNAs, Non-coding RNAs; lncRNAs, Long non-coding RNAs; lincRNAs, Long intergenic noncoding RNAs; AS, Antisense; TSS, Transcription start site; gDNA, Genomic DNA; shRNAs, Short hairpin RNAs; HEK293, Human embryonic kidney 293; TFBS, Transcription factor binding sites; PRC2, Polycomb repressive complex 2; H3K27me3, Histone H3 Lys27 trimethylation; saRNA, Small activating RNA

* Corresponding author.
E-mail addresses: a.hosseini.rad@postgrad.otago.ac.nz (S.M. Ali Hosseini Rad), alex.mclellan@otago.ac.nz (A.D. McLellan).

[1] Grace Min Yi Tan and Aarati Poudel contributed equally to this work.

https://doi.org/10.1016/j.gene.2020.145016
Received 2 April 2020; Received in revised form 21 May 2020; Accepted 30 July 2020
Available online 08 August 2020
0378-1119/

In addition to classification based on function, lncRNAs can also be categorized based on their location in the genome (Laurent et al., 2015). Long intergenic noncoding RNAs (lincRNAs) are expressed from intergenic regions and do not overlap with neighboring coding genes. On the other hand, natural antisense transcripts and intronic lncRNAs are expressed from coding regions (intron or exon). Lastly, antisense (AS) are the result of divergent transcription (Mercer et al., 2009; Atianand et al., 2017). Large portions of lncRNAs are antisense transcripts which usually exert their regulatory function on neighboring genes at different stages of transcription and translation (Su et al., 2010; Magistri et al., 2012). Up to 40% of human coding genes may be regulated by antisense transcripts (Chen et al., 2004; Werner et al., 2009). Antisense transcripts have variety of functions in biological processes, such as development, growth, migration and apoptosis (Lin et al., 2016).

Among the antisense transcripts, the ones derived from promoters of coding-genes are abundant in organisms from bacteria, plant and mammalians (Wei et al., 2011). lncRNAs are often transcribed near the transcription start site (TSS) and appear to be a widespread feature of active promoters (Seila et al., 2008; Sigova et al., 2013). However, the role of most of these antisense transcripts in regulation of their neighboring gene is unknown.

Several microRNAs such as miR-125b (Gong et al., 2013), miR-29 (Mott et al., 2007) and miR-101 (Su et al., 2009) target the Mcl-1 3́ UTR and downregulate its expression at a post-transcriptional level (Senichkin et al., 2020). However, the regulation of Mcl-1 expression by antisense transcripts has not yet been reported.

In the current study, we demonstrate that mcl1-AS1 lncRNA (NCBI Gene ID: 107985203) is expressed from the Mcl-1 proximal promoter and regulates Mcl-1 expression. Quantitative and functional studies showed that mcl1-AS1 negatively regulates Mcl-1 expression at both mRNA and protein levels in a time dependent manner, and impacts upon sensitivity to a chemotherapeutic agent. Using reporter assays, we confirmed that the mcl1-AS1 lncRNA promoter is located within Mcl-1 coding region. Bioinformatics surveys predicted that mcl1-AS1 lncRNA could bind Mcl-1 mRNA, suggesting a mechanism in Mcl-1 control at the transcriptional level, a common feature of most AS (Mercer et al., 2009; Werner et al., 2009; Guil and Esteller, 2012).

2. Experimental procedures

2.1. Cloning and plasmid construction

Mcl1-AS1 lncRNA (574 bp of NCBI reference sequence: XR_001738230.2) were synthesized as a gene block (gBlock, IDT) and cloned into a tetracycline inducible Sleeping beauty plasmid (pSBtet-GP) using asymmetric SfiI restriction sites (Kowarz et al., 2015). For screening of the potential promoter region for mcl1-AS1, fragments of Mcl-1 were amplified from human genomic DNA (gDNA) of PBMCs using primers provided in the supplementary data Table S1. These genomic fragments were cloned into pSB-bi-RFP-luciferase or dual reporter pSB-GFP-RFP plasmids (developed in our laboratory from Kowarz et al. (Kowarz et al., 2015); see Figs. 5 and 6) using NheI and NcoI restriction enzymes.

2.2. Short hairpin RNAs (shRNAs) design and construction

Five shRNAs were designed using three different software: shRNA1 & 2 were designed by Invitrogen Block-iT (https://rnaidesigner.thermofisher.com/rnaiexpress/), shRNA3 & 4 via WI siRNA (http://sirna.wi.mit.edu/) and sh-RNA5 using Sfold software (http://sfold.wadsworth.org/cgi-bin/sirna.pl). All shRNAs were synthesized as sense and antisense oligonucleotides (IDT) with SfiI overhangs, annealed as previously described (Rad et al., 2015) and cloned into Sleeping Beauty-based, tetracycline-inducible vector pSBtet-GP. shRNAs sequences are listed in supplementary data Table S2.

2.3. Genomic DNA and RNA extraction, cDNA synthesis and qPCR

gDNA was extracted using QIAamp DNA Mini Kit (Qiagen) according to the manufacturer's protocol. Total RNA was extracted using NucleoSpin® RNA Plus kit (MACHEREY-NAGEL) and was reverse transcribed to cDNAs by PrimeScript™ RT Reagent Kit (Takara), according to manufactures protocols. Next, 1 μl of cDNA was used as a template in the qPCR reaction with Luna® Universal qPCR Master Mix (NEB). The expression levels of mcl1-AS1 and Mcl-1 (isoform L) were measured by comparative CT ($2^{-\Delta\Delta ct}$) method and normalized to β-actin as a housekeeping gene. Primer sequences are provided in supplementary data Table S1.

2.4. Cell culture and transfection

Human embryonic kidney 293 (HEK293) cells were cultured in Dulbecco's modified eagle's medium (DMEM; Gibco, Auckland, NZ) supplemented with 10% fetal bovine serum (Pan Biotech, Aidenbach, Austria) and Pen-Strep (100 U/ml penicillin and 100 μg/ml streptomycin). Cells were maintained in 5% CO_2 at 37 °C.

For transfection, a total of 2×10^5 HEK293 cells were cultured per well in a 24-well plate and transfected with Sleeping Beauty transfer and transposase plasmids (a ratio of 5:1 SB transfer plasmid to transposase plasmid) using Lipofectamine 3000 following the manufacturer's protocol. After 24 h of transfection, media was replaced with fresh DMEM containing 10% FBS and cells maintained at 37 °C with 5% CO_2. For induction of mcl1-AS1, shRNAs or empty plasmid (control) cells were treated with 5 μg/ ml of doxycycline.

2.5. Western blot

Cells were lysed using RIPA lysis buffer (0.02% azide, 150 mM NaCl, 0.25% CHAPS, 0.5% Triton-X100, 100 mM Tris, pH 8.0 along with freshly added complete protease inhibitor; Roche #11–697-498–001). The total protein in the cell lysate was determined by Pierce™ BCA Protein Assay Kit (Thermo Fisher). A total of 20 μg of the protein was separated by Bolt 4–12% Bis-Tris Plus gels (Invitrogen) and transferred onto Nitrocellulose membranes (Protran, Amersham, Auckland, NZ). Membranes were blocked with 0.5% sodium caseinate (Arotech, Wellington, NZ) / PBS (Sigma) and was probed with rabbit anti-Mcl-1 antibody (Abcam # ab28147) at 1:1000 dilution as primary antibody and donkey anti-rabbit IgG DyLight 800 (SA5-10044) in 1:10000 dilution was used as secondary antibody. Mouse monoclonal β-actin at a concentration of 0.5 mg/ml was used as a primary antibody (Sigma-Aldrich #A2228) and Goat anti-mouse IgG DyLight 680 (Thermofisher #A3274) was used as secondary antibody. The membrane was scanned using an Odyssey Fc Imaging System (LI-COR Biosciences, Germany) and was analyzed using Image Studio Lite software.

2.6. Resazurin assay

Cell viability was measured by resazurin assay (Sigma-Aldrich). Briefly, cells were incubated with resazurin 1/10 diluted stock and incubated for 4 h at 37 °C. Supernatants (100 μl) were transferred to a black 96-well plate and fluorescence measured using a Varioskan™ LUX multimode microplate (Thermo Fisher).

2.7. Bioinformatics analysis

All the software used in this study for structure prediction, position in genome, alignments, RNA/RNA and TF binding prediction are listed in Table 1.

Table 1
Name, application and URL of bioinformatics software used in this study.

Name	*Application*	*URL*
NCBI Gene	Position, sequence and gene expression	https://www.ncbi.nlm.nih.gov/gene
UCSC genome Browser	Position, sequence and histone mark	https://genome.ucsc.edu/
DBTSS	TSS prediction and histone mark	https://dbtss.hgc.jp/
LNCpedia version 5.2	Position, sequence and structure	https://lncipedia.org/
YAPP	Promoter's element characterization	http://www.bioinformatics.org/yapp/cgi-bin/yapp.cgi
PROMO	TF binding site prediction	http://alggen.lsi.upc.es/cgi-bin/promo_v3/promo/promoinit.cgi?dirDB=TF_8.3
AliBaba2.1	TF binding site prediction	http://gene-regulation.com/pub/programs/alibaba2/
Geneious Prime®	Primer design, ClustalW sequence alignment	https://www.geneious.com/academic/
RNAfold	Secondary structure prediction	http://rna.tbi.univie.ac.at/cgi-bin/RNAWebSuite/RNAfold.cgi
RNAalifold	Structure alignment	http://rna.tbi.univie.ac.at/cgi-bin/RNAWebSuite/RNAalifold.cgi
LocARNA	Sequence-structure-based alignment	http://rna.informatik.uni-freiburg.de/LocARNA/Input.jsp
IntaRNA	RNA/RNA interaction prediction	http://rna.informatik.uni-freiburg.de/IntaRNA/Input.jsp
RNAup	RNA/RNA interaction prediction	http://rna.tbi.univie.ac.at//cgi-bin/RNAWebSuite/RNAup.cgi

2.8. Statistical analysis

All experiments were carried out at least three times, presented as mean ± standard deviation (SD) and analyzed by student T test and ANOVA test with Bonferroni post-test correction. The P values of ≤ 0.05 were considered statistically significant. (* $P < 0.05$, ** $P < 0.01$, *** $P < 0.001$, **** $P < 0.0001$)

3. Results

3.1. Characterization of mcl1-AS1 lncRNA and Mcl-1 genes

Mcl-1 is located on chromosome 1 between two lncRNAs expressed from its upstream (mcl1-AS1 lncRNA) and downstream (lnc-MCL1-2) regions (Fig. 1). The proximal promoter of Mcl-1 has binding sites for transcription factors, including STAT5, SRE, Ets, SP1, CRE-BP and NF-ƙB (Akgul et al., 2000). The Mcl-1 TSS is either located 80 bp upstream of the ATG translation initiation codon (ACTTC) (Akgul et al., 2000), or according to the DBTSS, is at position 150579738 (GCGCAA) (Fig. 1). At around exon 1 and 2, Mcl-1 gene shows enrichment for promoter marks such as H3K4me3, H3K27Ac and DNase I hypersensitivity, suggesting that mcl1-AS1 lncRNA promoter is located in the intragenic site of the Mcl-1 open reading frame (ORF) (Supplementary Figure S1 & 2).

Mcl1-AS1 lncRNA is expressed from a primary transcript encompassing two fused exons to create a 574 bp transcript (joining positions 1…404 and 24305…24474, NCBI Gene ID: 107985203). RNAseq data from normal tissue shows that mcl1-AS1 lncRNA is expressed in most tissues at low levels, with a higher level of expression in skin cells (Supplementary Figure S3).

3.2. mcl1-AS1 lncRNA regulates Mcl-1 expression at both mRNA and protein level

Firstly, a gain-of-function study was carried out to see the effect of mcl1-AS1 lncRNA up-expression on endogenous expression of Mcl-1. A doxycycline inducible sleeping beauty system was used in this study so that the expression of mcl1-AS1 lncRNA could be controlled accordingly. The expression level of mcl1-AS1 lncRNA upon treatment with 5 μg/ml of doxycycline was measured by qPCR to ensure inducible expression of mcl1-AS1 lncRNA (Fig. 2A). lncRNAs are involved in regulation of gene expression both at mRNA and protein level by binding to either transcriptional or mRNA maturation machinery. To assess the effect of mcl1-AS1 overexpression on Mcl-1 at protein level western blotting was performed on HEK293 cells at 24 to 72 h after mcl1-AS1 lncRNA induction by doxycycline. Induction of mcl1-AS1 did not alter Mcl-1 level at 24 and 48 h, but Mcl-1 levels were significantly downregulated at 72 h post-induction (Fig. 2 B&C). Similarly, mcl1-AS1 overexpression led to a decrease in Mcl-1 mRNA levels (Fig. 2 F), confirming negative regulation of mcl1-AS1 lncRNA of Mcl-1 expression at both mRNA and protein level.

Next, five shRNAs targeting different regions of mcl1-AS1 lncRNA were tested (Fig. 2D). To study the effect of mcl1-AS1 downregulation on endogenous Mcl-1 by shRNA, Mcl-1 expression was measured at both mRNA and protein levels following 72 h doxycycline induction of

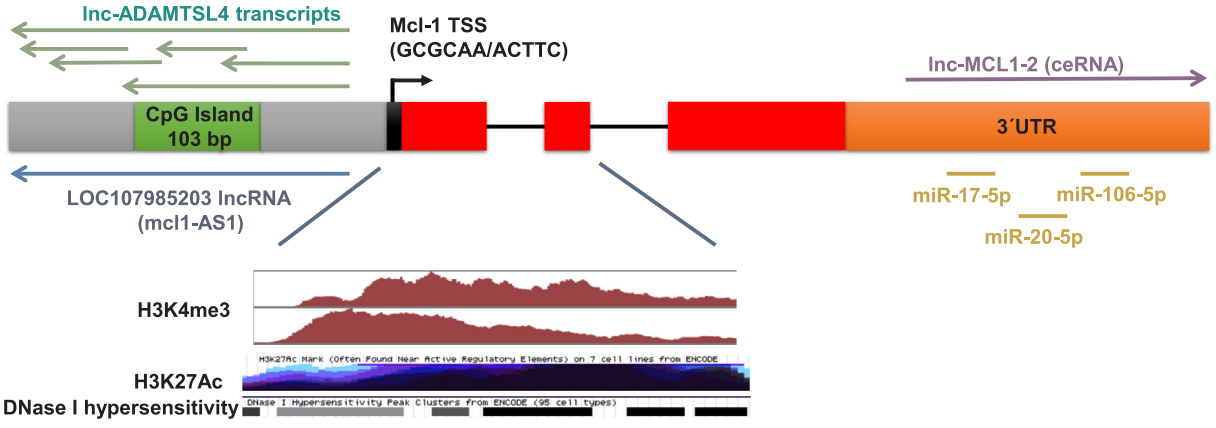

Fig. 1. Characterization of human Mcl-1 gene. Mcl-1 is located in chromosome 1 and has three exons (red boxes). The Mcl-1 proximal promoter contains a 103 bp CpG island. Two lncRNAs are driven from Mcl-1 gene. Mcl1-AS1 lncRNA is expressed from proximal promoter of Mcl-1 (classified as an 'anti-sense promoter') and lnc-MCL1-2 is expressed from the Mcl-1 3′ UTR and acts as ceRNA. Recently, lnc-ADAMTSL4 family which comprises 13 uncharacterized lncRNAs that may overlap the Mcl-1 promoter and enhancer. The first exon / intron of Mcl-1 shows enrichment for promoters marks such as H3K4me3, H3K27Ac and DNase I hypersensitivity according to DBTSS and UCSC databases. For more details please see Supplementary Figure S1 & 2. (For interpretation of the references to color in this figure legend, the reader is referred to the web version of this article.)

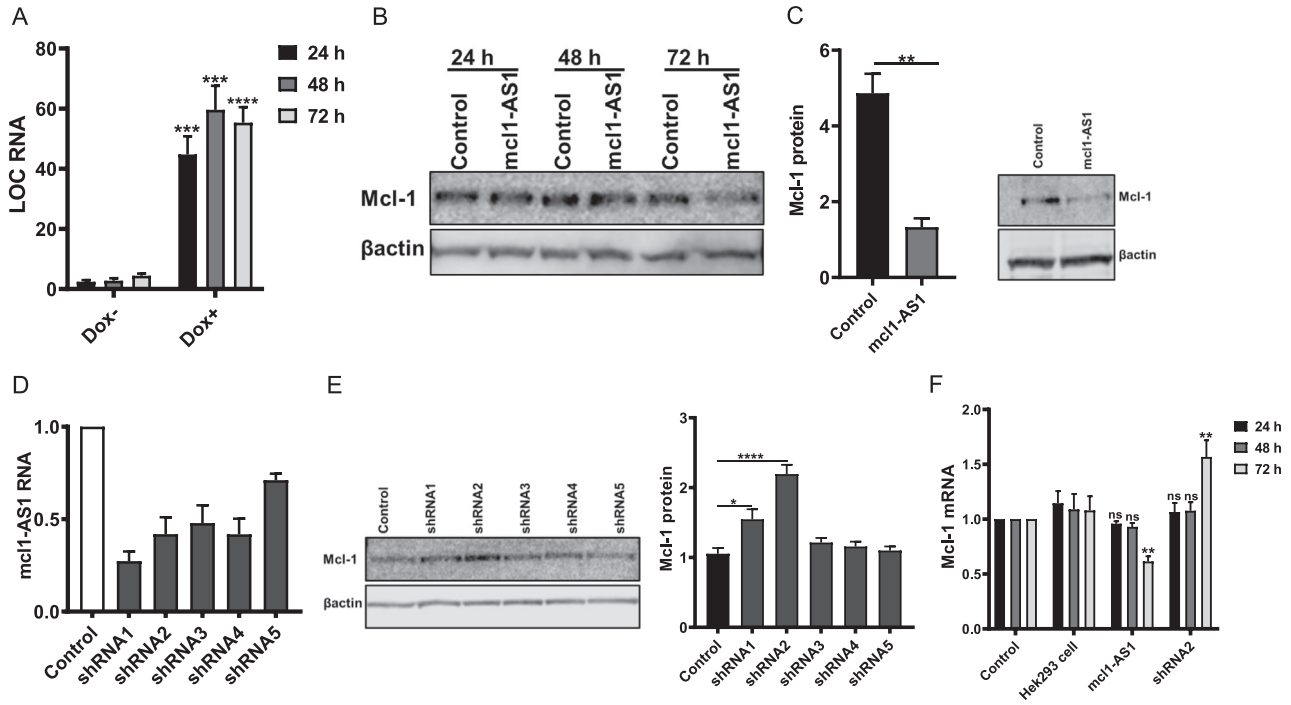

Fig. 2. Overexpression and knockdown of mcl1-AS1 lncRNA alter Mcl-1 expression. (A) Overexpression of mcl1-AS1 lncRNA in Tet-On SB system. Doxycycline (5 μg / ml) was added to induce mcl1-AS1 lncRNA. (B and C) Western blot of enforced expression of mcl1-AS1 lncRNA resulting in downregulation of Mcl-1 72 h post-induction. (D) The ability of synthetic shRNAs to inhibit mcl1-AS1 expression, as determined by qPCR assay. (E) Western blot analysis of Mcl-1 expression 72 h after transfection of HEK293 cells with shRNAs against mcl1-AS1. (F) Mcl-1 expression level quantified by qPCR, after upregulation or downregulation of mcl1-AS1 lncRNA. shRNA2 was used in qPCR experiment as it showed the most powerful shRNA. Control in all experiments is HEK293 cells transfected with empty plasmid and treated with 5 μg / ml of doxycycline.

shRNA expression. As shown in Fig. 2 E & F, downregulation of mcl1-AS1 lncRNA resulted in upregulation of endogenous Mcl-1 expression at 72 h. These results confirm that the overexpression of mcl1-AS1 lncRNA downregulates Mcl-1. To rule out that doxycycline was affecting mcl1-AS1 expression we tested the effect of 5 μg/ml of doxycycline on lncRNA expression, but observed no major perturbation in the expression of mcl1-AS1 (Supplementary Figure S4).

3.3. Regulation of Mcl-1 through mcl1-AS1 lncRNA affect cell viability of HEK293 cells

Mcl-1 is an anti-apoptotic protein that impacts on cell viability by modulating mitochondria function, particularly through its ability to stabilise membrane potential by interfering with Bak/ Bax- mediated pore formation in the mitochondrial outer membrane (Morciano et al., 2016). Previous studies have shown that downregulation of Mcl-1 by microRNAs, such as miR-101 and miR-193b sensitized cancer cells to doxorubicin, emphasizing on the role of Mcl-1 in cell survival (Long et al., 2015; He et al., 2016). HEK293 cells transfected with mcl1-AS1 or sh-mcl1-AS1s were treated with 10 μg/ml of doxorubicin, equivalent to the IC50 (Supplementary Figure S5). As shown in Fig. 3, altering Mcl-1 levels, by either overexpression or downregulation of mcl1-AS1 lncRNA, affects cellular sensitivity to doxorubicin.

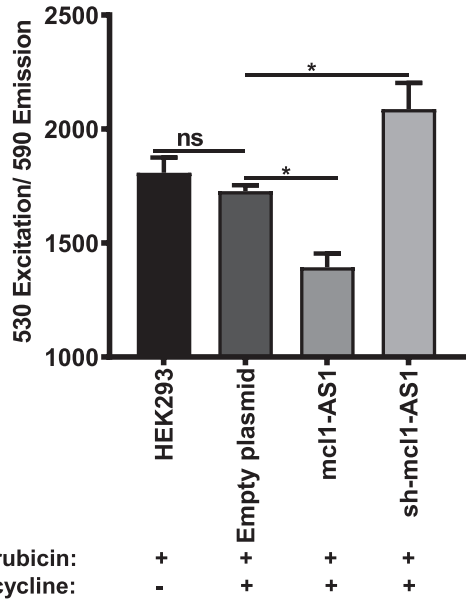

Fig. 3. Modulation of endogenous level of Mcl-1 through mcl1-AS1 lncRNA alters the sensitivity of HEK293 cells to doxorubicin. HEK293 cells were induced with 5 μg / ml of doxycycline to enhance (Tet-On-expressed mcl1-AS1) or downregulate (Tet-On expressed mcl1-AS1 shRNA-2) mcl1-AS1 lncRNA expression. HEK293 was treated with 10 μg / ml of doxorubicin at 48 h, and cell viability measured using resazurin assay at 72 h post doxycycline induction (see also Fig. S4).

3.4. Identification and characterization of mcl1-AS1 lncRNA promoter

Since the mcl1-AS1 lncRNA is complementary to the Mcl-1 proximal promoter, its promoter is likely present within the Mcl-1 coding region. As discussed above, exon 1 to exon 2 of Mcl-1 shows enrichment for promoter marks (Fig. 1). To confirm the activity of the predicted mcl1-AS1 promoter the Mcl-1 proximal to the second intron of Mcl-1 or fragments thereof, were cloned upstream of luciferase according to their orientation in the genome to determine if they act as a promoter for mcl1-AS1 or Mcl1 (Fig. 4 A). Both the Mcl-1 proximal promoter and the exon1-intron1 fragment showed promoter activity in inducing the luciferase gene 2-fold ($P < 0.0001$; Fig. 4B).

To further validate the exon1-intron1 as mcl1-AS1 lncRNA

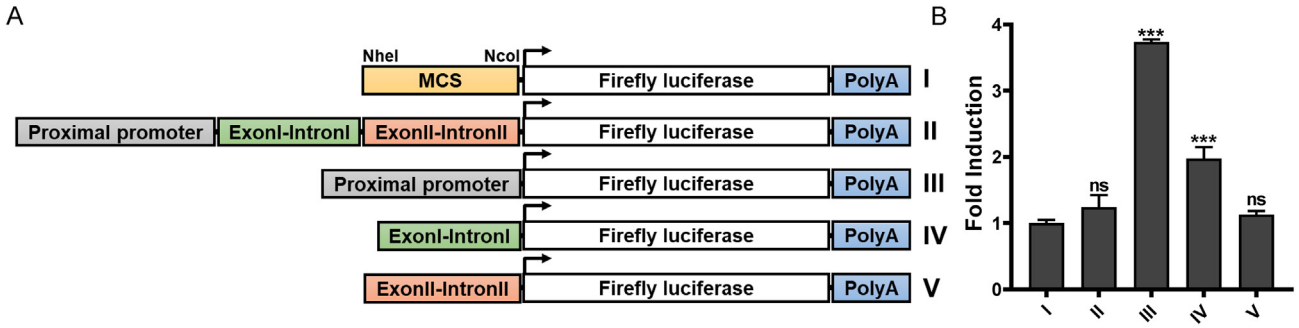

Fig. 4. Identification of the potential promoter region for mcl1-AS1 lncRNA within Mcl-1 coding regions. (A) Schematic illustration of the luciferase reporter constructs used to investigate the promoter activity of different regions of Mcl-1 gene. The luciferase plasmids lack the minimal promoter to reduce background expression. (B) Luciferase assay for HEK293 cells transfected with reporter plasmids carrying different Mcl-1 regions.

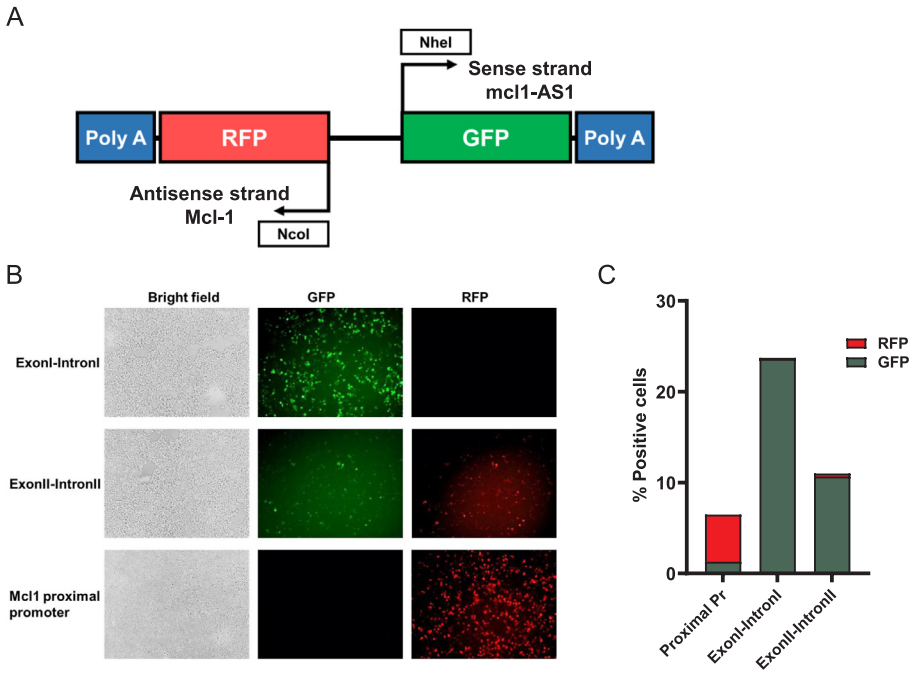

Fig. 5. Verification of mcl1-AS1 lncRNA promoter using a dual-reporter system. (A) Schematic illustration of the dual-reporter promoter for determining the promoter orientation relative to its position in the genome. Mcl-1 expresses from anti-sense strand while mcl1-AS1 lncRNA expresses from sense strand. Transcription from the antisense strand will result in RFP expression, while sense transcription results in GFP expression. (B) Fluorescent microscopy and (C) flow cytometric analysis of HEK293 cells transfected with dual-reporter plasmids carrying different region of Mcl-1 gene. Induction of GFP with the first exon-intron region verifies this sequence as the mcl1-AS1 lncRNA promoter in the sense orientation.

promoter, this region was cloned into a SB-based dual-reporter plasmid (Fig. 5 A). This dual reporter allowed us to determine the promoter direction according to its orientation in the genome. Therefore, if the region has promoter activity for the sense strand in the genome, GFP should be expressed and if activity is directed to the anti-sense strand RFP will be expressed. As Fig. 5B & C show, the proximal promoter of Mcl-1, located in the antisense strand, expressed RFP. The exon1-intron1 fragment drove GFP expressing, confirming this region as mcl1-AS1 lncRNA promoter. Weaker expression of GFP by the second exon and intron could be explained by the fact that this region is either an enhancer, or an upstream promoter element, resulting in only weak reporter expression, rather than acting as a core promoter.

To further characterize the mcl1-AS1 lncRNA promoter, we utilized bioinformatics tools to identify transcription factor binding sites (TFBS) and core promoter elements (Fig. 6). UCSC genome browser and PROMO software predicted enrichment for TFs such as STAT, C/EBP, NF-κB, Sp1 and Ets within the first exon and intron, similar to those binding the Mcl-1 promoter (Akgul et al., 2000). The mcl1-AS1 lncRNA core promoter contains a TATA box motif, similar to the one has been reported for Mcl-1 gene (Tullai et al., 2007).

3.5. *mcl1-AS1 lncRNA is similar to one of the members of the lnc-ADAMTSL4 lncRNAs family*

LNCipedia browser includes a new class of lncRNAs, lnc-ADAMTSL4, that vary in length (from 213 bp to 12066 bp) and are expressed from the Mcl-1 regulatory region (Supplementary Table S3 & 4). This family contains 13 uncharacterized lncRNAs. ClustalW alignment of mcl1-AS1 lncRNA against lnc-ADAMTSL4 family revealed mcl1-AS1 lncRNA is 100% similar to lnc-ADAMTSL4-5:1 (Table 2). Furthermore, structure based and sequence–structure-based alignments confirmed high similarity between mcl1-AS1 lncRNA and ADAMTSL4-5:1 (Fig. 7 A & B). In fact, ADAMTSL4-5:1 (418 bp) is shorter version of mcl1-AS1 lncRNA (574 bp) by 156 bps, suggesting that either both transcripts are same transcript with small differences in length (due to different sources of RNA-seq data) or mcl1-AS1 lncRNA is a new member of this family. Further information about the ADAMTSL4 family is provided in Supplementary Table S3 & 4.

3.6. *mcl1-AS1 lncRNA is predicted to bind to Mcl-1 mRNA*

lncRNAs can regulate genes at the transcriptional level by directly binding to the regulatory regions of gene, TFs, chromatin remodeling proteins and transcriptional machinery (Magistri et al., 2012; Zhang et al., 2017). At post-transcriptional level, they can bind to various RNA

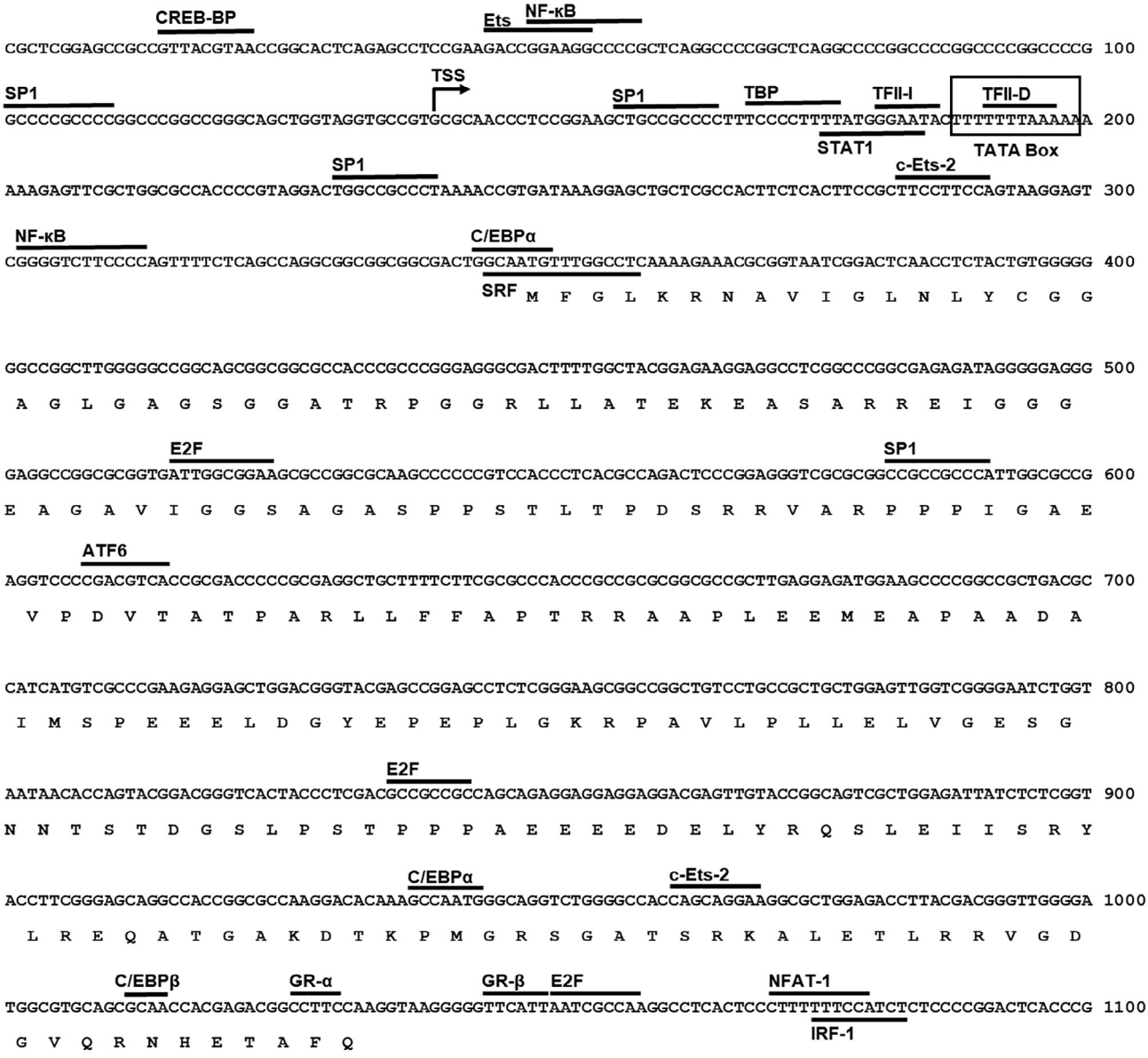

Fig. 6. Prediction of TF-binding sites within the mcl1-AS1 lncRNA promoter. TF binding sites were predicted using PROMO and AliBaba2.1 (both using different versions of the TRANSFAC database). The TATA box was predicted using YAPP software.

Table 2
ClustalW alignment of mcl1-AS1 lncRNA versus lnc-ADAMTSL4 family members.

Names	*% Pairwise Identity*
mcl1-AS1 vs lnc-ADAMTSL4-1:1	40.4%
mcl1-AS1 vs lnc-ADAMTSL4-1:2	40.5%
mcl1-AS1 vs lnc-ADAMTSL4-2:1	43.1%
mcl1-AS1 vs lnc-ADAMTSL4-4:1	42.1%
mcl1-AS1 lnc-ADAMTSL4-5:1	100%
mcl1-AS1 vs lnc-ADAMTSL4-6:1	40%
mcl1-AS1 A vs lnc-ADAMTSL4-7:1	43%
mcl1-AS1 vs lnc-ADAMTSL4-7:3	41.3%
mcl1-AS1 vs lnc-ADAMTSL4-7:4	43%
mcl1-AS1 vs lnc-ADAMTSL4-7:5	43%
mcl1-AS1 vs lnc-ADAMTSL4-7:6	43%
mcl1-AS1 vs lnc-ADAMTSL4-7:7	43%
mcl1-AS1 vs lnc-ADAMTSL4-7:8	48.5%

binding proteins or mRNA causing changes in stability, polyadenylation, splicing, exportation and subcellular localization of the mRNA (He et al., 2019). We looked for a possible direct interaction between mcl1-AS1 and Mcl-1 mRNA using two different software. IntaRNA predicted the interaction between mcl1-AS1 has different nucleotides ranged at position 114–176 that could bind to the Mcl-1 mRNA nucleotides from 613 to 682 (Fig. 8A). Furthermore, RNAup software predicted direct interactions of Mcl-1 and mcl1-AS1 at different positions compared to those predicted by IntaRNA (Fig. 8B). Secondary structure of mcl1-AS1 lncRNA predicted by RNAfold is shown in Fig. 8C (see also Fig. 9).

4. Discussion

This study has identified the regulation of Mcl-1 expression (expressed on the conventional anti-sense strand) by a divergent lncRNA expressed from the (conventional sense strand) Mcl-1 promoter (see Fig. 9). Activity of the mcl1-AS1 core promoter was demonstrated using reporter genes. Inducible overexpression of the mcl1-AS1 lncRNA decreased the abundance of endogenous Mcl-1 transcripts, confirming a

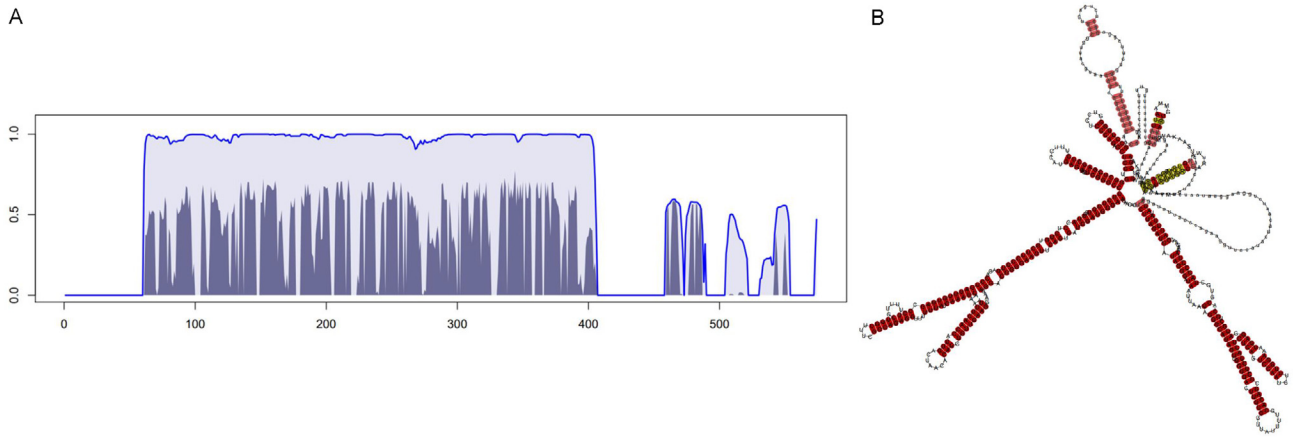

Fig. 7. Sequence-structure alignment between mcl1-AS1 lncRNA and lnc-ADAMTSL4-5:1: (A) Visualization of the local sequence–structure-based alignment reliability (STAR) between mcl1-AS1 lncRNA and lnc-ADAMTSL4-5:1 using LocARNA-P Reliability Profile (STAR Profile Plot). The profile consists of the reliabilities for each single alignment column. The dark regions indicate structure reliability, the light regions represent sequence reliability, and the thin line shows the combined column-reliability. The column-wise reliabilities are computed as sum-of-pairs over match probabilities, which are computed by LocARNA-P. (B) The consensus structure of the alignment, as predicted by RNAalifold, is shown in a 2D layout. Base pairs use the same color code as in "Colour and structure annotated alignment". The hue demonstrates sequence conservation, while saturation shows structural conservation. If gaps are present, lower case letters are used.

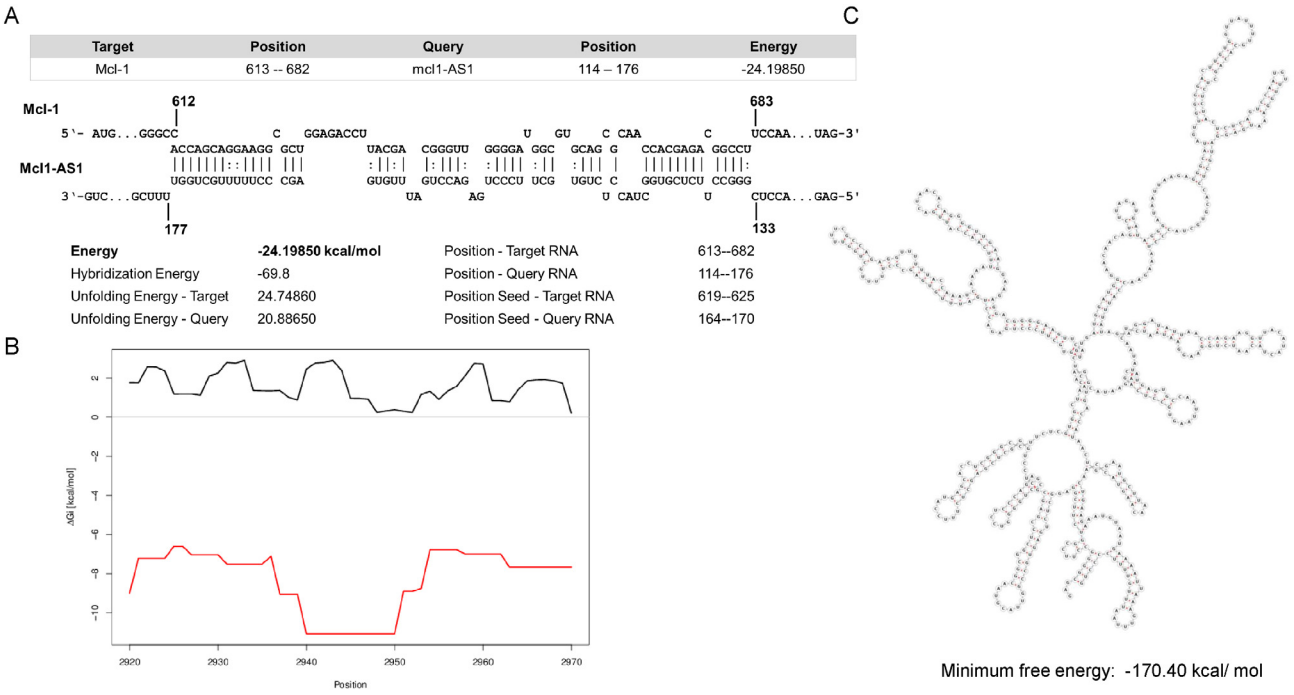

Fig. 8. Possible interaction between mcl1-AS1 lncRNA and Mcl-1 mRNA. (A) Possible interaction between mcl1-AS1 lncRNA and Mcl-1 mRNA at nucleotide position 114–176 of mcl1-AS1 with 613–682 nucleotides of Mcl-1 mRNA predicted by IntaRNA software. (B) Interaction at nucleotide mcl1-AS1 RNA (1492–502) with Mcl-1 mRNA (2940–2950), as predicted by RNAup software (C) Prediction of mcl1-AS1 secondary structure using RNAfold program.

functional interaction between these RNA species. Conversely, shRNA mediated knock-down of endogenous mcl1-AS1 led to a detectable increase in Mcl-1.

Mcl-1 expression in lymphocytes is rapidly induced by triggering T cell receptor signaling 24 h after activation with CD3 and CD28 antibodies followed by rapid downregulation 48 and 72 h after activation (Wensveen et al., 2010; Tripathi et al., 2013). Consistent with these findings, Mcl-1 and mcl1-AS1 RNA showed divergent expression in primary T cells upon CD3 and CD28 stimulation (Supplementary Figure S6).

It is not at this stage clear how mcl1-AS1 lncRNA influences Mcl-1 expression. Direct interaction of mcl1-AS1 with Mcl-1 mRNA was predicted with some certainty using a bioinformatics approach. It is possible that such an interaction could lead to transcriptional stalling, mRNA degradation or interference with the nuclear export of spliced Mcl-1 mRNA (Kopp and Mendell, 2018; He et al., 2019). Processing and export of mcl1-AS1 or fragments thereof, could theoretically impact upon protein translation in the cytoplasm. Another possibility is that mcl1-AS1 lncRNA is expressed from the Mcl-1 promoter and through its complementarity to Mcl-1 proximal promoter, mcl1-AS1 lncRNA interacts with the Mcl-1 regulatory region to interrupt Mcl-1 transcription, or to induce alternate splicing to pro-apoptotic Mcl-1S. Like most lncRNAs, mcl1-AS1 is predicted to form a stem-loop structure which could bind Suz12, a core component of the polycomb repressive complex 2 (PRC2). Such an RNA stem-loop sequence at the 5′ end of genes might allow histone H3 Lys27 trimethylation (H3K27me3) to inhibit

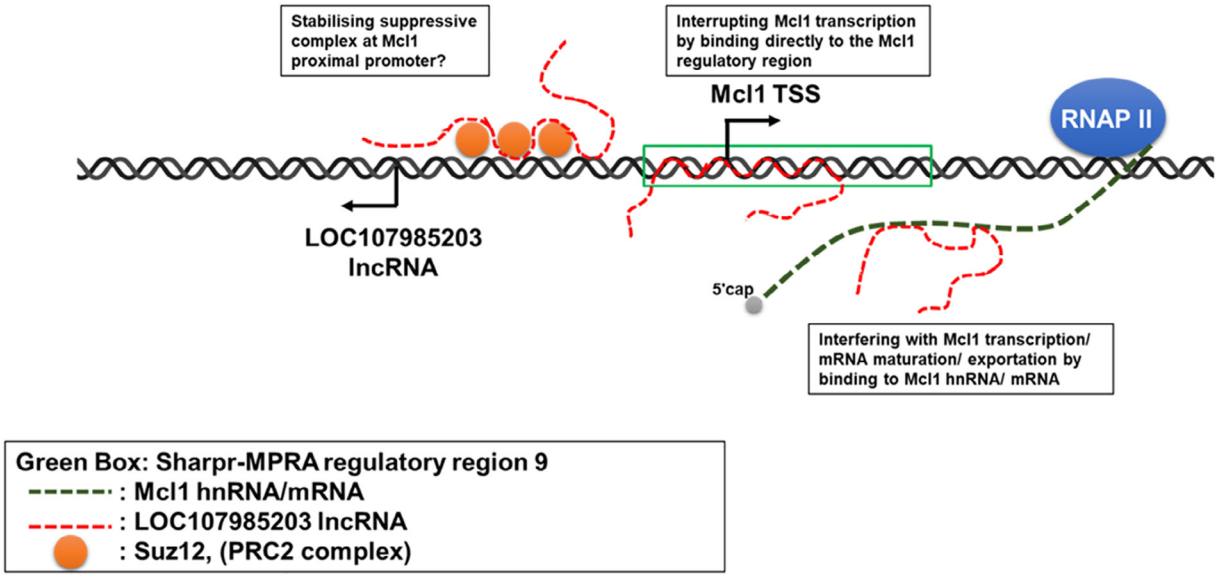

Fig. 9. Possible mechanisms for mcl1-AS1 lncRNA negative regulation of Mcl-1 expression. Direct interaction of mcl-AS1 lncRNA with Mcl-1 mRNA was predicted by two different bioinformatic tools as shown. The interaction could result in interference of mcl1-AS1 with Mcl-1 mRNA maturation and exportation. In addition, since mcl1-AS1 is complementary to the Mcl-1 promoter it is possible it directly interacts with the Mcl-1 regulatory region to interrupts transcription. LncRNAs with stem-loop structures have been shown to recruit the repressory complexes at regulatory regions of genes to suppress their expression.

transcription (Guil and Esteller, 2012; Senichkin et al., 2020).

One possibility to modulate the influence of AS is the use of small activating RNA (saRNA) that target promoter regions. These typically bind to CpG islands to upregulate gene expression. Interestingly, saRNA are slow to act compared to siRNA or miRNA, with maximal effects on gene expression observed at 72 h (Li et al., 2006), similar to our observed kinetics of shRNA-mediated relief of Mcl-1 inhibition by mcl1-AS1. Although theoretically designed to bind to promoter regions, saRNA have the potential to bind to AS transcripts expressed divergently from gene promoters (Portnoy et al., 2011). Not surprisingly, when we attempted to regulate Mcl-1 expression using a series of eight saRNA targeted to the upstream Mcl-1 promoter region, these failed to upregulate Mcl-1 gene expression (Supplementary Figure S7). Induction of endogenous Mcl-1 expression may require 'shRNA' to directly bind the AS transcripts and therefore effectively act as 'saRNA'.

Next generation RNA-sequencing data provided by projects such as ENCODE (https://www.encodeproject.org/) and FANTOM5 (http://fantom.gsc.riken.jp/5/) have led to the identification of thousands of ncRNAs. For instance, the ENCODE release (version 25) revealed that coding regions only account for ~2% of human genome, while ~75–90% of human genome is transcribed to ncRNAs, with an estimation of 80% of them being functional in at least one cell type (Laurent et al., 2015; Atianand et al., 2017). Furthermore, the FANTOM5 project led to identification of 20,000 new lncRNAs, which so far only a fraction have been characterized. The gap between raw RNA-sequencing data and characterization of lncRNAs is made wider by poor evolutionary conservation and limited tools to predict and functionally validate their interaction with DNA, RNA and protein (Thiel et al., 2019).

In addition to the transcription of coding sequences, antisense transcription is also abundant at active promoters and may drive the expression of short-lived, non-coding RNA (Seila et al., 2008; Werner et al., 2009). While the functions of most of these antisense transcripts are poorly known, previous studies suggest that AS may mainly play repressive roles (Shearwin et al., 2005). The regulatory pathway uncovered here further highlights the potential for anti-sense regulation of cell survival pathways and its relevance to cancer and the immune response (Zhang et al., 2017; Chen et al., 2018).

Among the lncRNAs, PVT1 and LINC00152 have been shown to enhance Mcl-1 expression by increasing Mcl-1 mRNA stability or act as competitive endogenous RNAs (ceRNAs) for miRNAs (Wu et al., 2017; Chen et al., 2018). Both PVT1 and LINCOO152 are located in different chromosomes (chromosome 8 and 2 respectively) than Mcl-1 (chromosome 1), hence they are acting in trans in Mcl-1 regulation. The only known lncRNA acting in cis in Mcl-1 regulation is lnc-MCL-1-2. Using in silico analysis, Ronchetti et al. suggested that lnc-MCL-1-2, which is expressed from Mcl-1 3́ UTR region, has potential binding sites for the miR-17 family (miR-106a, miR-18a & b, miR-20a and miR-17) and therefore could act as competing endogenous ceRNA to enhance Mcl-1 expression (Ronchetti et al., 2016).

Mcl1-AS1 may be a newly identified member of lnc-ADAMTSL4 lncRNA family, since ADAMTSL4-5:1 (418 bp) shares 100% similarity with mcl1-AS1 lncRNA (574 bp). Either both are transcribed as the same transcript, with small differences in length (possibly due to different sources of RNA-seq data), or mcl1-AS1 lncRNA is a new member of this family. Future investigations are necessary to validate the latter possibility.

Due to the critical role of Mcl-1 in both cancer and for T cell activity and lifespan, it may be possible to regulate Mcl-1 expression by modulating the level of endogenous lncRNA identified here. This has potential for enhancing susceptibility of cancer cells to chemotherapy, or enhancing the activity of anti-cancer T cells for immunotherapy. However, the diversity of potential transcripts expressed from the Mcl-1 regulatory region (see Fig. 1) highlights the extreme complexity of control mechanisms for Mcl-1 expression. It is also possible that the transcripts display tissue-specific roles in Mcl-1 regulation. Further research will be required to determine the potential for these transcripts in the regulation of Mcl-1 and neighboring genes.

Author contribution

AR and AM wrote the paper and supervised the study. AR performed experimental data in all figures, prepared the tables and performed the bioinformatics analysis. GT and AP contributed to viability and flow cytometry experiments and edited the first draft of manuscript. KH produced the dual reporter pSB-GFP-RFP plasmid backbone.

Declaration of Competing Interest

The authors declare that they have no known competing financial interests or personal relationships that could have appeared to influence the work reported in this paper.

Acknowledgments

We thank Dr. Sarah Saunderson for critical review of the manuscript. Funding was received from the Marsden Fund 18-UOO-18, The Cancer Society (NZ 2018) and a University of Otago Research Grant 2018.

Appendix A. Supplementary data

Supplementary data to this article can be found online at https://doi.org/10.1016/j.gene.2020.145016.

References

Akgul, C., Turner, P.C., White, M.R., Edwards, S.W., 2000. Functional analysis of the human MCL-1 gene. Cell. Mol. Life Sci. 57, 684–691.
Atianand, M.K., Caffrey, D.R., Fitzgerald, K.A., 2017. Immunobiology of long noncoding RNAs. Annu. Rev. Immunol. 35, 177–198.
Chen, J., Sun, M., Kent, W.J., Huang, X., Xie, H., Wang, W., Zhou, G., Shi, R.Z. and Rowley, J.D., 2004. Over 20% of human transcripts might form sense–antisense pairs. 32, 4812-4820.
Chen, P., Fang, X., Xia, B., Zhao, Y., Li, Q., Wu, X., 2018. Long noncoding RNA LINC00152 promotes cell proliferation through competitively binding endogenous miR-125b with MCL-1 by regulating mitochondrial apoptosis pathways in ovarian cancer. Cancer Med 7, 4530–4541.
Chen, Y.G., Satpathy, A.T., Chang, H.Y., 2017. Gene regulation in the immune system by long noncoding RNAs. Nat. Immunol. 18, 962.
Fleischer, B., Schulze-Bergkamen, H., Schuchmann, M., Weber, A., Biesterfeld, S., Müller, M., Krammer, P.H. and Galle, P.R., 2006. Mcl-1 is an anti-apoptotic factor for human hepatocellular carcinoma. 28, 25-32.
Gong, J., Zhang, J.P., Li, B., Zeng, C., You, K., Chen, M.X., Yuan, Y., Zhuang, S.M., 2013. MicroRNA-125b promotes apoptosis by regulating the expression of Mcl-1, Bcl-w and IL-6R. Oncogene 32, 3071–3079.
Gouill, S.L., Podar, K., Harousseau, J.-L. and Anderson, K.C., 2004. Mcl-1 regulation and its role in multiple myeloma. 3, 1259-1262.
Guil, S., Esteller, M., 2012. Cis-acting noncoding RNAs: friends and foes. Nat. Struct. Mol. Biol. 19, 1068–1075.
He, H., Tian, W., Chen, H., Deng, Y., 2016. MicroRNA-101 sensitizes hepatocellular carcinoma cells to doxorubicin-induced apoptosis via targeting Mcl-1. Mol. Med. Rep. 13, 1923–1929.
He, R.Z., Luo, D.-X., Mo, Y.-Y., 2019. Emerging roles of lncRNAs in the post-transcriptional regulation in cancer. Genes Diseases.
Kim, E.H., Neldner, B., Gui, J., Craig, R.W., Suresh, M., 2016. Mcl-1 regulates effector and memory CD8 T-cell differentiation during acute viral infection. Virology 490, 75–82.
Kopp, F., Mendell, J.T., 2018. Functional classification and experimental dissection of long noncoding RNAs. Cell 172, 393–407.
Kowarz, E., Löscher, D., Marschalek, R., 2015. Optimized Sleeping Beauty transposons rapidly generate stable transgenic cell lines. Biotechnol. J. 10, 647–653.
Laurent, G.S., Wahlestedt, C., Kapranov, P., 2015. The Landscape of long noncoding RNA classification. Trends Genet. 31, 239–251.
Li, L.-C., Okino, S.T., Zhao, H., Pookot, D., Place, R.F., Urakami, S., Enokida, H., Dahiya, R., 2006. Small dsRNAs induce transcriptional activation in human cells. Proc. Natl. Acad. Sci. 103, 17337–17342.
Lin, S., Zhang, L., Luo, W. and Zhang, X.J., 2016. Characteristics of antisense transcript promoters and the regulation of their activity. 17, 9.
Liu, H., Peng, H.-W., Cheng, Y.-S., Yuan, H.S., Yang-Yen, H.-F., 2005. Stabilization and enhancement of the antiapoptotic activity of mcl-1 by TCTP. Mol. Cell. Biol. 25, 3117–3126.
Long, J., Ji, Z., Jiang, K., Wang, Z. and Meng, G., 2015. miR-193b modulates resistance to doxorubicin in human breast cancer cells by downregulating MCL-1. BioMed research international 2015.
Magistri, M., Faghihi, M.A. and Wahlestedt, C.J., 2012. Regulation of chromatin structure by long noncoding RNAs: focus on natural antisense transcripts. 28, 389-396.
Mercer, T.R., Dinger, M.E., Mattick, J.S., 2009. Long non-coding RNAs: insights into functions. Nat. Rev. Genet. 10, 155–159.
Morciano, G., Giorgi, C., Balestra, D., Marchi, S., Perrone, D., Pinotti, M., Pinton, P., 2016. Mcl-1 involvement in mitochondrial dynamics is associated with apoptotic cell death. Mol. Biol. Cell 27, 20–34.
Mott, J.L., Kobayashi, S., Bronk, S.F., Gores, G.J., 2007. mir-29 regulates Mcl-1 protein expression and apoptosis. Oncogene 26, 6133–6140.
Portnoy, V., Huang, V., Place, R.F., Li, L.C., 2011. Small RNA and transcriptional upregulation. Wiley Interdisciplinary Reviews: RNA 2, 748–760.
Rad, S.M., Mohammadi-Sangcheshmeh, A., Bamdad, T., Langroudi, L., Atashi, A., Lotfinia, M., Arefian, E., Gastal, E.L., Soleimani, M., 2017. Pluripotency Crossroads: Junction of Transcription Factors, Epigenetic Mechanisms, MicroRNAs, and Long Non-coding RNAs. Curr. Stem Cell Res. Ther. 12, 300–311.
Rad, S.M.A.H., Bamdad, T., Sadeghizadeh, M., Arefian, E., Lotfinia, M., Ghanipour, M., 2015. Transcription factor decoy against stem cells master regulators, Nanog and Oct-4: a possible approach for differentiation therapy. Tumor Biology 36, 2621–2629.
Ronchetti, D., Manzoni, M., Todoerti, K., Neri, A., Agnelli, L., 2016. In Silico Characterization of miRNA and Long Non-Coding RNA Interplay in Multiple Myeloma. Genes (Basel) 7.
Rutenberg-Schoenberg, M., Sexton, A.N., Simon, M.D., 2016. The properties of long noncoding RNAs that regulate chromatin. Annu. Rev. Genomics Hum. Genet. 17, 69–94.
Seila, A.C., Calabrese, J.M., Levine, S.S., Yeo, G.W., Rahl, P.B., Flynn, R.A., Young, R.A. and Sharp, P.A., 2008. Divergent transcription from active promoters. 322, 1849-1851.
Senichkin, V.V., Streletskaia, A.Y., Gorbunova, A.S., Zhivotovsky, B., Kopeina, G.S., 2020. Saga of Mcl-1: regulation from transcription to degradation. Cell Death Differ. 1–15.
Senichkin, V.V., Streletskaia, A.Y., Zhivotovsky, B., Kopeina, G.S., 2019. Molecular comprehension of Mcl-1: from gene structure to cancer therapy. Trends Cell Biol.
Shearwin, K.E., Callen, B.P., Egan, J.B., 2005. Transcriptional interference–a crash course. Trends Genet. 21, 339–345.
Sigova, A.A., Mullen, A.C., Molinie, B., Gupta, S., Orlando, D.A., Guenther, M.G., Almada, A.E., Lin, C., Sharp, P.A. and Giallourakis, C.C., 2013. Divergent transcription of long noncoding RNA/mRNA gene pairs in embryonic stem cells. 110, 2876-2881.
Song, L., Coppola, D., Livingston, S., Cress, W.D., Haura, E.B. and therapy, 2005. Mcl-1 regulates survival and sensitivity to diverse apoptotic stimuli in human non-small cell lung cancer cells. 4, 267-276.
Su, H., Yang, J.R., Xu, T., Huang, J., Xu, L., Yuan, Y., Zhuang, S.M., 2009. MicroRNA-101, down-regulated in hepatocellular carcinoma, promotes apoptosis and suppresses tumorigenicity. Cancer Res. 69, 1135–1142.
Su, W.-Y., Xiong, H., Fang, J.-Y.J.B. and communications, b.r., 2010. Natural antisense transcripts regulate gene expression in an epigenetic manner. 396, 177-181.
Thiel, D., Conrad, N.D., Ntini, E., Peschutter, R.X., Siebert, H., Marsico, A., 2019. Identifying lncRNA-mediated regulatory modules via ChIA-PET network analysis. BMC Bioinf. 20, 292.
Thomas, L.W., Lam, C. and Edwards, S.W., 2010. Mcl-1; the molecular regulation of protein function. 584, 2981-2989.
Tripathi, P., Koss, B., Opferman, J., Hildeman, D., 2013. Mcl-1 antagonizes Bax/Bak to promote effector CD4+ and CD8+ T-cell responses. Cell Death Differ. 20, 998–1007.
Tullai, J.W., Schaffer, M.E., Mullenbrock, S., Sholder, G., Kasif, S., Cooper, G.M., 2007. Immediate-early and delayed primary response genes are distinct in function and genomic architecture. J. Biol. Chem. 282, 23981–23995.
Wei, W., Pelechano, V., Järvelin, A.I., Steinmetz, L.M., 2011. Functional consequences of bidirectional promoters. 27, 267-276.
Wensveen, F.M., van Gisbergen, K.P., Derks, I.A., Gerlach, C., Schumacher, T.N., van Lier, R.A., Eldering, E., 2010. Apoptosis threshold set by Noxa and Mcl-1 after T cell activation regulates competitive selection of high-affinity clones. Immunity 32, 754–765.
Werner, A., Carlile, M., Swan, D., 2009. What do natural antisense transcripts regulate? RNA Biol. 6, 43–48.
Wu, Q., Yang, F., Yang, Z., Fang, Z., Fu, W., Chen, W., Liu, X., Zhao, J., Wang, Q., Hu, X., Li, L., 2017. Long noncoding RNA PVT1 inhibits renal cancer cell apoptosis by up-regulating Mcl-1. Oncotarget 8, 101865–101875.
Zhang, X., Hamblin, M.H., Yin, K.-J., 2017. The long noncoding RNA Malat1: its physiological and pathophysiological functions. RNA Biol. 14, 1705–1714.

Supplemenatary data for Chapter II

A

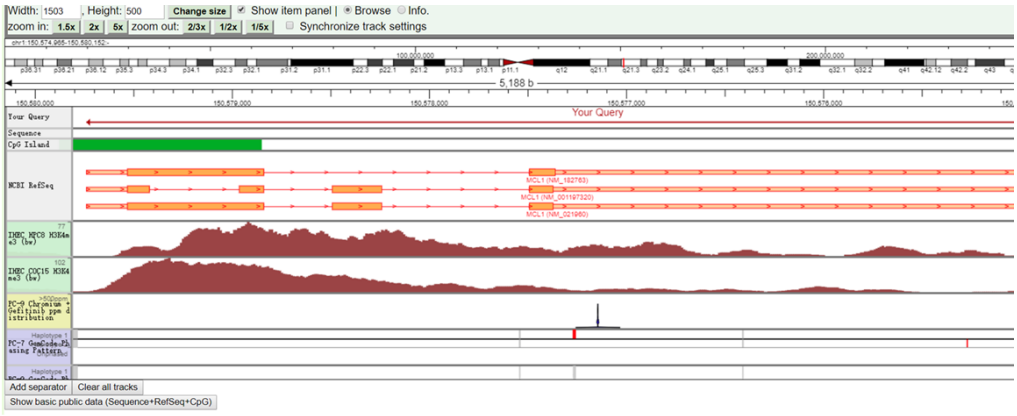

B

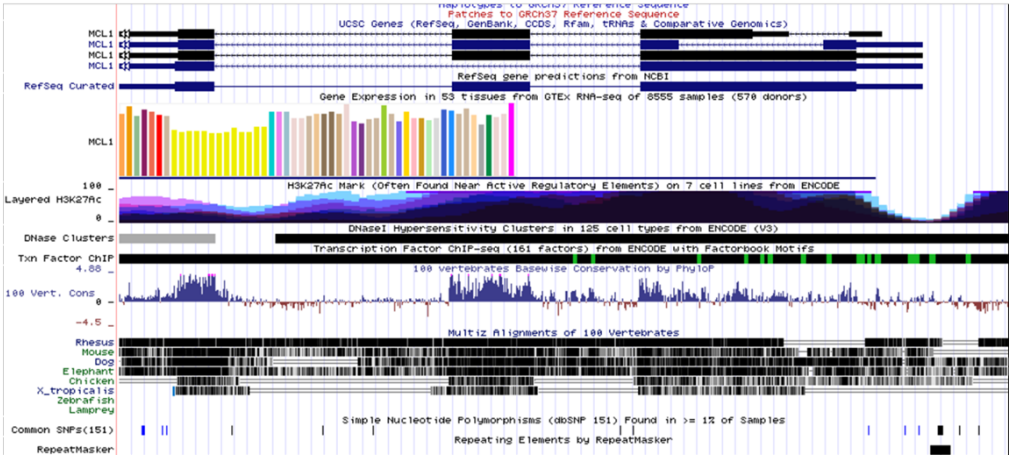

Figure S1. Chromatin status of Mcl-1 gene in A) DBTSS and B) UCSC databases. Enrichments for promoter marks such as H3K4me3, H3K2Ac and high DNaseI hypersensivity in the first exon and intron of Mcl-1 suggest the presence of a promoter for mcl1-AS1.

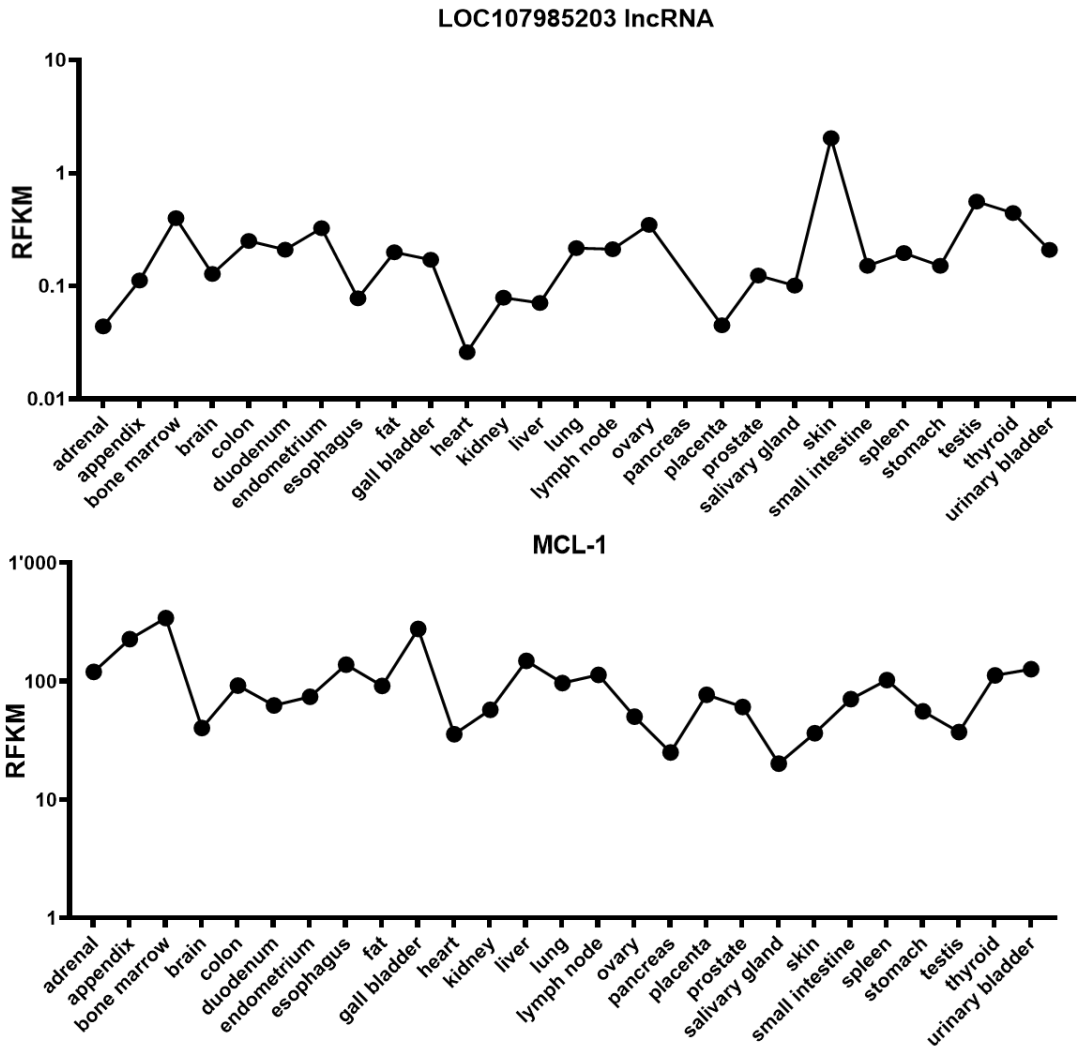

Figure S2. RNA-seq data of Mcl-1 and mcl1-AS1 expression 27 normal tissues extracted from NCBI-gene expression browser. Reads per kilobase per million reads (RPKM).

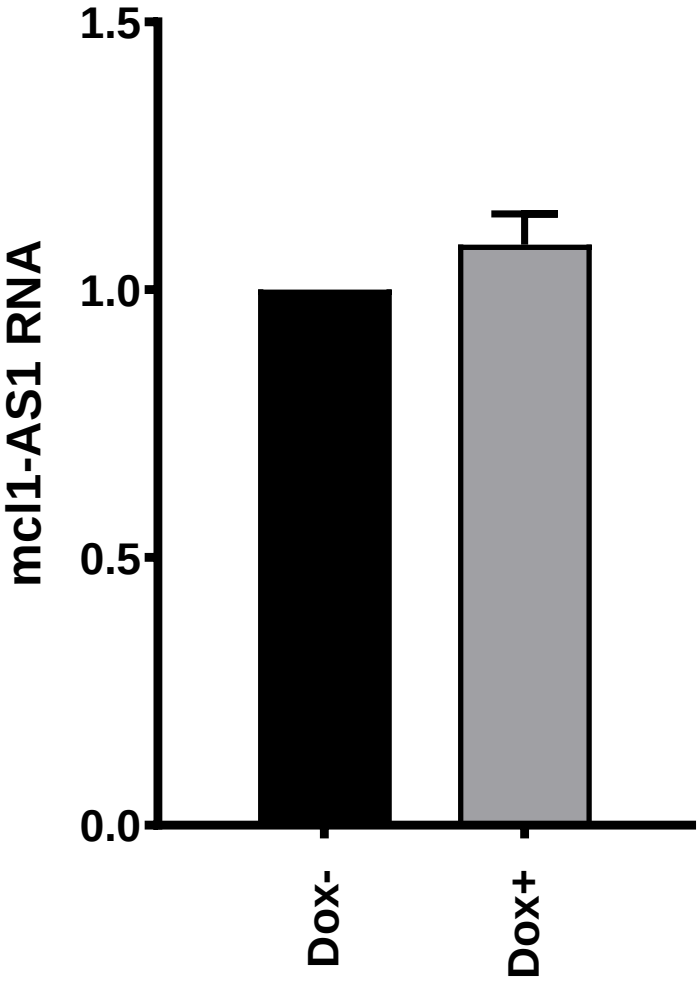

Figure S3. Effect of Doxycycline on mcl1-AS1 expression. Doxycycline does not alter the mcl1-AS1 expression in Hek293 cells. Hek293 cells were transfected with empty plasmid and treated with 5 µg/ml of doxycycline. 72 hrs after induction, qPCR performed for investigation of doxycycline effect on mcl1-AS1. As data shows, doxycycline does not alter the mcl1-AS1 expression in Hek293 cells.

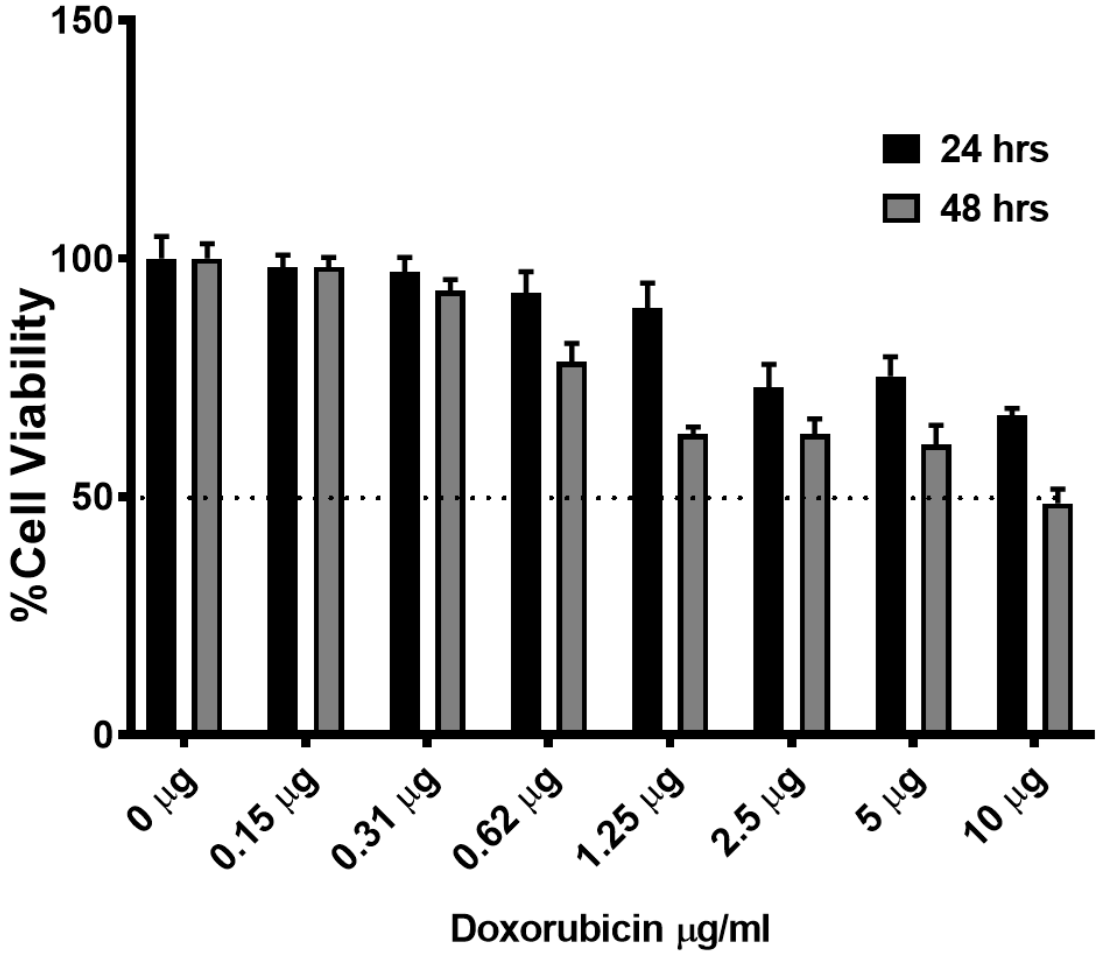

Figure S4. determination of Doxorubicin IC50 in HEK293 cells. Cells were treated with different concentration of doxorubicin and cell viability were measured using resazurin assay.

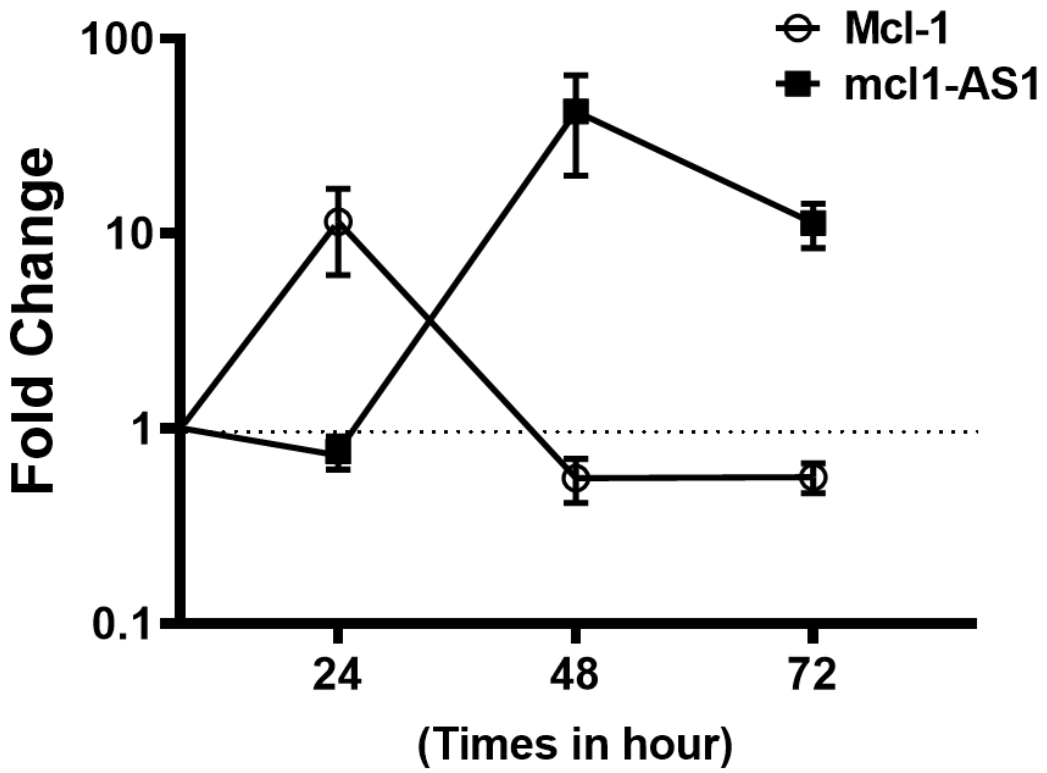

Figure S5. The expression level of Mcl-1 and mcl1-AS1 after activation of primary T cells with CD3/ CD28 antibodies 24, 48 and 72 hours after activation using qPCR.

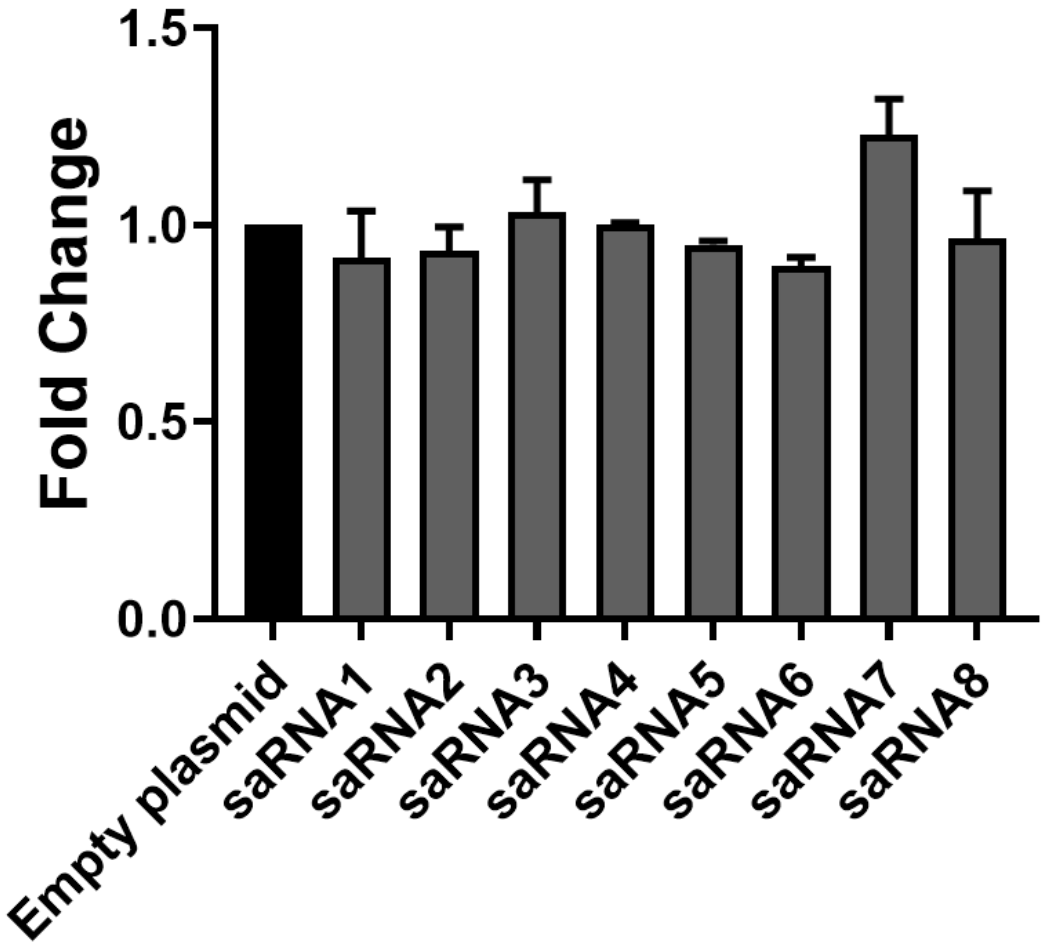

Figure S6. Mcl-1 expression 72 hours after HEK293 cells transfected with eight saRNAs targeting different regions of Mcl-1 promoter.

Table S1. Primer sequences used for qPCR experiments and cloning the different parts of human Mcl1 gene. Overhangs for restriction enzyme sites are underlined.

Name	Forward Primer	Reverse Primer
qPCR-βactin	CTTCCTTCCTGG GCATG	GTCTTTGCGGATGTCCAC
qPCR-mcl1-AS1	CTGTGCTTCCCTGAGACCTG	CACTGAACTTCCCCGTCCTC
qPCR-Mcl1 (isoform L)	CAGAGGAGGAGGACGAGTT	CGAGACAACGATTTCACATC
Proximal promoter	TATAGCTAGCATTCTAATGGATTAAGGCCTATATG	TTATCCATGGATAAAAGGGGAAAGGGGCGG
ExonI-IntronI	TATAGCTAGCAGCTGGTAGGTGCCGTGC	TTATCCATGGTCCAACCCACCCTTGGCGG
ExonII-IntronII	TATAGCTAGCTGGAAACCGAAACGAGTCAG	TTATCCATGGGCCTCAATTGCGCAGATCAG

Table S2. shRNA sequences with software used for designing them. Loop sequences are underlined.

Name	Software	Sequence (sense-loop-antisense)
shRNA1	BLOCK-iT™	GGGAACAACAGTCTTAGATGACGAATCATCTAAGACTGTTGTTCCC
shRNA2	BLOCK-iT™	GCACAGCTCTCTACTCTCAGTCGAAACTGAGAGTAGAGAGCTGTGC
shRNA3	WI siRNA	GTGCCTCAGAGAATACAAATTCAAGAGATTTGTATTCTCTGAGGCAC
shRNA4	WI siRNA	CCACGTGCTACCCTAAAGATTCAAGAGATCTTTAGGGTAGCACGTGG
shRNA5	Sfold	TACCCTAAAGAACCATTTATTCAAGAGATAAATGGTTCTTTAGGGTA

Table S3. Members of lnc-ADAMTSL4 family with their structure and source. Exons are shown in green boxes.

Transcript name	Source	Structure
lnc-ADAMTSL4-1:1	Broad Institute & NONCODE v4	
lnc-ADAMTSL4-1:2	Broad Institute	
lnc-ADAMTSL4-2:1	Biogazelle lncRNA chip, Ensembl release 64 - Sep 2011 & NONCODE v4	
lnc-ADAMTSL4-4:1	NONCODE v4 & Hangauer et al., 2013	
lnc-ADAMTSL4-5:1	NONCODE v4	
lnc-ADAMTSL4-6:1	Nielsen et al.,2014	
lnc-ADAMTSL4-7:1	NONCODE v4	
lnc-ADAMTSL4-7:3	FANTOM CAT (stringent)	
lnc-ADAMTSL4-7:4	FANTOM CAT (stringent)	
lnc-ADAMTSL4-7:5	FANTOM CAT (stringent)	
lnc-ADAMTSL4-7:6	FANTOM CAT (stringent)	
lnc-ADAMTSL4-7:7	FANTOM CAT (stringent)	
lnc-ADAMTSL4-7:8	FANTOM CAT (stringent)	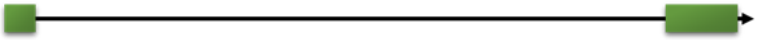

Table S4. 13 Members of lnc-ADAMTSL4 family classified as 3 antisense and 10 intergenic lncRNAs. Only lnc-ADAMTSL4-1:1 & 2 have potentially coding capacity. The family show low conservation compare to other animals. Data are available in LINipedia genome browser. Coding capacity was determined by two algorithms; CPAT and PhyloCSF. For locus conservation, Emsembl Compara API was used. CPAT: Coding-Potential Assessment Tool using an alignment-free logistic regression model. Human coding probability (CP) cutoff: 0.364 (CP ≥ 0.364 probability coding sequence, CP < 0.364 probability noncoding sequence). (http://rna-cpat.sourceforge.net/). PhyloCSF: Coding Potential of a multi-species nucleotide sequence alignment. CP cutoff: 60.7876 (CP ≥ 0.364 probability coding sequence, CP < 0.364 probability noncoding sequence) (https://github.com/mlin/PhyloCSF/wiki).

Transcript name	Alternative name(s)	Location (hg38)	Class	Length (bp)	Number of exon(s)	Protein coding potential		Locus conservation			
						PhyloCSF score	CPAT				
lnc-ADAMTSL4-1:1	TCONS_00001146 NONHSAT006302	Chr1:150532161-150537337	Intergenic	2034	3	-23.057	40.93%	×	×	×	×
lnc-ADAMTSL4-1:2	TCONS_00002162	Chr1:150532657-150537163	Intergenic	1627	2	-23.057	41.47%	×	×	×	×
lnc-ADAMTSL4-2:1	ENST00000500237 NONHSAT006317	Chr1:150592583-150617551	Antisense	1960	3	4.8876	2.98%	✓	×	×	×
lnc-ADAMTSL4-4:1	NONHSAT006304;	Chr1:150544762-150548321	Intergenic	3560	1	1.5471	0.62%	×	×	×	×
lnc-ADAMTSL4-5:1	NONHSAT006316	Chr1:150579876-150604193	Antisense	418	2	-78.7143	1.22%	✓	×	×	×
lnc-ADAMTSL4-6:1	l_134_chr1:150571617-150577187_ovary	Chr1:150599142-150604711	Antisense	405	3	-0.3061	0.44%	✓	×	×	×
lnc-ADAMTSL4-7:1	NONHSAT006322	Chr1:150629624-150637156	Intergenic	7533	1	20.8353	4.87%	×	×	×	×
lnc-ADAMTSL4-7:3	CATG00000017626.1 FTMT20300051582.1	Chr1:150629825-150635755	Intergenic	1094	2	20.8353	3.57%	×	×	×	×
lnc-ADAMTSL4-7:4	CATG00000017626.1 MICT00000020551.1	Chr1:150629825-150636987	Intergenic	6698	2	20.8353	2.56%	×	×	×	×
lnc-ADAMTSL4-7:5	CATG00000017626.1 HBMT00000028946.1	Chr1:150629825-150641890	Intergenic	11537	2	43.7732	2.09%	×	×	×	×
lnc-ADAMTSL4-7:6	CATG00000017626.1 HBMT00000028947.1	Chr1:150629825-150641890	Intergenic	12066	1	43.7732	2.03%	×	×	×	×
lnc-ADAMTSL4-7:7	CATG00000017626.1 MICT00000020555.1	Chr1:150629825-150636987	Intergenic	4470	3	20.8353	5.41%	×	×	×	×
lnc-ADAMTSL4-7:8	CATG00000017626.1 FTMT20300042953.1	Chr1:150629853-150634966	Intergenic	213	2	-2.9163	1.09%	×	×	×	×

Chapter III

Optimisation of Tet-On inducible system for Sleeping Beauty-based CAR T cell applications

In this chapter, we developed an inducible SB Tet-On system in order to control expression of Mcl-1 in CAR T cells. The most significant weakness of this system was high background expression in the absence of doxycycline. We used several approaches to improve the Tet-On system, including gene placement, codon-optimisation of rt-TA, a G72V mutation in the rtTA tet activator, removal of cryptic splice sites within rt-TA, creation of an autoregulatory Tet-On system, and through manipulation of regulatory elements in the tetracycline response element (TCE) promoter. Our final optimised construct showed high inducibility and a very low background expression compared to the original construct.

Author contributions:

A.R. and A.M. wrote the paper and supervised the study. A.R. contributed to experimental data in all figures, prepared the figures, tables and performed the bioinformatics analysis. G.T. and A.P. performed experiments.

SCIENTIFIC REPORTS
nature research

Check for updates

OPEN

Optimisation of Tet-On inducible systems for Sleeping Beauty-based chimeric antigen receptor (CAR) applications

S. M. Ali Hosseini Rad[1,2], Aarati Poudel[1,2], Grace Min Yi Tan[1,2] & Alexander D. McLellan[1]✉

Regulated expression of genetic elements that either encode polypeptides or various types of functional RNA is a fundamental goal for gene therapy. Inducible expression may be preferred over constitutive promoters to allow clinician-based control of gene expression. Existing Tet-On systems represent one of the tightest rheostats for control of gene expression in mammals. However, basal expression in absence of tetracycline compromises the widespread application of Tet-controlled systems in gene therapy. We demonstrate that the order of P2A-linked genes of interest was critical for maximal response and tightness of a chimeric antigen receptor (CAR)-based construct. The introduction of G72V mutation in the activation region of the TetR component of the rtTA further improved the fold response. Although the G72V mutation resulted in a removal of a cryptic splice site within rtTA, additional removal of this splice site led to only a modest improvement in the fold-response. Selective removal of key promoter elements (namely the BRE, TATA box, DPE and the four predicted Inr) confirmed the suitability of the minimal CMV promoter and its downstream sequences for supporting inducible expression. The results demonstrate marked improvement of the rtTA based Tet-On system in Sleeping Beauty for applications such as CAR T cell therapy.

Inducible-gene expression is one of the most sought-after elements of synthetic gene regulation systems. Engineering mammalian cells to express proteins or RNA in an inducible fashion offers opportunities for the development of safe cellular-based therapies to treat a wide spectrum of inborn and acquired diseases. Compared to prokaryote genetic systems, the development of tight, inducible gene expression in eukaryote cells has been challenging[1–3]. Unlike prokaryotes, mammalian genetic control is not usually mediated by single or oligo-component regulators, but rather by multiple transcription factors that bind to both promoters, as well as often distant enhancer regions located on different chromosomes. Moreover, both promoters and enhancers may be regulated by epigenetic control mechanisms, and the site of transgene insertion in the genome influences the response profile of transgenes[4]. Tet-On systems utilise a mutant TetR component that binds to tetracycline response elements (TRE) in the presence of tetracycline, or its stable analogue doxycycline[5]. To activate transcription, fusion of the herpes-simplex VP16 transcriptional activator to the C-terminus of the mutant TetR, recruits generalised transcription factors, as well as RNAP II to initiate gene transcription. Modified tetracycline-inducible systems represent the most widely used inducible system in eukaryotic systems, from yeast to human cells[5]. The potential exists for drug inducible systems to be used in cell-based immunotherapy to control the expression of genes or other sequences of interest (GOI). Although 10^3 to 10^6-fold induction of gene expression with tetracycline-based control systems has been reported, basal expression in the absence of inducer can result in undesirable GOI expression[5]. In vivo use would be compromised by such leakiness, particularly if the GOI was involved in T cell survival, or resistance to apoptosis. Unfortunately, compared to Tet-Off systems, Tet-On systems are less sensitive to tetracycline and generally exhibit a higher level of basal expression in the absence of induction[6]. On the other hand, Tet-Off systems are slow to respond to withdrawal of tetracycline and this may be compounded by sequestration of tetracycline in vivo, especially within bones[2,7].

[1]Department of Microbiology and Immunology, University of Otago, Dunedin, Otago 9010, New Zealand. [2]These authors contributed equally: S. M. Ali Hosseini Rad, Aarati Poudel and Grace Min Yi Tan. ✉email: alex.mclellan@otago.ac.nz

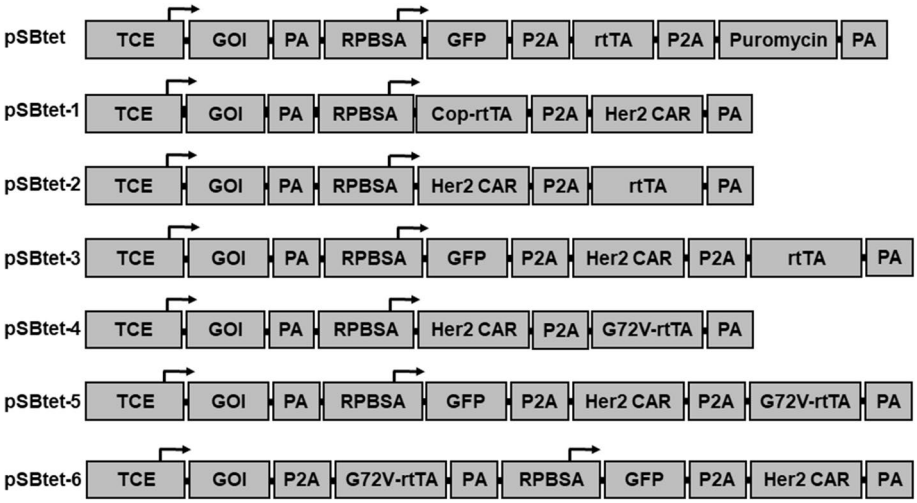

Figure 1. Schematic illustration of SB-based Tet-On systems used in this study. Constructs derived from original pSBtet-GP developed by Kowarz et al. TCE: tet-responsive promoter/ GOI: gene of interest (Mcl-1 or firefly luciferase); PA: polyadenylation site; P2A: 2A self-cleaving; rtTA-M2: reverse tetracycline-controlled transactivator; RPBSA: constitutive promoter comprised of the Rpl13a core promoter and exon 1, plus additional exon and intron elements from Rpl41.

The Sleeping Beauty (SB) transposon system was developed from extinct Salmonid transposons awoken after 10 million years of inactivity through consensus-based correction of accumulated mutations[8]. Compared to retroviral-based insertions into transcriptional units and their regulatory regions, SB vectors insert almost randomly into TA-sites throughout the genome. This property minimises deleterious integrations and helps maintain constitutive or inducible gene expression[9,10]. SB-based vectors carry a GOI along with optional markers or selection elements flanked by inverted terminal repeats (ITRs)[9–12]. Although the transposase has been re-engineered to enhance activity[12,13], a lower-activity SB-transposase is preferred for human clinical trials to minimise the incidence of multiple genome integrations. Along with piggy bac transposase systems, SB transposase systems have been used in CAR T cell therapy trials for B cell malignancies[14,15]. To expand the utility of SB-based vectors to express a CAR together with additional GOI under drug-control, we revisited the SB-based Tet-On system, through: (1) alterations in the placement of genes within the P2A-linked CAR cassette, (2) the introduction of a G72V mutation in rtTA-M2 – previously only described for yeast Tet-On control[16] (3) the placement of rtTA under auto-regulatory control, (4) the removal of cryptic splicing sites, and (5) modifications of the proximal promoter. To test the induction of the Tet-On system, we expressed myeloid leukaemia cell differentiation (Mcl-1) as a GOI involved in T cell survival and resistance to apoptosis.

Results

The rtTA location within a multi-gene cassette influences responsiveness of the Tet-On system. We reasoned that placing a codon-optimised rtTA-M2 gene proximal to the RPBSA promoter (pSBtet-1) should result in robust rtTA-M2 expression and therefore tight control of inducible gene expression (Fig. 1).

Surprisingly, this setting led to a decrease in both the fold-expression of luciferase and Mcl-1 mRNA (Fig. 2A,B). It has previously been reported that expression of rtTA-M2 by strong promoters compromises inducible expression[16,17]. We therefore relocated the original rtTA-M2 sequence distal to the RPBSA and downstream from either one (pSBtet-2) or two (pSBtet-3) additional GOI. However, inducibility of the GOI was still poor (Figs. 1, 2C,D).

Introduction of a G72V mutation in rtTA-M2 enhances the tightness of the Tet-On system. Roney et al.[16] reported that a GGG to GTG (G72V) missense mutation in rtTA mitigated basal gene expression in the absence of an inducer in *S. cerevisiae* clones. Because of the similarity of transcriptional machinery amongst eukaryote cells, we reasoned that this approach may give similar results in human cells. The G72V mutation was next introduced into pSBtet-2 and pSBtet-3 to create the pSBtet-4 and pSBtet-5 constructs (Fig. 1). The G72V mutation in rtTA-M2 decreased the background expression of TCE promoter in the absence of doxycycline at both the mRNA and protein level ($P < 0.001$, Fig. 3A,B). The G72V mutation also restored the maximal expression of pSBtet-2 and pSBtet-3 constructs following induction with doxycycline (Fig. 3C). As previously reported, G72V-rtTA-M2 appeared less sensitive to doxycycline compared to original rtTA-M2, though this was not statistically significant (Fig. 3C, $P > 0.9$)[16]. A similar pattern of results was obtained after two weeks passage of cells to ensure stable integration of the pSBtet-5 (Fig. 3D,E). Note, the GFP expression of the transfected cell lines dropped from ~ 90 to ~ 70% after two weeks of culture, most likely due to a shift from transient gene expression to that from integrated cassettes.

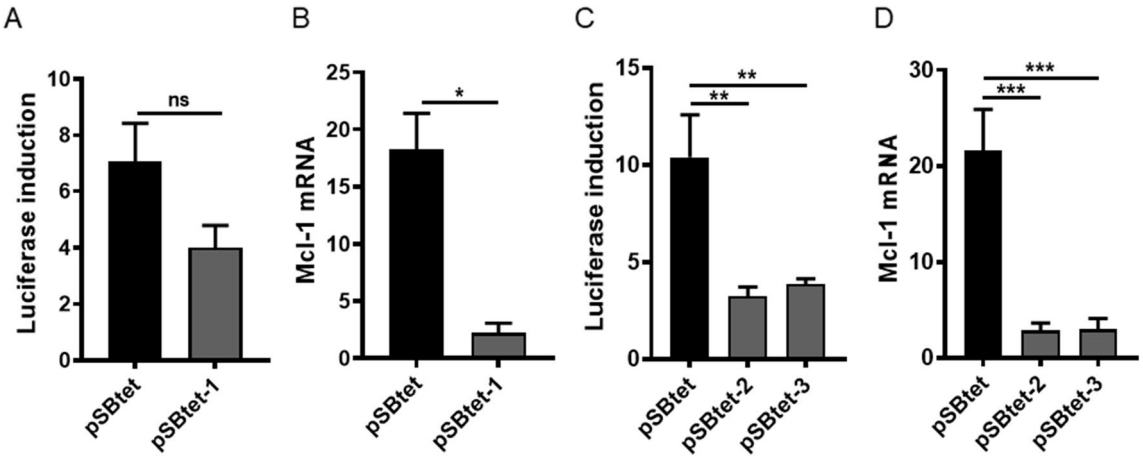

Figure 2. Locating a commercially-codon optimised rtTA-M2 (cop-rtTA; pSBtet-1) proximal to RPBSA increases the leakiness of TCE promoter as measured by (**A**) luciferase fold induction and (**B**) qPCR for Mcl-1 mRNA. Relocating the unmodified rtTA-M2 distal to the RPBSA in (pSBtet-2 &-3) did not improve the basal expression measured by (**C**) luciferase fold induction and (**D**) qPCR for Mcl-1 mRNA. Experiments were carried out 96 h post-transfection. Statistical analysis: (**A**, **B**) two-tailed t-test, (**C**, **D**) one-way ANOVA test with Bonferroni post-test correction (*P < 0.05, **P < 0.01, ***P < 0.001).

Investigation of autoregulatory strategy with G72V variant. We next investigated possible improvements in inducibility of multiple GOIs using positive feedback control in an autoregulatory cassette. Autoregulation can improve tetracycline-regulation in a retroviral vector[18] and in a bi-directional[19] or uni-directional lentiviral vector[7]. The bi-directional approach appears tight in transient transfection, however, high background was detected when cells were stably transduced[19]. Therefore, we utilised a uni-directional strategy with a P2A sequence in place of an Internal Ribosome Entry Site (IRES) sequence, to allow expression of GOI-P2A-G72VrtTA under TCE promoter (pSBtet-6,Fig. 1). We speculated that the leaky expression of the TCE would still allow sufficient levels of G72V-rtTA inducer to respond to doxycycline stimulation. Although the positive feedback system resulted in tight expression at the protein level (Fig. 4A), as previously reported[7,18,19], the system was leaky at the mRNA level for Mcl-1 (Fig. 4B). Basal expression of luciferase in pSBtet-6 was lower than for pSBtet (P < 0.05) and showed a higher response upon induction (P < 0.05, Fig. 4C). Compared to the constitutive expression of G72V-rtTA, the autoregulatory system showed greater sensitivity to doxycycline induction (P < 0.05; Fig. 4C), although the basal expression was higher (P = 0.0066).

Removing cryptic alternative splice sites within rtTA reduces the background expression. Since the first description of the eukaryotic Tet-On inducible system, most optimisation studies have focused on rtTA mutations: for example, the removal of cryptic splice sites (flanking amino acids 8–144) in the TetR sequence[20,21]. Using recently-developed software[22], we identified eight additional potential cryptic splice sites within the coding region of rtTA-M2 (Fig. 5A and Table S1). Because the G72V mutation resulted in the loss of a cryptic splice site at position 215 (Fig. 5A and Table S2, we determined if the success of the G72V mutation was due to the removal of the potential cryptic splice site at 215. These cryptic splice sites are located in two regions of rtTA; one in a surface residue (215 nt and seven in the dimerisation domains (320 nt, 326 nt, 367 nt, 392 nt, 408 nt, 456 nt and 541 nt; Fig. 5A, Figure S1). We therefore removed all eight cryptic splices sites by silent or conserved missense-mutations in the pSBtet construct (Table 1).

The removal of six cryptic splice sites modestly enhanced the tightness of Tet-On system 7.7–19.6 fold compared with original rtTA (P < 0.001, Fig. 5B). The remaining two mutations at position 320 (~ twofold, P = 0.8) and 367 (~ fivefold, P = 0.08) did not significantly affect Tet-On performance. The mutation at position 320 produced E106Q, while 367 (Q122) was a silent mutation (Table 1). It is possible these two splice sites are weak 5′ acceptor splice sites which are only used if other competing splice sites are removed[23]. Indeed, positions 320 and 367 have low score and confidence which represent strength and the probable occurrence of a splice site, respectively (Table S1). Combining all mutations together, improved the leaky background of the Tet-On system ~ 40 fold compared to original rtTA (P < 0.0001, Fig. 5B). However, superior results were still seen with G72V mutation (Fig. 5C).

Surprisingly, combining the G72V mutation and removing all cryptic splice sites abolished responsiveness and inducibility of Tet-On system (Fig. 5C,D). There are four altered amino acid positions within rtTA-M2 that result in a reverse activator phenotype, as compared to the original TetR: E71K, D95N, L101S and G102D[2]. In TetR, E71 is a surface residue amino acid, D95 connects the DNA reading head to the core domain, while L101 and G102 are crucial for dimerisation and the tetracycline response, respectively[2]. In TetR the E71 and G72 amino acids create the turn between α-helix-4 and 5 (Fig. 6). This region bridges the DNA binding domain to the tetracycline binding domain and the combination of both the E71K and G72V mutations might destroy the structure of this critical turn, causing a loss of rtTA-M2 activity. This may also explain the drop in tetracycline-induction observed with the position 320 mutant (E107 to Q107, Fig. 5D), since this residue is close to a 'high sensitivity

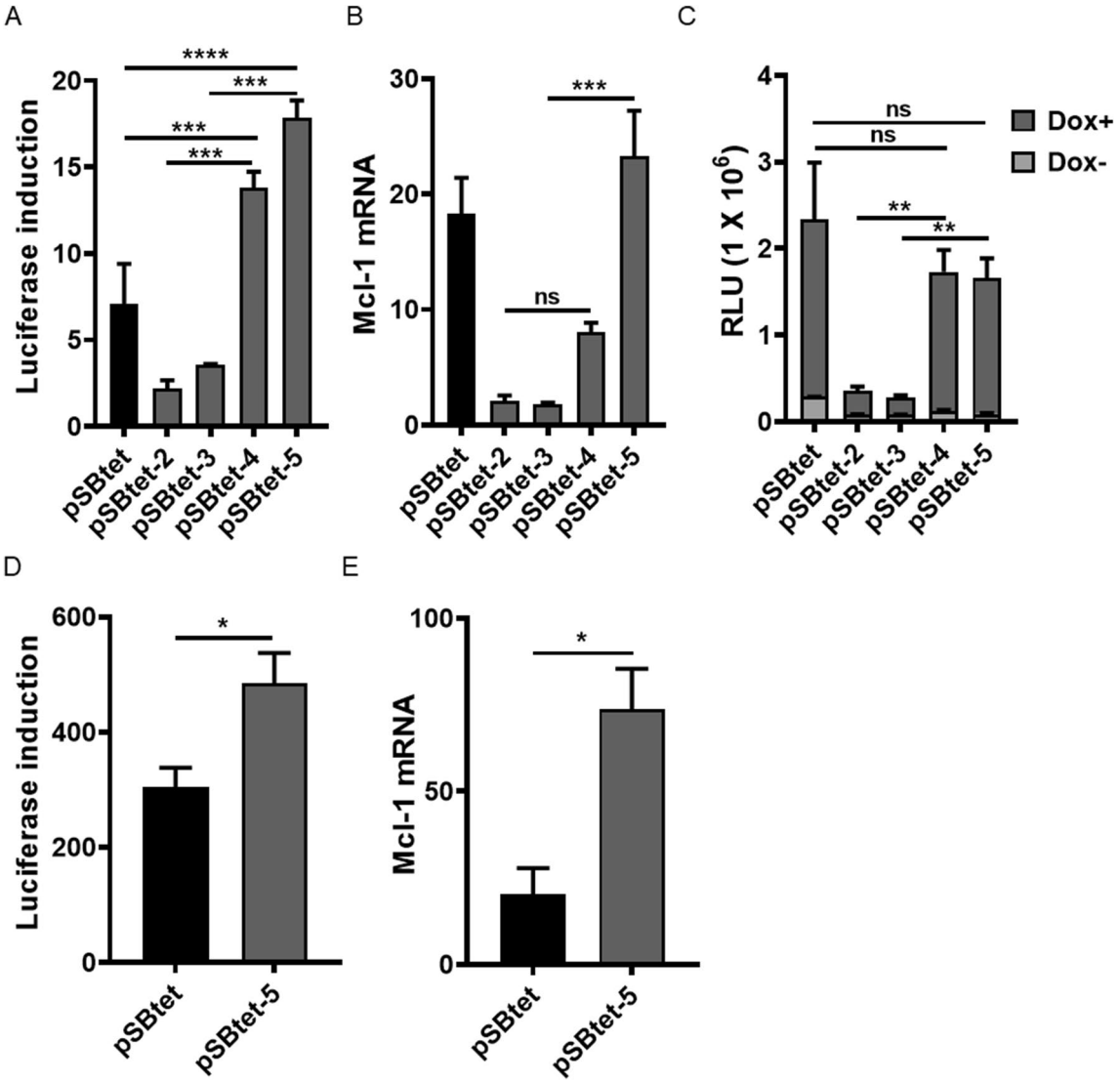

Figure 3. Introducing the G72V mutation into pSBtet-2 & -3 and generation of pSBtet-4 & -5. The efficacy of G72V-rtTA SB based Tet-On system was measured at 96 h by (**A**) luciferase fold induction and (**B**) qPCR for Mcl-1 mRNA. (**C**) The G72V mutation restores the inducibility of pSBtet-2 and pSBtet-3 upon doxycycline induction. (**D**, **E**) Confirmation of the improvement of SB-based Tet-On system after two weeks passaging, as quantified by luciferase fold induction and qPCR for Mcl-1 mRNA. Statistical analysis: (**A**–**C**) one-way ANOVA test with Bonferroni post-test correction, (**D**, **E**) two-tailed t-test (*P < 0.05, **P < 0.01, ***P < 0.001, ****P < 0.0001).

region' (Figure S2)[21,24–26]. It is possible that the G72V mutation affected the secondary structure of rtTA[16], rather than simply removing a cryptic splice site. It is interesting to note that further commercial algorithm-mediated codon optimisation of rt-TA-M2 attempted in pSBtet-1 (see Fig. 2) re-introduced 13 cryptic alternative splice sites with high score and confidence (Fig. 5A, Table S3) within the rtTA coding region. This may have contributed to the poor performance of the first pSBtet-1 construct analysed, since cryptic splice sites might be associated with poor performance of Tet-On systems[20,21] (Fig. 2A,B).

Dissection of the TCE proximal promoter. Modification of the minimal CMV promoter can affect TCE promoter performance[27]. Removing elements downstream of the TATA box can reduce the maximal expression, whereas deleting the upstream elements can decrease the leakiness[27]. We therefore revisited the design of pTIGHT to ensure optimal performance in our setting. Core promoter elements were identified using the YAAP program (Fig. 7A). It is possible that the presence of alternative initiator element (Inr) might lead to a loss of control of the TCE-promoter. We therefore removed these elements in single or combinatorial mutation fashion from pSBtet and monitored the tightness and maximal expression of TCE promoter.

Removal of each, or all, downstream elements of the TATA box (Inr-1, -2, -3 and -4 sites, and the DPE element) markedly decreased the tightness of the TCE promoter (Fig. 7B), and also reduced the maximal expression, as previously reported[27] (Fig. 7C). Specifically, removing Inr-3 increased the background expression remarkably

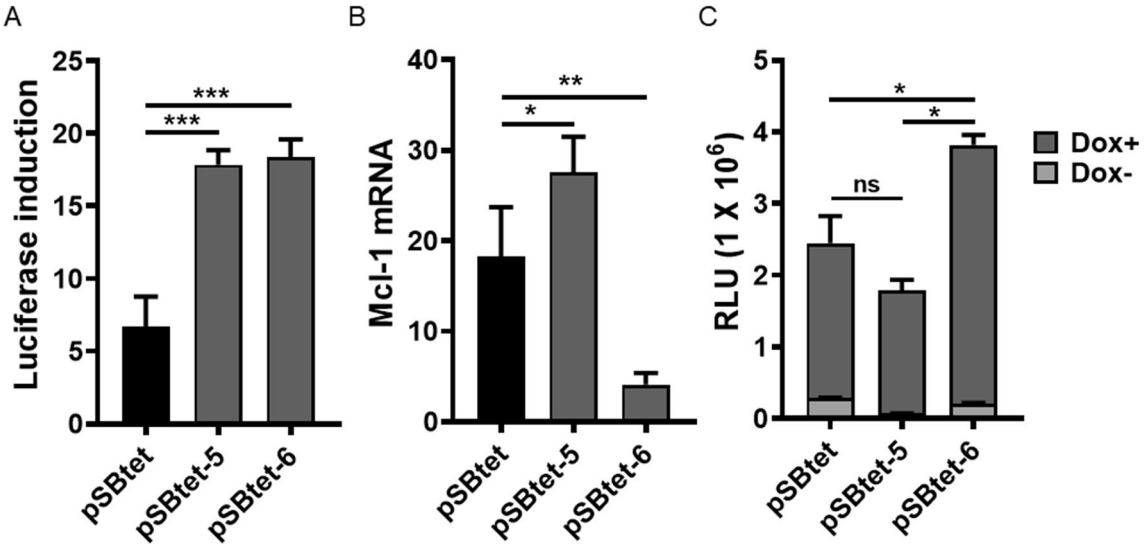

Figure 4. pSBtet-6 autoregulatory system showed superior regulation to pSBtet with (**A**) luciferase fold induction, but (**B**) higher background expression at the mRNA level for Mcl-1. (**C**) Comparison of maximal expression of luciferase in pSBtet-6 versus constitutive expression of G72V (psBtet-5) after induction with doxycycline. pSBtet-6 showed higher sensitivity, but higher background expression in the absence of doxycycline compared to pSBtet-5. Experiments were carried out 96 h post-transfection. Statistical analysis: one-way ANOVA test with Bonferroni post-test correction (*$P < 0.05$, **$P < 0.01$, ***$P < 0.001$).

($P < 0.01$). Inr-3 contains two CTF/NF1 binding sites that bind to DNA as dimers[28] (Fig. 7A). CTF/NF1 is an enhancer-blocker element which specifically blocks the interaction of other enhancers with the promoter[29]. A general explanation would be that deletion of the CTF/NF1 binding site could increase the interaction of neighbouring enhancers to the TCE promoter, resulting in high background.

The only core promoter element found upstream of the TATA box is B recognition element (BREu). As shown in Fig. 7D,E, removing BREu did not improve the tightness and the basal expression of the TCE promoter ($P > 0.19$) and optimal transcription through the TCE promoter was dependent on the TATA box. However, deleting the BREu site increased the response of the TCE promoter to doxycycline (Fig. 7E, $P < 0.01$).

Discussion

Several strategies have been proposed to reduce the leakiness and enhance the inducibility of Tet-On systems, with only some tested in human cells. Such approaches include: (1) increased expression of rtTA using a strong promoter and codon optimisation[21,30,31], (2) mutation of rtTA to increase binding to doxycycline or DNA[16,20,21,26], (3) autoregulatory systems[7,18,19,32], (4) removing a cryptic splice sites in the rtTA coding region[20], and (5) alteration of the core promoter elements within the proximal region of the TCE promoter [27]. We revisited these strategies for use in the SB-based Tet-On system in a human cell line for future investigation in CAR T cell therapy.

The introduction of a single mutation G72V, gave the optimal induction results at both mRNA and protein level, as reported in *S. cerevisiae*[16]. Future studies may explore the use of a G72P instead of G72V in our system as a candidate amino acid at position G72, though G72P appeared to result in a small loss in sensitivity, as compared to G72V[16]. It is interesting that independent efforts into the rtTA structure have resulted in distinct amino acid changes in different studies, but with similar outcomes. For example, mutations introduced into the rtTA-M2 gene used here are present in distinct positions, as compared to the original four mutations in rtTA[6,20]. Moreover, introducing sensitivity enhancing (SE) mutations[24–26] (V9I, F67S, G72P, F86Y, and R171K) could further increase the sensitivity to doxycycline, without increasing the background, as demonstrated in yeast[16].

Autoregulatory systems have recently generated interest, with both the rtTA and GOI transcribed by a single TCE promoter, using either a bi-directional promoter[19] or an IRES sequence[7,18,32]. However, our constitutive expression of G72V-rtTA gave tighter expression, but was less sensitive to doxycycline compared to the autoregulatory system. The autoregulatory system may be preferred for controllable expression of a toxic rtTA or toxic GOI in mammalian protein production[32–35].

Next, our analysis found evidence of cryptic splice sites within an rtTA, a sequence that was previously optimised for mammalian expression by Urlinger et al.[30] Removing these splice sites reduced the basal expression and further increased the maximal expression. Unfortunately, using the combination of the G72V mutation with all splice sites removed (using predominantly silent, but with two necessarily non-silent, mutations) created a non-responsive system. It appears likely that the combination of the E71Q and G72V mutations disrupted the turn between two critical α-helixes 4 and 5.

It is also noteworthy that different programs identified other possible splice sites that needed to be investigated (Table S4). At least three independent approaches for codon optimisation of rtTA have been reported to enhance Tet-On function[21,30,31]. For example, Urlinger et al. modified the *S. cerevisiae*-developed rtTA-M2 sequence to remove potential hairpin, splice, and endonuclease sites, as well as codon optimising the sequence for use within mammalian systems[21].

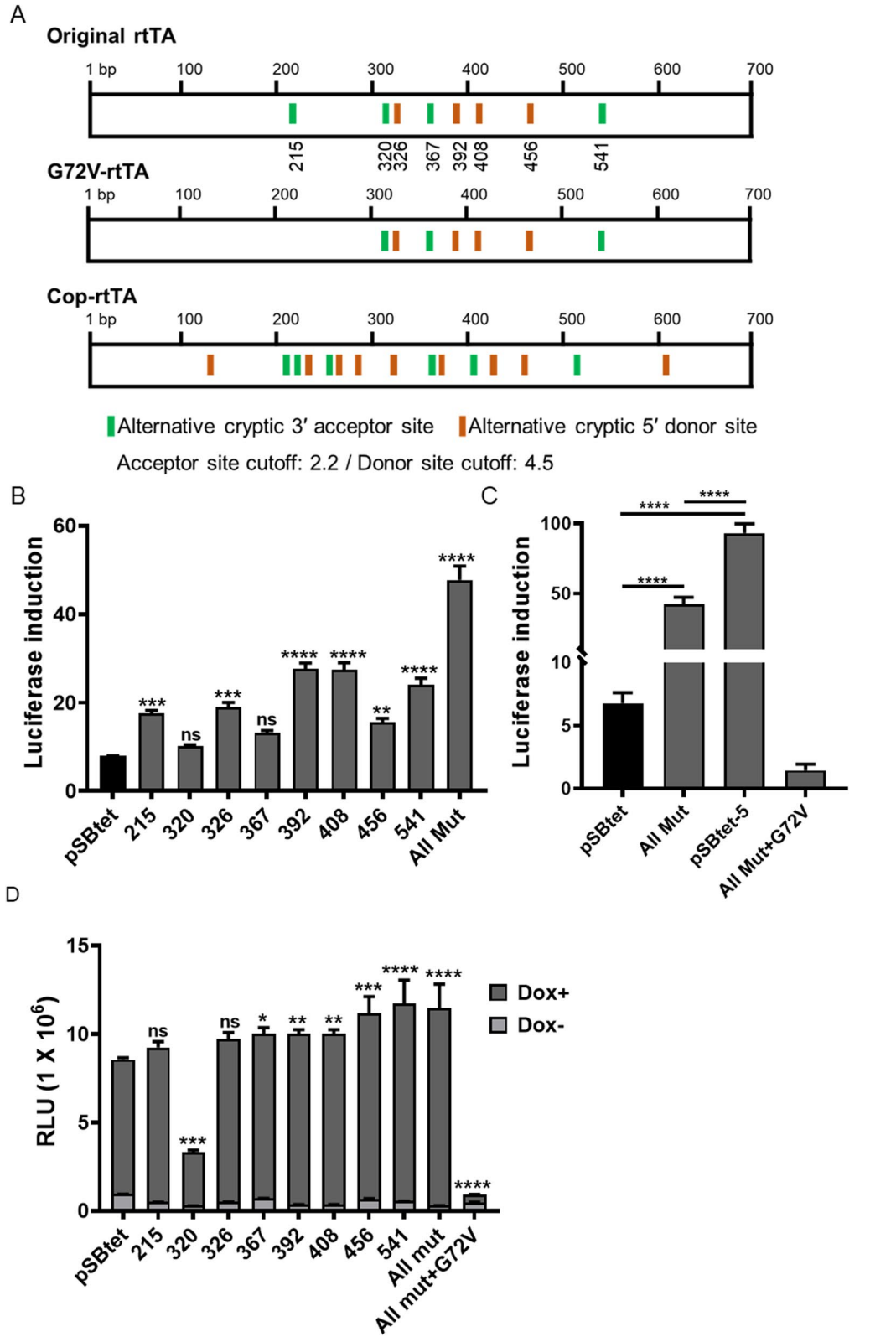

Figure 5. Investigation of potential cryptic splice sites within rtTA. (**A**) Predicted cryptic alternative splice sites within (top): original rtTA-M2, (middle): G72V-rtTA-M2 and (below): commercially codon optimised (cop)-rtTA-M2 using ASSP program. The default cut-off values of the ASSP program was used. The cut-off 2.2 for acceptor sites and 4.5 for donor sites have shown to correctly predict 75 to 80% of cryptic splice sites (Wang M and et al. 2006). (**B**) Removing the eight potential cryptic splice sites alone, or combination of all eight, improved the tightness of Tet-On system. (**C**) Comparison of the fold induction of pSBtet-5 with removing all cryptic splice sites in pSBtet-5. Combining G72V mutation with the eight cryptic splice sites removed, resulted in a non-responsiveness Tet-On system (**D**) Induction of luciferase expression in mutated rtTA-M2 proteins upon doxycycline induction. The missense E107Q mutation at position 320 bp showed lower induction. Experiments were carried out 96 h post-transfection. Statistical analysis: one-way ANOVA test with Bonferroni post-test correction (*P < 0.05, **P < 0.01, ***P < 0.001, ****P < 0.0001).

Name	Type	Original sequence	Mutated sequence	Mutation type
215	Acceptor	CCC CTG GA**A** **G**GC GAG TCA Pro Leu Glu Gly Glu Ser	CCC CTG GA**T** **G**GC GAG TCA Pro Leu Asp Gly Glu Ser	Missense (conservative)
320	Acceptor	CCA AC**A** **G**AG AAA CAG TAC Pro Thr Glu Lys Gln Tyr	CCA AC**A** **C**AA AAA CAG TAC Pro Thr Gln Lys Gln Tyr	Missense (conservative)
326	Donor	CCA ACA GAG AAA CA**G** **T**AC Pro Thr Glu Lys Gln Tyr	CCA ACA GAG AAA CA**A** **T**AC Pro Thr Glu Lys Gln Tyr	Silent
367	Acceptor	TGT C**AG** CAA GGC TTC TCC Cys Gln Gln Gly Phe Ser	TGT CA**A** CAA GGC TTC TCC Cys Gln Gln Gly Phe Ser	Silent
392	Donor	AAC GCA CT**G** **T**AC GCT CTG Asn Ala Leu Tyr Ala Leu	AAC GCA TT**A** **T**AC GCT CTG Asn Ala Leu Tyr Ala Leu	Silent
408	Donor	TCC GCC **GT**G GGC CAC TTT Ser Ala Val Gly His Phe	TCC GCC **AT**C GGC CAC TTT Ser Ala Ile Gly His Phe	Missense (conservative)
456	Donor	GAG CAT CAA **GT**A GCA AAA Glu His Gln Val Ala Lys	GAG CAT CAA **GT**G GCA AAA Glu His Gln Val Ala Lys	Silent
541	Acceptor	GAC CGG C**AG** GGA GCC GAA Asp Arg Gln Gly Ala Glu	GAC CGG C**A**A GGA GCC GAA Asp Arg Gln Gly Ala Glu	Silent

Table 1. Putative cryptic acceptor and donor splice sites within rtTA. Dinucleotide splice sites (AG or GT) are highlighted in bold and mutated sequences are underlined.

In the proximal region of the TCE promoter, we confirmed that the TATA box was essential for the function of the TCE promoter[27]. Removal of the BREu element increased maximal expression, but did not markedly affect the tightness of the TCE. The deletion of the BRE site might enhance the elongation and / or reduce the TFIIB-rtTA sequestration. BRE plays a role in the preinitiation complex (PIC), leading to the dissociation of TFIIB from the promoter which is necessary for RNA polymerase II to initiate the elongation step[36–38]. Hence, interrupting the BRE-TFIIB interaction may enhance transcription via the enhancement of elongation[39]. Alternatively, direct sequestration VP16 on TFIIB has been reported[40,41] that may act to reduce VP16-mediated transcriptional activation.

Collectively, our results demonstrate marked improvements to the rtTA-M2 based Tet-On system in a Sleeping Beauty system through the yeast-optimised G72V mutation. The results especially highlight the necessity to investigate the placement of individual GOI and rtTA within an expression cassette. The use of the clinically relevant CAR cassette within this setting offer the possibility to enhance adoptive cell therapy though drug-inducible expression of cell-survival and memory enhancing genes, or death switches to conditionally ablate CAR T cells following the onset of cytokine release syndrome.

Material and methods

Plasmid construction and cloning. The Tet-On SB (pSBtet-GP) contains the tetracycline-inducible pTIGHT promoter upstream of two asymmetric SfiI sites for cloning genes of interest (GOI), with a downstream RPBSA promoter driving GFP-P2A-rtTA-P2A-puromycin. pSBtet-GP and the SB-transposase vector (pCMV(CAT)T7-SB100) were purchased from Addgene. The pTIGHT promoter is a derivative of (Ptet-14) with shorter spacer (16–17 bp) sequences[27] between the TRE and the minimal CMV promoter (see Fig. 7)[9,27,42]. To generate the modified SB plasmids, a multiple cloning site (MCS) with Bsu36I and BstBI sites was cloned into pSBtet to remove GFP-P2A-rtTA-P2A-puromycin to create pSBtet-MCS. The codon optimised rtTA-M2 gene and FRP5 scFv Her2-CAR[43] were synthesised as gene blocks (IDT Singapore) and cloned into pSBtet MCS to create pSBtet-1. Other plasmids were generated by splicing by overlap extension (SOE) PCR to fuse the original rtTA2S-M2 (rtTA)[9,21], GFP and Her2CAR in different combinations as illustrated in Fig. 1. Mutations into rtTA was introduced using inverse or SOEing PCR. Codon optimised-mouse Mcl-1 (Cop-Mcl-1) was synthetised as a gene block (IDT) with SfiI overhangs to replace the Firefly luciferase gene in the pSB-tet constructs. Both the Mcl-1 and firefly luciferase genes were used as GOI in this study. To modify the core promoters elements (Fig. 5A), the proximal promoter of TCE was PCR amplified from pSBtet and then subcloned into a pUC19 vector (Addgene) using conventional restriction fragment ligation method with EcoRI and NcoI enzymes. Inverse PCR with primers carrying point mutations were used to change the core promoter elements. Finally, each of the modified fragments were PCR amplified from pUC19 and cloned back to pSBtet using PshAI and NcoI restriction sites. To alter the cryptic splice sites within rtTA (Table 1), rtTA was sub-cloned into PUC19 and mutations introduced using inverse PCR.

Bioinformatics analysis. Analysis of the TCE proximal promoter for core promoter elements, including the initiation repeats (Inr1, 2, 3 and 4), TATA box, B recognition element (BRE) site and downstream promoter element (DPE), was carried out using YAPP Eukaryotic Core promoter predictor. TF binding sites were predicted using AliBaba 2.1[44] and PROMO[45,46] programs. The transcriptional start site (TSS) was predicted as reported previously for the minimal CMV promoter[47]. Screening of rtTA for cryptic splice sites was carried out using Alternative Splice Site Predictor (ASSP) software and Human Splicing Finder (HSF)[22,48]. The protein structure of TetR and the prediction of secondary structure were obtained from Protein Data Bank (PBD).

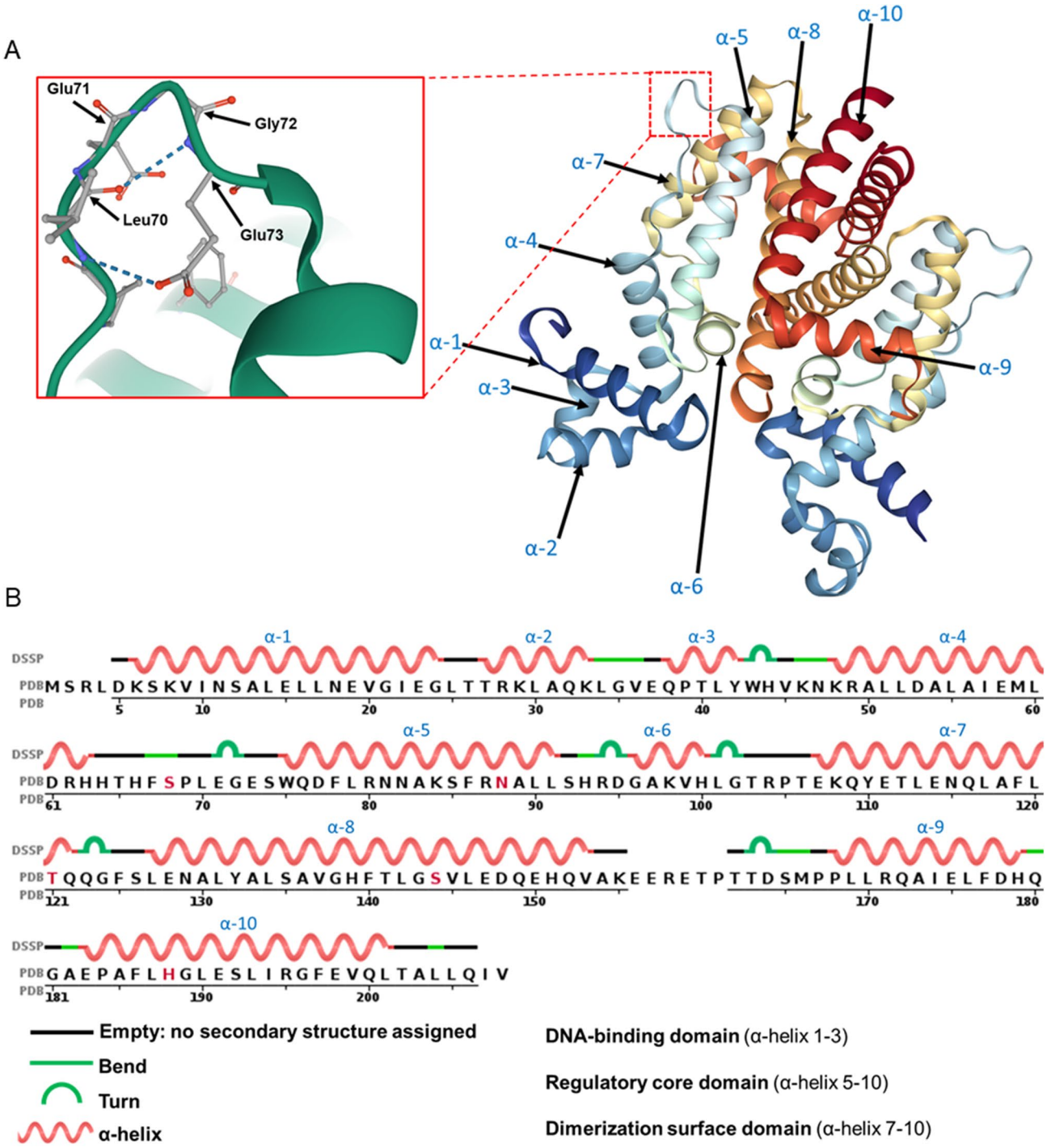

Figure 6. (**A**) Secondary structure of TetR obtained from protein data bank (PBD) with focus on the E71 and G72 (highlighted by red box) that form a turn between α-helix-4 and 5. Mutating both amino acids may cause a conformational change in rtTA. (**B**) Annotation of TetR protein sequence and position of the ten α-helices.

Cell culture and transfection. The human embryonic kidney 293 (HEK293; ATCC CRL-1573) cell line was cultured in high glucose Dulbecco's Modified Essential medium (DMEM) supplemented with tetracycline-free 10% foetal bovine serum (FBS; Pan Biotech), Pen-Strep (100 U/mL penicillin and 100 µg/mL streptomycin) (Gibco) at 37 °C with 5% CO_2. One day prior to transfection, HEK293 cells were cultured in a 24 well plate at 2×10^5 cells/ mL. A ratio of 5:1 (transfer plasmid: transposase) was used to stably transfect HEK293 cell line using Lipofectamine 3,000 (Thermo Fisher) and the medium was replaced at 24 h post transfection. For induction of the TCE promoter, at 72 h post transfection, cells from each well were detached and divided into four wells in a 96-well plate. Two wells were cultured with DMEM containing 5 µg / mL of doxycycline (Sigma), while control wells were maintained with only DMEM, for additional 24 h. Doxycycline-induced and control values for each construct are derived from each independent transfection to eliminate the possibility of different

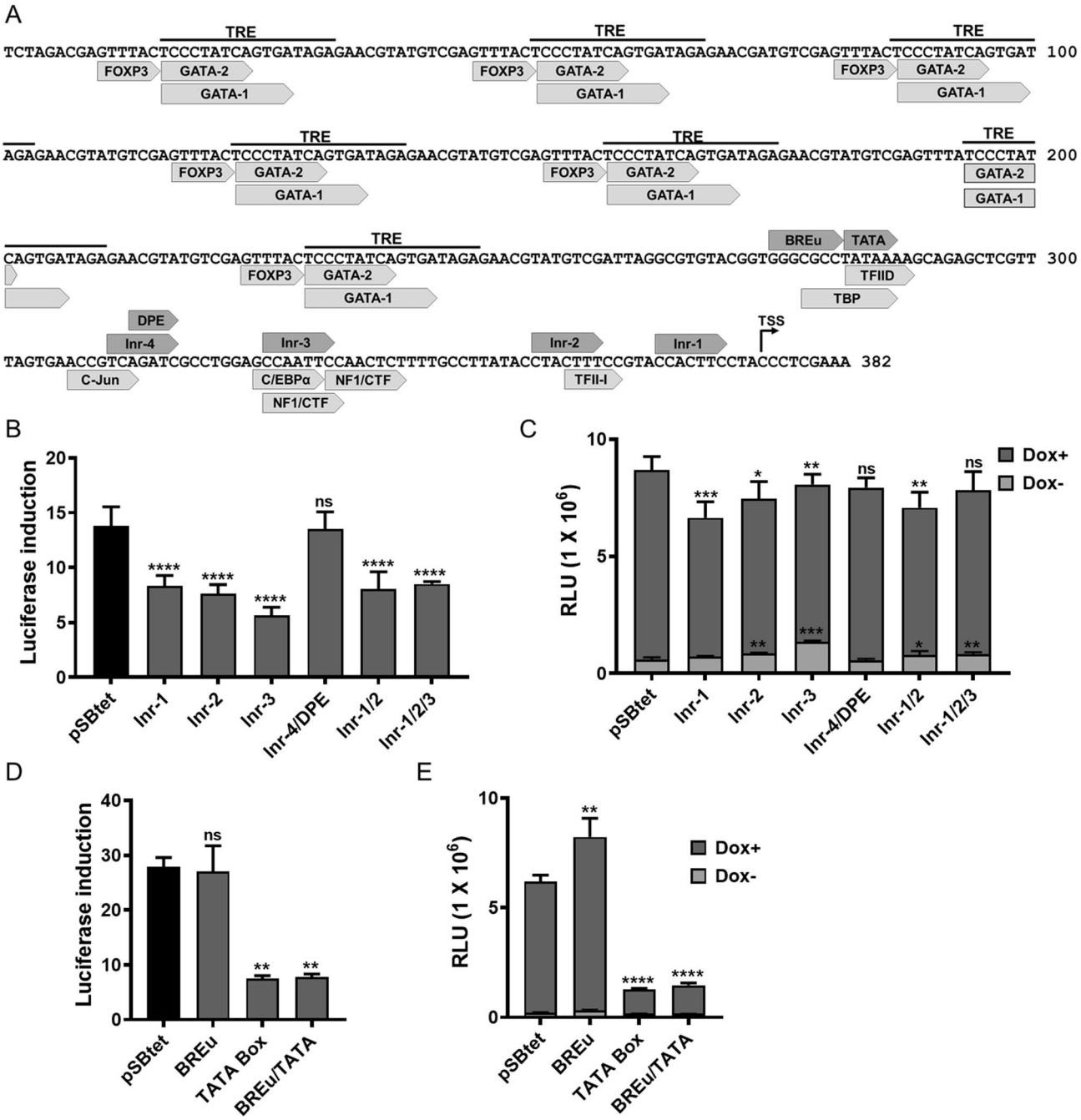

Figure 7. Investigation of core promoter elements in the proximal region of TCE promoter. (**A**) Annotated TCE promoter sequence for core promoter elements and TF binding sites. (**B**, **C**) Deleting elements downstream of TATA box including Inr-1, -2, -3, -4 and DPE in single or combination form increases leaky expression of TCE as well as reduction in TCE promoter induction (**D**, **E**) The effect of removing TATA box and BREu on luciferase induction with or without induction by doxycycline. Removing BREu does not affect the tightness of TCE promoter, whereas TCE showed to be sensitive over loss of TATA box. Only removing BREu improved the inducibility of TCE promoter, without increasing the basal expression. Experiments were carried out 96 h post-transfection. Statistical analysis: one-way ANOVA test with Bonferroni post-test correction (*$P < 0.05$, **$P < 0.01$, ***$P < 0.001$, ****$P < 0.0001$). Inr: initiation repeats; BRE: B recognition element (BRE); DPE: downstream promoter element; TSS: transcriptional start site.

transfection efficiencies between Dox + and Dox- wells. Then, cells were proceed either with qPCR or luciferase assays. For Fig. 3D,E cells were maintained for to two weeks to confirm the consistency of gene-regulation over longer time periods.

RNA extraction, cDNA synthesis and quantitative PCR (qPCR). Total RNA was extracted using NucleoSpin RNA Plus kit (Macherey–Nagel, Germany) and cDNA prepared using PrimeScript RT Reagent Kit (Takara Bio, USA). QPCR was carried out using Luna Universal qPCR Master Mix (NEB) in a ViiA 6 Real-Time PCR (Applied Biosystems, Foster City, CA). The comparative CT ($2^{-\Delta\Delta ct}$) method was used to analyse the relative expression level of cop-Mcl1, by normalising to β-actin. Primers used for the qPCR reactions were: Mcl1-Fwd: GCA GAA TTG TGA CAC TGA TAA G, Mcl1-Rev: TTT TGT TCT AAC CAA TAC ATC G, β-actin-Fwd: CTT CCT TCC TGG GCA TG, β-actin-Rev: GTC TTT GCG GAT GTC CAC.

Reporter assay. Luciferase assays were carried out using Pierce Firefly Luc one-step glow assay kit (ThermoFisher #16197) with cells at 10^5 cells per 100 µL in a 96 well plate. Firefly Luc One-Step Glow assay working solution (100 µL) was added to each well. Cells were incubated at room temperature for one hour before reading with a Varioskan LUX multimode microplate reader (Thermo Fisher, USA). Luciferase data was presented either as relative luminescence units (RLU) or fold change. Fold change was calculated with the following formula:

$$\text{Fold change} = \frac{\text{Luciferase read from cells treated with doxycyline}}{\text{Luciferase read from same cells untreated with doxycycline}}$$

Statistical analysis. All data are presented as mean ± standard deviation (SD) and pooled from three independent experiments. Statistical analysis was performed by two-tailed t-test or one-way ANOVA test with Bonferroni post-test correction in GraphPad prism (version 8). The P values of ≤ 0.05 were considered statistically significant (* $P < 0.05$, ** $P < 0.01$, *** $P < 0.001$, **** $P < 0.0001$). (* $P < 0.05$, ** $P < 0.01$, *** $P < 0.001$, **** $P < 0.0001$).

Received: 23 April 2020; Accepted: 8 July 2020
Published online: 04 August 2020

References

1. Daniel, B., Nagy, G. & Nagy, L. The intriguing complexities of mammalian gene regulation: how to link enhancers to regulated genes. Are we there yet?. *FEBS Lett.* **588**, 2379–2391. https://doi.org/10.1016/j.febslet.2014.05.041 (2014).
2. Gossen, M. *et al.* Transcriptional activation by tetracyclines in mammalian cells. *Science* **268**, 1766–1769 (1995).
3. Bashor, C. J. *et al.* Complex signal processing in synthetic gene circuits using cooperative regulatory assemblies. *Science (New York, N.Y.)* **364**, 593–597 (2019).
4. Haruyama, N., Cho, A. & Kulkarni, A. B. Overview: engineering transgenic constructs and mice. *Curr. Protoc. Cell Biol.* **42**, 19.10. 11-19.10. 19 (2009).
5. Das, A. T., Tenenbaum, L. & Berkhout, B. Tet-on systems for doxycycline-inducible gene expression. *Curr. Gene Ther.* **16**, 156–167 (2016).
6. Berens, C. & Hillen, W. Gene regulation by tetracyclines. Constraints of resistance regulation in bacteria shape TetR for application in eukaryotes. *Eur. J. Biochem.* **270**, 3109–3121. https://doi.org/10.1046/j.1432-1033.2003.03694.x (2003).
7. Markusic, D., Oude-Elferink, R., Das, A. T., Berkhout, B. & Seppen, J. Comparison of single regulated lentiviral vectors with rtTA expression driven by an autoregulatory loop or a constitutive promoter. *Nucl. Acids Res.* **33**, e63–e63 (2005).
8. Ivics, Z., Hackett, P. B., Plasterk, R. H. & Izsvak, Z. Molecular reconstruction of Sleeping Beauty, a Tc1-like transposon from fish, and its transposition in human cells. *Cell* **91**, 501–510. https://doi.org/10.1016/s0092-8674(00)80436-5 (1997).
9. Kowarz, E., Loscher, D. & Marschalek, R. Optimized Sleeping Beauty transposons rapidly generate stable transgenic cell lines. *Biotechnol. J.* **10**, 647–653. https://doi.org/10.1002/biot.201400821 (2015).
10. Vink, C. A. *et al.* Sleeping beauty transposition from nonintegrating lentivirus. *Mol. Ther.* **17**, 1197–1204 (2009).
11. Moldt, B. *et al.* Comparative genomic integration profiling of Sleeping Beauty transposons mobilized with high efficacy from integrase-defective lentiviral vectors in primary human cells. *Mol. Ther.* **19**, 1499–1510. https://doi.org/10.1038/mt.2011.47 (2011).
12. Mates, L. *et al.* Molecular evolution of a novel hyperactive Sleeping Beauty transposase enables robust stable gene transfer in vertebrates. *Nat. Genet.* **41**, 753–761. https://doi.org/10.1038/ng.343 (2009).
13. Geurts, A. M. *et al.* Gene transfer into genomes of human cells by the sleeping beauty transposon system. *Mol. Ther.* **8**, 108–117 (2003).
14. Magnani, C. F. *et al.* Preclinical efficacy and safety of CD19CAR cytokine-induced killer cells transfected with sleeping beauty transposon for the treatment of acute lymphoblastic leukemia. *Hum. Gene Ther.* **29**, 602–613. https://doi.org/10.1089/hum.2017.207 (2018).
15. Bishop, D. C. *et al.* PiggyBac-engineered T cells expressing CD19-specific CARs that lack IgG1 Fc spacers have potent activity against B-ALL xenografts. *Mol. Ther.* **26**, 1883–1895. https://doi.org/10.1016/j.ymthe.2018.05.007 (2018).
16. Roney, I. J., Rudner, A. D., Couture, J. F. & Kaern, M. Improvement of the reverse tetracycline transactivator by single amino acid substitutions that reduce leaky target gene expression to undetectable levels. *Sci. Rep.* **6**, 27697. https://doi.org/10.1038/srep27697 (2016).
17. Kang, K. *et al.* An improved Tet-on system in microRNA overexpression and CRISPR/Cas9-mediated gene editing. *J. Anim. Sci. Biotechnol.* **10**, 43 (2019).
18. Hofmann, A., Nolan, G. P. & Blau, H. M. Rapid retroviral delivery of tetracycline-inducible genes in a single autoregulatory cassette. *Proc. Natl. Acad. Sci.* **93**, 5185–5190 (1996).
19. Yang, T., Burrows, C. & Park, J. H. Development of a doxycycline-inducible lentiviral plasmid with an instant regulatory feature. *Plasmid* **72**, 29–35. https://doi.org/10.1016/j.plasmid.2014.04.001 (2014).
20. Stebbins, M. J. *et al.* Tetracycline-inducible systems for Drosophila. *Proc. Natl. Acad. Sci.* **98**, 10775–10780 (2001).
21. Urlinger, S. *et al.* Exploring the sequence space for tetracycline-dependent transcriptional activators: novel mutations yield expanded range and sensitivity. *Proc. Natl. Acad. Sci. USA* **97**, 7963–7968. https://doi.org/10.1073/pnas.130192197 (2000).
22. Wang, M. & Marín, A. Characterization and prediction of alternative splice sites. *Gene* **366**, 219–227 (2006).
23. Roca, X., Sachidanandam, R. & Krainer, A. R. Determinants of the inherent strength of human 5′ splice sites. *RNA* **11**, 683–698 (2005).

24. Das, A. T. *et al.* Viral evolution as a tool to improve the tetracycline-regulated gene expression system. *J. Biol. Chem.* **279**, 18776–18782 (2004).
25. Hinrichs, W. *et al.* Structure of the Tet repressor-tetracycline complex and regulation of antibiotic resistance. *Science (New York, N.Y.)* **264**, 418–420 (1994).
26. Zhou, X., Vink, M., Klaver, B., Berkhout, B. & Das, A. Optimization of the Tet-On system for regulated gene expression through viral evolution. *Gene Ther.* **13**, 1382–1390 (2006).
27. Agha-Mohammadi, S. *et al.* Second-generation tetracycline-regulatable promoter: repositioned Tet operator elements optimize transactivator synergy while shorter minimal promoter offers tight basal leakiness. *J. Gene Med.* **6**, 817–828. https://doi.org/10.1002/jgm.566 (2004).
28. Gronostajski, R. M. Roles of the NFI/CTF gene family in transcription and development. *Gene* **249**, 31–45 (2000).
29. Gaussin, A. *et al.* CTF/NF1 transcription factors act as potent genetic insulators for integrating gene transfer vectors. *Gene Ther.* **19**, 15–24 (2012).
30. Valencik, M. L. & McDonald, J. A. Codon optimization markedly improves doxycycline regulated gene expression in the mouse heart. *Transgenic Res.* **10**, 269–275 (2001).
31. Wells, K. D., Foster, J. A., Moore, K., Pursel, V. G. & Wall, R. J. Codon optimization, genetic insulation, and an rtTA reporter improve performance of the tetracycline switch. *Transgenic Res.* **8**, 371–382 (1999).
32. Anastassiadis, K. *et al.* A predictable ligand regulated expression strategy for stably integrated transgenes in mammalian cells in culture. *Gene* **298**, 159–172 (2002).
33. Balasubramanian, S. *et al.* Rapid recombinant protein production from piggyBac transposon-mediated stable CHO cell pools. *J. Biotechnol.* **200**, 61–69 (2015).
34. Barnes, L. M., Bentley, C. M. & Dickson, A. J. Characterization of the stability of recombinant protein production in the GS-NS0 expression system. *Biotechnol. Bioeng.* **73**, 261–270 (2001).
35. Massie, B. *et al.* Inducible overexpression of a toxic protein by an adenovirus vector with a tetracycline-regulatable expression cassette. *J. Virol.* **72**, 2289–2296 (1998).
36. Roberts, S. G., Choy, B., Walker, S. S., Lin, Y.-S. & Green, M. R. A role for activator-mediated TFIIB recruitment in diverse aspects of transcriptional regulation. *Curr. Biol.* **5**, 508–516 (1995).
37. Zawel, L., Kumar, K. P. & Reinberg, D. Recycling of the general transcription factors during RNA polymerase II transcription. *Genes Dev.* **9**, 1479–1490 (1995).
38. Buratowski, S. & Zhou, H. Functional domains of transcription factor TFIIB. *Proc. Natl. Acad. Sci.* **90**, 5633–5637 (1993).
39. Evans, R., Fairley, J. A. & Roberts, S. G. Activator-mediated disruption of sequence-specific DNA contacts by the general transcription factor TFIIB. *Genes Dev.* **15**, 2945–2949. https://doi.org/10.1101/gad.206901 (2001).
40. Roberts, S. G., Ha, I., Maldonado, E., Reinberg, D. & Green, M. R. Interaction between an acidic activator and transcription factor TFIIB is required for transcriptional activation. *Nature* **363**, 741–744 (1993).
41. Hori, R., Pyo, S. & Carey, M. Protease footprinting reveals a surface on transcription factor TFIIB that serves as an interface for activators and coactivators. *Proc. Natl. Acad. Sci.* **92**, 6047–6051 (1995).
42. Loew, R., Heinz, N., Hampf, M., Bujard, H. & Gossen, M. Improved Tet-responsive promoters with minimized background expression. *BMC Biotechnol.* **10**, 81. https://doi.org/10.1186/1472-6750-10-81 (2010).
43. Schonfeld, K. *et al.* Selective inhibition of tumor growth by clonal NK cells expressing an ErbB2/HER2-specific chimeric antigen receptor. *Mol. Ther.* **23**, 330–338. https://doi.org/10.1038/mt.2014.219 (2015).
44. Grabe, N. AliBaba2: context specific identification of transcription factor binding sites. *In Silico Biol.* **2**, S1–S15 (2002).
45. Farré, D. *et al.* Identification of patterns in biological sequences at the ALGGEN server: PROMO and MALGEN. *Nucl. Acids Res.* **31**, 3651–3653 (2003).
46. Messeguer, X. *et al.* PROMO: detection of known transcription regulatory elements using species-tailored searches. *Bioinformatics* **18**, 333–334 (2002).
47. Even, D. Y. *et al.* Engineered promoters for potent transient overexpression. *PLoS ONE* **11**, 1–19 (2016).
48. Desmet, F.-O. *et al.* Human Splicing Finder: an online bioinformatics tool to predict splicing signals. *Nucl. Acids Res.* **37**, e67–e67 (2009).

Acknowledgements

We thank Dr. Sarah Saunderson for critical reading of the manuscript.

Author contributions

A.R. and A.M. wrote the paper and supervised the study. A.R. contributed to experimental data in all figures, prepared the figures, tables and performed the bioinformatics analysis. G.T. and A.P. performed experiments.

Competing interests

The authors declare no competing interests.

Additional information

Supplementary information is available for this paper at https://doi.org/10.1038/s41598-020-70022-0.

Correspondence and requests for materials should be addressed to A.D.M.

Reprints and permissions information is available at www.nature.com/reprints.

Publisher's note Springer Nature remains neutral with regard to jurisdictional claims in published maps and institutional affiliations.

Optimisation of Tet-On inducible systems for Sleeping Beauty-based chimeric antigen receptor (CAR) applications

Ali Hosseini Rad SM¶, Aarati Poudel¶, Grace Min Yi Tan¶ and Alexander D. McLellan*

¶ These authors contributed equally to this work.

Department of Microbiology and Immunology, University of Otago, Dunedin 9010, Otago, New Zealand.

*To whom correspondence should be addressed: Alexander D. McLellan Department of Microbiology and Immunology, University of Otago, Dunedin 9010, Otago, New Zealand; alex.mclellan@otago.ac.nz.

Table S1. Potential cryptic alternative splice sites within rtTA coding region by ASSP program.

Position	Splice site type	Sequence	Score*	Confidence**
215	Acceptor	cccctggaagGCGAGTCATG	3.637	0.768
320	Acceptor	cgcccaacagAGAAACAGTA	2.567	0.552
326	Donor	CAGAGAAACAgtacgaaacc	6.389	0.894
367	Acceptor	cctgtgtcagCAAGGCTTCT	3.704	0.849
392	Donor	AGAACGCACTgtacgctctg	4.895	0.919
408	Donor	TCTGTCCGCCgtgggccact	5.697	0.609
456	Donor	GGAGCATCAAgtagcaaaag	5.673	0.903
541	Acceptor	cgaccggcagGGAGCCGAAC	5.154	0.858

Table S2. Potential cryptic alternative splice sites within G72V-rtTA coding region by ASSP program.

Position	Splice site type	Sequence	Score*	Confidence*
320	Acceptor	cgcccaacagAGAAACAGTA	2.567	0.552
326	Donor	CAGAGAAACAgtacgaaacc	6.389	0.894
367	Acceptor	cctgtgtcagCAAGGCTTCT	3.704	0.849
392	Donor	AGAACGCACTgtacgctctg	4.895	0.919
408	Donor	TCTGTCCGCCgtgggccact	5.697	0.609
456	Donor	GGAGCATCAAgtagcaaaag	5.673	0.903
541	Acceptor	cgaccggcagGGAGCCGAAC	5.154	0.858

Table S3. Potential cryptic alternative splice sites within Cop-rtTA coding region by ASSP program.

Position	Splice site type	Sequence	Score*	Confidence*
132	Donor	GTACTGGCATgtaaaaaaca	5.127	0.917
214	Acceptor	tcccttggagGGAGAAAGTT	3.729	0.612
240	Acceptor	atttcctcagGAATAACGCC	3.586	0.352
260	Donor	AGAGTTTTAGgtgtgcgctc	8.709	0.966
282	Acceptor	tgtctcacagAGATGGTGCG	8.920	0.112
286	Donor	CACAGAGATGgtgcgaaggt	6.777	0.911
294	Donor	TGGTGCGAAGgttcacttgg	4.538	0.936
326	Donor	CCGAGAAACAgtatgaaacc	6.194	0.951
367	Acceptor	cctgtgccagCAAGGTTTCT	3.470	0.807
370	Donor	TGCCAGCAAGgtttctcact	5.293	0.863
407	Acceptor	gcactctcagCCGTTGGTCA	3.323	0.932

428	Donor	TTACTCTCGGgtgcgtcctc	7.722	0.959
456	Donor	GGAACATCAGgtggctaaag	7.849	0.871
517	Acceptor	gcttcgccagGCCATTGAAC	6.456	0.275
605	Donor	AGCAATTGAAgtgtgagagt	5.391	0.896
607	Donor	CAATTGAAGTgtgagagtgg	8.156	0.832

***** Score reflects splice site strength and ranges between one to ten.

****** Confidence reflects the probable occurrence of splicing and ranges between zero to one.

Table S4. Potential splice sites within rtTA coding region predicted by Human Splice Finder (HSF) program.

Position	Splice site type	Sequence	Consensus value (0-100)
7	Acceptor	agactggacaagAG	65.22
9	Acceptor	actggacaagagCA	67.25
22	Donor	AAAgtcata	68.79
47	Acceptor	tactcaatggagTC	73.33
55	Donor	GGAgtcggt	69.44
59	Acceptor	tcggtatcgaagGC	76.38
59	Donor	TCGgtatcg	70.52
72	Acceptor	cctgacgacaagGA	73.99
88	Acceptor	ctcgctcaaaagCT	76.86
100	Acceptor	ctgggagttgagCA	68.08
103	Acceptor	ggagttgagcagCC	73.18
104	Donor	GAGttgagc	68.07
127	Acceptor	tggcacgtgaagAA	72.07
130	Donor	CACgtgaag	73.73
163	Acceptor	ctgccaatcgagAT	75.06
174	Acceptor	gatgctggacagGC	80.9
199	Acceptor	ttctgccccctgGA	66.14
203	Acceptor	gccccctggaagGC	77.96
212	Donor	AAGgcgagt	71.05
216	Donor	CGAgtcatg	65.29
218	Acceptor	agtcatggcaagAC	68.31
222	Donor	ATGgcaaga	65.13
241	Acceptor	aacaacgccaagTC	67.3
249	Donor	CAAgtcatt	72.08
284	Acceptor	acggggctaaagTG	68.62
292	Donor	AAAgtgcat	66.34
308	Acceptor	cccgcccaacagAG	85.25
310	Acceptor	cgcccaacagagAA	71.56
316	Acceptor	acagagaaacagTA	70.69
324	Donor	ACAgtacga	72.58
337	Acceptor	ctggaaaatcagCT	75.6
355	Acceptor	ttcctgtgtcagCA	85.01
359	Acceptor	tgtgtcagcaagGC	75.35
359	Donor	TGTgtcagc	75.1
373	Acceptor	ttctccctggagAA	84.47
390	Donor	ACTgtacgc	72.45
399	Donor	TCTgtccgc	66.4

406	Donor	GCCgtgggc	70.8
430	Acceptor	tgcgtattggagGA	77.01
436	Acceptor	ttggaggaacagGA	80.23
446	Acceptor	aggagcatcaagTA	66.28
449	Acceptor	agcatcaagtagCA	68.24
454	Donor	CAAgtagca	66.73
455	Acceptor	aagtagcaaaagAG	67.2
457	Acceptor	agactggacaagAG	65.22
466	Donor	GAGgaaaga	69.07
501	Acceptor	cccacttctgagAC	76.08
506	Acceptor	ttctgagacaagCA	72.82
514	Acceptor	caagcaattgagCT	67.43
525	Donor	GCTgttcga	66.46
529	Acceptor	ttcgaccggcagGG	88.74
533	Acceptor	accggcagggagCC	65.49
583	Acceptor	tgtggcctggagAA	75.88
589	Acceptor	ctggagaaacagCT	75.66
595	Acceptor	aaacagctaaagTG	68.29
603	Donor	AAAgtgcga	76.17
641	Acceptor	attttgacttagAC	76.79
653	Acceptor	acatgctcccagCC	82.52

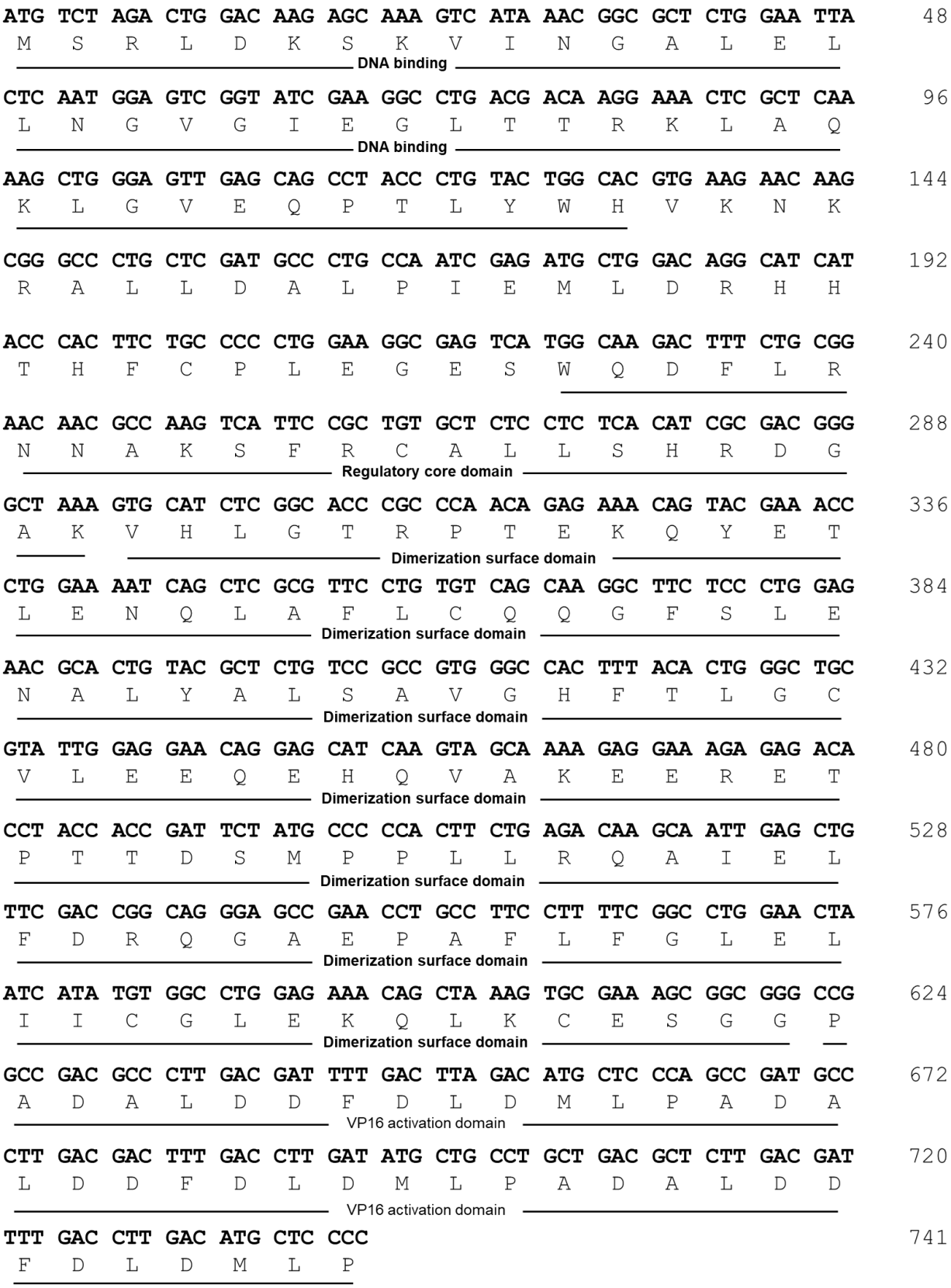

Figure S1. The whole rtTA sequence with translation and position of each domain.

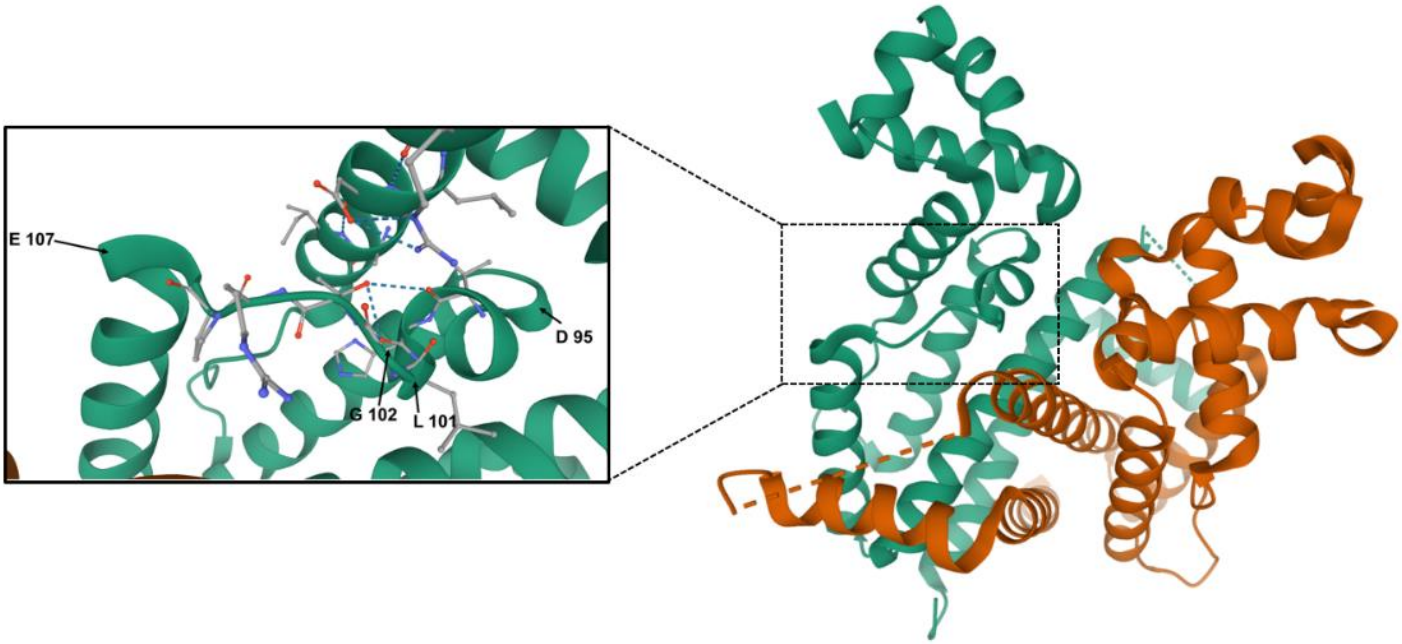

Figure S2. Secondary structure of TetR with focus on the high sensitivity region comprising D95, L101 and G102. Modifying the splice site at nucleotide 320 (E107) resulted in a conformational change that decreased TCE-induction upon doxycycline treatment.

Chapter IV

Functional analysis of promoters for driving long RNA transcripts in CAR T cells

In this chapter, using a series of experiments, we tested the strength of four commonly used promoters, EF-1, CMV, RPBSA, and hPGK, in running short and long transcripts. EF-1 was shown to be the best promoter in running short and long RNA in T cells. As a result, we chose EF-1 to run the GFP-P2A-Her2CAR and hPGK to transcribe Mcl-1 or miR429 in our next experiments.

Author contributions:

AR and AM conceived of and supervised the study, and wrote the paper and carried out the revisions. AR carried out experiments in all figures. AP and GT contributed to analysis and edited the first draft.

PLOS ONE

RESEARCH ARTICLE

Promoter choice: Who should drive the CAR in T cells?

**Ali Hosseini Rad S. M.*, Aarati Poudel☯, Grace Min Yi Tan☯, Alexander D. McLellan*

Department of Microbiology and Immunology, University of Otago, Dunedin, New Zealand

☯ These authors contributed equally to this work.
* a.hosseini.rad@postgrad.otago.ac.nz (RSMAH); alex.mclellan@otago.ac.nz (ADM)

OPEN ACCESS

Citation: Rad S. M. AH, Poudel A, Tan GMY, McLellan AD (2020) Promoter choice: Who should drive the CAR in T cells? PLoS ONE 15(7): e0232915. https://doi.org/10.1371/journal.pone.0232915

Editor: Joe W. Ramos, University of Hawai'i at Manoa, UNITED STATES

Received: April 22, 2020

Accepted: July 7, 2020

Published: July 24, 2020

Data Availability Statement: All relevant data are within the paper and its Supporting Information files.

Funding: This study was funded by The Cancer Society New Zealand (19.11) and The University of Otago Research Grant Committee (2019). ADM and AR received salary support from the Royal Society Marsden fund 18-UOO-188. The funders had no role in study design, data collection and analysis, decision to publish, or preparation of the manuscript.

Abstract

Chimeric antigen receptor (CAR) T cell therapy is an effective treatment for B cell malignancies, with emerging potential for the treatment of other hematologic cancers and solid tumors. The strength of the promoter within the CAR cassette will alter CAR-polypeptide levels on the cell surface of the T cell–impacting on the kinetics of activation, survival and memory cell formation in T cells. In addition to the CAR, promoters can be used to drive other genes of interest to enhance CAR T cell function. Expressing multiple genes from a single RNA transcript can be effectively achieved by linking the genes via a ribosomal skip site. However, promoters may differ in their ability to transcribe longer RNAs, or could interfere with lentiviral production, or transduction frequencies. In this study we compared the ability of the strong well-characterized promoters CMV, EF-1, hPGK and RPBSA to drive functional expression of a single RNA encoding three products: GFP, CAR, plus an additional cell-survival gene, Mcl-1. Although the four promoters produced similarly high lentiviral titres, EF-1 gave the best transduction efficacy of primary T cells. Major differences were found in the ability of the promoters to drive expression of long RNA encoding GFP, CAR and Mcl-1, highlighting promoter choice as an important consideration for gene therapy applications requiring the expression of long and complex mRNA.

Introduction

Promoters are of critical importance for expressing optimal levels of the transgene in CAR T cells for the production of functional proteins or non-coding RNA [1–5]. It is also clear that high expression of the CAR can result in antigen-independent CAR signaling, resulting in T cell exhaustion and sub-optimal anti-tumor responses, or lead to the inappropriate recognition of tumor antigen on self-tissue [1, 2]. In addition, controlling CAR T cell signaling is critical for proper memory cell formation [6]. Because surface expression of the CAR may be limited by mRNA levels, the choice of promoter is critical [1, 2].

There have been limited studies that directly compare the efficiency of different promoters for driving long mRNA comprising multiple genes within CAR T cells [1, 2, 7]. Recent studies investigating promoter performance in mouse or human T cells were usually limited to either the CAR, a single gene of interest alone, or single fluorescent reporter genes of limited size [1,

Competing interests: Authors have no competing interests

2, 7–9]. For the generation of lentiviral particles for transduction, using multiple internal promoters or internal ribosome entry sites (IRES) for multiple genes may interfere with transcription or reverse transcription of viral genomic RNA (vgRNA), impacting upon lentiviral particle titre, and/or on the efficiency of integration into the target cell [8, 10]. Therefore, strategies that employ single promoters to drive multiple genes may be preferred for CAR T cell engineering [9].

Although all current, clinically-approved second and third generation CAR T cells rely on the expression of a single gene encoding a single polypeptide, it may be advantageous to express longer RNA containing the CAR, together with one or more genes of interest. For example, endogenous growth factors or membrane bound or secreted cytokines could improve T cell expansion and survival [6, 11]. Alternatively, markers of transduction efficiency or death switches could be incorporated into the CAR element [4, 12–14]. Promoter choice for such applications is crucial to obtain optimised gene expression of multiple, linked genes.

Because requirements for driving short versus long RNA might be distinct in CAR T cell genetic elements, we investigated the ability of several promoters to drive an extended downstream genetic sequence comprised of GFP, anti-Her2-CAR and an additional cell survival gene Myeloid leukemia cell differentiation protein (Mcl-1), an anti-apoptotic Bcl2 family member. Mcl-1 aids in T cell development, mitochondrial function and lifespan and appears to a suitable candidate for enhancing CAR T cell performance [15, 16]. Mcl-1 inhibits the action of pro-apoptotic BIM / BAK / BAX at the mitochondrial membrane and is expressed throughout T cell differentiation and is essential for memory T cell formation [16–20].

The individual elements were tested at protein level and for functional activity. The results demonstrated clear differences in the ability of these internal promoters to drive expression of multiple CAR-cassette associated transgenes.

Material and methods

Plasmid construction

The third-generation lentiviral vector pCCLsin.cPPT.hPGK.GFP.WPRE (pCCLsin) and VSV-G-based packaging plasmids were a kind gift from Prof. Dr. Naldini and have been described elsewhere [21]. The anti-Her-2 CAR FRP5, anti-CD19 CAR FMC63 (with–EQKLISEEDL–c-myc tag between scFv and CD8 hinge) and codon-optimized human Mcl-1 (cop-Mcl-1) were synthesized as gene blocks (IDT Technologies). Both CAR constructs are second generation CAR with CD28 costimulatory domains (Fig 1A). Sap I Type IIs restriction enzyme cloning was utilized for scarless assembly of the eGFP-P2A-CAR-P2A-Mcl-1. This cassette was then cloned into the BamHI and SalI sites of the pCCLsin (Fig 1A). Promoters were amplified with 5' EcoRV and 3' BamHI sites from respective plasmids: CMV from pcDNA3.1(-), EF-1 from Sleeping Beauty (pSBbiRP) and RPBSA from Sleeping Beauty (pSBtet-GP) and ligated upstream of the GFP-CAR-mcl1 cassette. Codon optimized Leucine Zipper CD95 (LZ-CD95L) gene was synthesized by IDT with EcoRI and BamHI sites and cloned into pcDNA3.1(-) (Addgene #104349).

Cell culture

Cell lines were cultured in a humidified atmosphere at 37˚C, 5% CO_2 (or with 8% CO_2 for LV-Max and Expi293F). Human embryonic kidney 293T (ATCC CRL-1573) and MCF-7 (ATCC HTB-22) cell lines were cultured in high glucose Dulbecco's Modified Essential medium (DMEM) supplemented with 10% fetal bovine serum (FBS; Pan-Biotech GmbH), penicillin (100 U/mL) and streptomycin (100 μg/mL) (Gibco). MCF-7 and HEK293T cells were transfected using Lipofectamine 3000 according to manufacturer's protocol. Human

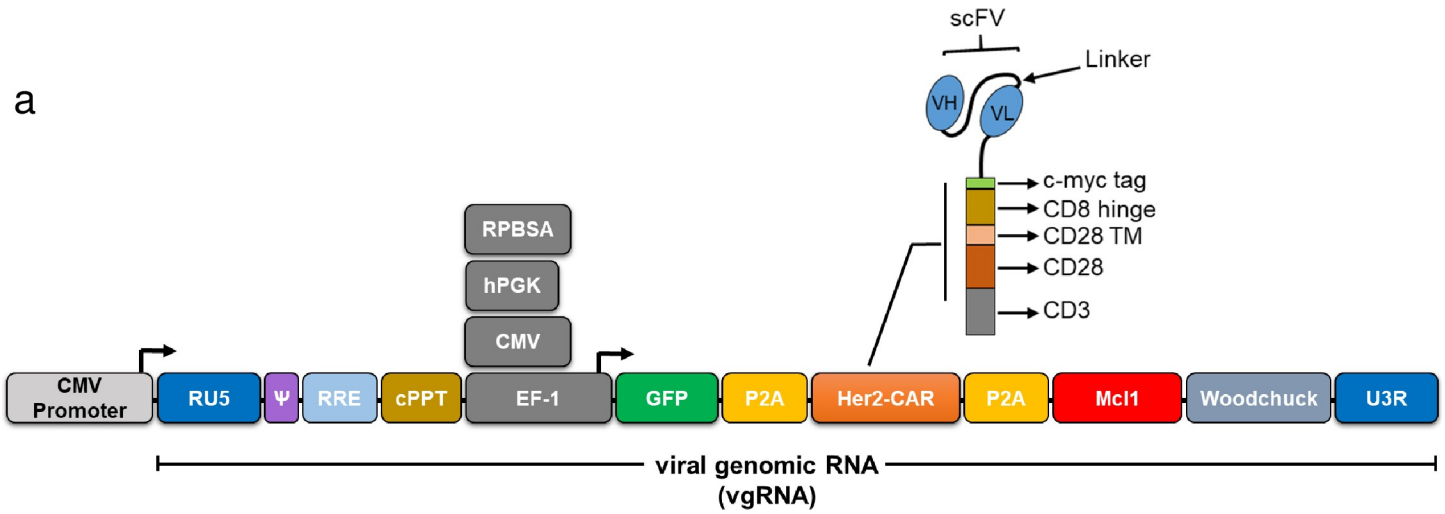
a
scFV
Linker
VH
VL
c-myc tag
CD8 hinge
CD28 TM
CD28
CD3
RPBSA
hPGK
CMV
CMV Promoter
RU5
Ψ
RRE
cPPT
EF-1
GFP
P2A
Her2-CAR
P2A
Mcl1
Woodchuck
U3R
viral genomic RNA
(vgRNA)

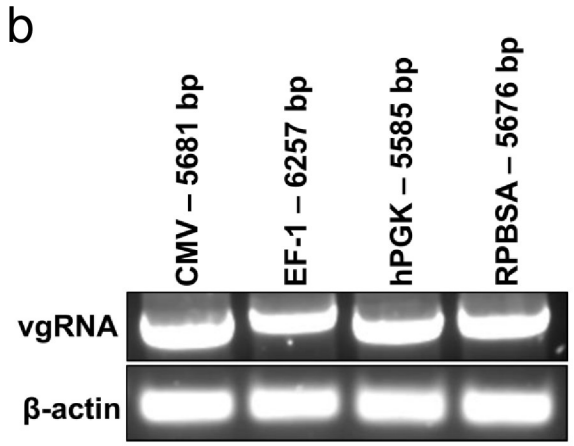
b
CMV – 5681 bp
EF-1 – 6257 bp
hPGK – 5585 bp
RPBSA – 5676 bp
vgRNA
β-actin

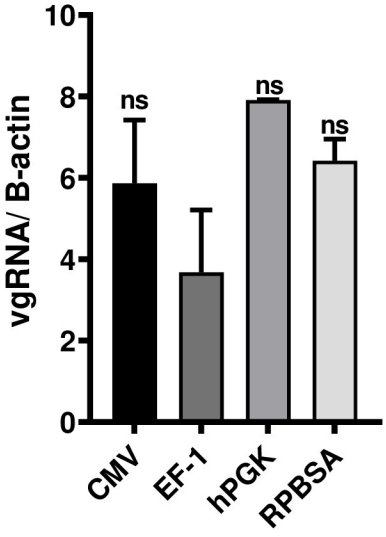
vgRNA/ B-actin
10
8
6
4
2
0
ns
ns
ns
CMV
EF-1
hPGK
RPBSA

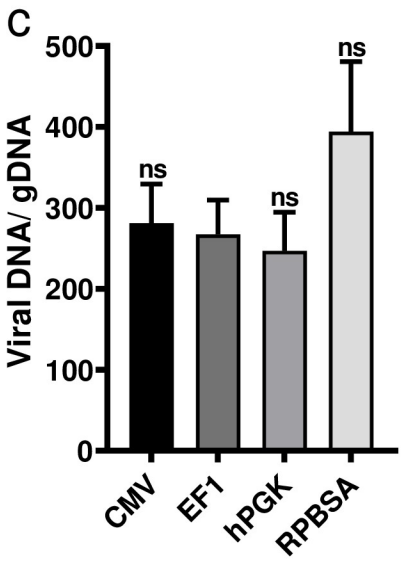
c
Viral DNA/ gDNA
500
400
300
200
100
0
ns
ns
ns
CMV
EF1
hPGK
RPBSA

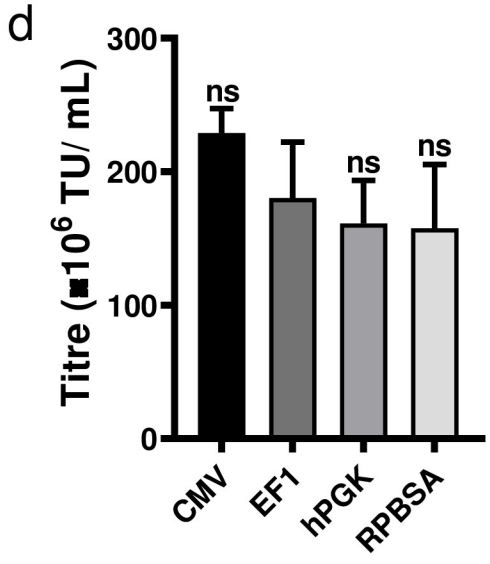
d
Titre (■10^6 TU/ mL)
300
200
100
0
ns
ns
ns
CMV
EF1
hPGK
RPBSA

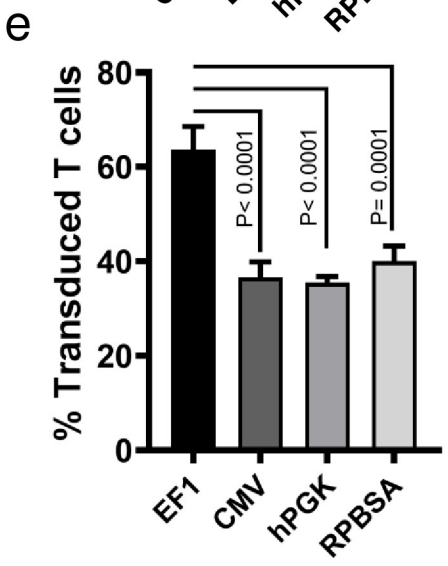
e
% Transduced T cells
80
60
40
20
0
P< 0.0001
P< 0.0001
P= 0.0001
EF1
CMV
hPGK
RPBSA

Fig 1. The effect of internal promoters in producing functional lentiviral particles. (a) Schematic illustration of the pCCLsin backbone bearing four different internal promoters (CMV, EF-1, hPGK and RPBSA) for driving a long RNA consist of GFP-P2A-Her2CAR-P2A-Mcl-1, (b) HEK293T cells were transfected with lentiviral constructs containing different promoters along with packaging plasmids. At 24 h post transfection, total RNA was extracted and 1 μg of RNA was converted to cDNA. PCR was carried out using specific primers binding to PPT and woodchuck region. Agarose gel electrophoresis displays the PCR product band of each construct. Lower band displays the PCR product of β-actin serving as a loading control. The ratio between viral genomic RNA (vgRNA) to β-actin was quantified and presented in the bar graph (right) using Image Studio Lite. There was no statistically significant difference between promoters ($P>0.05$). (c) Shows the ratio between integrated viral cassettes to gDNA 48 h post-transduction. Genomic DNA was extracted from cell lysates and qPCR was performed using Gag for integrated lentivirus and β2 microglobulin and β-actin as a housekeeping genes for host gDNA quantification. There was no statistically significant difference between promoters ($P>0.05$). (d) Comparison of the viral particle titration of four different constructs through analysis of the percent GFP expression in HEK293T cells using flow cytometry. Bar graph values represent the titre unit/mL (TU/mL) from three independent repeats. There was no statistically significant difference between promoters ($P>0.05$). (e) Transduction efficiency of primary T cells for the four lentivectors. CD3 / CD28 stimulated human primary T cells were transduced at MOI 40 and cells were analyzed for GFP expression at 72 h post-transduction by flow cytometry. A representative experiment, and all GFP MFI values relating to graph, are presented in Fig 3A. Dead cells were excluded with Zombie NIR viability dye gating at analysis. Bar graph values represent the mean values ± SD from three independent repeats. scFv; single-chain variable fragment, VH; variable heavy chain, VL; variable light chain, TM; transmembrane domain.

https://doi.org/10.1371/journal.pone.0232915.g001

peripheral blood mononuclear cells (PBMC) were isolated from healthy donors. The University of Otago Human Ethics Committee (Health; Ethics Approval# H18/089) approved this study and written consent was obtained from blood donors. Frozen PBMCs were thawed and then rested overnight in T cell expansion media (Thermofisher #A1048501) supplemented with 50 U/mL of hIL-2 (Peprotech, #200–02), L-glutamine and 10 U/mL penicillin and streptomycin (Gibco), prior to CD4 and CD8 T cells isolation using EasySep Human T cell isolation kit (STEMCELL Technology, #17951). Isolated T cells were activated with Dynabeads Human T-Activator CD3/CD28 (Thermo Fisher, #111.32D).

Lentiviral production, titration and T cell transduction

Lentiviral production and titration were carried out using LV-Max Viral production system (ThermoFisher #A35684) according to manufacturer's protocol. HEK293T cells were transduced at MOI 2:1 with 8 μg/mL of polybrene (Sigma-Aldrich). One day before T cell transduction, plates were coated with 40 μg/mL retronectin (TAKARA, #T100A/B) overnight at 4˚C, blocked with 2% FBS/PBS for 15 min, before adding LV at 40:1 MOI to the plate; followed by centrifugation at 800 ×g for 2.5 h at room temperature. After 48 h of activation with a 1:1 ratio of CD3/CD28 Dynabeads, T cells were added to virus-coated wells and spinoculation carried out at 500 ×g for 5 min. The next day, T cells were debeaded and cultured in media plus 50 U/mL of hIL-2. Media was changed with fresh medium supplemented with 50 U/mL hIL-2 every three days.

RNA extraction, long cDNA synthesis and RT-PCR

Total cellular RNA (containing viral genomic RNA) was extracted 48 h after transfection using NucleoSpin RNA Plus kit (Macherey-Nagel, Germany) according to the manufacturer's protocol. Then RNA was reverse transcribed using PrimeScript™ RT Reagent Kit (Takara Bio, USA) according to manufacturer's protocol RT-PCR was performed using internal primers PPT-Fwd: `GGGTACAGTGCAGGGGAAAG` and Woodchuck-Rev: `AAGCAGCGTATCCACATAGCG` for comparison with β-actin Fwd: `CTTCCTTCCTGGGCATG` and β-actin-Rev: `GTCTTTGCGGA TGTCCAC`.

Quantification of gDNA/ integrated viral DNA ratio

At 48 h post transduction, integrated lentiviral DNA was quantified by extracting genomic DNA using Qiamp DNA Mini kit (Qiagen, Germany) and the ratio of viral genome: human gDNA were estimated using qPCR via Luna Universal qPCR Master Mix (New England Biolabs) using designed primers Gag-Fwd: `GGA GCT AGA ACG ATT CGC AGT TA`, Gag-Rev:

GGT TGT AGC TGT CCC AGT ATT TG TC, PBS-Fwd: TCT CGA CGC AGG ACT CG; PBS-Rev: TAC TGA CGC TCT CGC ACC, and β-actin forward and reverse primers described above. All reactions were run in triplicate and were presented as mean ± SD.

Western blot

Cell lysates were prepared using RIPA lysis buffer and blotting carried out using mouse monoclonal anti-EGFP antibody (Abcam, #ab184601), rabbit anti-human Mcl-1 (Abcam, #ab28147), biotin anti-c-myc (Biolegend #908805). Mouse monoclonal β-actin primary antibody (Sigma-Aldrich #A2228) was used as loading control. goat anti-mouse IgG DyLight 680 (Thermo Fisher #A3274), goat anti-rabbit IgG 800, streptavidin-800 in 1:10000 dilution as secondary antibody (#A32730 and # A32735). The membrane was scanned using an Odyssey Fc imaging system (Licor, Germany) and analyzed using Image Studio Lite software.

Mitochondrial membrane potential assay (TMRE)

Transduced T cells were incubated overnight with 1 μg/mL LZ-CD95L, then 4 μM TMRE (Invitrogen) was added at 37˚C for 30 min. DAPI (50 ng /mL) was added immediately prior to flow cytometric analysis and GFP positive cells electronically gated for quantification of TMRE and DAPI signals using the YG586/16 and BV421 channels.

Cytotoxicity and cytokine release assay

Luciferase-based cytotoxicity assay was carried out for Her2 and CD19 CAR T cells as previously described [22] at a 10:1 ratio of effector to target cells of using Firefly Luc One-Step Glow assay (Thermo Fisher #16197). For analysis of cytokine release, CAR T cells were added to target cells in a 2:1 ratio. IL-2 and IFN-γ concentration secreted in cell supernatant were measured using sandwich ELISA according to manufacturer's protocol (BD Biosciences, USA). Plates were read on a Varioskan Lux multimode microplate reader (Thermo Fisher, USA).

Flow cytometry

CAR T cells were stained with biotin anti-c-myc antibody (Biolegend #908805) detected with Streptavidin-Brilliant Violet 421 (Biolegend #405225). Antigen stimulated CAR T cells were stained for CD69 expression using APC-conjugated anti-human CD69 antibody (Biolegend #310910). Flow cytometric data was acquired using a BD LSRFortessa with BD FACSDiva software. Data was analysed with FlowJo v10.6.2 software. Cells were subject to FSc and SSc doublet discrimination and dead cells were excluded from analysis using Zombie NIR viability dye (Biolegend #423106).

Statistical analysis

All experiments were carried out at least three times, presented as mean ± standard deviation (SD) and analyzed by one-way ANOVA test with Bonferroni post-test correction. The P values of ≤ 0.05 were considered statistically significant. (* $P<0.05$, ** $P<0.01$, *** $P<0.001$, **** $P<0.0001$)

Results

Compatibility of the promoter systems with a third-generation lentiviral system

The four promoters were chosen based on their widespread use in the literature and documented ability to drive high level expression of transgenes in either lentiviral vectors, or in

Sleeping Beauty transposon vectors [1, 8, 9, 21, 23]. Each of the four promoters were cloned upstream of the series of P2A-linked genes comprised of GFP, the FRP5 anti-Her2 CAR followed by human Mcl-1 (Fig 1A), a Bcl2 family member–the latter gene as a strategy to protect CAR T cells against activation-induced cell death (AICD). A first consideration for the choice of internal promoter driving transgenes within lentiviral systems is the effect on viral titration and transduction efficiency. Generally, there is a difference in the degree of transcriptional interference between the internal promoters and the promoter driving expression of genomic RNA, resulting in a lower number of full-length viral genomic RNAs (vgRNA) particularly when the CMV or EF-1 promoter is being used [10, 24]. In order to test the promoter interference, HEK293 cells were transfected with four constructs along with helper plasmids and the levels of vgRNA for four promoters were measured ($P>0.05$, Fig 1B). Similar levels of full-length transcripts were obtained using all constructs, as assessed by RT-PCR carried out with primers binding to cPPT and woodchuck regions (Fig 1B). Next, the effect of internal promoter interference with provirus production was estimated. QPCR was performed on gDNA extracted from HEK293 cells transduced with all constructs. The ratio between integrated cassette to gDNA did not show significant differences among constructs ($P>0.05$, Fig 1C), suggesting that the selected promoters do not adversely affect reverse transcription or integration steps.

Next, we determined if the choice of internal promoter affects titre and transduction of primary T cells. As shown in Fig 1D, constructs containing any of the four promoters were able to produce similar viral titres, as determined by transduction of the GFP marker into HEK293T cells. To determine if the sequences of internal promoters altered primary T cells transduction, we transduced primary T cells obtained from different donors and analyzed for GFP expression by flow cytometry three days later. EF-1 gave superior transduction efficacy compared to the other three promoters ($P\leq 0.0001$, Fig 1E).

Promoter comparison for long and complex gene expression

To determine if the promoters differed in their ability to transcribe individual gene products within a long gene, the expression of individual genes were assessed in HEK293T and primary T cells. From the data obtained with HEK293T, CMV and EF-1 were superior to hPGK and RPBSA in producing all three products (Fig 2). We next examined the strength of the four promoters in primary T cells by analyzing GFP and CAR expression. Live primary T cells were gated for GFP, for determining the intensity of CAR and GFP expression. As shown in Fig 3, EF-1 gave stronger expression of GFP and Her2 CAR compared to the other promoters. CMV was weaker in primary T cells, as compared to its activity in HEK293T cells. This could be due to the differences in the transcriptome of both cell types and / or the different techniques that have been used to measure the protein level.

Functional effect of CAR T cells in tumour and T cell engagement

We next examined the function of the CAR T cells transduced with each of the promoter constructs, measuring cytokine release (IL-2 and IFN-γ), cytotoxicity and activation following incubation of CAR T cells with the $Her2^{+}$ MCF-7 breast cancer cell line. Although the expression of CD69 as an activation marker was similarly expressed among the CAR T cells with different promoters (Fig 4A), EF-1 and CMV CAR T cells showed optimal cytokine release after engaging MCF-7 cells (Fig 4B & 4C). CAR T cells transduced with hPGK were less active and those with the RPBSA construct failed to release detectable IL-2 and IFN-γ. Cytotoxicity assay with the four constructs showed similar results with strong killing with CAR T cells expressing under the EF-1 promoter at 24 h time points (Fig 4D).

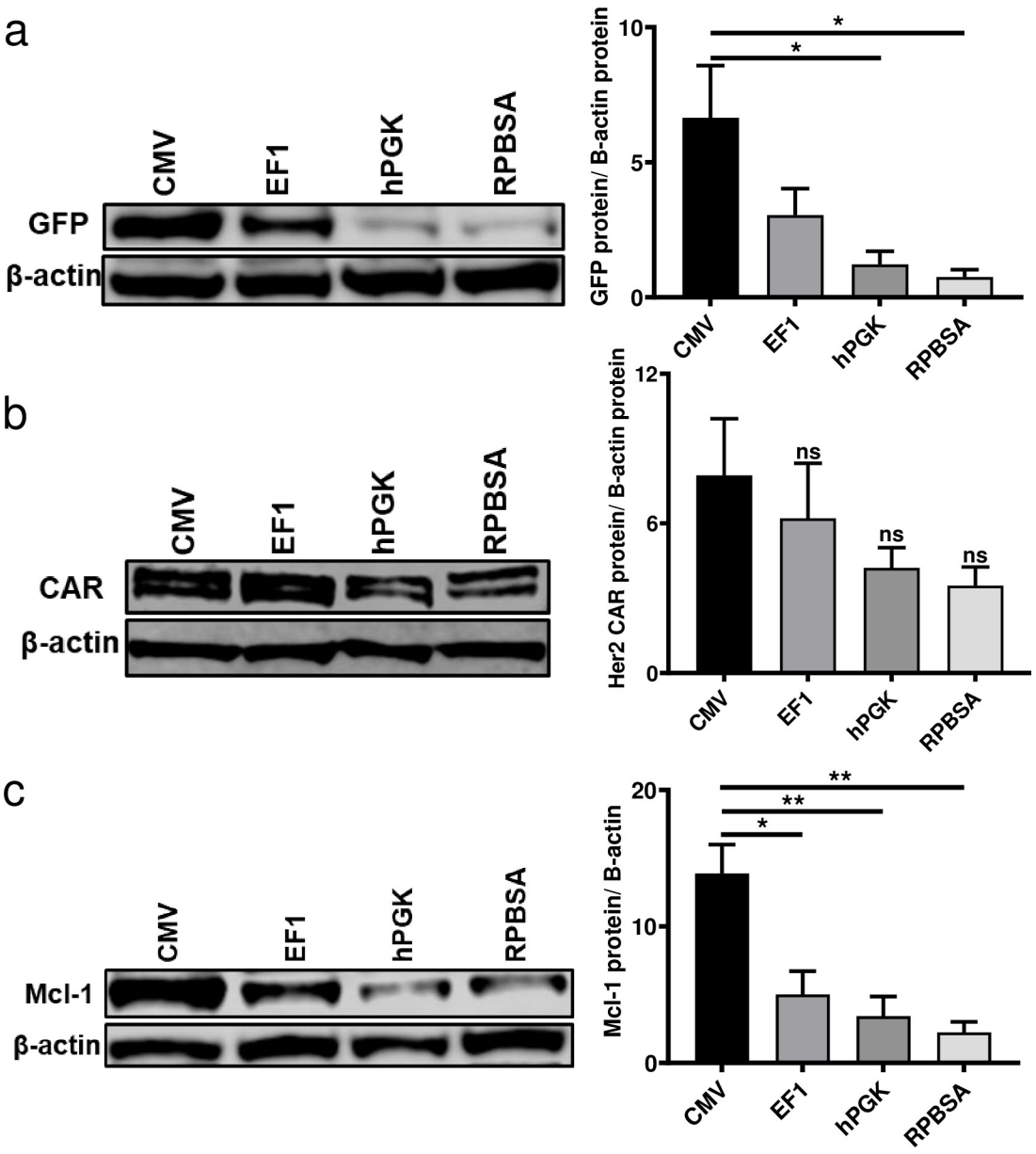

Fig 2. Protein expression from four different constitutive promoters driving long mRNA. Transfected HEK293T cells were lysed with RIPA buffer and processed for immunoblotting using antibodies to detect (a) GFP (b) c-Myc tag for Her2 CAR and (c) Mcl-1 expression with β-actin used as a loading control for the Western blots. All representative blots above are repeated three times and quantified and presented in the bar graph (right) using Image Studio Lite. Bar graph values represent the mean values ± SD from three independent repeats.

https://doi.org/10.1371/journal.pone.0232915.g002

To functionally test the relationship between the expression level of the most distal gene Mcl-1, and resistance to AICD, CAR T cells carrying four different promoters were challenged with 1 μg/mL LZ-CD95L and mitochondrial depolarisation monitored by TMRE staining and flow cytometry. In the absence of CD95L-triggering, there was little difference in cell viability or CAR T cell yields using the four different promoters (Fig 5A and data not shown). Again, EF-1 provided the most potent protection against CD95L-induced cell death (Fig 5). Note, the protection against AICD observed here could reflect a contribution of both Mcl-1, as well as

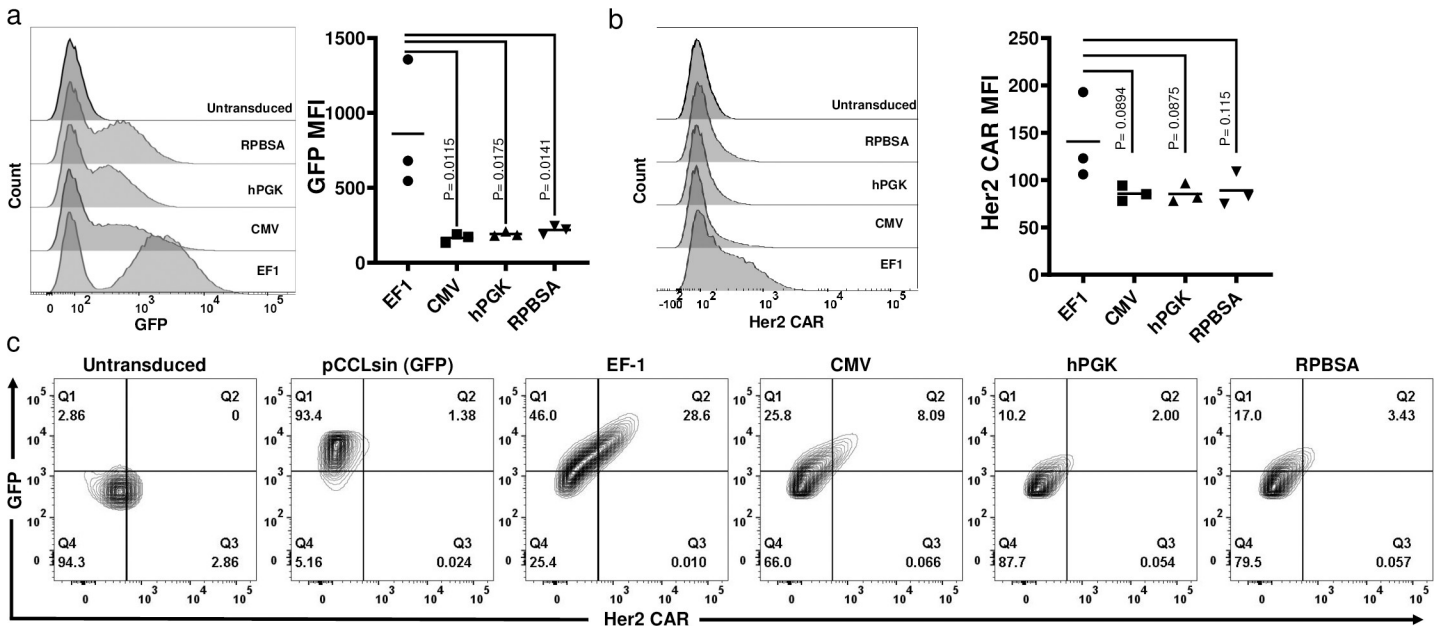

Fig 3. GFP and Her2 CAR expression of the four constructs in primary human T cells. Flow cytometry carried out to measure the expression of (a) GFP and (b) Her2 CAR (c-myc tag). Dead cells were excluded by Zombie NIR viability dye at analysis. GFP positive cells were gated and MFI assessment of CAR and GFP is shown for three individual donors are shown in graphs. (c) Live T cells positive for GFP (Y-axis) and / or Her2 CAR (anti-c-myc; X-axis).

https://doi.org/10.1371/journal.pone.0232915.g003

the pro-survival effect of the CD28 domain in the CAR. For example, CD28 has been shown to enhance the T cell survival by upregulating Bcl2-xL [25]. However, in this setting (without CAR triggering), the presence of the CD28 domain-CAR makes only a minor contribution to the observed protection against CD95L-induced cell death, as compared to the major anti-apoptotic action of Mcl-1 (manuscript in preparation).

Promoter comparison for driving short transcripts

We compared the ability of the four promoters in transcribing GFP linked to an FMC63 CD19 CAR, the most studied CAR construct and the first CAR T cell design approved by the FDA. The FMC63 CAR transcript is 1.2 kb shorter than the GFP-Her2CAR-Mcl1. Viral titres and transduction efficacies were similar among all promoters driving the shorter FMC63 CAR mRNA (Fig 6A & 6B). Protein expression of the shorter GFP-CAR constructs was enhanced in HEK293T transduced with EF-1 and CMV constructs (Fig 6C). In primary T cells, EF-1 gave the highest expression for GFP and CD19 CAR, while CMV gave a more heterogenous expression, but this was not statistically significantly lower than EF-1 (Fig 6D & 6E).

Although CD69 expression on antigen stimulated CAR T cells was similar for all promoter constructs (Fig 7A), EF-1 constructs drove higher levels of CAR triggering in terms of cytokine release and cytotoxicity. RPBSA was more effective in driving short transcripts, as compared to performance observed earlier for long and complex RNA (Fig 7B–7D), further emphasizing that promoter activity is dependent on the nature of the downstream transcript.

Core promoter elements, CpG island and TF binding sites are varying between promoters

Although all four selected promoters are assumed to be constitutive and active in most cell types, bioinformatic analysis showed that the four promoters vary in terms of core promoter

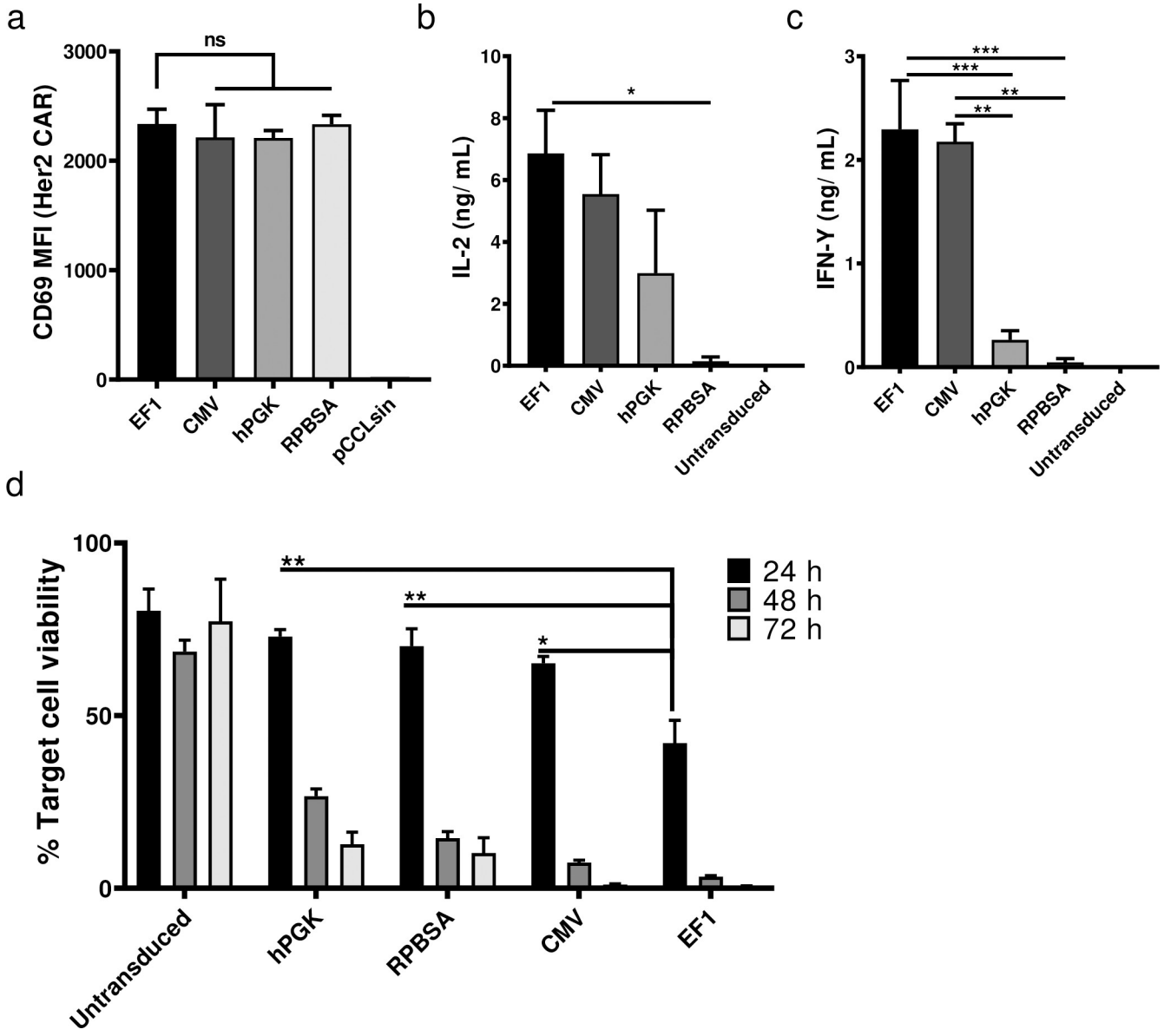

Fig 4. Comparison of anti-tumor activity using different promoters in CAR T cells. (a) Flow cytometric analysis of Her2 CAR T cells 18 h after co-culture with Her2^{+} / MCF-7 cells. Data shows the MFI of CD69 expression from three different donors. Bar graphs show the secretion of (b) IL-2 and (c) IFN-γ by different CAR T cells measured by ELISA. CAR T cells were incubated with Her-2^{+} MCF-7 cell line for 24 h before supernatants were collected. Cytokines were measured in ng/mL. (d) Luciferase based cytotoxicity assay assessed 24, 48 and after 72 h after incubation of CAR T cells with MCF-7 cells stably expressing the firefly luciferase gene. The graph shows the percent of cell viability, calculated by dividing the luciferase of the sample well over the luciferase reading of untreated MCF-7.

https://doi.org/10.1371/journal.pone.0232915.g004

elements and potential TF binding sites. While there is no universal core promoter elements for RNA polymerase II, the TATA box, initiator (Inr) element, TFIIB recognition element (BRE), downstream core promoter element (DPE) and motif ten element (MTE) are well-established core promoter elements (Fig 8A). Overall, EF-1 had more core promoter elements, such as GC box, DPE and MTE (Fig 8B, Table 1). Except for hPGK, all promoters contain a TATA box.

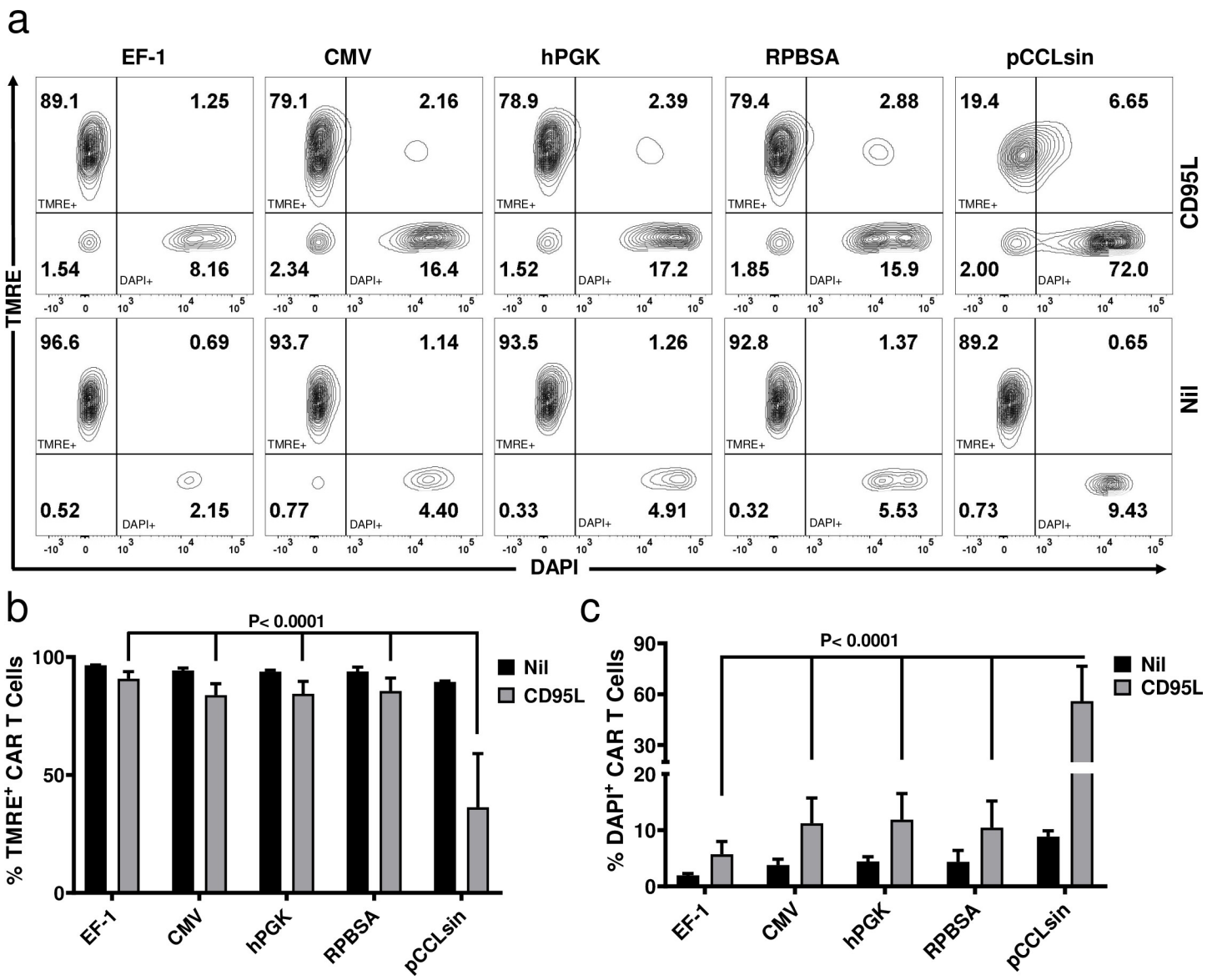

Fig 5. TMRE assay for monitoring mitochondrial membrane potential. (a) CAR T cells expressing Mcl-1 as an anti-apoptotic gene as the most distal gene in the cassette were challenged with 1 μg/mL (top) or 0 μg/mL (below) LZ-CD95L to mimic AICD. $TMRE^{+}$ events represent intact cells with healthy mitochondria, while $TMRE^{-}$ are cells with depolarised mitochondria. pCCLsin (lentivector expressing only GFP) was used as control. Graphs represent the percent of (b) TMRE and c) DAPI positive CAR T cells.

https://doi.org/10.1371/journal.pone.0232915.g005

Another feature of eukaryotic promoters is the presence of CpG islands. CpG islands could result in hypermethylation and gene silencing. However, promoters with CpG islands containing multiple Sp1 binding sites exhibit a hypomethylated state and are typically stronger promoters [26]. We therefore searched for CpG islands within our promoters using two different programs (Table 2). Except for CMV, all promoters were expected to have at least one CpG island. When we searched the Sp1 binding sites within the CpG islands, EF-1 and hPGK showed the highest number of Sp1 binding sites in their CpG islands (Table 3). EMBOSS Cpgplot program predicted two CpG island for EF-1 with 37 Sp1 binding sites. Fig 8C represents the total number of TFBS within the four promoters. Of these identified TFBS, sixteen TFs were selected based on their function and expression in T cells [27–29] and the relative

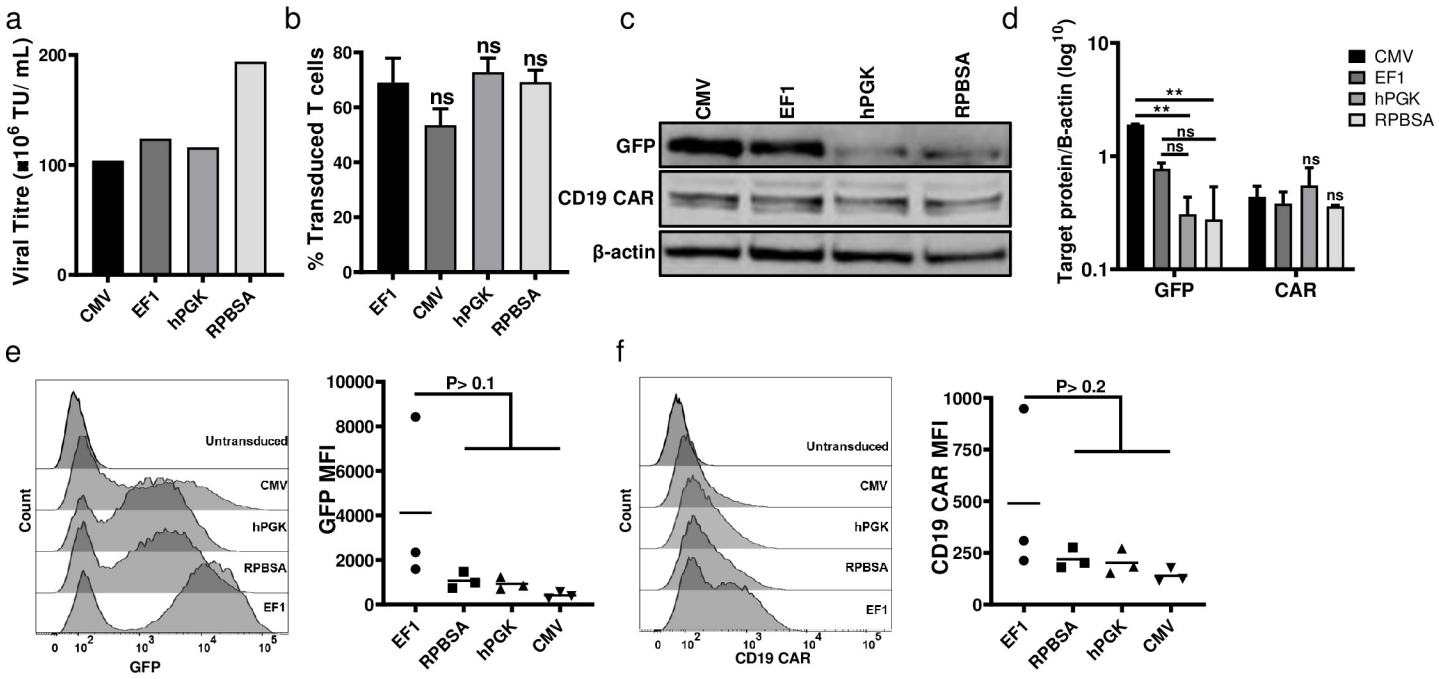

Fig 6. Comparison of four constructs for transcribing short RNA. The eGFP gene linked to FMC63 CD19 CAR was cloned under the control of the four promoters. (a) Titration and (b) transduction efficacy among four constructs (c) Western blot analysis for GFP and CD19 CAR level of HEK293T cells transduced at MOI 2:1 plus 1 μg/mL polybrene (d) Quantification representation of western blot using Image Studio Lite. Bar graph values represent the mean values ± SD from three different repeats. (e) GFP and f) CD19 CAR expression in CAR T cells by flow cytometry.

https://doi.org/10.1371/journal.pone.0232915.g006

enrichment of their corresponding TFBS in each promoter plotted (Fig 8D) [27–29]. Fig 8D highlights promoters that demonstrate a specific enrichment of binding sites for T cell-associated TF, relative to the other promoters. Essentially, the graph illustrates the number of TFBS present in each promoter, expressed as percentage of those present in all promoters. EF-1 possessed binding sites for all these TFs (Fig 8D). CMV is the next promoter enriched for T cell-specific TFs, excluding GATA3, LEF-1, STAT5 and IF-2 (Fig 8D). It should be noted that EF-1 is almost twice the length of other promoters (>600 bp), and this length allows a greater possible enrichment of TFBS and core promoter elements.

Who should drive the CAR?

In order to have a broader view in comparing the strength of each promoter, scores from 0–10 were assigned to all functional assays carried out in primary T cells (Fig 9). Scores were calculated using the following formula:

$$\text{Score} = \frac{\text{Mean of each value}}{\text{Mean of maximum value}} \times 10$$

Based on data from Fig 9A, the promoter strengths for short transcript were in the following order: EF-1 > RPBSA > hPGK > CMV. For long transcripts carrying another accessory gene (Mcl-1) in addition to GFP-CAR, the promoter strengths were as follow: EF-1 > CMV > hPGK > RPBSA (Fig 9B). Taken together, EF-1 displayed the best function in driving both short and long RNA transcripts. However, if the insert size between two LTR increases beyond 10 kb, other promoters could be considered to mitigate drops in the viral titre and transduction efficiency [30]. In our study, the largest insert utilised was 6.8 kb.

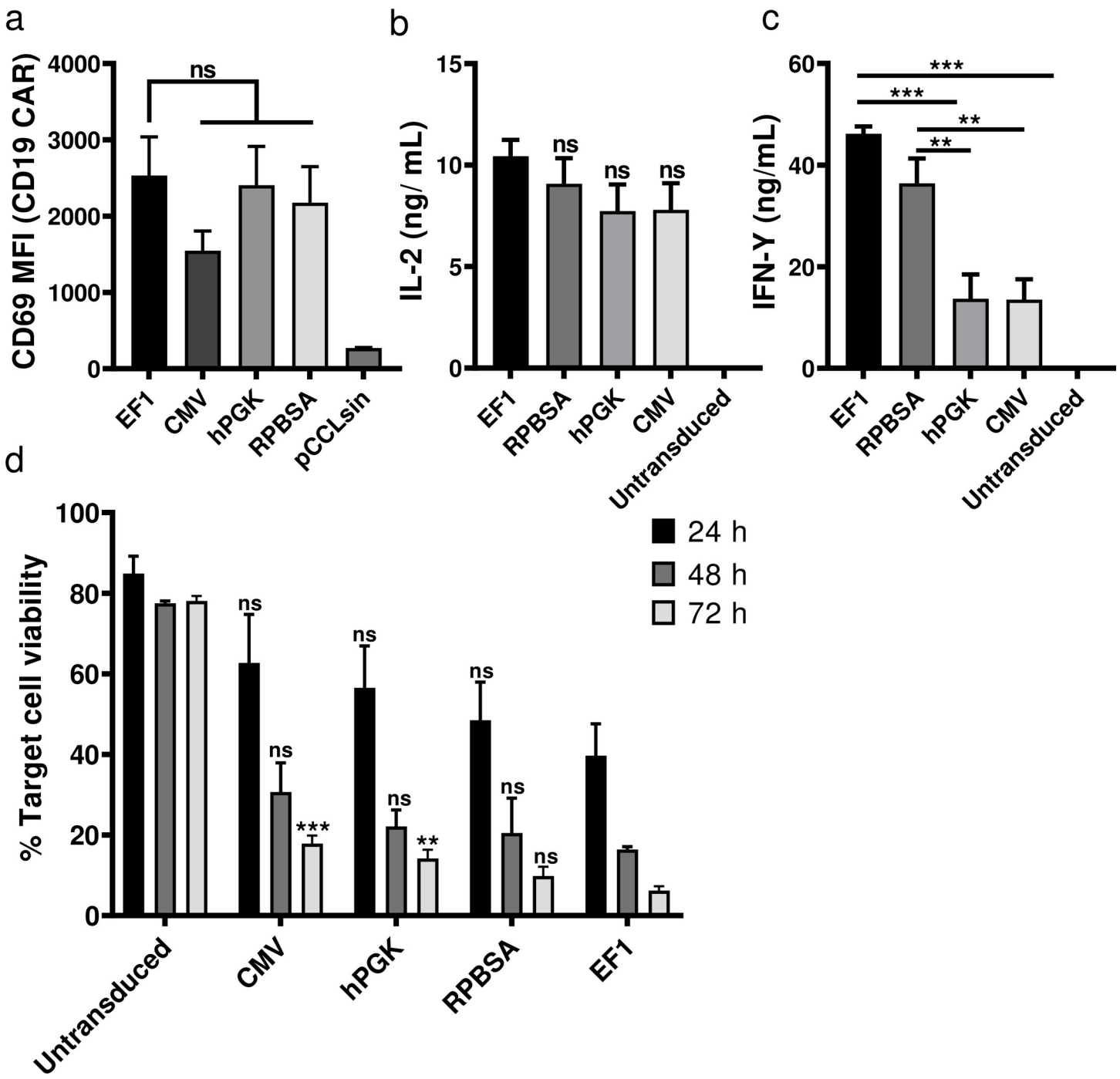

Fig 7. Functional analysis of CAR T cells expressing short RNA. (a) CD69 activation assay was carried out 18 hours after incubation of the four types of promoter-driven CD19 CAR T cells with $CD19^+$ HEK293T cells. (b, c) Cytokine release assay for secretion of (b) IL-2 and (c) IFN-γ. CAR T cells were co-cultured with $CD19^+$ HEK239T and supernatant were collected after 24 h. (d) Luciferase based cytotoxicity assay assessed 24, 48 and 72 h after incubation of CD19 CAR T cells with $CD19^+$ HEK293 cells stably expressing the firefly luciferase gene. The graph shows the percent of cell viability, calculated by dividing the luciferase of test wells divided by the luciferase signal of untreated HEK293T.

https://doi.org/10.1371/journal.pone.0232915.g007

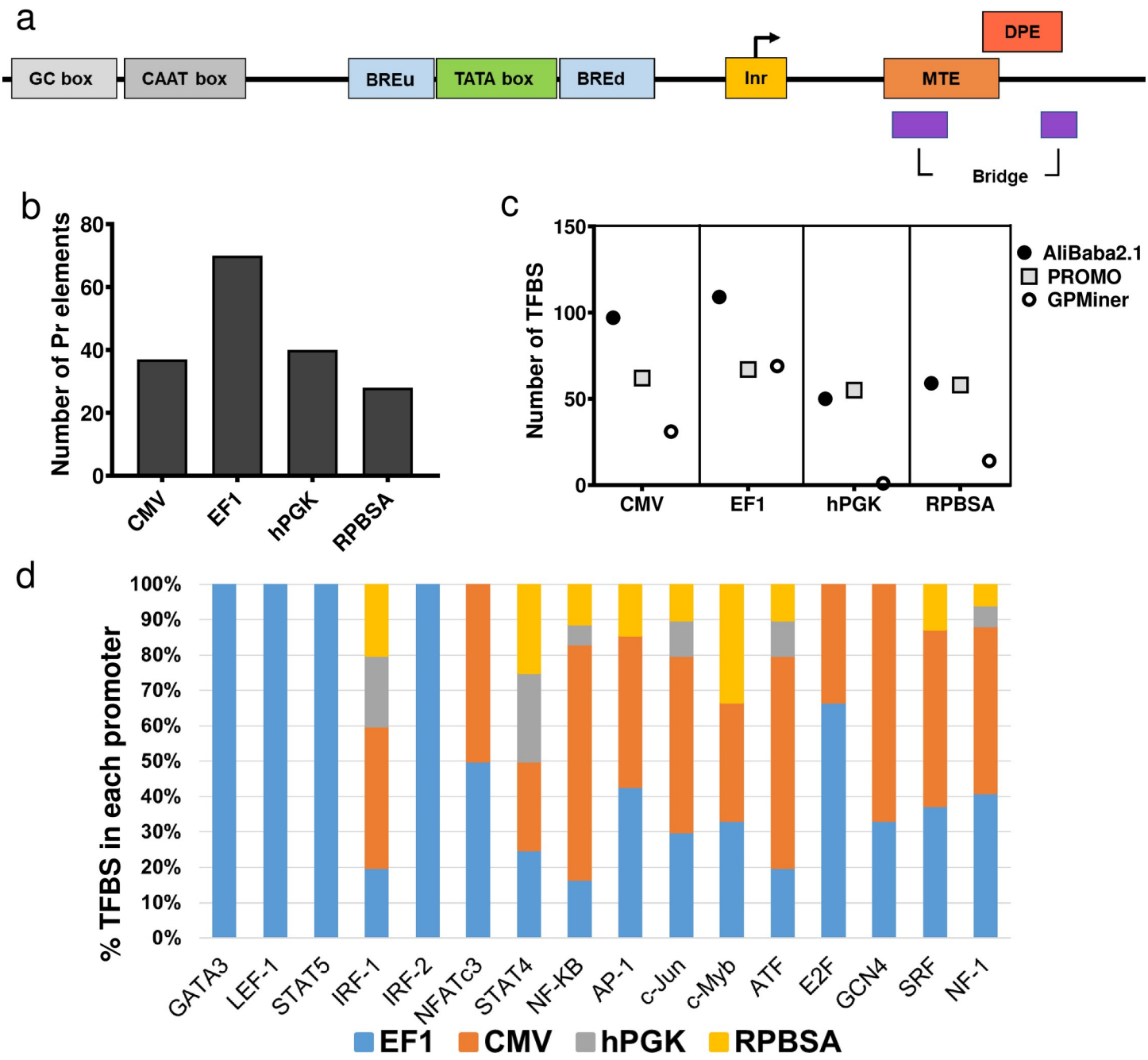

Fig 8. Structure and bioinformatic analysis of the four different promoters. (a) Structure of a typical eukaryotic core promoter and the position of core elements within a promoter were investigated in the four different promoters (b) Total number of core promoter elements predicted by YAPP, GPMiner and ElemeNT algorithms (details provided in Table 1) (c) The number of TF binding sites in promoters sequenced analyzed by AliBaba2.1, PROMO and GPMiner programs d) Enrichment of sixteen TFs highly-expressed in T cells in the four promoters. The data shows the percentage of total number predicted binding sites for the four promoters.

https://doi.org/10.1371/journal.pone.0232915.g008

Discussion

In this study, we compared four promoters for optimal expression of long RNA encoding multiple gene products in CAR T cells. Our results suggest that promoter requirements are stringent for driving long RNA, and that EF-1 is the best choice for driving short or long RNA in CAR T cells, similar to an early study [31]. In contrast to the poor results obtained here for

Table 1. The number of core promoter elements and TF binding sites predicted for four promoters with YAPP, GPMiner and ElemeNT algorithms.

Promoter	Size (bp)	Core prompter elements							
		GC box	CAAT box	BRE	TATA box	Inr	MTE	DPE	Bridge
CMV	617	3	4	-	2	10	-	6	12
EF-1	1192	11	-	2	2	7	2	24	22
hPGK	516	8	2	3	-	3	2	12	10
RPBSA	612	3	1	1	2	3	-	10	8

https://doi.org/10.1371/journal.pone.0232915.t001

hPGK and RPBSA in driving long and complex RNA, these same promoters demonstrated little difference to the so-called strong promoters CMV and EF-1 in lentiviral based systems driving shorter RNA sequences, such as CAR and fluorescent reporter genes (see Fig 6E)–consistent with other studies [1, 8, 9, 21, 23].

To determine the functional role of additional accessory genes expressed in long constructs, we utilised Mcl-1, a bcl2 family member with an essential role in T cell development, mitochondrial function and lifespan. To our knowledge, this is the first study to demonstrate that Mcl-1 is a suitable candidate for enhancing CAR T cell performance [15, 16]. Expression of mcl1 in a position distal to the CAR allowed protection from CD95-induced cell death. Interestingly, although protection was noted with all promoters, EF-1 driven-cassettes consistently gave the best protection. The fact that protection was observed with Mcl-1 driven by the weaker promoters RPBSA and hPGK contrasts with the stringent requirement for a strong promoter to drive CAR expression for optimal cytotoxicity and cytokine release.

Our analysis of promoter motifs demonstrates clear differences in transcription factor binding sites and core promoter elements between the strong (EF-1 and CMV) and weaker (hPGK and RPBSA) promoters. Although not all the predicted core promoter elements might be functional in primary T cells, the high number of the core elements can correlate with the strength of the promoter [26]. In addition EF-1 and CMV predominantly enriched for TFs specific or highly expressed in T cells [27–29, 32, 33] such as GATA3, NFATc3, NF-kB, AP1 and c-Jun, The number of transcription factor and core promoter element sites predicted within the promoters may provide some explanation for the ability of the CMV and EF-1 promoters to direct long mRNA expression (Fig 1, S1 Data). However, it should be noted that EF-1 is almost twice the length of the other promoters, therefore has the potential to house more TFBS and core promoter elements.

The activity of promoters with predicted 'ubiquitous' expression, such as the four studied here, will still depend greatly on the lineage of the host cell [34]. However, EF-1 promoter was found to be active and resistant to silencing in cells where other viral promoters may become silenced [35]. Therefore, future work will be required to determine if the superior performance

Table 2. Bioinformatic tools used for studying promoter structure and TF binding sites.

Program	Promoter element	CpG island	TF binding sites
YAPP	✓	-	-
GPMiner	✓	✓	✓
ElemeNT	✓	-	-
AliBaba2.1	-	-	✓
PROMO	-	-	✓
EMBOSS Cpgplot	-	✓	-
CpGFinder	-	✓	-

https://doi.org/10.1371/journal.pone.0232915.t002

Table 3. The number of CpG islands and Sp1 binding sites within selected promoters.

Promoter	Number of CpG islands	Position	Number of Sp1 binding sites
EF-1	1	604–868	17
CMV	0	-	-
hPGK	1	54–392	16
RPBSA	1	194–405	8

https://doi.org/10.1371/journal.pone.0232915.t003

of EF-1 and CMV in expressing long RNA sequences can be extrapolated to other cell primary cell types.

In our study, the lower expression of CAR within a long mRNA transcript driven by the RPBSA and hPGK translated into lower lytic function for a Her2-expressing tumor cell line. Given the profound effects that CAR density has on T cell activation, our results will be useful for developing strategies to titrate CAR expression at the T cell. Promoter choice would be expected to be a critical consideration for controlling the levels of surface expressed CAR, which in turn would dictate the level of T cell activation, lytic function, as well as undesirable tonic (antigen-independent) signaling [2, 36–39]. Optimal CAR expression will be critical for minimizing tonic signaling, while optimizing signal transduction during antigen-specific signaling. In addition, lowering the level of CAR expression could contribute desirable avidity effects to T cell recognition of antigen, thereby minimizing CAR T cell activation by tumor-associated antigen on self-tissue [14]. Interestingly, despite CMV inducing a noticeably higher level expression of GFP, CAR and Mcl-1 in HEK293T cells, as compared to EF-1, functional analysis showed superior activation of primary human CAR T cells driven by EF-1 in terms of cytokine release and cytotoxicity against MCF-7. EF-1 is enriched in binding sites of TFs expressed in T cells (Fig 8C), suggesting a mechanism for the increased EF-1 activity in T cells, as compared to HEK293T cells. In addition functional experiments demonstrated that EF-1

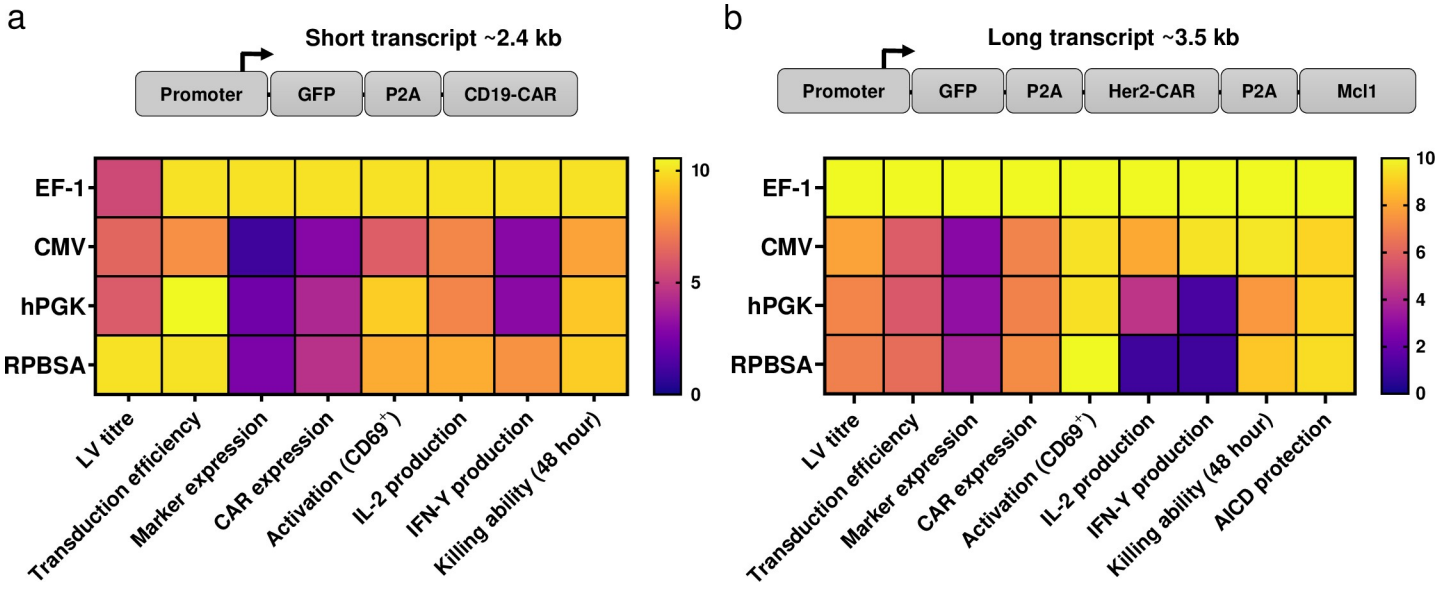

Fig 9. Heat map charts representing the strength of each promoter in functional assays for a) short transcripts and b) long transcripts. Each promoter was assigned a score from 0–10 based on the data obtained from primary T cell experiments, and values were calculated by dividing mean of each data set by mean of the maximum value obtained in the experiment and multiplied by ten.

https://doi.org/10.1371/journal.pone.0232915.g009

driven expression of Mcl-1 provided the best protection of CAR T cells to AICD induced by CD95L.

A further consideration for promoter choice is possible silencing *in vivo*. In particular, CMV can be silenced after a period of weeks post-transduction [34, 40]. However, the effects of promoter silencing might be overshadowed by the long term CAR T cell downregulation that occurs in a methylation-independent fashion following CAR triggering both *in vitro* and *in vivo* [14, 41, 42]. In conclusion, the study of long mRNA production will improve our ability to express multiple genes in CAR T cells to improve cell survival and persistence of infused CAR T cells.

Supporting information

S1 Raw images.
(PDF)

S1 Data.
(DOCX)

Acknowledgments

We thank Dr. Sarah Saunderson for critical review of the manuscript.

Author Contributions

Conceptualization: Ali Hosseini Rad S. M., Alexander D. McLellan.

Formal analysis: Ali Hosseini Rad S. M., Aarati Poudel, Grace Min Yi Tan, Alexander D. McLellan.

Funding acquisition: Alexander D. McLellan.

Investigation: Ali Hosseini Rad S. M., Aarati Poudel, Grace Min Yi Tan, Alexander D. McLellan.

Methodology: Ali Hosseini Rad S. M., Aarati Poudel, Grace Min Yi Tan, Alexander D. McLellan.

Project administration: Ali Hosseini Rad S. M.

Resources: Ali Hosseini Rad S. M., Alexander D. McLellan.

Supervision: Ali Hosseini Rad S. M., Alexander D. McLellan.

Writing – original draft: Ali Hosseini Rad S. M., Aarati Poudel, Grace Min Yi Tan, Alexander D. McLellan.

Writing – review & editing: Ali Hosseini Rad S. M., Alexander D. McLellan.

References

1. Milone MC, Fish JD, Carpenito C, Carroll RG, Binder GK, Teachey D, et al. Chimeric receptors containing CD137 signal transduction domains mediate enhanced survival of T cells and increased antileukemic efficacy in vivo. Molecular therapy: the journal of the American Society of Gene Therapy. 2009; 17 (8):1453–64.
2. Frigault MJ, Lee J, Basil MC, Carpenito C, Motohashi S, Scholler J, et al. Identification of chimeric antigen receptors that mediate constitutive or inducible proliferation of T cells. Cancer immunology research. 2015; 3(4):356–67. https://doi.org/10.1158/2326-6066.CIR-14-0186 PMID: 25600436

3. Drent E, Poels R, Mulders MJ, van de Donk N, Themeli M, Lokhorst HM, et al. Feasibility of controlling CD38-CAR T cell activity with a Tet-on inducible CAR design. PloS one. 2018; 13(5):e0197349. https://doi.org/10.1371/journal.pone.0197349 PMID: 29847570
4. Stoiber S, Cadilha BL, Benmebarek MR, Lesch S, Endres S, Kobold S. Limitations in the Design of Chimeric Antigen Receptors for Cancer Therapy. Cells. 2019; 8(5).
5. Naldini L, Trono D, Verma IM. Lentiviral vectors, two decades later. Science (New York, NY). 2016; 353 (6304):1101–2.
6. McLellan AD, Ali Hosseini Rad SM. Chimeric antigen receptor T cell persistence and memory cell formation. Immunology and cell biology. 2019.
7. Gilham DE, Lie ALM, Taylor N, Hawkins RE. Cytokine stimulation and the choice of promoter are critical factors for the efficient transduction of mouse T cells with HIV-1 vectors. The journal of gene medicine. 2010; 12(2):129–36. https://doi.org/10.1002/jgm.1421 PMID: 20033928
8. Jones S, Peng PD, Yang S, Hsu C, Cohen CJ, Zhao Y, et al. Lentiviral vector design for optimal T cell receptor gene expression in the transduction of peripheral blood lymphocytes and tumor-infiltrating lymphocytes. Human gene therapy. 2009; 20(6):630–40. https://doi.org/10.1089/hum.2008.048 PMID: 19265475
9. Amendola M, Venneri MA, Biffi A, Vigna E, Naldini L. Coordinate dual-gene transgenesis by lentiviral vectors carrying synthetic bidirectional promoters. Nature biotechnology. 2005; 23(1):108–16. https://doi.org/10.1038/nbt1049 PMID: 15619618
10. Curtin JA, Dane AP, Swanson A, Alexander IE, Ginn SL. Bidirectional promoter interference between two widely used internal heterologous promoters in a late-generation lentiviral construct. Gene therapy. 2008; 15(5):384–90. https://doi.org/10.1038/sj.gt.3303105 PMID: 18283290
11. Wang D, Shao Y, Zhang X, Lu G, Liu B. IL-23 and PSMA-targeted duo-CAR T cells in Prostate Cancer Eradication in a preclinical model. Journal of translational medicine. 2020; 18(1):23. https://doi.org/10.1186/s12967-019-02206-w PMID: 31937346
12. Hoyos V, Savoldo B, Quintarelli C, Mahendravada A, Zhang M, Vera J, et al. Engineering CD19-specific T lymphocytes with interleukin-15 and a suicide gene to enhance their anti-lymphoma/leukemia effects and safety. Leukemia. 2010; 24(6):1160–70. https://doi.org/10.1038/leu.2010.75 PMID: 20428207
13. Philip B, Kokalaki E, Mekkaoui L, Thomas S, Straathof K, Flutter B, et al. A highly compact epitope-based marker/suicide gene for easier and safer T-cell therapy. Blood. 2014; 124(8):1277–87. https://doi.org/10.1182/blood-2014-01-545020 PMID: 24970931
14. Eyquem J, Mansilla-Soto J, Giavridis T, van der Stegen SJ, Hamieh M, Cunanan KM, et al. Targeting a CAR to the TRAC locus with CRISPR/Cas9 enhances tumour rejection. Nature. 2017; 543(7643):113–7. https://doi.org/10.1038/nature21405 PMID: 28225754
15. Andersen JL, Kornbluth S. Mcl-1 rescues a glitch in the matrix. Nat Cell Biol. 2012; 14(6):563–5. https://doi.org/10.1038/ncb2511 PMID: 22643875
16. Morciano G, Pedriali G, Sbano L, Iannitti T, Giorgi C, Pinton P. Intersection of mitochondrial fission and fusion machinery with apoptotic pathways: Role of Mcl-1. Biol Cell. 2016; 108(10):279–93. https://doi.org/10.1111/boc.201600019 PMID: 27234233
17. Kim EH, Neldner B, Gui J, Craig RW, Suresh M. Mcl-1 regulates effector and memory CD8 T-cell differentiation during acute viral infection. Virology. 2016; 490:75–82. https://doi.org/10.1016/j.virol.2016.01.008 PMID: 26855329
18. Dzhagalov I, Dunkle A, He YW. The anti-apoptotic Bcl-2 family member Mcl-1 promotes T lymphocyte survival at multiple stages. Journal of immunology (Baltimore, Md: 1950). 2008; 181(1):521–8.
19. Dunkle A, Dzhagalov I, He YW. Cytokine-dependent and cytokine-independent roles for Mcl-1: genetic evidence for multiple mechanisms by which Mcl-1 promotes survival in primary T lymphocytes. Cell death & disease. 2011; 2:e214.
20. Stewart DP, Koss B, Bathina M, Perciavalle RM, Bisanz K, Opferman JT. Ubiquitin-independent degradation of antiapoptotic MCL-1. Mol Cell Biol. 2010; 30(12):3099–110. https://doi.org/10.1128/MCB.01266-09 PMID: 20385764
21. Dull T, Zufferey R, Kelly M, Mandel RJ, Nguyen M, Trono D, et al. A third-generation lentivirus vector with a conditional packaging system. Journal of virology. 1998; 72(11):8463–71. PMID: 9765382
22. Fu X, Tao L, Rivera A, Williamson S, Song X-T, Ahmed N, et al. A simple and sensitive method for measuring tumor-specific T cell cytotoxicity. PloS one. 2010; 5(7).
23. Kowarz E, Loscher D, Marschalek R. Optimized Sleeping Beauty transposons rapidly generate stable transgenic cell lines. Biotechnol J. 2015; 10(4):647–53. https://doi.org/10.1002/biot.201400821 PMID: 25650551

24. Yee J-K, Moores JC, Jolly DJ, Wolff JA, Respess JG, Friedmann T. Gene expression from transcriptionally disabled retroviral vectors. Proceedings of the National Academy of Sciences. 1987; 84(15):5197–201.

25. Watts TH. Staying alive: T cell costimulation, CD28, and Bcl-xL. The Journal of Immunology. 2010; 185 (7):3785–7. https://doi.org/10.4049/jimmunol.1090085 PMID: 20858889

26. Butler JE, Kadonaga JT. The RNA polymerase II core promoter: a key component in the regulation of gene expression. Genes & development. 2002; 16(20):2583–92.

27. Naito T, Tanaka H, Naoe Y, Taniuchi I. Transcriptional control of T-cell development. Int Immunol. 2011; 23(11):661–8. https://doi.org/10.1093/intimm/dxr078 PMID: 21948191

28. Hosokawa H, Rothenberg EV. Cytokines, Transcription Factors, and the Initiation of T-Cell Development. Cold Spring Harb Perspect Biol. 2018; 10(5). https://doi.org/10.1101/cshperspect.a028621 PMID: 28716889

29. Rothenberg EV. The chromatin landscape and transcription factors in T cell programming. Trends Immunol. 2014; 35(5):195–204. https://doi.org/10.1016/j.it.2014.03.001 PMID: 24703587

30. Escors D, Breckpot K. Lentiviral vectors in gene therapy: their current status and future potential. Archivum immunologiae et therapiae experimentalis. 2010; 58(2):107–19. https://doi.org/10.1007/s00005-010-0063-4 PMID: 20143172

31. Frigault MJ, Lee J, Basil MC, Carpenito C, Motohashi S, Scholler J, et al. Identification of chimeric antigen receptors that mediate constitutive or inducible proliferation of T cells. Cancer immunology research. 2015; 3(4):356–67. https://doi.org/10.1158/2326-6066.CIR-14-0186 PMID: 25600436

32. Urso K, Alfranca A, Martinez-Martinez S, Escolano A, Ortega I, Rodriguez A, et al. NFATc3 regulates the transcription of genes involved in T-cell activation and angiogenesis. Blood. 2011; 118(3):795–803. https://doi.org/10.1182/blood-2010-12-322701 PMID: 21642596

33. Lynn RC, Weber EW, Sotillo E, Gennert D, Xu P, Good Z, et al. c-Jun overexpression in CAR T cells induces exhaustion resistance. Nature. 2019; 576(7786):293–300. https://doi.org/10.1038/s41586-019-1805-z PMID: 31802004

34. Hong S, Hwang DY, Yoon S, Isacson O, Ramezani A, Hawley RG, et al. Functional analysis of various promoters in lentiviral vectors at different stages of in vitro differentiation of mouse embryonic stem cells. Molecular therapy: the journal of the American Society of Gene Therapy. 2007; 15(9):1630–9.

35. Wang X, Xu Z, Tian Z, Zhang X, Xu D, Li Q, et al. The EF-1alpha promoter maintains high-level transgene expression from episomal vectors in transfected CHO-K1 cells. J Cell Mol Med. 2017; 21 (11):3044–54. https://doi.org/10.1111/jcmm.13216 PMID: 28557288

36. Chang ZL, Silver PA, Chen YY. Identification and selective expansion of functionally superior T cells expressing chimeric antigen receptors. Journal of translational medicine. 2015; 13:161. https://doi.org/10.1186/s12967-015-0519-8 PMID: 25990251

37. Chmielewski M, Hombach A, Heuser C, Adams GP, Abken H. T cell activation by antibody-like immunoreceptors: increase in affinity of the single-chain fragment domain above threshold does not increase T cell activation against antigen-positive target cells but decreases selectivity. Journal of immunology (Baltimore, Md: 1950). 2004; 173(12):7647–53.

38. Han C, Sim SJ, Kim SH, Singh R, Hwang S, Kim YI, et al. Desensitized chimeric antigen receptor T cells selectively recognize target cells with enhanced antigen expression. Nature communications. 2018; 9(1):468. https://doi.org/10.1038/s41467-018-02912-x PMID: 29391449

39. Sakemura R, Terakura S, Watanabe K, Julamanee J, Takagi E, Miyao K, et al. A Tet-On Inducible System for Controlling CD19-Chimeric Antigen Receptor Expression upon Drug Administration. Cancer immunology research. 2016; 4(8):658–68. https://doi.org/10.1158/2326-6066.CIR-16-0043 PMID: 27329987

40. Brooks AR, Harkins RN, Wang P, Qian HS, Liu P, Rubanyi GM. Transcriptional silencing is associated with extensive methylation of the CMV promoter following adenoviral gene delivery to muscle. The journal of gene medicine. 2004; 6(4):395–404. https://doi.org/10.1002/jgm.516 PMID: 15079814

41. Burns WR, Zheng Z, Rosenberg SA, Morgan RA. Lack of specific gamma-retroviral vector long terminal repeat promoter silencing in patients receiving genetically engineered lymphocytes and activation upon lymphocyte restimulation. Blood. 2009; 114(14):2888–99. https://doi.org/10.1182/blood-2009-01-199216 PMID: 19589923

42. Gallegos AM, Xiong H, Leiner IM, Susac B, Glickman MS, Pamer EG, et al. Control of T cell antigen reactivity via programmed TCR downregulation. Nature immunology. 2016; 17(4):379–86. https://doi.org/10.1038/ni.3386 PMID: 26901151

LZ-CD95L production and Resazurin assay

The pcDNA3.1(-)-LZ-CD95L plasmid containing isoleucine zipped human CD95 ligand (LZ-CD95L) with histidine tag (made in house and available from Addgene #104349) was transfected into Expi293 cells (1.0 µg DNA per mL of culture volume with exp293 transfection reagent; Thermofisher) and LZ-CD95L isolated by nickel chromatography.

The ability of LZ-CD95L to induce activation-induced cell death (AICD) was determined using the resazurin assay. Jurkat cells (50×10^3 seeded in 96-well plate in 100 µl) were treated with variety of concentrations 0-1.5 µg/ ml) LZ-CD95L. After 24 hours, 10 µl of resazurin solution (12 mg/L of resazurin, 10 mg/ L methylene blue, 40 µM potassium ferricyanide, 40 µM potassium ferrocyanide and 100 mM phosphate buffer pH 7.4) was added to the wells. After a further 4 hours culture, fluorescence (ex540 nm / em585 nm) was determined using Varioskan LUX multimode microplate reader (Thermo Fisher, USA).

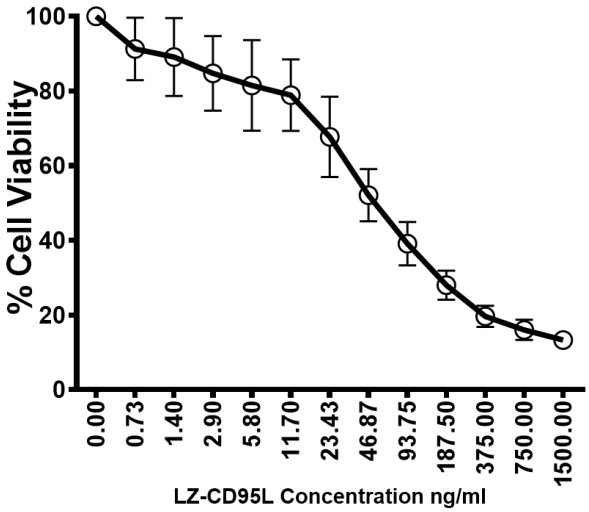

S 1. Ability of LZ-CD95L in inducing AICD in Jurkat cells.

CMV promoter sequence

```
ACATTGATTATTGACTAGTTATTAATAGTAATCAATTACGGGGTCATTAG 50

TTCATAGCCCATATATGGAGTTCCGCGTTACATAACTTACGGTAAATGGC 100

CCGCCTGGCTGACCGCCCAACGACCCCCGCCCATTGACGTCAATAATGAC 150

GTATGTTCCCATAGTAACGCCAATAGGGACTTTCCATTGACGTCAATGGG 200

TGGAGTATTTACGGTAAACTGCCCACTTGGCAGTACATCAAGTGTATCAT 250

ATGCCAAGTACGCCCCCTATTGACGTCAATGACGGTAAATGGCCCGCCTG 300

GCATTATGCCCAGTACATGACCTTATGGGACTTTCCTACTTGGCAGTACA 350

TCTACGTATTAGTCATCGCTATTACCATGGTGATGCGGTTTTGGCAGTAC 400

ATCAATGGGCGTGGATAGCGGTTTGACTCACGGGGATTTCCAAGTCTCCA 450

CCCCATTGACGTCAATGGGAGTTTGTTTTGGCACCAAAATCAACGGGACT 500

TTCCAAAATGTCGTAACAACTCCGCCCCATTGACGCAAATGGGCGGTAGG 550

CGTGTACGGTGGGAGGTCTATATAAGCAGAGCTCTCTGGCTAACTAGAGA 600

ACCCACTGCTTACTGGC                                   617
```

EF1 promoter sequence

```
AAGCTTGATATCGGGCTCCGGTGCCCGTCAGTGGGCAGAGCGCACATCGC 50

CCACAGTCCCCGAGAAGTTGGGGGGAGGGGTCGGCAATTGAACCGGTGCC 100

TAGAGAAGGTGGCGCGGGGTAAACTGGGAAAGTGATGTCGTGTACTGGCT 150

CCGCCTTTTTCCCGAGGGTGGGGGAGAACCGTATATAAGTGCAGTAGTCG 200

CCGTGAACGTTCTTTTTCGCAACGGGTTTGCCGCCAGAACACAGGTAAGT 250

GCCGTGTGTGGTTCCCGCGGGCCTGGCCTCTTTACGGGTTATGGCCCTTG 300

CGTGCCTTGAATTACTTCCACGCCCCTGGCTGCAGTACGTGATTCTTGAT 350

CCCGAGCTTCGGGTTGGAAGTGGGTGGGAGAGTTCGAGGCCTTGCGCTTA 400

AGGAGCCCCTTCGCCTCGTGCTTGAGTTGAGGCTTGGCCTGGGCGCTGGG 450
```

GCCGCCGCGTGCGAATCTGGTGGCACCTTCGCGCCTGTCTCGCTGCTTTC 500

GATAAGTCTCTAGCCATTTAAAATTTTTGATGACCTGCTGCGACGCTTTT 550

TTTCTGGCAAGATAGTCTTGTAAATGCGGGCCAAGATCTGCACACTGGTA 600

TTTCGGTTTTTGGGGCCGCGGGCGGCGACGGGGCCCGTGCGTCCCAGCGC 650

ACATGTTCGGCGAGGCGGGGCCTGCGAGCGCGGCCACCGAGAATCGGACG 700

GGGGTAGTCTCAAGCTGGCCGGCCTGCTCTGGTGCCTGGCCTCGCGCCGC 750

CGTGTATCGCCCCGCCCTGGGCGGCAAGGCTGGCCCGGTCGGCACCAGTT 800

GCGTGAGCGGAAAGATGGCCGCTTCCCGGCCCTGCTGCAGGGAGCTCAAA 850

ATGGAGGACGCGGCGCTCGGGAGAGCGGGCGGGTGAGTCACCCACACAAA 900

GGAAAAGGGCCTTTCCGTCCTCAGCCGTCGCTTCATGTGACTCCACGGAG 950

TACCGGGCGCCGTCCAGGCACCTCGATTAGTTCTCGAGCTTTTGGAGTAC 1000

GTCGTCTTTAGGTTGGGGGGAGGGGTTTTATGCGATGGAGTTTCCCCATA 1050

CTGAGTGGGTGGAGACTGAAGTTAGGCCAGCTTGGCACTTGATGTAATTC 1100

TCCTTGGAATTTGCCCTTTTTGAGTTTGGATCTTGGTTCATTCTCAAGCC 1150

TCAGACAGTGGTTCAAAGTTTTTTTCTTCCATTTAAGGTGTCGTGAAAAC 1200

TACCCCGGATCCGTGGT 1217

hPGK promoter sequence

CCACGGGGTTGGGGTTGCGCCTTTTCCAAGGCAGCCCTGGGTTTGCGCAG 50

GGACGCGGCTGCTCTGGGCGTGGTTCCGGGAAACGCAGCGGCGCCGACCC 100

TGGGTCTCGCACATTCTTCACGTCCGTTCGCAGCGTCACCCGGATCTTCG 150

CCGCTACCCTTGTGGGCCCCCCGGCGACGCTTCCTGCTCCGCCCCTAAGT 200

CGGGAAGGTTCCTTGCGGTTCGCGGCGTGCCGGACGTGACAAACGGAAGC 250

CGCACGTCTCACTAGTACCCTCGCAGACGGACAGCGCCAGGGAGCAATGG 300

CAGCGCGCCGACCGCGATGGGCTGTGGCCAATAGCGGCTGCTCAGCGGGG 350

CGCGCCGAGAGCAGCGGCCGGGAAGGGGCGGTGCGGGAGGCGGGGTGTGG 400

GGCGGTAGTGTGGGCCCTGTTCCTGCCCGCGCGGTGTTCCGCATTCTGCA 450

AGCCTCCGGAGCGCACGTCGGCAGTCGGCTCCCTCGTTGACCGAATCACC 500

GACCTCTCTCCCCAGG 516

RPBSA promoter sequence

AAGCTTGATATCGCGAGACCCTGTCTCACAAAATAAAGTAAGCCCGGACT 50

GAGTGCGGAAAGGCGGGCCTGGCGGGTCTGGTCTCCCCATGCGGGCCACC 100

AGAGGCCCTGCAGCCTTCAGTCGCTTGAAGGGGTAATGGCGCTTCCACTC 150

ACAAACATGGCGGACAGAGCGTGTGAACGAGATGAACAGCCCCTCAAAAA 200

TATGGCCGCCGAGGCTGGACGGCCGTGCCCCAGCAGCACCGCCTCCGCGC 250

CCCACGTGATCTCTCGCCGGGCACAGCGCTGACCGCGGAGGTCCAACCGG 300

AAGAATGTCCGGATTGGACATTCGGAAGAGGGCCCGCCTTCCCTGGGGAA 350

TCTCTGCGCACGCGCAGAACGCTTCGACCAATGAAAACACAGGAAGCCGT 400

CCGCGCAACCGCGTTGCGTCACTTCTGCCGCCCCTGTTTCAAGGTATATA 450

GCCGTAGACGGAACTTCGCCTTTCTCTCGGCCTTAGCGCCATTTTTTTGG 500

GTGAGTGTTTTTTGGTTCCTGCGTTGGGATTCCGTGTACAATCCATAGAC 550

ATCTGACCTCGGCACTTAGCATCATCACAGCAAACTAACTGTAGCCTTTC 600

TCTCTTTCCCTGTAGAAACCTCTGCGGATCCGTGGT 636

Table. 1 Core promoter element predicted for CMV promoter

Motif	Pos	Score	Sequence
INR	310	0.96	CCAGTAC
INR	223	0.95	CCACTTG
INR	170	0.91	CCAATAG
INR	44	0.88	TCATTAG
INR	47	0.85	TTAGTTC
INR	369	0.84	CTATTAC
INR	503	0.83	CCAAAAT
INR	484	0.83	CCAAAAT
INR	336	0.82	CTACTTG
INR	247	0.82	TCATATG
TATA	567	0.93	TCTATATAAGCA
TATA	58	0.85	CCCATATATGGA
DPE	413	0.92	GGATA
DPE	361	0.91	AGTCA
DPE	42	0.90	GGTCA
DPE	69	0.89	AGTTC
DPE	49	0.89	AGTTC
DPE	17	0.88	AGTTA

Table. 2 Core promoter element predicted for EF1 promoter

Motif	Pos	Score	Sequence
INR	782	0.95	CCAGTTG
INR	1125	0.94	TCATTCT
INR	1033	0.87	CCATACT
INR	221	0.86	CCAGAAC
INR	299	0.85	TTACTTC
INR	964	0.85	TTAGTTC
INR	833	0.81	TCAAAAT
TATA	167	0.92	CGTATATAAGTG
TATA	502	0.84	CATTTAAAATTT
MTE	698	0.87	CAAGCTGGCCGG
MTE	662	0.81	CGAGCGCGGCCA
DPE	843	0.99	GGACG
DPE	683	0.99	GGACG
DPE	800	0.97	AGATG
DPE	1140	0.96	AGACA
DPE	183	0.95	AGTCG
DPE	571	0.94	AGATC
DPE	774	0.94	GGTCG
DPE	66	0.94	GGTCG
DPE	1115	0.93	GGATC
DPE	547	0.93	AGATA
DPE	784	0.92	AGTTG
DPE	53	0.92	AGTTG
DPE	412	0.92	AGTTG
DPE	42	0.92	AGTCC
DPE	998	0.91	GGTTG
DPE	349	0.91	GGTTG
DPE	873	0.91	AGTCA
DPE	966	0.89	AGTTC
DPE	368	0.89	AGTTC
DPE	247	0.89	GGTTC
DPE	1122	0.89	GGTTC
DPE	1147	0.89	GGTTC
DPE	1057	0.88	AGTTA
DPE	274	0.87	GGTTA
BRE	305	0.97	CCACGCC
BRE	942	0.91	GGGCGCC

Table. 3 Core promoter element predicted for hPGK promoter

Motif	Pos	Score	Sequence
INR	328	0.91	CCAATAG
INR	259	0.89	TCACTAG
INR	262	0.84	CTAGTAC
MTE	300	0.93	GCAGCGCGCCGA
MTE	80	0.90	GAAACGCAGCGG
DPE	275	1.00	AGACG
DPE	51	0.99	GGACG
DPE	232	0.99	GGACG
DPE	198	0.95	AGTCG
DPE	473	0.95	AGTCG
DPE	279	0.95	GGACA
DPE	142	0.93	GGATC
DPE	7	0.91	GGTTG
DPE	13	0.91	GGTTG
DPE	207	0.89	GGTTC
DPE	72	0.89	GGTTC
DPE	217	0.89	GGTTC
BRE	89	0.96	CGGCGCC
BRE	350	0.96	GCGCGCC
BRE	303	0.96	GCGCGCC

Table. 4 Core promoter element predicted for RPBSA promoter

Motif	Pos	Score	Sequence
INR	406	0.97	TCACTTC
INR	476	0.97	CCATTTT
INR	104	0.92	TCAGTCG
TATA	430	0.88	GGTATATAGCCG
TATA	17	0.86	AAAATAAAGTAA
DPE	443	1.00	AGACG
DPE	204	0.99	GGACG
DPE	167	0.97	AGATG
DPE	3	0.97	AGACC
DPE	534	0.96	AGACA
DPE	106	0.95	AGTCG
DPE	303	0.95	GGACA
DPE	149	0.95	GGACA
DPE	277	0.91	GGTCC
DPE	501	0.89	GGTTC
BRE	232	1.00	CCGCGCC

Table. 5 The TF binding sites predicted by AliBaba program for CMV promoter.

Promoter: CMV
Length: 617 bp
Number of sites found: 97

Class	Factor	Start	Stop
4.3.1.1	MEB-1	17	26
1.2.8.0	Id3	29	38
3.1.1.12	HNF-1C	29	38
4.1.3.0	NF-ATc3	29	38
9.9.29	AP-1	37	46
2.1.2.3	T3R	38	47
4.3.2.0	SRF	58	68
1.1.3.0	C/EBPalpha	75	84
2.3.1.0	Sp1	96	108
1.1.1.1	c-Jun	103	112
2.3.1.0	Sp1	109	118
2.3.1.0	Sp1	122	134
2.3.2.1	Egr-1	123	132
1.1.1.6	CRE-BP1	131	140
1.1.2.0	CREB	131	140
2.3.3.0	CPE_binding_pro	131	140
9.9.51	ATF	131	140
1.1.1.6	CRE-BP1	142	151
2.3.3.0	CPE_binding_pro	143	152
9.9.51	ATF	144	153
4.3.2.0	SRF	169	178
2.3.4.0	MBP-1_(1)	175	184
9.9.588	NF-kappaB	175	184
9.9.591	NF-kappaB(-like	175	184
4.1.1.0	c-Rel	176	185
9.9.590	NF-kappaB	176	185
1.1.1.6	CRE-BP1	184	193
1.1.2.0	CREB	184	193
2.3.3.0	CPE_binding_pro	184	193
9.9.51	ATF	184	193
2.3.1.0	Sp1	193	205
9.9.77	CACCC-binding_f	195	204
2.3.1.0	Sp1	217	230
9.9.539	NF-1	224	233
2.2.1.1	GATA-1	244	253
3.1.2.2	Oct-1	244	255
9.9.539	NF-1	249	260
1.1.1.6	CRE-BP1	267	276
1.1.2.0	CREB	267	276
2.3.1.0	YY1	289	301
2.3.1.0	Sp1	307	316
2.1.2.1	RAR-alpha1	315	324
2.1.2.3	T3R-alpha	315	325
2.1.1.4	ER	316	325
2.2.2.0	Ttx	316	325
2.3.4.0	KBP-1	326	335
4.1.1.0	c-Rel	326	335
9.9.213	EBP-1	326	335
9.9.588	NF-kappaB	326	335
9.9.590	NF-kappaB	326	335
9.9.591	NF-kappaB(-like	326	335
9.9.539	NF-1	337	346
1.1.1.2	c-Fos	355	366

1.1.1.5	GCN4	356	365
1.1.1.1	c-Jun	357	366
9.9.29	AP-1	357	366
1.1.3.0	C/EBPalpha(p20)	369	378
9.9.539	NF-1	386	395
2.3.1.0	Sp1	403	413
1.1.1.1	c-Jun	420	429
1.1.1.2	c-Fos	420	429
9.9.29	AP-1	423	432
2.3.4.0	AGIE-BP1	431	440
9.9.213	EBP-1	431	440
9.9.588	NF-kappaB	431	440
9.9.590	NF-kappaB	431	440
9.9.594	RelA	431	440
4.1.1.0	NF-kappaB	432	441
1.1.3.0	C/EBPalpha	434	443
9.9.537	NF-1	437	446
2.3.1.0	Sp1	444	456
1.1.1.6	CRE-BP1	453	462
1.1.2.0	CREB	453	462
2.3.3.0	CPE_binding_pro	453	462
9.9.51	ATF	453	462
9.9.539	NF-1	474	483
2.3.4.0	MBP-1_(1)	494	503
4.1.1.0	c-Rel	494	503
9.9.588	NF-kappaB	494	503
9.9.590	NF-kappaB	494	503
9.9.591	NF-kappaB(-like	494	503
9.9.594	RelA	494	503
1.1.3.0	C/EBPalpha	497	506
9.9.1469	Ik-1	498	507
9.9.1470	Ik-2	498	507
9.9.1471	Ik-3	498	507
9.9.535	NF-1	500	509
9.9.539	NF-1	500	509
2.3.1.0	YY1	503	512
9.9.51	ATF	505	514
2.3.1.0	Sp1	517	527
9.9.51	ATF	525	534
1.1.3.0	C/EBPalpha	528	537
2.3.1.0	Sp1	536	545
2.3.1.0	Sp1	555	565
4.3.2.0	SRF	566	575
1.1.1.1	c-Jun	585	594

Table. 6 The TF binding sites predicted by AliBaba program for EF-1 promoter.

Promoter: EF1
Length: 1192 bp
Number of sites found: 109

Class	Factor	Start	Stop
9.9.51	ATF	12	21
2.3.1.0	Sp1	15	27
1.1.3.0	C/EBPalpha	30	39
2.3.1.0	Sp1	38	47
2.3.3.0	MIG1	55	64
2.3.1.0	Sp1	56	70
2.3.1.0	Sp1	94	106
1.3.1.2	USF	97	106
9.9.701	PTF1-beta	111	120
9.9.428	ISGF-3	112	121
2.3.1.0	Sp1	132	143
9.9.77	CACCC-binding_f	150	159
2.3.1.0	Sp1	150	162
2.3.3.0	MIG1	154	163
9.9.535	NF-1	199	208
1.3.2.3	E2F	213	222
9.9.726	repressor_of_CA	214	223
2.1.1.1	GR	221	230
2.3.1.0	Sp1	250	264
2.3.1.0	Sp1	257	266
4.3.2.0	SRF	275	284
1.1.3.0	C/EBPalpha	280	289
1.2.8.0	Id3	297	306
3.1.1.12	HNF-1C	297	306
4.1.3.0	NF-ATc3	297	306
2.3.1.0	Sp1	303	316
9.9.539	NF-1	310	319
2.3.1.0	Sp1	354	364
2.3.1.0	Sp1	392	403
1.6.1.0	AP-2alphaA	398	407
2.3.1.0	Sp1	414	423
9.9.539	NF-1	420	429
2.3.1.0	Sp1	421	431
2.3.1.0	Sp1	430	443
2.3.1.0	Sp1	437	446
3.1.1.2	Ubx	497	506
2.3.1.0	Sp1	500	509
3.1.2.1	Pit-1a	502	511
2.1.1.4	ER	514	523
1.1.1.5	GCN4	532	541
9.9.535	NF-1	537	546
1.1.3.0	C/EBPalpha	551	560
9.9.539	NF-1	561	572
2.3.1.0	Sp1	562	571
9.9.537	NF-1	562	571
2.3.1.0	Sp1	571	580
3.5.3.0	IRF-1	587	596
2.1.1.1	GR	589	598
2.3.1.0	Sp1	598	610
1.6.1.0	AP-2alphaA	599	608
2.3.1.0	Sp1	604	613
2.3.1.0	Sp1	611	620

2.3.1.0	Sp1	617	626
9.9.270	ETF	645	654
2.3.1.0	Sp1	647	658
2.3.1.0	Sp1	666	675
2.3.1.0	Sp1	681	690
2.3.1.0	Sp1	697	709
2.3.1.0	Sp1	720	731
2.3.1.0	Sp1	729	739
2.3.2.1	Egr-1	744	753
2.3.1.0	Sp1	744	754
9.9.270	ETF	745	754
9.9.537	NF-1	749	758
2.3.1.0	Sp1	753	764
2.3.1.0	Sp1	764	777
2.3.1.0	Sp1	770	779
9.9.561	NF-muE1	799	808
4.3.2.0	SRF	802	811
2.3.1.0	Sp1	804	818
2.3.1.0	Sp1	811	821
2.3.1.0	YY1	833	842
2.3.1.0	Sp1	842	851
2.3.1.0	Sp1	861	870
3.5.1.2	REB1	862	871
1.1.1.5	CPC1	867	876
9.9.29	AP-1	867	877
1.1.1.1	c-Jun	868	877
9.9.32	AP-1	869	878
2.3.1.0	Sp1	874	883
3.5.1.2	RAP1	874	883
4.3.2.0	SRF	885	894
1.1.3.0	C/EBPalpha	903	912
1.3.1.2	USF	919	928
1.1.1.1	c-Jun	923	932
1.1.2.0	ATF-1	924	933
2.3.2.2	CF2-III	924	933
2.3.1.0	Sp1	939	948
2.3.3.0	MIG1	1000	1009
2.3.1.0	Sp1	1001	1011
9.9.588	NF-kappaB	1022	1031
2.3.4.0	MBP-2	1023	1032
4.1.1.0	c-Rel	1023	1032
9.9.213	EBP-1	1023	1032
9.9.590	NF-kappaB	1023	1032
9.9.592	NF-kappaB(-like	1023	1032
9.9.594	RelA	1023	1032
3.5.1.2	RAP1	1038	1047
9.9.77	CACCC-binding_f	1041	1050
2.3.1.0	Sp1	1041	1051
3.1.1.0	MATalpha2	1076	1085
2.3.1.0	Sp1	1086	1095
2.1.2.3	REV-ErbAalpha	1096	1105
1.1.3.0	C/EBPalpha	1118	1127
9.9.29	AP-1	1131	1140
1.1.3.0	C/EBPgamma	1150	1159
1.1.1.5	GCN4	1154	1163
2.3.2.2	Hb	1155	1164
4.3.2.0	SRF	1165	1174

Table. 7 The TF binding sites predicted by AliBaba program for hPGK promoter.

Promoter: hPGK
Length: 516 bp
Number of sites found: 50

Class	Factor	Start	Stop
1.1.3.0	C/EBPalpha	11	20
1.1.3.0	C/EBPalpha	19	28
2.3.1.0	Sp1	49	58
2.3.1.0	Sp1	64	73
9.9.1299	MPBF	72	81
3.5.1.2	FlbD	73	82
2.3.1.0	Sp1	84	98
2.3.1.0	Sp1	93	102
1.1.1.6	CRE-BP1	132	141
9.9.51	ATF	132	141
2.3.3.0	CPE_binding_pro	133	142
1.1.2.0	CREB	134	143
3.5.1.2	REB1	135	144
2.3.1.0	Sp1	162	174
1.6.1.0	AP-2alphaA	166	175
2.3.1.0	Sp1	168	181
2.3.3.0	CPE_binding_pro	169	178
3.5.2.0	c-Ets-1_68	177	186
2.3.1.0	Sp1	179	188
2.3.1.0	Sp1	185	195
3.4.1.0	TSF3	202	211
2.3.1.0	Sp1	221	235
3.5.2.0	GABP	241	250
1.1.1.6	CRE-BP1	251	260
2.3.1.0	YY1	285	294
1.1.3.0	C/EBPalpha	288	297
3.5.1.2	Adf-1	295	304
2.3.1.0	Sp1	298	312
2.3.1.0	Sp1	305	314
2.3.1.0	Sp1	314	327
9.9.150	CP1	323	332
9.9.539	NF-1	324	333
3.5.1.2	Adf-1	331	340
2.3.1.0	Sp1	342	354
2.3.1.0	Sp1	361	372
2.3.1.0	Sp1	369	383
2.3.1.0	Sp1	377	389
2.3.1.0	Sp1	384	397
2.3.1.0	Sp1	392	404
2.3.1.0	Sp1	398	407
2.2.1.1	GATA-1	410	419
2.3.1.0	Sp1	420	430
2.3.1.0	Sp1	426	435
3.6.1.0	TEC1	437	446
2.3.1.0	Sp1	452	461
1.3.1.2	USF	462	471
2.3.1.0	Sp1	503	512
1.6.1.0	AP-2	505	514
2.2.1.1	GATA-1	505	514
2.3.3.0	MIG1	509	518

Table. 8 The TF binding sites predicted by AliBaba program for RPBSA promoter.

Promoter: RPBSA
Length: 612 bp
Number of sites found: 59

Class	Factor	Start	Stop
1.1.3.0	C/EBPalpha	14	23
2.3.1.0	Sp1	28	41
2.3.1.0	Sp1	48	57
1.6.1.0	AP-2alphaA	66	75
2.3.1.0	Sp1	73	82
2.3.1.0	Sp1	88	99
1.6.1.0	AP-2alphaA	93	102
3.5.1.2	REB1	117	126
1.2.8.0	Id3	138	147
2.3.1.0	Sp1	138	147
2.2.1.1	GATA-3	166	175
2.3.1.0	Sp1	172	181
4.3.2.0	SRF	183	192
2.3.1.0	Sp1	194	203
2.3.1.0	Sp1	205	217
1.1.3.0	C/EBPalpha	211	220
1.6.1.0	AP-2alphaA	213	222
2.3.1.0	Sp1	223	234
2.3.2.1	Krox-20	225	234
2.3.1.0	Sp1	229	242
1.3.1.2	USF	237	246
1.1.1.6	ATF-a	240	249
1.1.2.0	CREB	240	249
2.3.3.0	CPE_binding_pro	240	249
2.3.1.0	Sp1	270	279
3.5.1.2	RAP1	291	300
1.1.3.0	C/EBPdelta	297	306
2.3.1.0	Sp1	310	319
2.3.1.0	Sp1	316	325
2.3.4.0	MBP-2	331	340
4.1.1.0	c-Rel	331	340
9.9.213	EBP-1	331	340
9.9.590	NF-kappaB	331	340
9.9.594	RelA	331	340
9.9.637	NRF-1	341	350
9.9.1197	NRF-1	341	350
9.9.150	CP1	359	368
3.5.2.0	c-Ets-1_68	374	383
2.3.1.0	Sp1	383	392
1.1.1.6	CRE-BP1	398	407
1.1.3.0	C/EBPalpha	398	407
2.3.3.0	CPE_binding_pro	398	407
9.9.29	AP-1	400	409
2.3.1.0	Sp1	411	420
4.5.1.0	TBP	427	436
4.4.1.0	E2	437	446
3.4.1.0	HSTF	446	455
2.3.1.0	YY1	473	482
2.3.2.2	Hb	474	483
2.3.2.2	Hb	492	501

3.5.3.0	NF-EM5	496	505
3.5.2.0	PU.1	499	508
4.1.1.0	NF-kappaB	510	519
9.9.539	NF-1	522	531
2.1.2.10	COUP	535	544
1.1.3.0	C/EBPalpha	565	574
2.2.1.1	GATA-1	583	592
9.9.701	PTF1-beta	587	596
3.4.1.0	HSE-binding_pro	600	609

Table. 9 The TF binding sites predicted by PROMO program.

EF1 (67 TFBDs)	CMV (62 TFBDs)	hPGK (55 TFBDs)	RPBSA (58 TFBDs)
Pax-5	C/EBPbeta	C/EBPbeta	RXR-alpha
p53	C/EBPalpha	NF-1	TFIID
c-Jun	GR-beta	TFII-I	HNF-3alpha
Egr-3	HOXD9	STAT4	GR
ETF	HOXD10	NF-AT1	GR-beta
TFII-I	c-Jun	c-Ets-1	Pax-5
C/EBPbeta	Pax-5	STAT1beta	p53
NF-1	p53	GR-alpha	IRF-1
GR-alpha	YY1	AP-2alphaA	GR-alpha
GR-beta	SRF	NFI/CTF	AP-2alphaA
C/EBPalpha	TFII-I	Pax-5	NF-AT1
VDR	STAT4	p53	ENKTF-1
PXR-1:RXR-alpha	E2F-1	EBF	TFII-I
ENKTF-1	c-Ets-1	IRF-1	YY1
FOXP3	HNF-1C	FOXP3	XBP-1
c-Myb	FOXP3	NF-AT1	C/EBPbeta
IRF-1	HNF-1B	GCF	STAT4
TFIID	c-Myb	RXR-alpha	c-Ets-1
NF-AT1	XBP-1	c-Jun	Elk-1
IRF-2	ENKTF-1	T3R-beta1	FOXP3
XBP-1	ER-alpha	E2F-1	PR B
E2F-1	Sp1	Elk-1	PR A
NF-AT2	NFI/CTF	Sp1	VDR
STAT4	RXR-alpha	TFIID	PXR-1:RXR-alpha
c-Ets-1	ETF	HIF-1	MEF-2A
PR B	ATF-1	GR-beta	E2F-1
PR A	CREB	XBP-1	PPAR-alpha:RXR-alpha
RelA	ATF3	ENKTF-1	WT1
Elk-1	ATF-2	ER-alpha	GCF
AhR:Arnt	ATF	ATF3	c-Myc
AP-2alphaA	NF-kappaB	PR B	USF1
YY1	RBP-Jkappa	PR A	ER-alpha

HNF-3alpha	GR-alpha	c-Ets-2	NFI/CTF
ER-alpha	NF-AT2	ETF	AR
GATA-3	NF-AT1	C/EBPalpha	C/EBPalpha
NFI/CTF	NF-1	CTF	NF-Y
PPAR-alpha:RXR-alpha	GATA-1	NF-Y	NF-1
GCF	STAT1beta	YY1	ETF
GATA-1	AP-1	AR	AhR:Arnt
Sp1	HNF-3alpha	AhR:Arnt	c-Ets-2
GR	GR	NF-kappaB	c-Jun
AP-1	TFIID	PPAR-alpha:RXR-alpha	Sp1
RXR-alpha	PR B	RelA	c-Myb
c-Fos	PR A	GR	HNF-1C
T3R-beta1	AP-2alphaA	RAR-beta	HNF-1B
SRY	RAR-beta		NF-AT2
TCF-4E	Egr-3		STAT1beta
c-Ets-2	AhR:Arnt		COUP-TF1
STAT1beta	POU2F1		
ATF3	IRF-1		
NF-kappaB	NF-AT1		
NF-kappaB1	NF-kappaB1		
HNF-4alpha	c-Fos		
SRF	GATA-2		
LEF-1	T3R-beta1		
TCF-4	c-Ets-2		
RAR-beta	CTF		
MAZ	NF-Y		
AhR	E2F		
EBF	VDR		
HOXD9	PXR-1:RXR-alpha		
HOXD10	RAR-alpha1		
STAT5A			
Ik-1			
ATF-1			
E2F			
RBP-Jkappa			

Chapter V:

The potential improvement of CAR T cell function by Mcl-1 and miR429 overexpression

As noted in the Introduction, the mitochondrial dynamic has a central role in T cell persistence and memory development. We therefore selected two genes based on their role in mitochondrial dynamics; Mcl-1 and TCAIM. Mcl-1 upregulation protects T cells from AICD and enhances T cell persistence (1). Also, Mcl-1 promotes mitochondrial fusion, an essential step in T_M formation (2-4). TCAIM downregulation was correlated with an increase in T_M and mitochondrial fusion (5-7). Our bioinformatic analysis predicted miR429 as a negative regulator of TCAIM. We hypothesized that overexpression of Mcl-1 and miR429 would facilitate mitochondria fusion and T_M development in Her2-CAR T cells.

First, we used the Tet-On Sleeping Beauty (SB) system to overexpress GOI (construct has been optimized in chapter III). However, utilizing different protocols, transfection efficiency remained lower than 10%. Hence, we created a Tet-On lentiviral (LV) system to improve the efficiency of gene delivery. This system also had several drawbacks, including low transduction efficiency and weak inducibility. Therefore, we decided to use a constitutive system to overexpress Mcl-1 and miR429, along with a GFP-P2A-Her2CAR in T cells.

This chapter is an unfinished story of Mcl-1, the work being affected by the SARS-CoV-2 pandemic. Our laboratory only received permission to work with the LV system in July 2019. The first steps were making the LV constructs, cloning, optimization methods of LV production, and transduction methods. In this time, I tried to complete at least a proof of concept that suggests Mcl-1 promotes T_M development possibly via mitochondrial fusion.

5.1. Investigation of Tet-On inducible system in SB system

In order to have controlled expression of Mcl-1, we used the Tet-On SB that was developed and described in chapter 3. This system showed high inducibility and low background expression. Hence, Jurkat T cells were electroporated with Tet-On SB plasmids with or without cop-Mcl-1 (here named 'Mcl-1') under TCE promoter. Transfected Jurkat cells were purified by 2 µg/mL of Puromycin for two weeks. Mcl-1 upregulation was verified at RNA and protein levels using qPCR and western blot assays, respectively (Figure 5.1). In line with previous reports, the expression of Mcl-1S (in our intronless sequence) indicated that protease cleavage of Mcl-1L by caspase 3/8 is probably the primary mechanism for Mcl-1S production (8, 9).

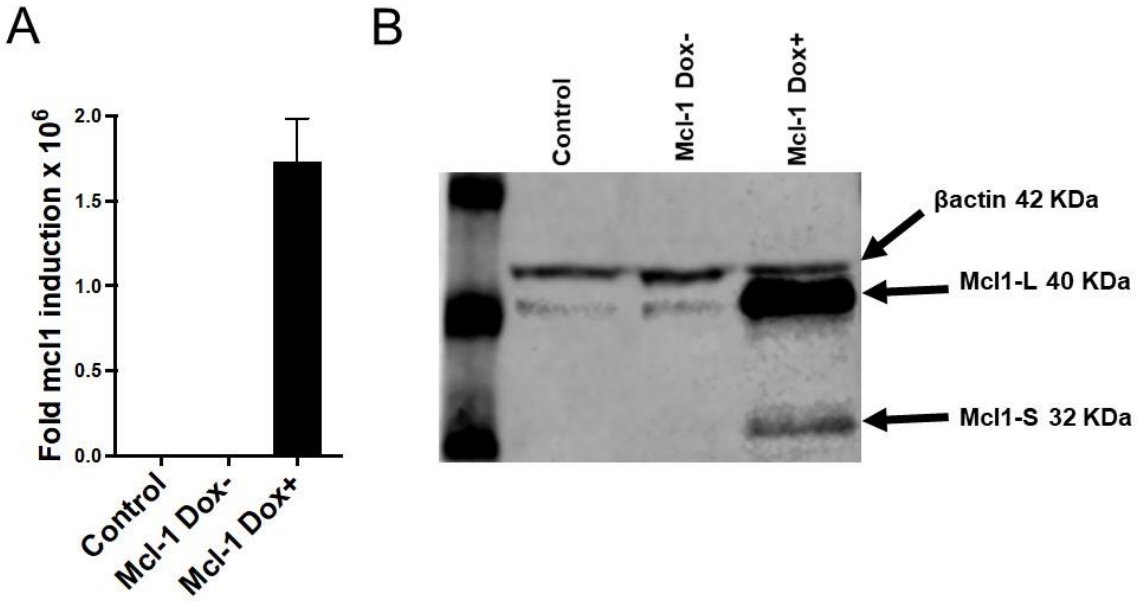

Figure 5.1. Quantification of Mcl-1 expression 24 hours after treatment of cells with 5 µg/mL of doxycycline. Jurkat cells were lysed for RNA or protein extraction. **(A)** Mcl-1 expression at mRNA level using qPCR assay, and **(B)** Western blot analysis for Mcl-1 protein verified the upregulation of long and short isoforms of Mcl-1. The graph represents the mean ± SD of three independent experiments.

Next, two electroporation methods, Neon electroporation (Thermo Fisher) and 4D-Nucleofector (Lonza), were used to transfect primary T cells (10). However, the transfection efficiency was lower than 10%. Since artificial antigen presenting cells have

only just been developed in the lab but, were not available at this time to expand CAR T cells (Lawrence Cooper's group), we decided to develop a Tet-On LV system.

5.2 Investigation of Tet-On inducible system in lentiviral (LV) system

In order to improve gene delivery efficiency, we decided to use the LV system. First, we removed the Poly(A) site downstream of Mcl-1 and then sub-cloned the construct into a third-generation LV system, pCCLSin (Figure 5.2A). After producing LV particles, HEK293T cells were transduced at MOI 2 with 8 µg/mL of polybrene. After 48 hours, cells were treated with 0 to 10 µg/mL of doxycycline. The expression level of Mcl-1 was measured at RNA (Figure 5.2B) and protein level (Figure 5.2B) and compared to constitutive expression. Unfortunately, Tet-On lost its inducibility in LV, and even 10 µg/mL of doxycycline did not significantly increase the Mcl-1 level. In addition, transduction efficiency was ~10%, and increasing the MOI to 30 did not increase the percentage of transduced T cells (Figure 5.2C).

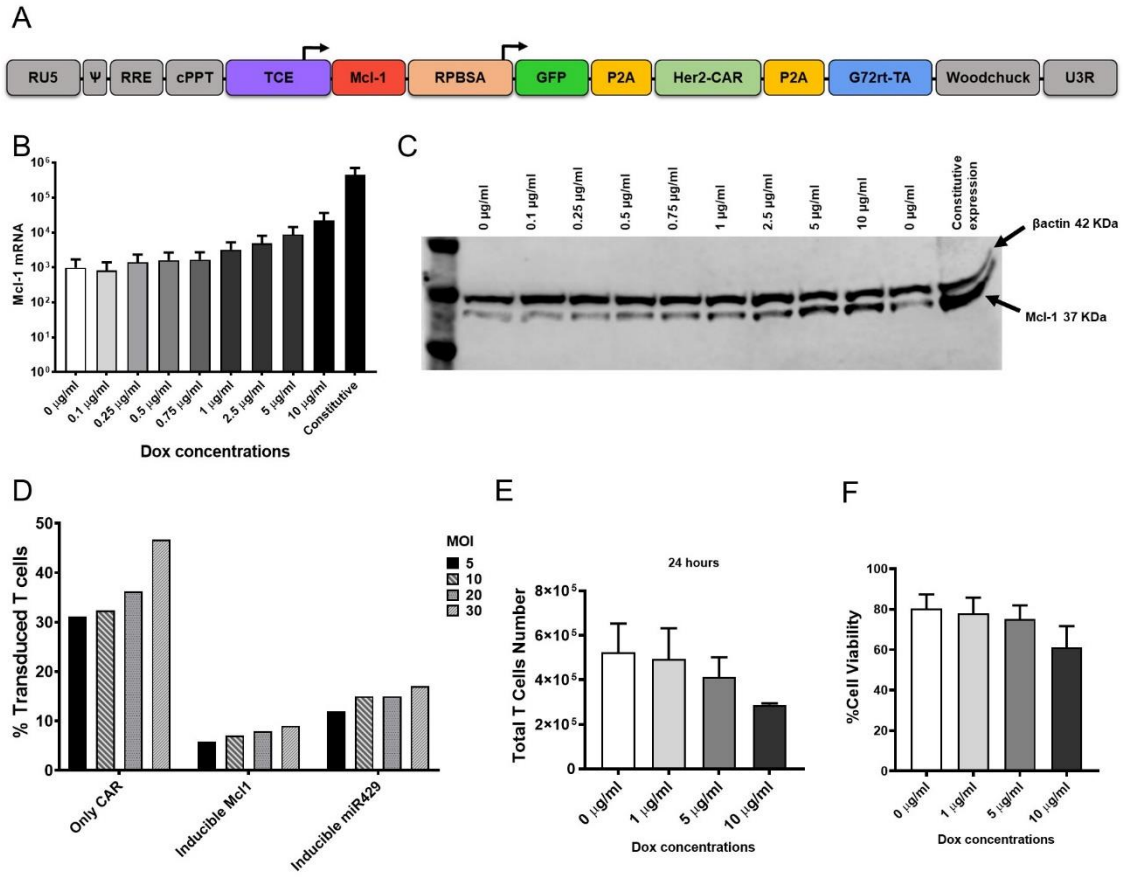

Figure 5.2. Tet-On system showed poor inducibility in the LV system. **(A)** Schematic representation of the Tet-On LV system. **(B & C)** HEK93T cells were transduced with LV particles at MOI 2 along with 8 μg/mL of polybrene. After 48 hours, HEK293T cells were treated with different concentrations of doxycycline. After overnight treatment, HEK293T cells were proceeded to measure Mcl-1 expression at RNA and protein level using qPCR and western blot. **(D)** A pilot experiment using the Tet-On LV system for Mcl-1 and miR429 showed low transduction efficiency compared to the LV expressing only Her2-CAR. **(E & F)** Human primary T cells cultured for 24 hours in the presence of 0, 1, 5, and 10 μg/mL of doxycline. LUNA-II™ automated cell counter (Thermo Fisher) was used to measure the total cell number. Cell viability was determined by the resazurin assay. Three experiments were performed in triplicate, except (D) pilot experiment only.

doxycycline is an antibiotic which blocks bacterial protein translation. In human cell lines, doxycycline was shown to reduce proliferation, increase apoptosis, and promote glycolytic metabolism (11). Consistent with this, a 10 μg/mL of doxycycline treatment for 24 hours decreased the cell number and cell viability (Figure 5.2E & F).

5.3 Constitutive overexpression of Mcl-1 and miR429 in Her2-CAR T cells

5.3.1 Construct design

Since the Tet-On system failed to operate in an inducible manner in LV-transduced cells, we decided to use the constitutive overexpression of Mcl-1 and miR429 in Her2-CAR T cells. We chose EF-1 to express the GFP-P2A-Her2CAR and hPGK to transcribe Mcl-1 or miR429. The promoter choice for longer RNA (GFP-P2A-Her2CAR, ~2.3 kb) was EF-1, while for transcribing Mcl-1/miR429 (≤1 kb), we selected hPGK (see chapter IV) (4). pCCLsin group represents T cells that underwent CD3/CD28 activation, LV transduction procedure, and expresses GFP marker (Figure 5.3A). Her2CAR is the control group and expresses GFP and Her2-CAR (Figure 5.3A).

It has been shown that CD28- CD3ζ -CAR T cells aggregate at the cell surface and cause an antigen-independent CAR stimulation (12). CD28 stimulation of CAR promotes CAR T cell survival as well as CAR T cell exhaustion (12, 13). Besides, the level of Her2-CAR expression is correlated with the extent of CAR T cell cytotoxicity (1). Therefore, the

level of the CAR should be similar in the control and treated groups. To express a GOI in the treatment group, we had three options (Figure 5.3B). The first option was to express all genes under EF-1 using two P2A sequences (Figure 5.3B) (1). The advantage of this system is the higher LV titer and transduction rate since this design has a smaller size and contains only one promoter. However, the expression level of Her2-CAR at the protein level between the control and treatment groups will not be equal (see chapter IV).

The second design produces two RNA, one from hPGK and another from EF-1. Since there is no poly(A) site after Mcl-1, both RNA encode Her2-CAR (Figure 5.3B). Therefore, the amount of CAR protein is slightly different in the two compared groups. Adding a Poly(A) site after Mcl-1 would most likely reduce the LV titer and transduction. Only the third strategy resulted in the robust expression of Her2-CAR in the treatment and control group (Figure 5.3B). It worth mentioning that we have tested miR429 expression in the first and second designs, and fold induction was 10 to 25 compared to 50 fold change in the third design.

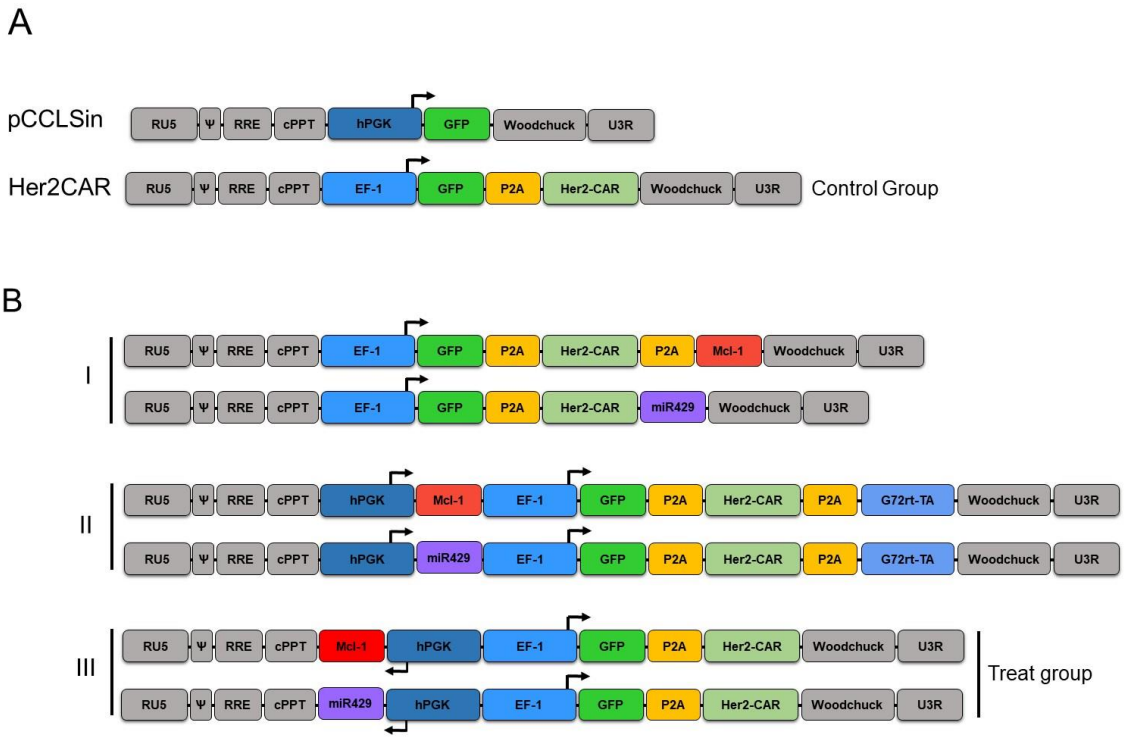

Figure 5.3. LV constructs have been used in this study. **(A)** pCCLsin is the original vector that only expresses a GFP. The control group expresses both GFP and Her2-CAR under

EF-1 promoter **(B)** Strategies to express GOI along with a HER2-CAR. We used the third strategy to acquire a ubiquitous expression of Her-CAR in the control and treated group.

5.3.2 miR429 targets TCAIM by binding to its 3′ UTR

Bioinformatics analysis predicted miR429 has potential binding sites within TCAIM, MFF, and TET-2 3'UTR (Figure 5.4A). TCAIM is a mitochondrial gene, and its downregulation has been linked to an increase in mitochondrial fusion and T_M development (5-7). MFF enhances mitochondrial fission by recruiting Drp1 at OMM (14), and the downregulation of MFF by miR27 increased the mitochondrial fusion in human cells (15). Downregulation of TET-2 also has been associated with long-term CAR T cell persistence and complete remission (16). Further studies showed that inhibition of TET-2 improves the CAR T cell therapy via epigenetic changes that encourage T_M differentiation (16, 17).

First, stem-loop qRT-PCR (18) confirmed that the genomic sequence ranged from 1168816 to 1169361 in chromosome 1 (GRCh38.p12) and that this produced a 22 bp mature miR429-3p (Figure 5.4B). As flanking sequences, we arbitrarily cloned 190 bp upstream and 274 bp downstream of the miR429 pre-miRNA sequence. miR429 overexpression in HEK293 cells resulted in the downregulation of TCAIM, MFF, and TET-2 at mRNA level (Figure 5.4C). To verify the predicted miR429 binding sites in Figure 5.3B, three repeats of each binding site were cloned downstream of a luciferase gene (pmirGLO dual-luciferase vector). Mutated sequences of each binding site were also cloned as the negative control. The reporter vectors were transfected into HEk293T cells overexpressing miR429, and luciferase assay carried out 48 hours post-transfection. Reporter assay confirmed the direct binding of miR429 to the TCAIM, MFF and TET-2 3′ UTR (Figure 5.4D). Since the main focus of this study was mitochondrial related genes (Mcl-1 and TCAIM); we only confirmed the TCAIM downregulation by miR429 at the protein level (Figure 5.4E).

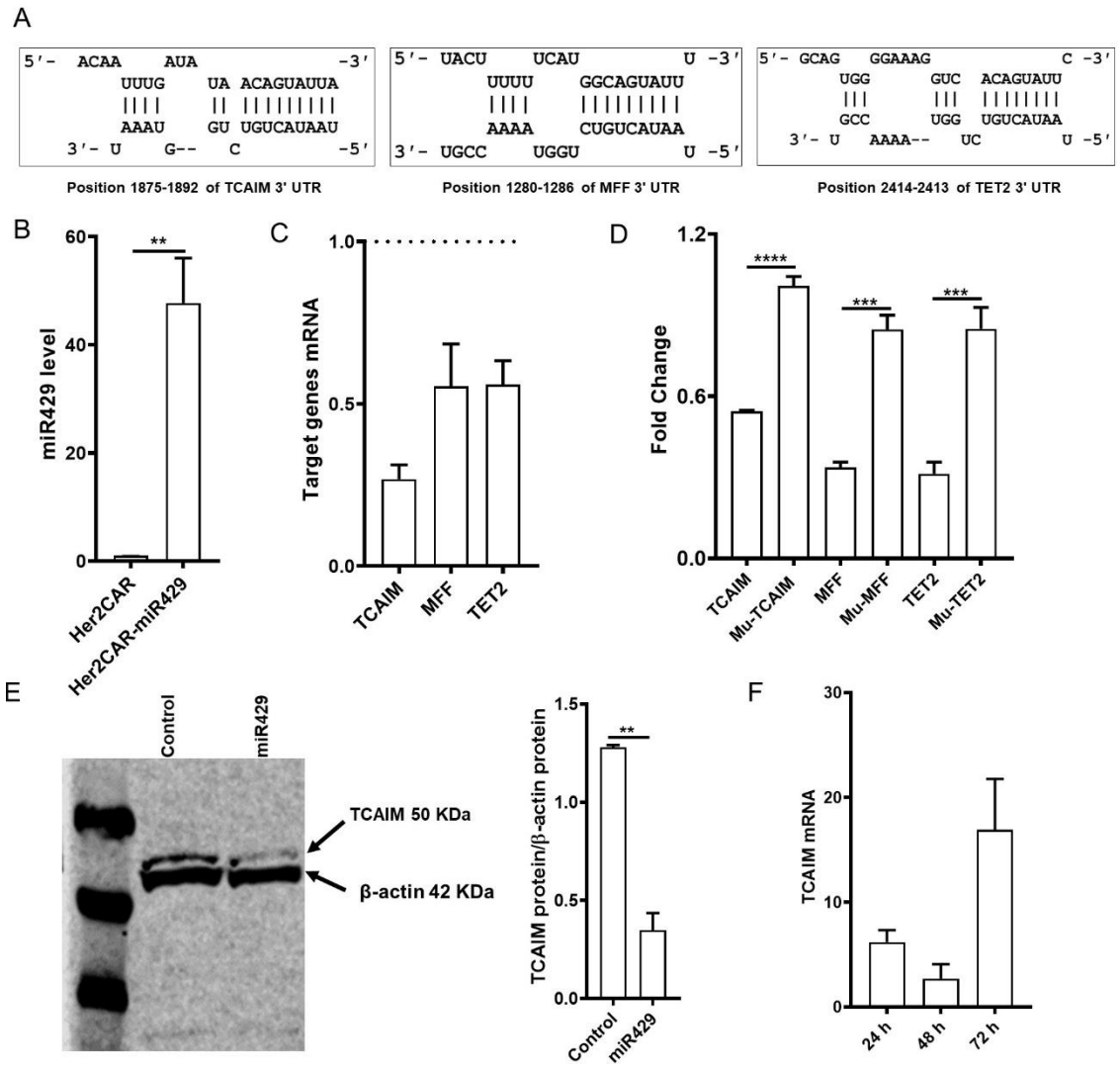

Figure 5.4. Confirmation of TCAIM, MFF, and TET-2 as miR429 targets **(A)** miR429 binding sites within 3′ UTR of TCAIM, MFF, and TET-2 predicted by DIANA-microT tool (19, 20). **(B)** Stem-loop RT-qPCR assay verified the elevated level of mature miR429, 48 hours post-transduction. **(C)** SYBR green qPCR assay for TCAIM, MFF, and TET-2 showed miR429 upregulation led to target gene downregulation in HEK293T cells. The comparative CT ($2^{-\Delta\Delta CT}$) method was utilised to analyse the relative expression level of target genes. β-actin was used as the housekeeping gene. **(D)** HEK293T overexpressing miR429 were transfected with the reporter vectors carrying wild type or mutated miR429 binding sites of TCAIM, MFF, and TET-2. This reporter expresses a second luciferase gene (Renilla) under the SV40 promoter as an internal control to minimize the transfection error. Fold induction was calculated by the following formula:

Fold induction $= \frac{\text{Read from Firefly gene}}{\text{Read from Renilla gene}}$. **(E)** Western blot analysis of TCAIM and β-actin on the HEK293T cell lysate 48 after transduction. Statistical analysis: all data are presented as the mean ± SEM and pooled from three independent experiments, (B & E) two-tailed t-test; (D) one-way ANOVA test with Bonferroni post-test correction (*P < 0.05, **P < 0.01, ***P < 0.001, ****P < 0.0001).

5.4 Functional analysis of Her2-CAR T cells overexpressing Mcl-1 or miR429

5.4.1 An overview of workflow and study design

The workflow of *in vitro* assays is briefly described in Figure 5.5. Cytotoxicity and IL-2/INF-γ release assays carried out one week after transduction while the majority of CAR T cells were still T_{EFF} or T_{EM}. TMRE assay was also carried out at this time point because T_{EFF} cells are more susceptible to the AICD. Ten days post-transduction, CD4/CD8 Her-CAR T cells were stained for T_{reg} markers ($CD25^{+}CD127^{-}$) and T cell activation marker CD69. Three weeks post-transduction, CD4/CD8 CAR T cells were stained for T_M cell markers (CCR7, CD45RO, CD45RA, CD27, CXCR3, CD95 and CD57). At this time point, mitochondrial mass (Mitotracker staining) and the ratio of mitochondrial (mt)DNA:gDNA were also measured.

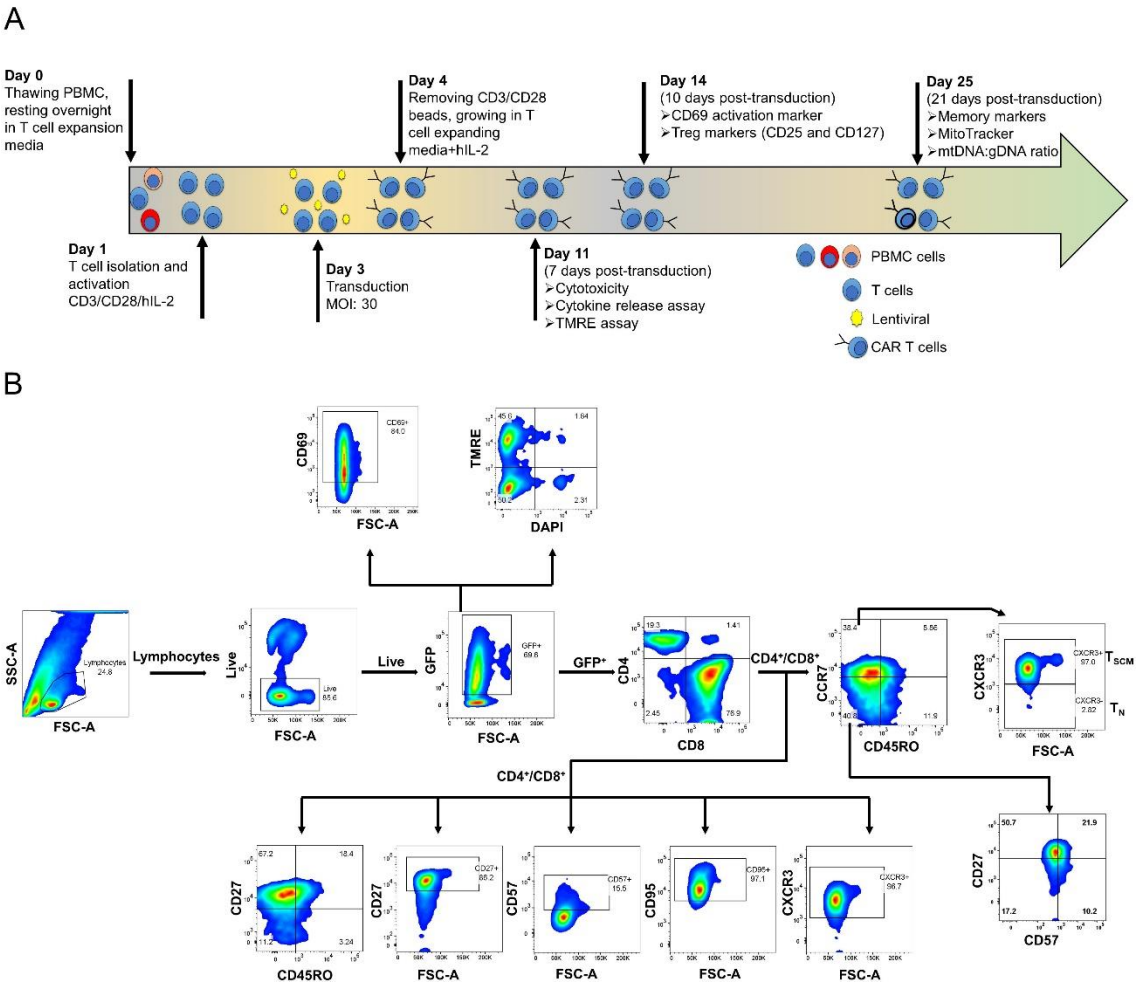

Figure 5.5. An overview of **(A)** workflow and **(B)** gating strategy used in this study. The fluorescence minus one (FMO) control was used for two colour plots.

5.4.2 Experiments seven days post-transduction

5.4.2.1 Transduction, cytotoxicity and cytokine release assays

CD95L induces AICD in T cells via two cascades. First, at the high level of activated caspase 8, caspase 8 directly activates caspase 3 and initiates apoptosis independent of mitochondria. Second, the mitochondria-dependent pathway, which leads to the release of cytochrome C into the cytosol (21). T cells with elevated expression of Bcl2/Mcl-1 (e.g., T_M) are protected against AICD through the second pathway while they benefit from non-apoptotic functions of the CD95 (see introduction). Plus, culturing CAR T cells with 46 ng/mL of CD95L enhanced the CAR T cell functions and the number of T_M cells (22-

25). Accordingly, we hypothesized that treatment of Her2CAR-Mcl-1 T cells with 46 ng/mL of CD95L would improve TM development while most of CAR T cells are protected against AICD.

Viral titer ranged from 6-10 × 10^7 TU/mL, even when two promoters were used (1). However, Her2CAR-Mcl1 had lower transduction efficacy (~30%) compared to the other constructs (Figure 5.6A). The use of two promoters (EF-1 and hPGK), higher size (1.5 kb more compared to the control), and complexity of the Mcl-1 transcript can negatively affect the reverse transcriptase activity during the transduction process.

Cytotoxicity assay carried out by the co-culturing of CAR T cells with Luciferase$^+$/Her2$^+$ MCF-7 cells in a 5:1 ratio, as described before in chapter IV (1). Luciferase expression was read 24 and 48 hours after incubation of the Her2-CAR T cells with MCF-7 cells. The percentage of the live cells was calculated using the following formula:

$$\%\text{Target cell viability} = \frac{\text{read from the sample well}}{\text{read from untransduced T cells} + \text{MCF} - 7 \text{ cells}} \times 100$$

Her2-CAR T cells in the control group had ~10% more cytotoxicity activity at the 24 hour time point (P> 0.9). All CAR T cells killed MCF-7 cells within 48 hours of post-incubation (Figure 5.6B).

Next, CAR T cells were incubated with MCF-7 cells (ratio 2:1) for 24 hours, and supernatant were analysed for IL-2 and IFN-γ secretion by ELISA (Figure 6C & D). All CAR T cells had similar levels of cytokine secretion. For both cytotoxicity and cytokine release experiments, samples were checked for the percentage of CAR T cells (GFP$^+$ cells) before co-culturing with MCF-7. We admixed in untransduced cells to normalise the total number of T cells and CAR T cells among samples.

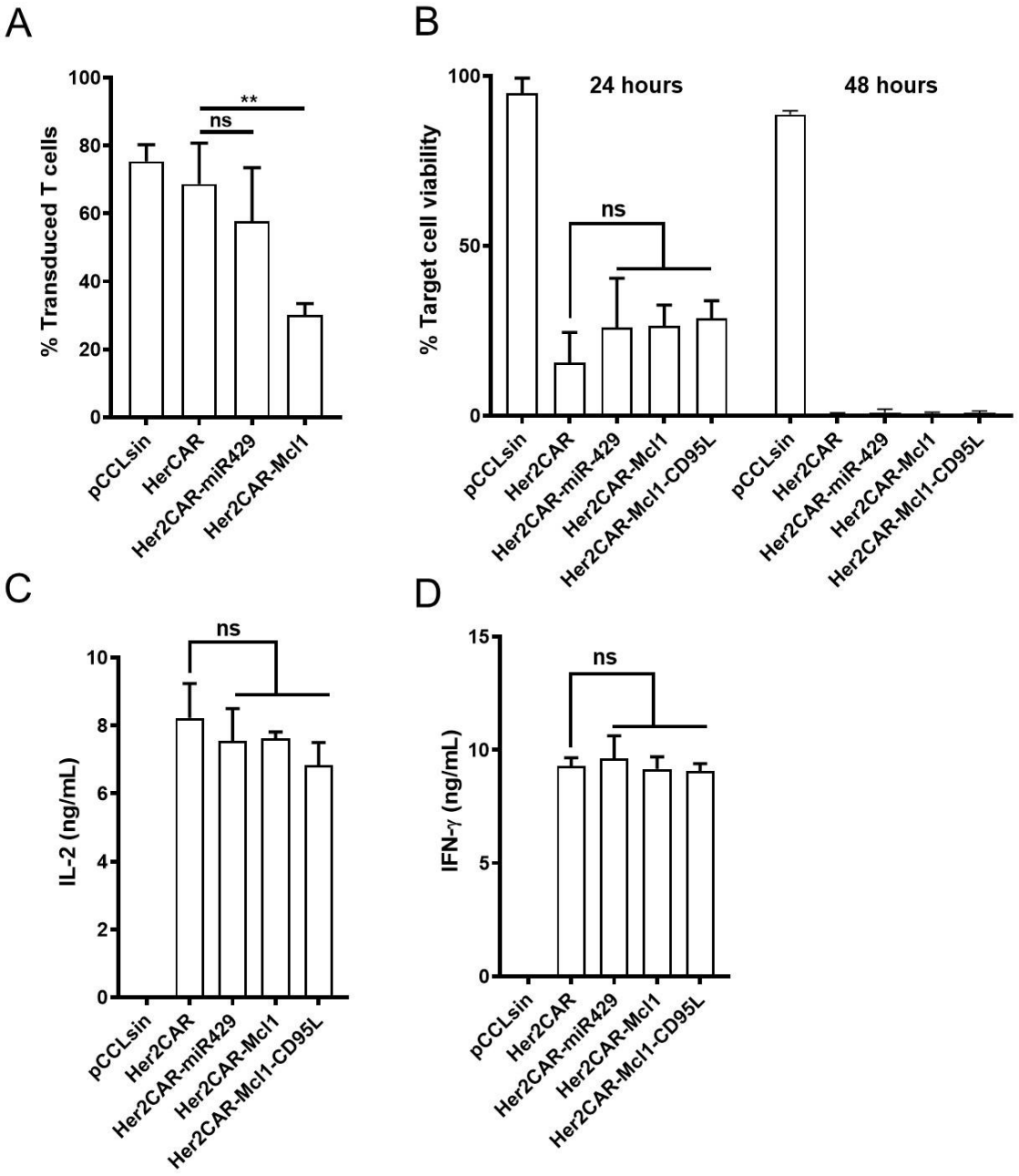

Figure 5.6. Functional analysis of Her2-CAR T cells. **(A)** Percentage of transduced T cells at MOI:30. **(B)** Cytotoxicity assay of Her2-CAR T cells 24 and 48 hours after incubation with Luciferase^{+}/Her-2^{+} MCF-7 cells (ratio 5:1). **(C & D)** Cytokine release capability of Her-CAR T cells measured by ELISA. Supernatants were collected 24 hours after incubation of CAR T cells with MCF-7 cells (ratio 2:1). Statistical analysis: data represent the mean ± SD of three independent experiments. (A, C & D) one-way (B) two-way ANOVA test with Bonferroni post-test correction (**P=0.005).

5.4.2.2 Activation-induced cell death (AICD) mediated by CD95L

Healthy mitochondria with high membrane potential ($\Delta\Psi m$) will retain the TMRE dye, whereas depolarised mitochondria release it. DAPI binds to the AT-rich regions in DNA exposed in cells with compromised plasma and nuclear membrane integrity, thus discriminating between live ($DAPI^-$) and dead cells ($DAPI^+$). Hence, in an AICD experiment stained with TMRE and DAPI dyes, four distinct cell populations can be seen (Figure 5.7A).

Previously we showed that ~90% CAR T cells overexpressing Mcl-1 are protected against AICD triggered by 1 µg/mL of CD95L (see chapter IV) (1). In this chapter, we increased the CD95L concentration to 3 µg/mL to test the protection at the highest concentration. As shown before (1), overexpression of Mcl-1 decreased the AICD in CAR T cells. Her2-CAR-Mcl1 and Her2CAR-Mcl1-CD95L T cells showed the highest number of healthy CAR T cells compared to the control (Figure 5.7B). Interestingly, cells were grown with 46 ng/mL of CD95L had higher content of fully viable cells (~38%) compared to the control (~12%). Her2CAR-miR429 T cells were more susceptible to AICD, possibly due to Bcl-2 downregulation via miR429 (26).

All samples had ≥90% viable CAR T cells (Figure 5.7D). CAR T cells overexpressing Mcl-1 had ~2% higher viable cells compared to the control. CAR T cells upregulated Mcl-1 and have been grown with 46 ng/mL CD95L, had the lowest content of fully viable cells (90%) with more early apoptotic cells. The presence of early apoptotic cells could be due to the AICD activation through the mitochondria-independent pathway (21, 27).

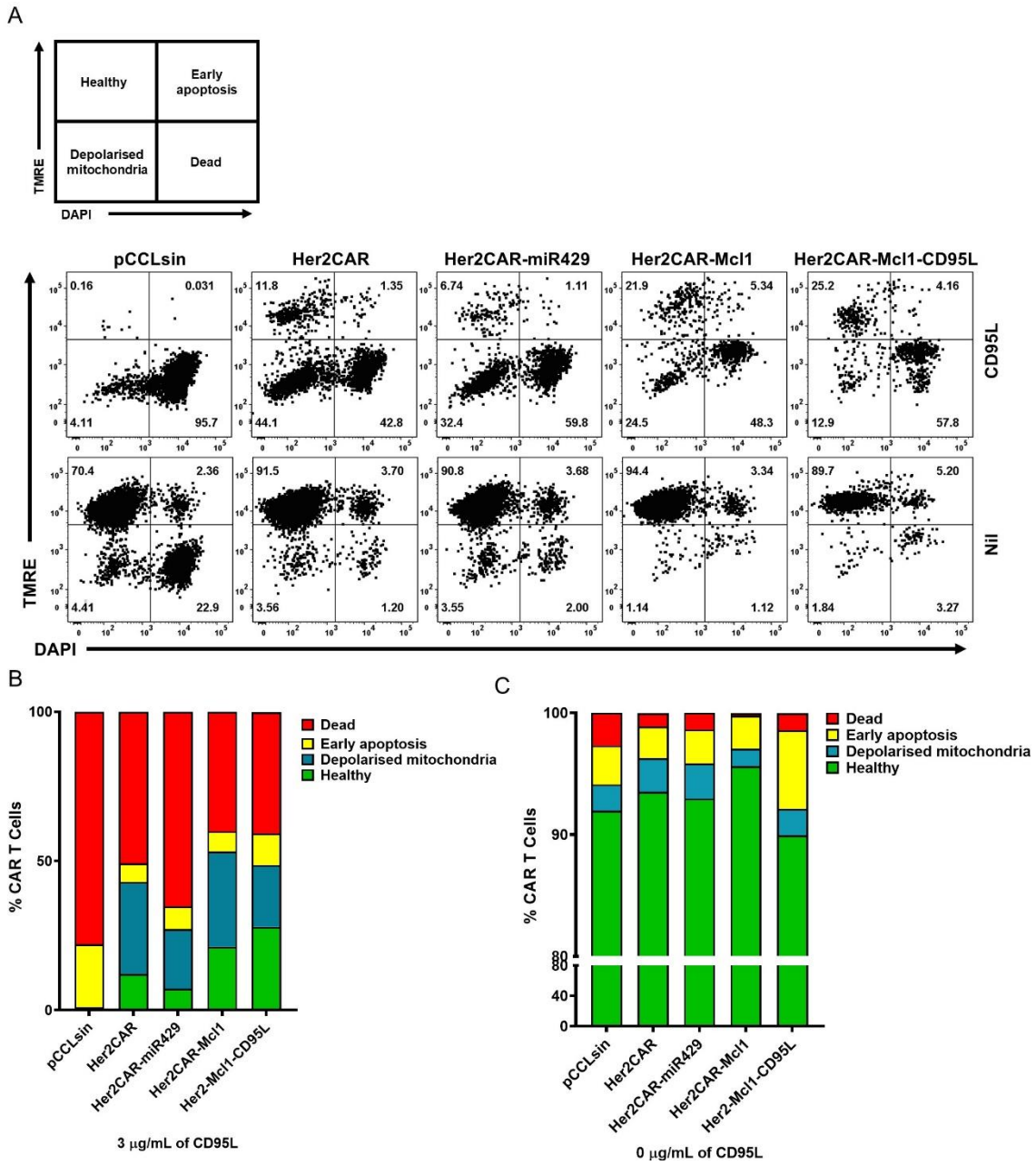

Figure 5.7. TMRE assay following overnight treatment with 3 μg/mL of CD95L. **(A)** Her2-CAR T cells were stained with 4 μM TMRE and 50 ng/mL DAPI dyes. GFP^+ CAR T cells were electronically gated for quantification of TMRE and DAPI signals using the YG586/16 and BV421 channels. **(B & C)** Graphs represent the mean of two independent experiments.

5.4.3 Experiments ten days post-transduction

5.4.3.1 CD69 expression following antigen stimulation

Following one hour after TCR engagement with antigen, the phosphorylation of ITAM domains lead to CD69 expression in T_N cells (28). CD69 protein was maintained on the cell surface for several days, suggesting relatively stable protein. CD69 stimulation on T cells induces proliferation, Ca^{2+} efflux, and IL-2/INF-γ/TNF production (28).

Her2-CAR T cells had a higher population of $CD96^{+,}$ although it was not statistically significant (P>0.9) (Figure 5.8). The control group, at this time point, comprises more T_{EFF} compared to other samples (Figure 5.9). Therefore, it is not surprising that the control group also had higher $CD69^{+}$ CAR T cells.

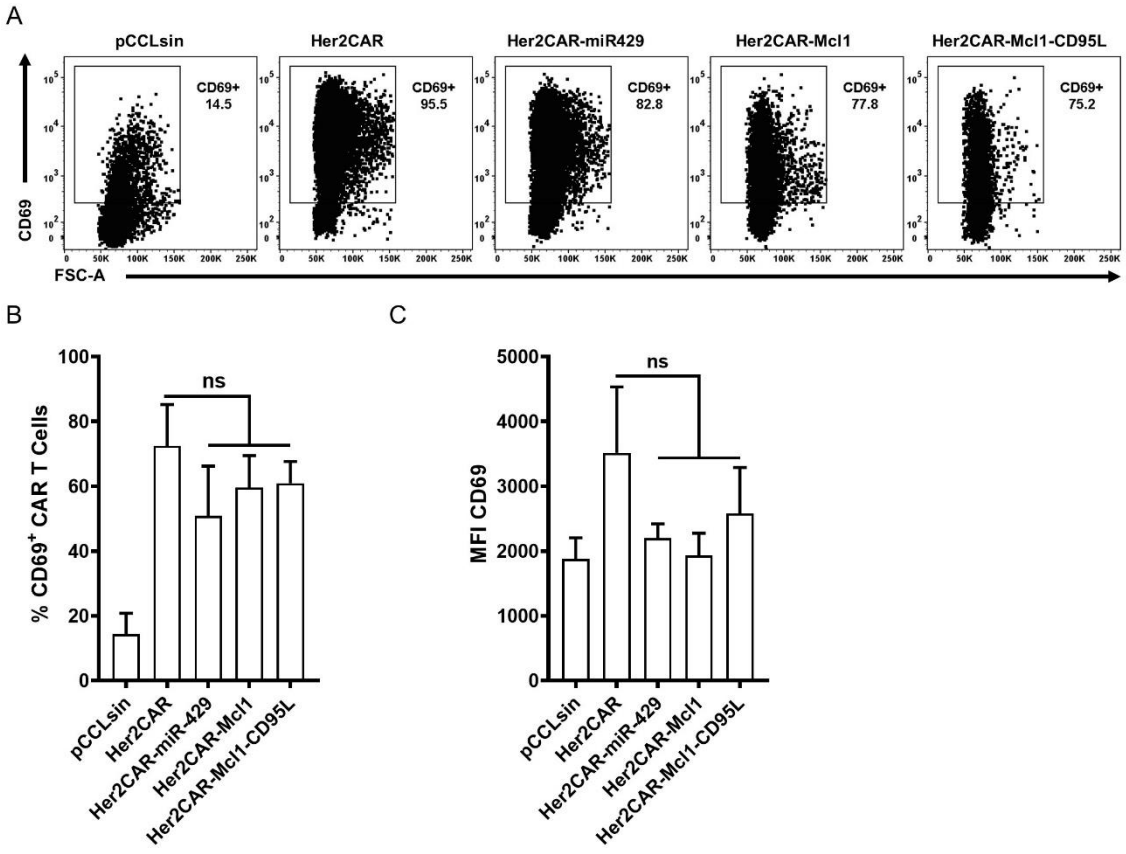

Figure 5.8. (A) Her2-CAR T cells were co-cultured with MCF-7 cells overnight. Live GFP^{+} cells were gated for CD69, as previously described in chapter IV (1). **(B & C)** Graphs represent the mean ± SEM of three independent experiments. Statistical analysis:

One-way ANOVA test with Bonferroni post-test correction. MFI: mean fluorescent intensity.

5.4.3.2 Composition of Her2-CAR T cells ten days post-transduction (focus on T_{reg})

Despite the vital role of T_{reg} in self-tolerance and autoimmune diseases, T_{reg} dampen T cell responses, particularly CAR T cell therapy (29-31). Although the majority of T_{reg} are $CD4^+$ T cells, several subsets of $CD8^+$ T_{reg} cells have been characterized (32, 33). Generally, T_{reg} cells are divided into natural T_{reg} (developed in the thymus) and adaptive T_{reg} (generated after antigen stimulation) (34). Several markers have been used to define the adaptive $CD4^+$ and $CD8^+$ T_{reg} (33, 35). CD25 and FoxP3 are the common markers that have been used to identify $CD4^+$ T_{reg} (32-34). However, the intracellular expression of FoxP3 limits its application. It has been shown that using $CD25^+CD127^{-/low}$ signature is comparable to the conventional markers, $CD25^+Foxop3^+$, in defining $CD4^+$ and $CD8^+$ T_{reg} (33, 36). Furthermore, CD25 and CD127 expression distinguishes between T_{reg}, T_{EFF}, $T_{CM,}$ and T_{EM} within a mixed T cell population (Figure 5.9A) (37, 38).

CD4/CD8 Her2CAR-Mcl1 and Her2CAR-Mcl1-CD95L had the lowest percentage of phenotypes resemble to T_{EFF} and T_{reg} cells compared to the control (Figure 5.9B & C). At this time point, Her2CAR-Mcl1-CD95L CAR T cells were mainly composed of phenotypes similar to T_{EM} ($P<0.05$). I will discuss these results in the next section.

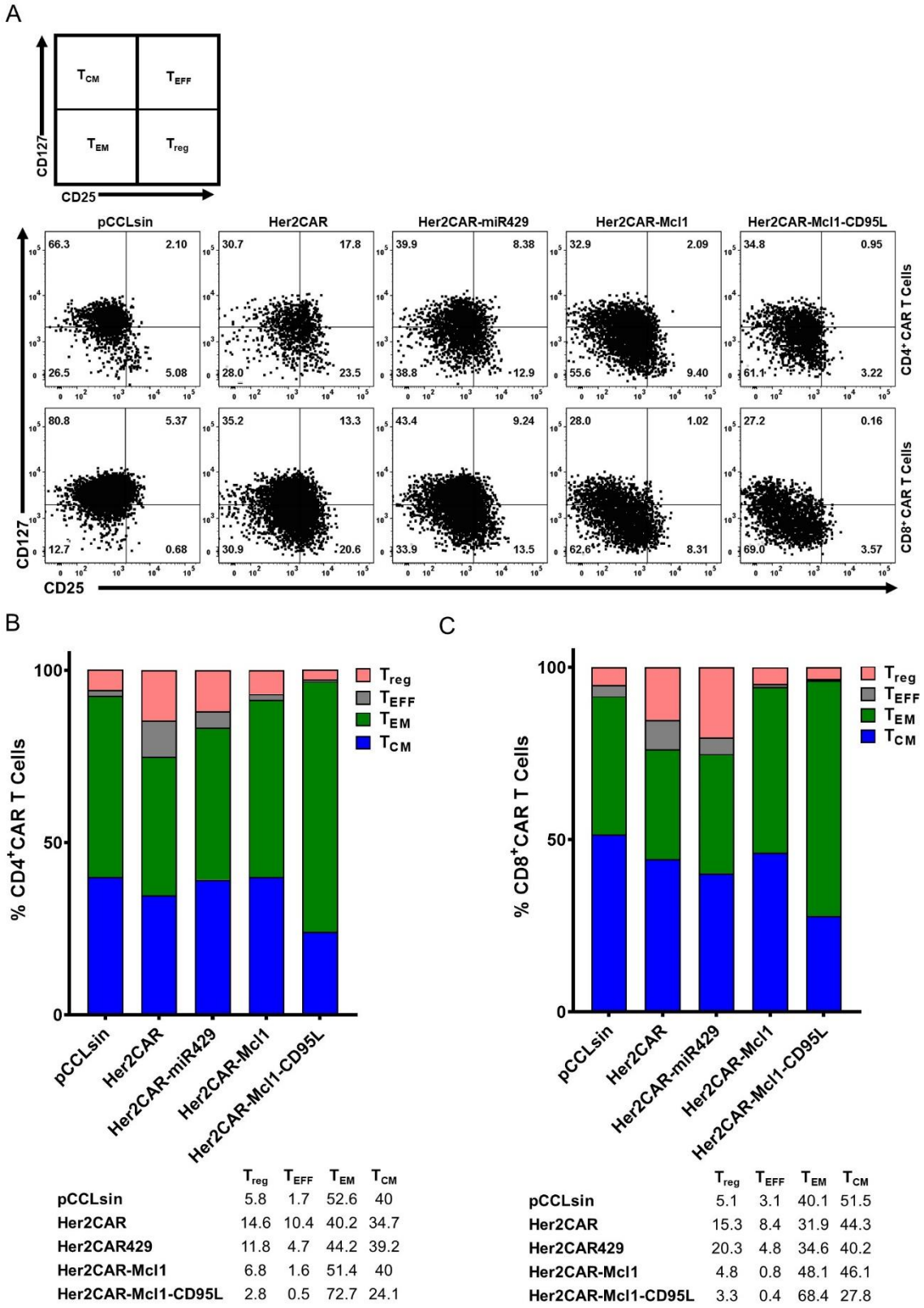

	T_{reg}	T_{EFF}	T_{EM}	T_{CM}
pCCLsin	5.8	1.7	52.6	40
Her2CAR	14.6	10.4	40.2	34.7
Her2CAR429	11.8	4.7	44.2	39.2
Her2CAR-Mcl1	6.8	1.6	51.4	40
Her2CAR-Mcl1-CD95L	2.8	0.5	72.7	24.1

	T_{reg}	T_{EFF}	T_{EM}	T_{CM}
pCCLsin	5.1	3.1	40.1	51.5
Her2CAR	15.3	8.4	31.9	44.3
Her2CAR429	20.3	4.8	34.6	40.2
Her2CAR-Mcl1	4.8	0.8	48.1	46.1
Her2CAR-Mcl1-CD95L	3.3	0.4	68.4	27.8

Figure 5.9. The composition of Her2-CAR T cells ten days post-transduction. **(A)** Defining CAR T cell population based on CD25 and CD127 expression. Live GFP$^+$ Her2-

CAR T cells were gated for CD25 and CD127. CAR T cells upregulating Mcl-1 had lower T_{reg} compare to the control. **(B & C)** Graphs represent the mean of three independent experiments. Statistical analysis: two-way ANOVA test with Bonferroni post-test correction.

5.4.4 Experiments twenty-one days post-transduction

5.4.4.1 Memory T cell subsets

In general, it takes 18-21 days for T_M cells to develop, and most of CAR T cell studies use this time point to investigate T_M commitment (39-41). First, CD4/CD8 Her2-CAR T cells were gated for CD45RO and CCR7 to differentiate between $T_{N/SCM}$, T_{CM}, $T_{EM,}$ and T_{EMRA} (T_{EM} cells re-express CD45RA) (42, 43). CXCR3 was used to separate T_N from T_{SCM} populations (Figure 5.10). Thereby, T_M subsets were categorized as follows: T_N; $CD45RO^-CCR7^-CXCR3^-$, T_{SCM}; $CD45RO^-CCR7^-CXCR3^+$, T_{CM}; $CD45RO^+CCR7^+$, T_{EM}; $CD5RO^+CCR7^-$ and T_{EMRA} (T_{EM} re-expressing CD45RA); $CD45RO^-CCR7^-$.

CAR T cells overexpressing Mcl-1 with or without CD95L treatment had a high frequency of phenotypes similar to T_{SCM} and T_{CM} subsets, while the number of T_{EM} and T_{EMRA}-like cells was reduced compared to the control (Figure 5.10B). The origin of T_{SCM} cells is still unknown: they may arise from T_N cells in the early stage of T cell activation or originate from T_{CM}. Several studies have shown that T_{SCM} (and less T_{CM} cells) have excessive self-renewing capacity, longevity, and can reconstitute all the T_M subsets (44, 45). T_{SCM} cells have shown remarkable persistence and tumour killing in clinical and preclinical studies (46).

Interestingly at day-10, Her2CAR-Mcl1 and Her2CAR-Mcl1-CD95L cells were enriched for T_{EM}-like phenotypes (Figure 5.9B). At day-21, T_{SCM} and T_{CM} cells were predominant in $CD8^+$ and $CD4^+$ CAR T cells, respectively. Differentiation of T_M subsets after antigen encounter is varied, and several paths have been suggested for T_M development (please see the discussion). However, $T_N \rightarrow T_{EEF} \rightarrow T_{EM} \rightarrow T_{CM}$ is known as the leading route (40). Thus, Mcl-1 induction in CAR T cells probably increases the T_{CM} number through the same path. T_{CM} cells have high proliferation and cytotoxicity capacity; they can last for years after development and are able to differentiate to T_{EM} and T_{EFF} cells (45).

The upregulation of miR429 did not change the T_M composition in $CD8^+$ Her2-CAR T cells. However, phenotypes similar to T_{SCM} and T_{CM} cells in this group were 2.5% and 8.6% higher in $CD4^+$ CAR T cells, respectively (Figure 5.10). miRNA target selection is a cell- and context-dependent; notably, various immune cells express different isoforms of a gene with distinct 3′ UTR (47). Interestingly, highly proliferative cells tend to use alternative polyadenylation to remove the negative regulators (e.g., miRNA binding sites) in the 3′ UTR of essential genes (48). For instance, both ZEB1 and ZEB2 genes are well-known targets of miR429 (49, 50). However, in $CD8^+$ T cells, miR429 selectively only targets ZEB2, not ZEB1 (51). Therefore, it is possible that miR429 targets different genes in $CD4^+$ and $CD8^+$ T cells.

The number of, phenotypes similar to T_{EM} and T_{EMRA} cells in Her2-CAR T cells overexpressing Mcl-1 (with or without CD95L treatment) and miR429 were lower compared to the control. T_{EM} cells similar to their progeny T_{EFF} have effector functions but with higher lifespan, proliferation, and multipotency capacity. However, T_{EM} cells do not possess self-renewal capacity, identical to T_{CM} and T_{SCM}. Single-cell serial transfer of T_M subsets showed that T_{CM} and T_{SCM} were able to reconstitute the murine immune system, while an infusion of 100-fold T_{EM} cells in mice failed to rebuild the host immune system (45, 52). In another study, the T_{SCM} number was unchanged for decades, whereas the population of T_{CM} and T_{EM} shrunk 10- to 100-fold, respectively (53). T_{SCM} number was constant in patients receiving engineered T cells decades after ACT (54, 55). Remarkably, vaccination with yellow fever created $CD8^+$ T_{SCM} cells that remained unchanged after 25 years (56).

T_{EMRA} cells are usually considered as terminally differentiated cells with an intermediate phenotype between T_{EM} and T_{EFF} cells. T_{EMRA} cells have a lower proliferation capacity, IL-2/INF-γ secretion, and lifespan. These cells have $CD95^{high}$/$Bcl\text{-}2^{low}$ signature that makes them susceptible to apoptosis, even more than T_{EFF} cells (57, 58). Her2CAR-Mcl1and Her2CAR-Mcl1-CD95L CAR T cells contain lower T_{EMRA} cells compared to the control (Figure 5.10).

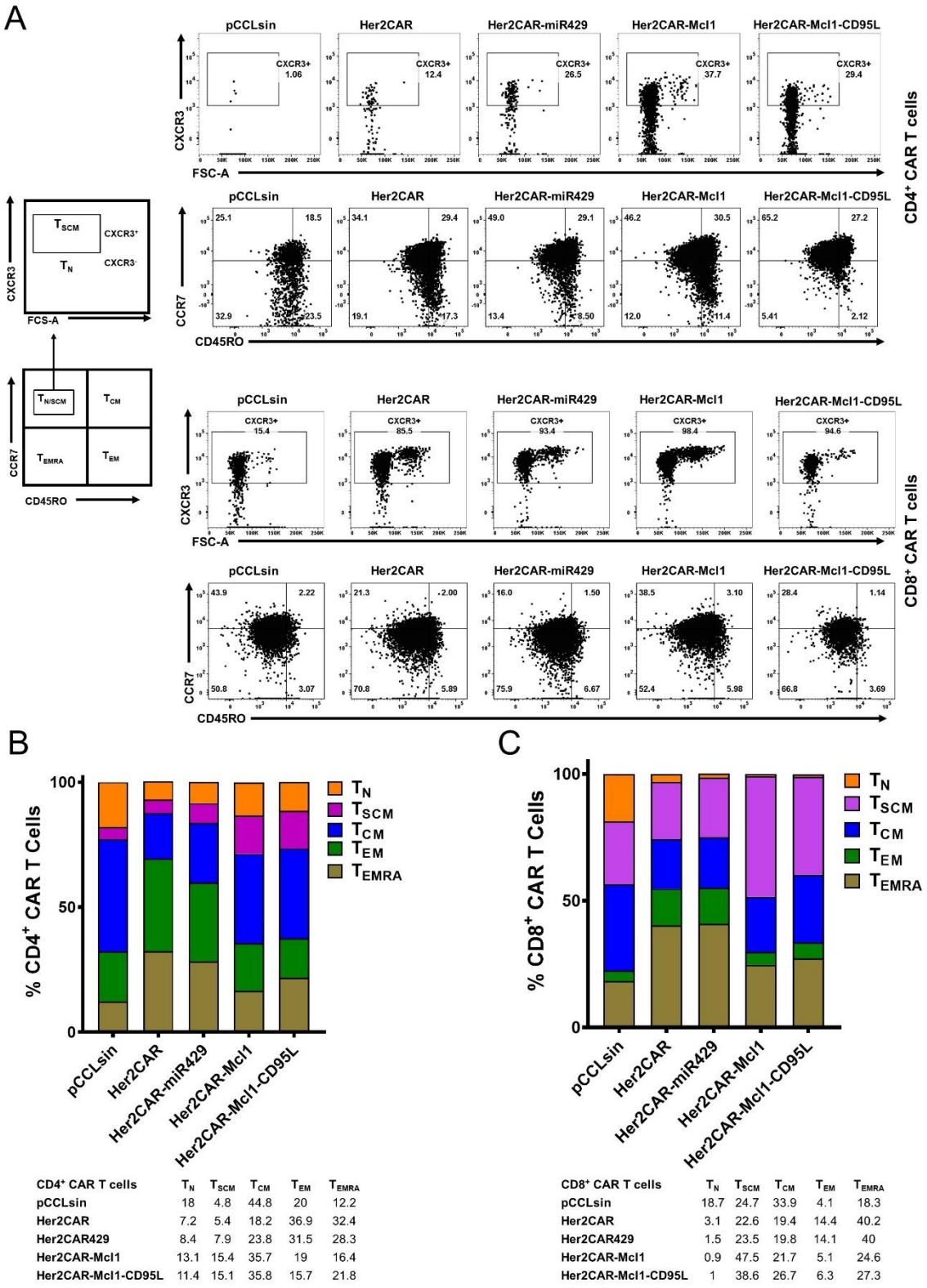

CD4+ CAR T cells	T_N	T_{SCM}	T_{CM}	T_{EM}	T_{EMRA}
pCCLsin	18	4.8	44.8	20	12.2
Her2CAR	7.2	5.4	18.2	36.9	32.4
Her2CAR429	8.4	7.9	23.8	31.5	28.3
Her2CAR-Mcl1	13.1	15.4	35.7	19	16.4
Her2CAR-Mcl1-CD95L	11.4	15.1	35.8	15.7	21.8

CD8+ CAR T cells	T_N	T_{SCM}	T_{CM}	T_{EM}	T_{EMRA}
pCCLsin	18.7	24.7	33.9	4.1	18.3
Her2CAR	3.1	22.6	19.4	14.4	40.2
Her2CAR429	1.5	23.5	19.8	14.1	40
Her2CAR-Mcl1	0.9	47.5	21.7	5.1	24.6
Her2CAR-Mcl1-CD95L	1	38.6	26.7	6.3	27.3

Figure 5.10. Memory T cell subsets within the Her2-CAR T cell population. CD45RO and CCR7 were used to distinguish between live CD4/CD8 $T_{N/SCM}$ ($CD45RO^-CCR7^+$),

T_{CM} ($CD45RO^-CCR7^+$), T_{EM} ($CD45RO^-CCR7^+$), and T_{EMRA} ($CD45RO^-CCR7^+$) Her2-CAR T cells. CXCR3 was used to separate T_{SCM} ($CXCR3^+$) and T_N ($CSXCR3^-$). **(B & C)** Graphs represent the mean of three independent experiments. Statistical analysis: two-way ANOVA test with Bonferroni post-test correction.

Recently, it has been shown that T_{EMRA} cells include functional cytotoxic and cytokine secreting cells. These cells do not express CD57 but induce CD27 expression (59-61). Functionally, T_{EMRA} cells are not senescent, yet possess effector functions such as IL-2/INF-γ secretion, cytotoxicity, and showed decreased sensitivity to apoptosis (59, 61). The number of non-functional T_{EMRA} cells is higher in older people (60). Strikingly, Her2CAR-Mcl1, and Her2CAR-Mcl1-CD95L T cells demonstrated higher $CD57^-CD27^+$ cells within their T_{EMRA} cell population (Figure 5.11).

5.4.4.2 $CD45RO^-CD27^+$ Her2-CAR T cells

Several clinical trials have shown that responder patients have an elevated frequency of $CD45RO^-CD27^+$ CAR T cells (62-64). Further analysis showed $CD45RO^-CD27^+$ CAR T cells resemble the $T_{N/SCM}$ phenotype (62-64). Interestingly a decade before, this population has been visualised in patients responding to vaccination or anti-viral therapy and was known as "true resting" T_M cells (65-67). Overexpression of Mcl-1, especially cells treated with CD95L, had a greater number of CD4/CD8 $CD45RO^-CD27^+$ CAR T cells (Figure 5.12). Forced expression of miR429 slightly increased the number of these cells exclusively in $CD4^+$ CAR T cells (Figure 5.12).

Another criterion to predict the outcome of CAR T cell therapy is the CD4:CD8 ratio at the time of infusion. Although $CD8^+$ CAR T cells are known to be responsible for the direct tumour killing, $CD4^+$ CAR T cells have been shown to have a cytotoxic capacity comparable to the $CD8^+$ CAR T cells (68). Interestingly, TCR engagement in CAR T cells induced apoptosis and exhaustion in $CD8^+$, but not $CD4^+$ CAR T cells (68). Early studies suggested a 1:1 ratio as the optimal composition for CAR T cell therapy in ALL and NHL (69, 70). More recent clinical trials in multiple myeloma showed that a larger number of $CD4^+$ CAR T cells is correlated with durable remission and desire *in vivo* expansion (62, 64). The CD4:CD8 ratio in our study differed between treatments:

Her2CAR = 0.39, Her2CAR-miR429 = 0.43, Her2CAR-Mcl1 = 1.21 and Her2CAR-Mcl1-CD95L = 2.63 (mean ratios; n=3).

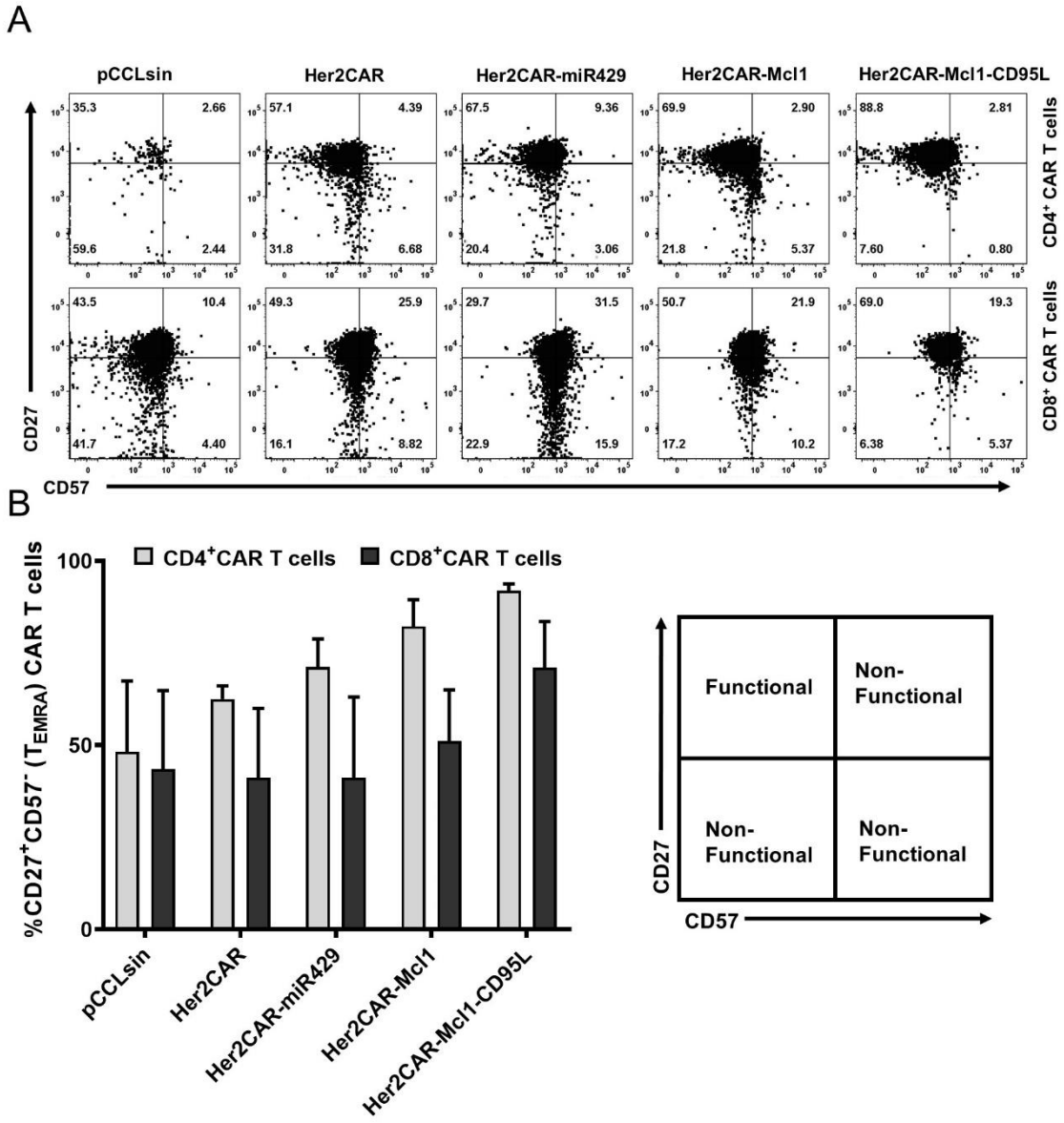

Figure 5.11. Discriminating between functional ($CD57^{-}CD27^{+}$) and non-functional T_{EMRA} Her2-CAR T cells. CAR T cells upregulating Mcl-1 had lower non-functional T_{EMRA} cells. Graphs represent the mean ± SEM of three independent experiments. Statistical analysis: two-way ANOVA test with Bonferroni post-test correction.

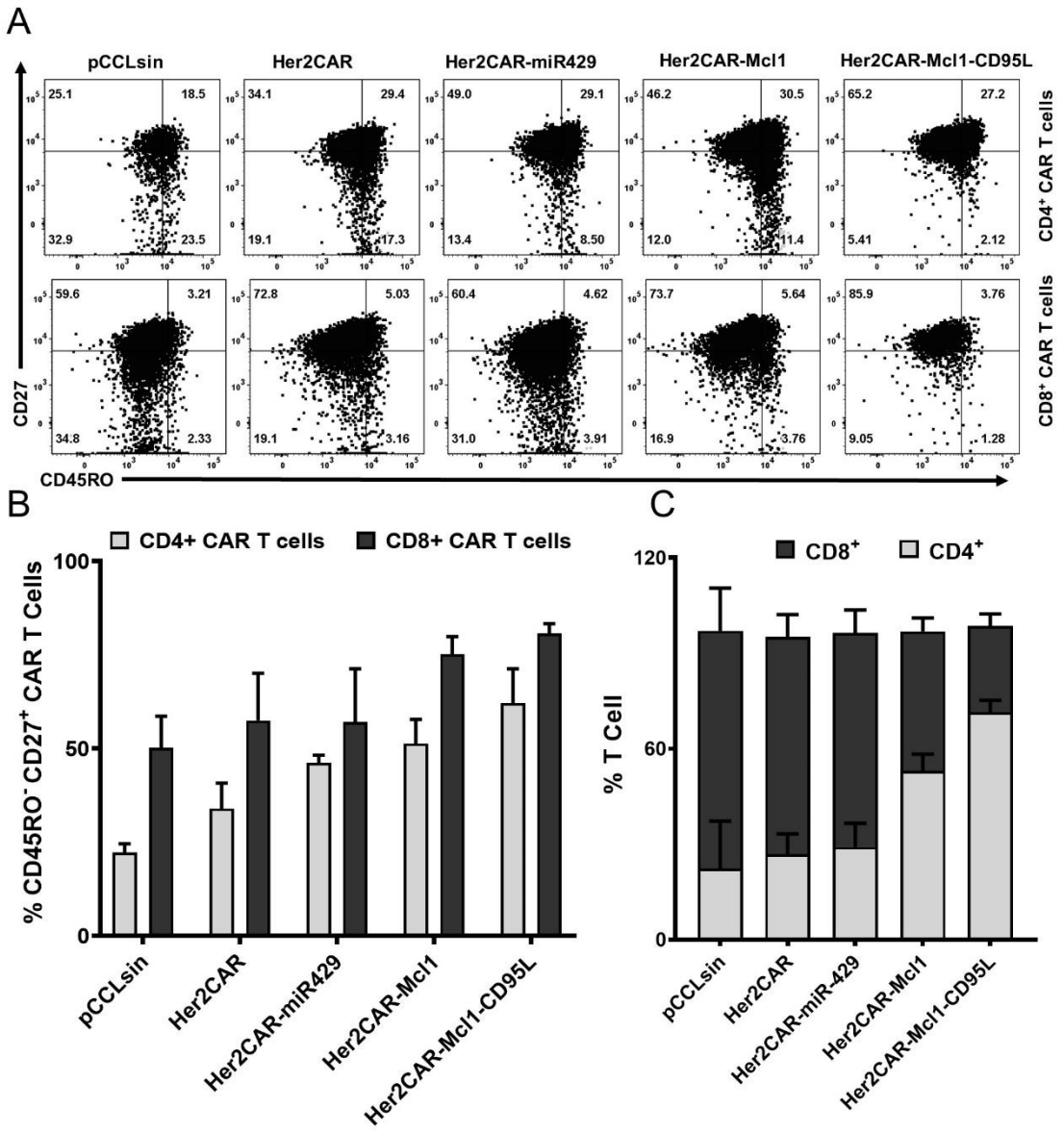

Figure 5.12. (A & B) Live GFP$^+$ CD4/CD8 Her2-CAR T cells were gated for CD27 and CD45RO. Overexpression of Mcl-1 improved the number of CD4/CD8 CD45RO$^-$CD27$^+$ CAR T cells. The graph represents the mean ± SEM of three independent experiments. **(C)** The chart shows the number of CD4$^+$and CD8$^+$ Her2-CAR T cells at day 21 post-transduction. Statistical analysis: two-way ANOVA test with Bonferroni post-test correction.

5.4.4.3 Expression of memory T cells markers

5.4.4.3.1 CD27

CD27 belongs to the TNF family and, alike to CD137 and CD134 has a costimulatory role in T cells. T_N cells express CD27; its expression induces upon TCR activation and gets lost after several rounds of proliferation and activation (71). CD27 ligand (CD70) is expressed on antigen presenting cells (APC), and stimulation of CD27 enhances T cell persistence, proliferation, and T_M development (71). Less differentiated T_M cells such as T_{SCM} and T_{CM} overexpress CD27, T_{EM} cells do not express CD27 (or express at a low level), and T_{EMRA} cells are negative for CD27 (72). Her2-CAR T cells overexpressing Mcl-1 had a higher $CD27^+$ CAR T cells (Figure 5.13). These results are in line with the findings in Figure 5.10, in which these CAR T cells contain higher T_{SCM} and T_{CM} and lower T_{EMRA} population (Figure 5.10). miR429 upregulation resulted in a higher number of $CD4^+CD27^+$ CAR T cells, as this population has shown to include more T_{CM} cells (Figure 5.10).

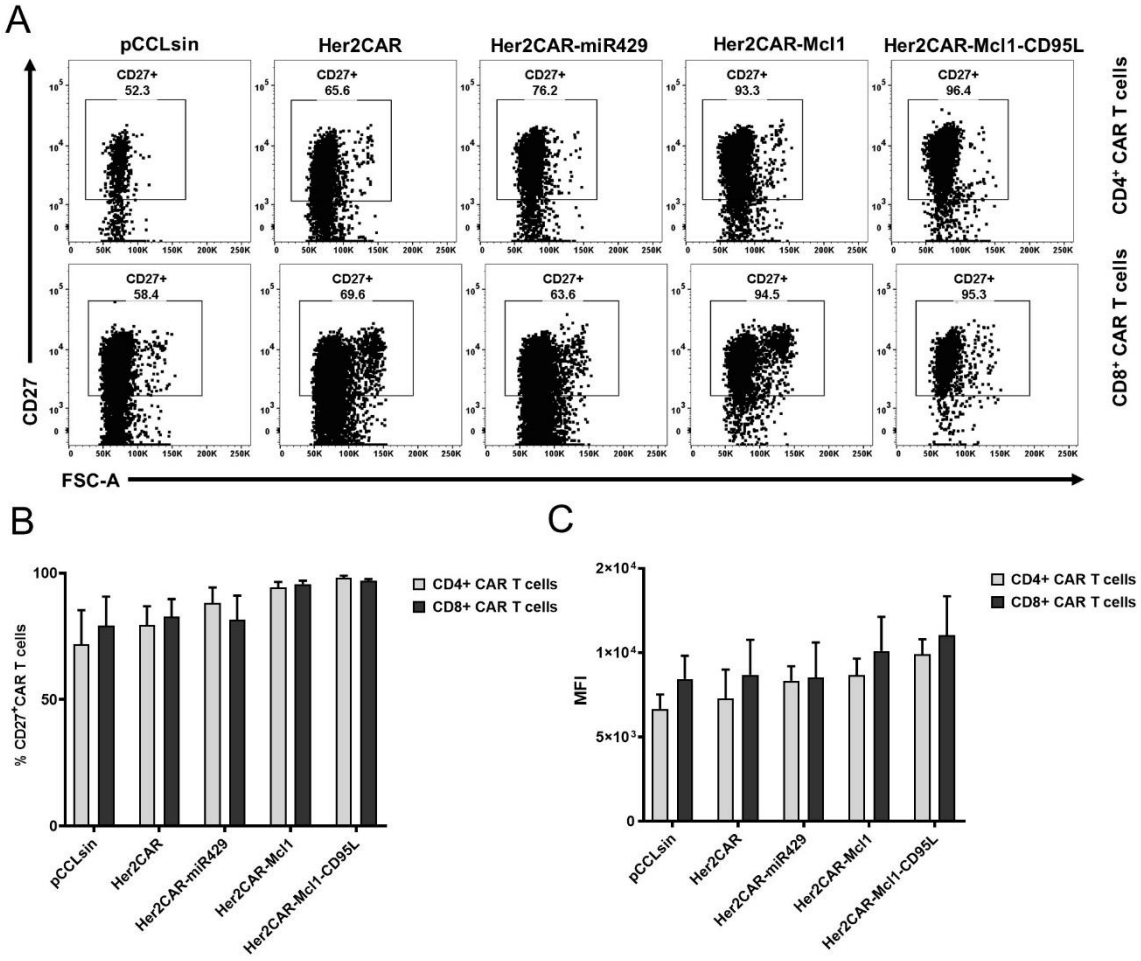

Figure 5.13. Flow cytometry analysis of CD27 expression. **(A)** Live GFP^+ $CD4^+$ or $CD8^+$ CAR T cells were gated for CD27 expression. **(B & C)** Graphs represent the mean ± SEM of three independent experiments. Statistical analysis: two-way ANOVA test with Bonferroni post-test correction.

5.4.4.3.2 CCR7 and CD62L

CCR7 and CD62L (L-selectin) play a crucial role in adaptive immunity and T cell migration into lymph nodes during infections. CCR7 and CD62L expression separates T_N, T_{SCM}, T_{CM} ($CCR7^+CD62L^+$) and T_{EFF}, T_{EM} and T_{EMRA} ($CCR7^-CD62L^-$) (67, 72, 73). $CD62L^+CCR7^+$ T cells have shown to be the optimal cells for ACT purposes, such as CAR T cell therapy, as they contain high T_{SCM} and T_{CM} cells (74, 75). Her2-CAR T with elevated Mcl-1 expression had higher $CD62L^+CCR7^+$ as they also contain more T_N, T_{SCM}, T_{CM} (Figure 5.14 & 5.15).

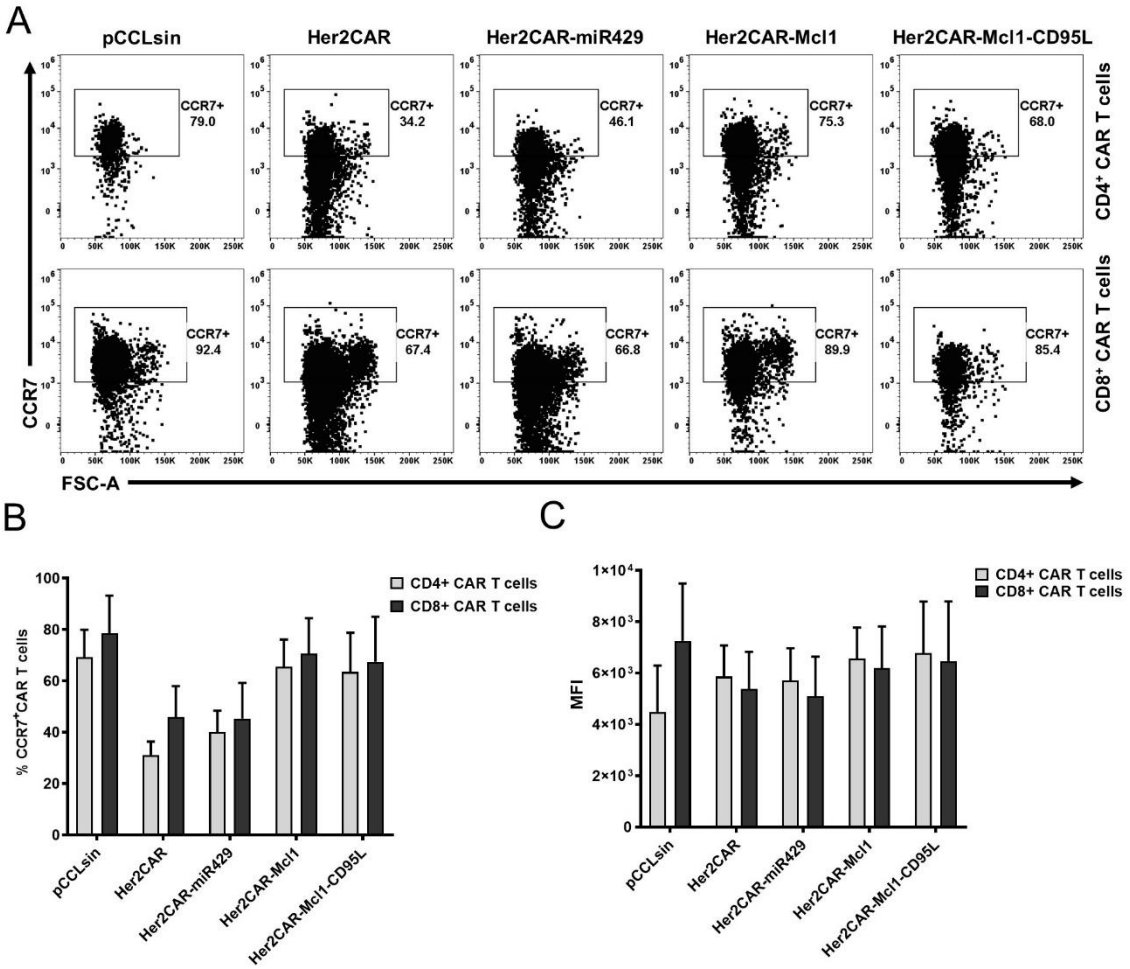

Figure 5.14. Flow cytometry analysis of CCR7 expression. **(A)** Live GFP$^+$ CD4$^+$ or CD8$^+$ CAR T cells were gated for CCR7 expression. **(B & C)** Graphs represent the mean ± SEM of three independent experiments. Statistical analysis: two-way ANOVA test with Bonferroni post-test correction.

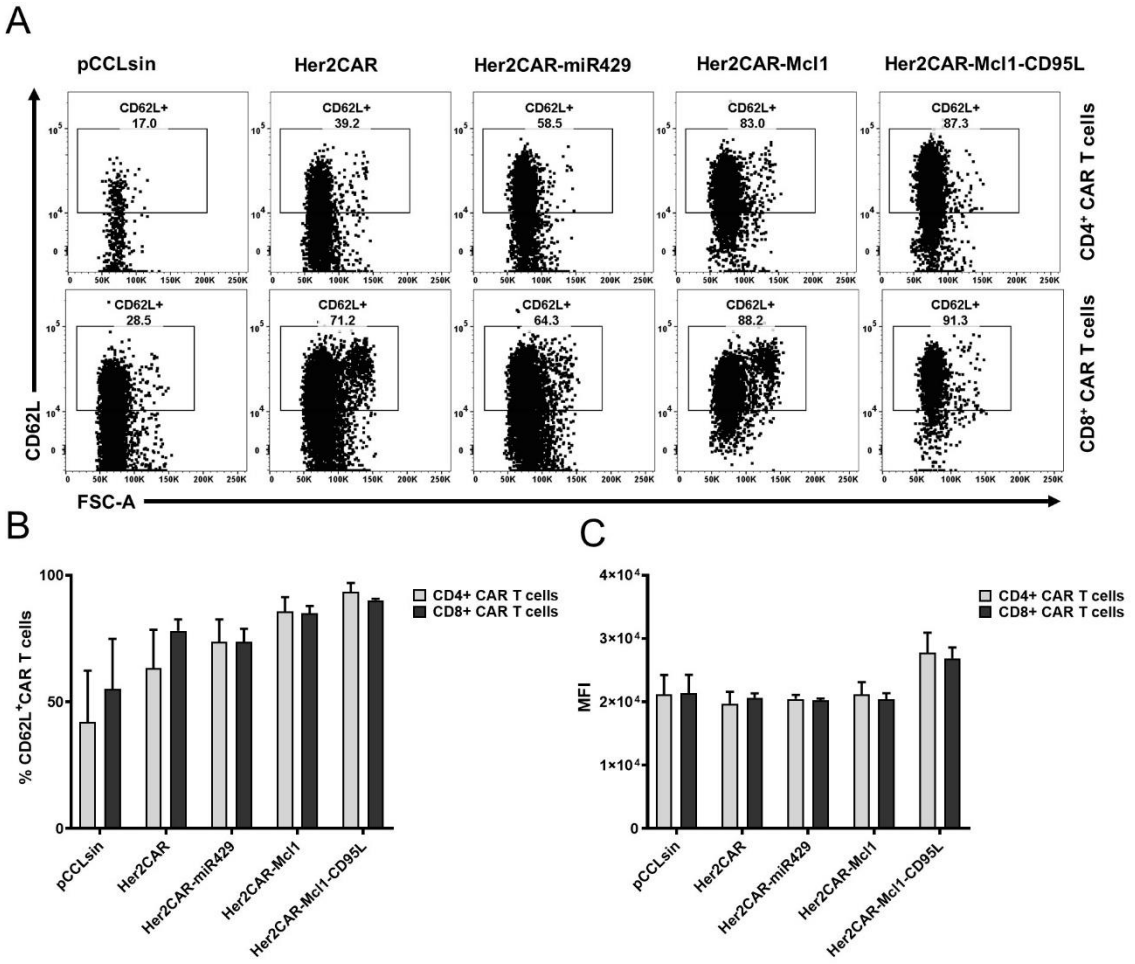

Figure 5.15. Flow cytometric analysis of CD62L expression. **(A)** Live GFP$^+$ CD4$^+$ or CD8$^+$ CAR T cells were gated for CD62L expression. **(B & C)** Graphs represent mean ± SEM of three independent experiments. Statistical analysis: two-way ANOVA test with Bonferroni post-test correction.

5.4.4.3.3 CD95

CD95 belongs to the TNF family, and it is well-known for its role in AICD. Upon T cell activation, CD95 expression elevates in T_{EFF} cells, while they also upregulate CD95L

(76). Following Bcl-2 and Mcl-1 downregulation (contraction), T_{EFF} cells undergo AICD, while T_M cells, which overexpress Bcl-2 and Mcl-1, are protected against AICD. For more information about the apoptotic and non-apoptotic functions of CD95, please see the introduction.

The frequency of $CD95^+$ Her2-CAR T cells was similar in all groups, with a minor reduction in CAR T cells overexpressing Mcl-1 (Figure 5.16). As I discussed above, Her2CAR and Her2CAR-miR429, which have higher $CD95^+$ cells, also contain a greater number of $CD62L^-CCR7^-$ cells (T_{EFF}, T_{EM}, and T_{EMRA} - Figure 5.14 & 5.15). Except for T_N cells, all T cells have been shown to express CD95 (72, 77). It should be noted that CD95 expression in T_N cells is still controversial as some studies showed that a percentage of T_N cells are positive for CD95 and prone to AICD (78, 79). Therefore, a ~2-5% lower $CD95^+$ in CAR T cells upregulating Mcl-1 can be explained due to the lower number of T_{EFF}, $T_{EM,}$ and T_{EMRA} cells.

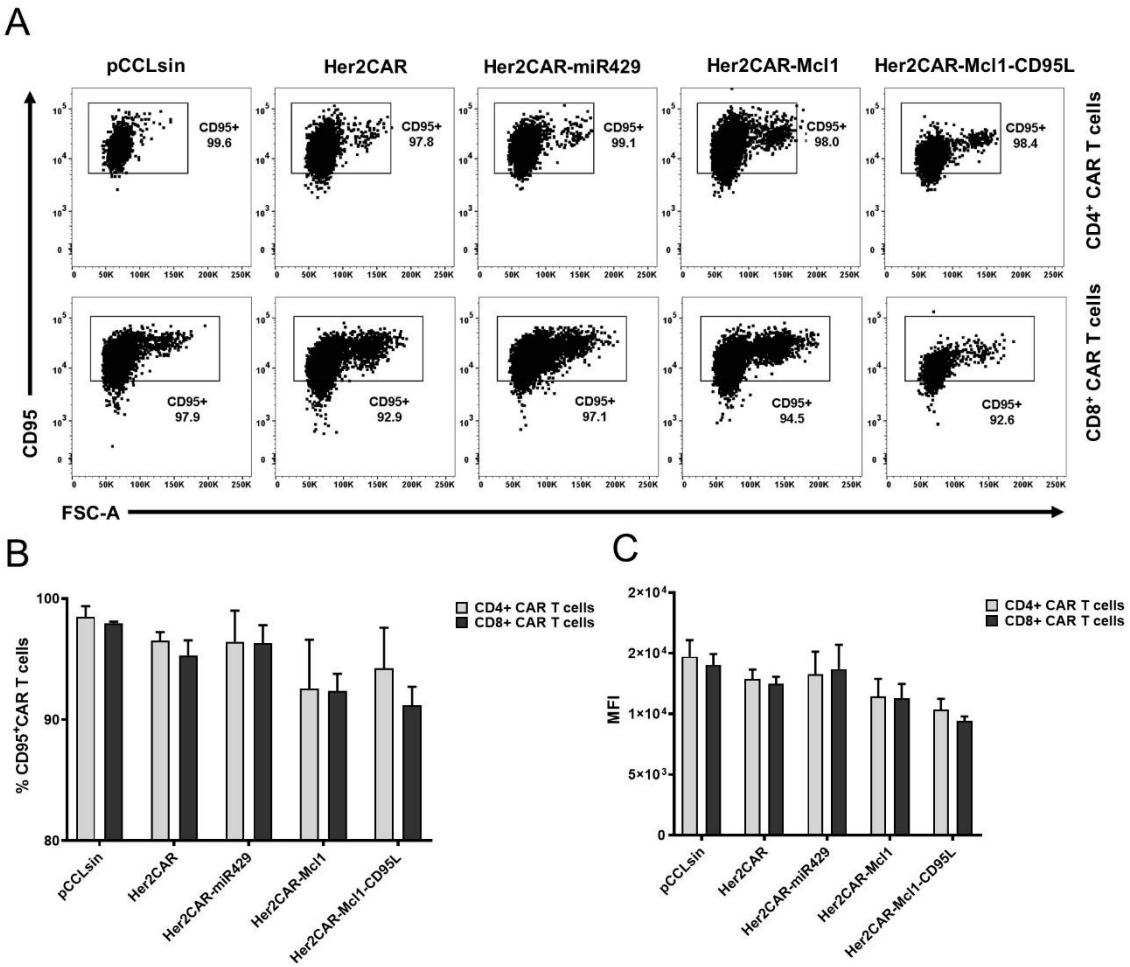

Figure 5.16. Flow cytometry analysis of CD95 expression. **(A)** Live GFP$^+$ CD4$^+$ or CD8$^+$ CAR T cells were gated for CD95 expression. **(B & C)** Graphs represent the mean ± SEM of three independent experiments. Statistical analysis: two-way ANOVA test with Bonferroni post-test correction.

5.4.4.3.4 CXCR3

CXCR3 is an inflammatory chemokine receptor responsible for the migration of T cells towards the inflammation site. Tumour cells expressing CXCR3 ligands (CXCL9, CXCL10 and CXCL11) have better T cell infiltration and improved response to immunotherapy (80).

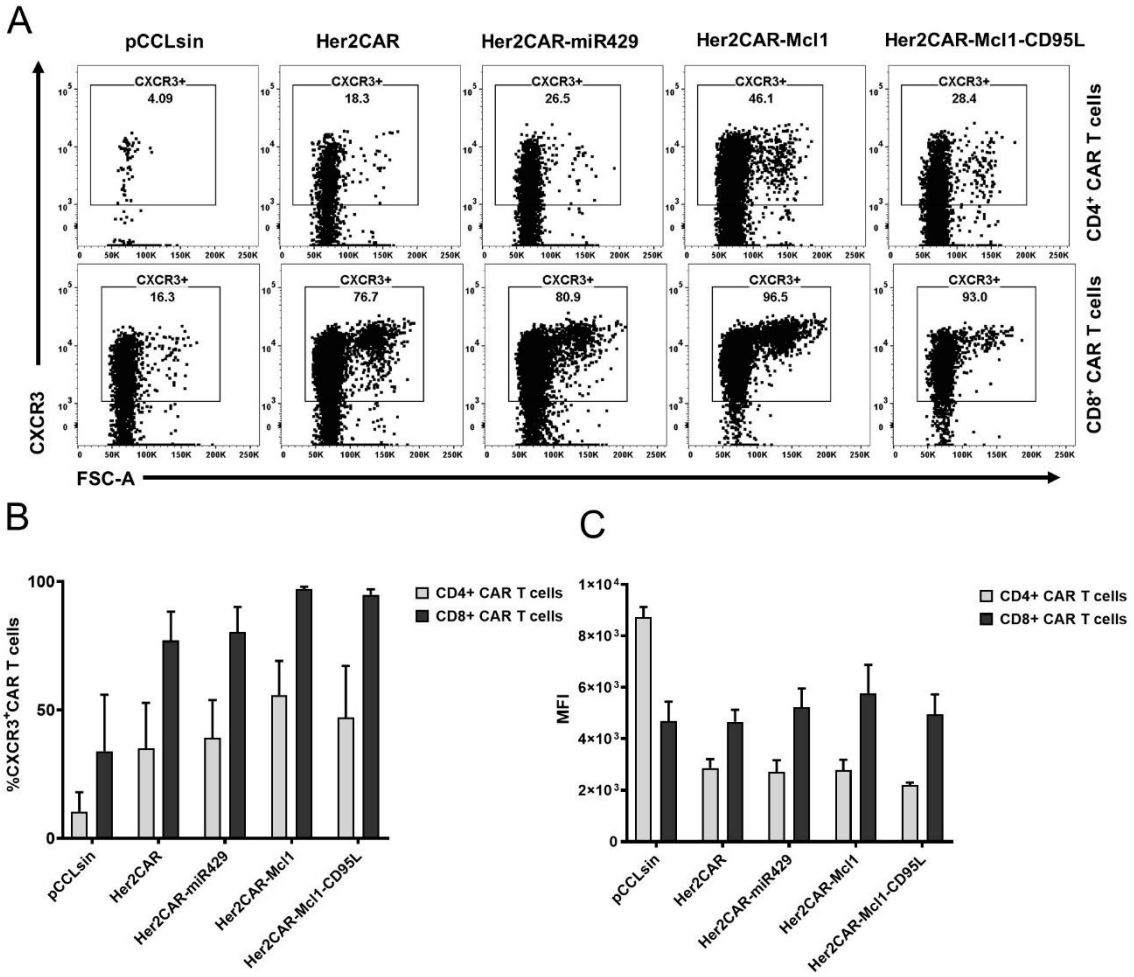

Figure 5.17. Flow cytometry analysis of CXCR3 expression. **(A)** Live GFP$^+$ CD4$^+$ or CD8$^+$ CAR T cells were gated for CXCR3 expression. **(B & C)** Graphs represent mean ±

SEM of three independent experiments. Statistical analysis: two-way ANOVA test with Bonferroni post-test correction.

Similar to CD95, all T cells except T_N express CXCR3 with different expression levels. Her2-CAR T cells upregulating Mcl-1 had 12-20% higher $CXCR3^+$ cells, probably due to the presence of higher T_{SCM} and T_{CM} numbers (Figure 5.17). Besides, $CXCR3^+$ CAR T cells were higher in $CD8^+$ compare to $CD4^+$ CAR T cells, since they contain more T_{SCM} (Figure 5.10). Forced expression of miR429 only increased 2-4% $CXCR3^+$Her2CAR T cells.

5.4.4.3.5 CD57

CD57, also known as HNK-1, is expressed in terminally differentiated cells and has been used routinely as a senescence and exhaustion marker for T cells (81). T cells expressing CD57 have low proliferation and cytotoxicity capability and susceptible to apoptosis (81). Manufacturing low $CD57^+$ CAR T cells population enhances the efficacy of CAR T cell therapy (82). Interestingly, the upregulation of Mcl-1, especially with CD95L treatment, decreases the number of $CD4^+$ (2-6%) and $CD8^+$ (3-10%) Her2-CAR T cells (Figure 5.18).

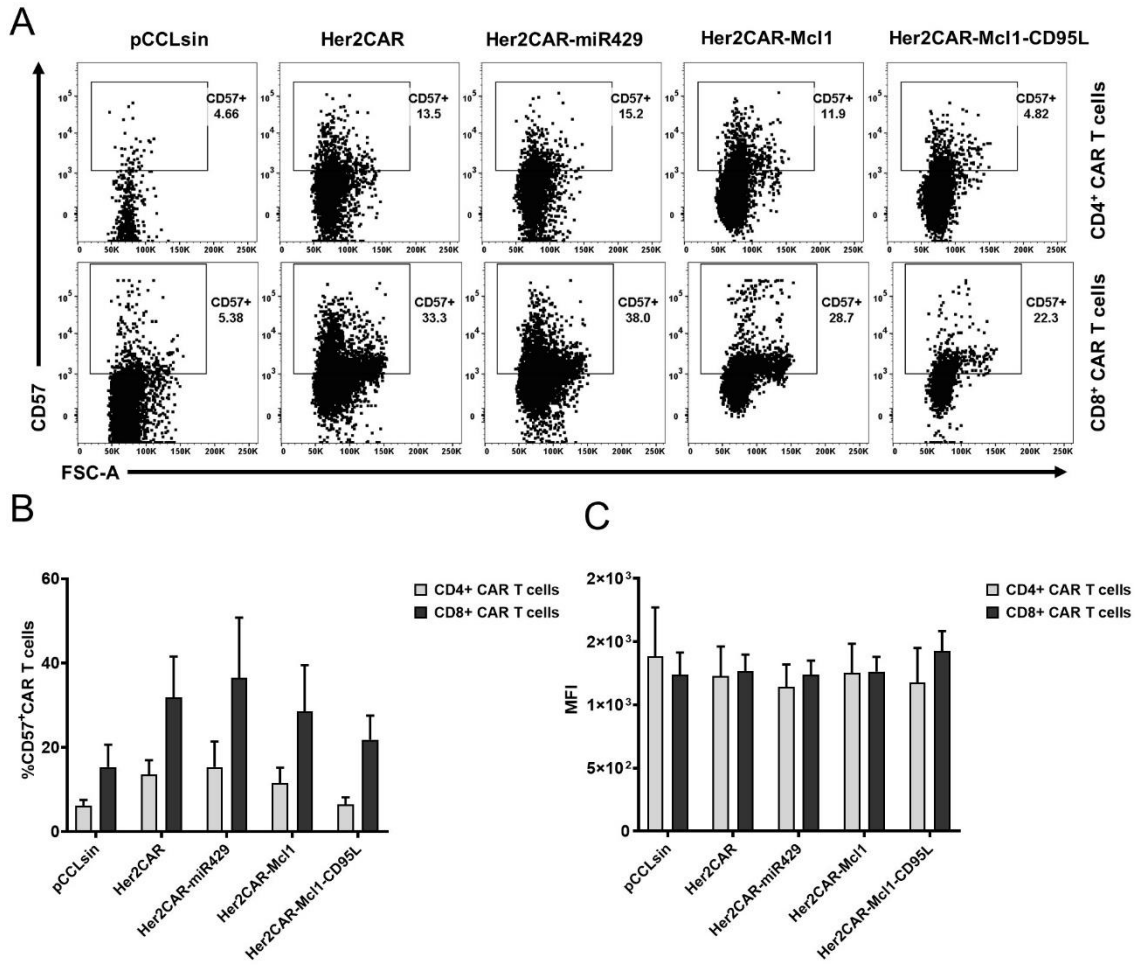

Figure 5.18. Flow cytometry analysis of CD57 expression. **(A)** Live GFP$^+$ CD4$^+$ or CD8$^+$ CAR T cells were gated for CD57 expression. **(B & C)** Graphs represent the mean ± SEM of three independent experiments. Statistical analysis: two-way ANOVA test with Bonferroni post-test correction.

5.4.4.4 Mitochondrial mass

Similar to the surface markers, T_N, T_M, and T_{EFF} cells have morphologically distinct mitochondria with different metabolism program. T_N and T_M cells have larger mitochondrial mass (fusion) and rely on OXPHOS metabolism. T_{EFF} cells have smaller mitochondria (fission) and use glycolysis to produce ATP (for more information, please see the introduction). Both Mcl-1 isoforms facilitate mitochondrial fusion; Mcl-1L inhibits fission by interacting with Drp-1 and MFF, while Mcl-1S promotes fusion

through binding to OPA-1, MFN1, and MFN2 (2-4). In addition, miR429 might enhance fusion by downregulating the TCAIM and MFF. Overexpression of Mcl-1, particularly with CD95L treatment, increases mitochondrial mass and mtDNA:gDNA ratio in Her2-CAR T cells (Figure 5.19), suggesting Mcl-1 (and less miR429) increase the T_M differentiation probably by expediting mitochondrial fusion.

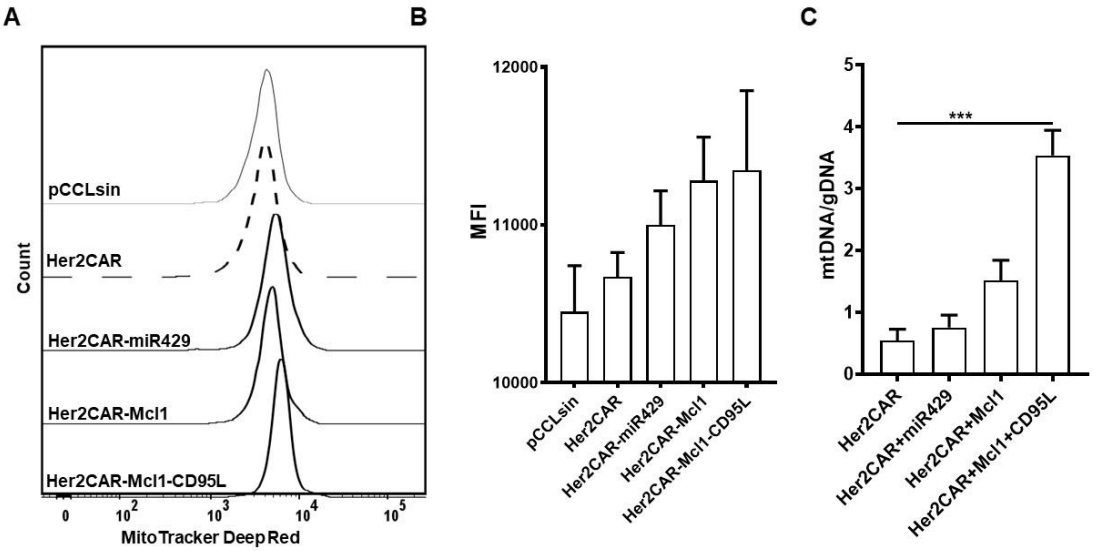

Figure 5.19. Estimation of mitochondrial mass. **(A & B)** Her2-CAR T cells were stained with MitoTracker deep red and flow cytometric analysis carried to determine the mitochondrial mass. The graph shows the MFI of MitoTracker for three independent repeats **(C)** qPCR analysis of mtDNA:gDNA ratio. Genomic DNA was extracted from cell lysates and qPCR was performed using primers for β2-microglobulin and β-actin (nuclear genes), Leu-tRNA and Cytochrome C (mitochondrial genes). The comparative CT (2−ΔΔCT) method was used to analyses the fold change against Gag and PBS as internal genes. Statistical analysis: all data are presented as mean ± SEM and pooled from three independent experiments. One-way ANOVA test with Bonferroni post-test correction (***$P < 0.001$).

5.5 Conclusion

We investigated the overexpression of a non-coding gene (miR429) and a coding gene (Mcl-1) in Her2-CAR T cells. These genes were selected based on their role in the mitochondrial dynamic. First, we used a Tet-On system we have established in chapter III. Despite trying several protocols, the transfection efficiency was lower than 10%. Hence, we created a Tet-On LV vector. Unfortunately, this system had several drawbacks that made it inapplicable. First, at least 10 µg/mL was needed to achieve an adequate level of Mcl-1 (Figure 5.2B & C). The high concentration of doxycycline decreased the cell viability and cell number of human primary T cells (Figure 5.2 E & F). Also, transduction efficiency was still low. Hence, miR429 and Mcl-1 constitutively were expressed under the hPGK promoter. We divided CAR T cells overexpressing Mcl-1 into two groups; grown with or without 46 ng/ mL CD95L.

We screened TCAIM 3′UTR for potential miRNA binding sites. miR429 was chosen among candidate miRNA since this miRNA also was predicted to target MFF and TET-2. qPCR and reporter assays confirmed TCAIM, MFF, and TET-2 as miR429 targets. TCAIM downregulation, as the primary target, was also verified by at protein level (Figure 5.2). Compared to the control, overexpression of miR429 had limited benefits such as 5% lower T_{reg}, 2-5% higher $T_{CM,}$ and T_{SCM} CAR T cells.

In terms of cytotoxicity, IL-2 and IFN-γ secretion, all Her2-CAR T cells had a similar activity (Figure 5.6). The upregulation of Mcl-1 protects CAR T cells from AICD-mediated by CD95L (Figure 5.7). Her2-CAR T cells overexpressing Mcl-1 had a reduced number of $CD69^+$ CAR T cells after stimulating with antigen (Figure 5.8), probably due to the lower number of T_{EFF} cells (Figure 5.9). These CAR T cells contained a lower number of $CD25^+CD127^-$ T_{reg} compares to the control (Figure 5.9). On the other hand, the upregulation of Mcl-1, especially along with CD95L stimulation, enhanced the T_{SCM} and T_{CM} development (Figure 5.10). Interestingly, these CAR T cells also had lower non-functional exhausted T_{EMRA} cells (Figure 5.11). Although more experiments need to be done, measuring mitochondrial mass and mtDNA:gDNA ratio suggested that Mcl-1 probably improves T_M differentiation via promoting mitochondrial fusion (Figure 5.11).

References

1. Rad S. M. AH PA, Tan GMY, McLellan AD. Promoter choice: Who should drive the CAR in T cells? PLoS ONE. 2020;15(7):e0232915.
2. Escudero S, Zaganjor E, Lee S, Mill CP, Morgan AM, Crawford EB, et al. Dynamic regulation of long-chain fatty acid oxidation by a noncanonical interaction between the MCL-1 BH3 helix and VLCAD. Molecular cell. 2018;69(5):729-43. e7.
3. Liu Y, Ma Y, Tu Z, Zhang C, Du M, Wang Y, et al. Mcl-1 inhibits Mff-mediated mitochondrial fragmentation and apoptosis. Biochemical and Biophysical Research Communications. 2020;523(3):620-6.
4. Morciano G, Giorgi C, Balestra D, Marchi S, Perrone D, Pinotti M, et al. Mcl-1 involvement in mitochondrial dynamics is associated with apoptotic cell death. Molecular biology of the cell. 2016;27(1):20-34.
5. Keeren K, Friedrich M, Gebuhr I, Philipp S, Sabat R, Sterry W, et al. Expression of tolerance associated gene-1, a mitochondrial protein inhibiting T cell activation, can be used to predict response to immune modulating therapies. The Journal of Immunology. 2009;183(6):4077-87.
6. Sawitzki B, Bushell A, Steger U, Jones N, Risch K, Siepert A, et al. Identification of gene markers for the prediction of allograft rejection or permanent acceptance. American Journal of Transplantation. 2007;7(5):1091-102.
7. Schumann J, Stanko K, Woertge S, Appelt C, Schumann M, Kühl A, et al. The mitochondrial protein TCAIM regulates activation of T cells and thereby promotes tolerance induction of allogeneic transplants. American Journal of Transplantation. 2014;14(12):2723-35.
8. Perciavalle RM, Stewart DP, Koss B, Lynch J, Milasta S, Bathina M, et al. Anti-apoptotic MCL-1 localizes to the mitochondrial matrix and couples mitochondrial fusion to respiration. Nature cell biology. 2012;14(6):575-83.
9. Weng C, Li Y, Xu D, Shi Y, Tang H. Specific cleavage of Mcl-1 by caspase-3 in tumor necrosis factor-related apoptosis-inducing ligand (TRAIL)-induced apoptosis in Jurkat leukemia T cells. Journal of Biological Chemistry. 2005;280(11):10491-500.
10. Rad SAH, Poudel A, Tan GMY, McLellan AD. Optimisation of Tet-On inducible systems for Sleeping Beauty-based chimeric antigen receptor (CAR) applications. Scientific Reports. 2020;10(1):1-12.

11. Ahler E, Sullivan WJ, Cass A, Braas D, York AG, Bensinger SJ, et al. Doxycycline alters metabolism and proliferation of human cell lines. PloS one. 2013;8(5):e64561.

12. Ajina A, Maher J. Strategies to address chimeric antigen receptor tonic signaling. Molecular cancer therapeutics. 2018;17(9):1795-815.

13. Long AH, Haso WM, Shern JF, Wanhainen KM, Murgai M, Ingaramo M, et al. 4-1BB costimulation ameliorates T cell exhaustion induced by tonic signaling of chimeric antigen receptors. Nature medicine. 2015;21(6):581-90.

14. Youle RJ, Van Der Bliek AM. Mitochondrial fission, fusion, and stress. Science. 2012;337(6098):1062-5.

15. Tak H, Kim J, Jayabalan AK, Lee H, Kang H, Cho D-H, et al. miR-27 regulates mitochondrial networks by directly targeting the mitochondrial fission factor. Experimental & molecular medicine. 2014;46(11):e123-e.

16. Fraietta JA, Nobles CL, Sammons MA, Lundh S, Carty SA, Reich TJ, et al. Disruption of TET2 promotes the therapeutic efficacy of CD19-targeted T cells. Nature. 2018;558(7709):307-12.

17. Ladle BH, Li K-P, Phillips MJ, Pucsek AB, Haile A, Powell JD, et al. De novo DNA methylation by DNA methyltransferase 3a controls early effector CD8+ T-cell fate decisions following activation. Proceedings of the National Academy of Sciences. 2016;113(38):10631-6.

18. Mohammadi-Yeganeh S, Paryan M, Samiee SM, Soleimani M, Arefian E, Azadmanesh K, et al. Development of a robust, low cost stem-loop real-time quantification PCR technique for miRNA expression analysis. Molecular Biology Reports. 2013;40(5):3665-74.

19. Paraskevopoulou MD, Georgakilas G, Kostoulas N, Vlachos IS, Vergoulis T, Reczko M, et al. DIANA-microT web server v5. 0: service integration into miRNA functional analysis workflows. Nucleic acids research. 2013;41(W1):W169-W73.

20. Reczko M, Maragkakis M, Alexiou P, Grosse I, Hatzigeorgiou AG. Functional microRNA targets in protein coding sequences. Bioinformatics. 2012;28(6):771-6.

21. Peter ME, Budd RC, Desbarats J, Hedrick SM, Hueber A-O, Newell MK, et al. The CD95 receptor: apoptosis revisited. Cell. 2007;129(3):447-50.

22. He B, Wang L, Neuber B, Schmitt A, Kneisel N, Hoeger T, et al. Blockade of CD95/CD95L Death Signaling Enhances CAR T Cell Persistence and Antitumor Efficacy. American Society of Hematology Washington, DC; 2019.
23. Klebanoff CA, Scott CD, Leonardi AJ, Yamamoto TN, Cruz AC, Ouyang C, et al. Memory T cell–driven differentiation of naive cells impairs adoptive immunotherapy. The Journal of clinical investigation. 2016;126(1):318-34.
24. Künkele A, Johnson AJ, Rolczynski LS, Chang CA, Hoglund V, Kelly-Spratt KS, et al. Functional tuning of CARs reveals signaling threshold above which CD8+ CTL antitumor potency is attenuated due to cell Fas–FasL-dependent AICD. Cancer immunology research. 2015;3(4):368-79.
25. Yamamoto TN, Lee P-H, Vodnala SK, Gurusamy D, Kishton RJ, Yu Z, et al. T cells genetically engineered to overcome death signaling enhance adoptive cancer immunotherapy. The Journal of clinical investigation. 2019;129(4).
26. Wang Y, Li M, Zang W, Ma Y, Wang N, Li P, et al. MiR-429 up-regulation induces apoptosis and suppresses invasion by targeting Bcl-2 and SP-1 in esophageal carcinoma. Cellular oncology. 2013;36(5):385-94.
27. Özören N, El-Deiry WS. Defining characteristics of Types I and II apoptotic cells in response to TRAIL. Neoplasia. 2002;4(6):551-7.
28. Ziegler SF, Ramsdell F, Alderson MR. The activation antigen CD69. Stem cells. 1994;12(5):456-65.
29. McLellan AD, Ali Hosseini Rad SM. Chimeric antigen receptor T cell persistence and memory cell formation. Immunology & Cell Biology. 2019;97(7):664-74.
30. Zhang C, Liu J, Zhong JF, Zhang X. Engineering car-t cells. Biomarker research. 2017;5(1):22.
31. Hou AJ, Chang ZL, Lorenzini MH, Zah E, Chen YY. TGF-β–responsive CAR-T cells promote anti-tumor immune function. Bioengineering & translational medicine. 2018;3(2):75-86.
32. Wang YM, Alexander SI. CD8 regulatory T cells: what's old is now new. Immunology and cell biology. 2009;87(3):192.
33. Wang R-F. CD8+ regulatory T cells, their suppressive mechanisms, and regulation in cancer. Human immunology. 2008;69(11):811-4.

34. Bluestone JA, Abbas AK. Natural versus adaptive regulatory T cells. Nature Reviews Immunology. 2003;3(3):253-7.

35. Smith TR, Kumar V. Revival of CD8+ Treg–mediated suppression. Trends in immunology. 2008;29(7):337-42.

36. Hartigan-O'Connor DJ, Poon C, Sinclair E, McCune JM. Human CD4+ regulatory T cells express lower levels of the IL-7 receptor alpha chain (CD127), allowing consistent identification and sorting of live cells. Journal of immunological methods. 2007;319(1-2):41-52.

37. Dunham RM, Cervasi B, Brenchley JM, Albrecht H, Weintrob A, Sumpter B, et al. CD127 and CD25 expression defines CD4+ T cell subsets that are differentially depleted during HIV infection. The Journal of Immunology. 2008;180(8):5582-92.

38. Saunders JAH, Estes KA, Kosloski LM, Allen HE, Dempsey KM, Torres-Russotto DR, et al. CD4+ regulatory and effector/memory T cell subsets profile motor dysfunction in Parkinson's disease. Journal of Neuroimmune Pharmacology. 2012;7(4):927-38.

39. Alizadeh D, Wong RA, Yang X, Wang D, Pecoraro JR, Kuo C-F, et al. IL15 enhances CAR-T cell antitumor activity by reducing mTORC1 activity and preserving their stem cell memory phenotype. Cancer immunology research. 2019;7(5):759-72.

40. Ho LP, San Yit P, Ng LH, Linn YC, Zhao Y, Sun L, et al. The road to memory: an early rest for the long journey. The Journal of Immunology. 2013;191(11):5603-14.

41. Kaech SM, Hemby S, Kersh E, Ahmed R. Molecular and functional profiling of memory CD8 T cell differentiation. Cell. 2002;111(6):837-51.

42. Schmueck-Henneresse M, Omer B, Shum T, Tashiro H, Mamonkin M, Lapteva N, et al. Comprehensive approach for identifying the T cell subset origin of CD3 and CD28 antibody–activated chimeric antigen receptor–modified T cells. The Journal of Immunology. 2017;199(1):348-62.

43. Golubovskaya V, Wu L. Different subsets of T cells, memory, effector functions, and CAR-T immunotherapy. Cancers. 2016;8(3):36.

44. Gattinoni L, Lugli E, Ji Y, Pos Z, Paulos CM, Quigley MF, et al. A human memory T cell subset with stem cell–like properties. Nature medicine. 2011;17(10):1290.

45. Gattinoni L, Speiser DE, Lichterfeld M, Bonini C. T memory stem cells in health and disease. Nature medicine. 2017;23(1):18-27.

46. Arcangeli S, Falcone L, Camisa B, De Girardi F, Biondi M, Giglio F, et al. Next-Generation Manufacturing Protocols Enriching TSCM CAR T Cells Can Overcome Disease-Specific T Cell Defects in Cancer Patients. Frontiers in Immunology. 2020;11:1217.

47. Jia Y, Wei Y. Modulators of MicroRNA Function in the Immune System. International Journal of Molecular Sciences. 2020;21(7):2357.

48. Tamaddon M, Shokri G, Rad SMAH, Rad I, Razavi ÀE, Kouhkan F. involved microRNAs in alternative polyadenylation intervene in breast cancer via regulation of cleavage factor "CFIm25". Scientific reports. 2020;10(1):1-11.

49. Humphries B, Yang C. The microRNA-200 family: small molecules with novel roles in cancer development, progression and therapy. Oncotarget. 2015;6(9):6472.

50. Muralidhar GG, Barbolina MV. The miR-200 family: versatile players in epithelial ovarian cancer. International journal of molecular sciences. 2015;16(8):16833-47.

51. Guan T, Dominguez CX, Amezquita RA, Laidlaw BJ, Cheng J, Henao-Mejia J, et al. ZEB1, ZEB2, and the miR-200 family form a counterregulatory network to regulate CD8+ T cell fates. Journal of Experimental Medicine. 2018;215(4):1153-68.

52. Buchholz VR, Flossdorf M, Hensel I, Kretschmer L, Weissbrich B, Gräf P, et al. Disparate individual fates compose robust CD8+ T cell immunity. Science. 2013;340(6132):630-5.

53. Lugli E, Dominguez MH, Gattinoni L, Chattopadhyay PK, Bolton DL, Song K, et al. Superior T memory stem cell persistence supports long-lived T cell memory. The Journal of clinical investigation. 2013;123(2).

54. Biasco L, Scala S, Basso Ricci L, Dionisio F, Baricordi C, Calabria A, et al. In vivo tracking of T cells in humans unveils decade-long survival and activity of genetically modified T memory stem cells. Sci Transl Med 7 (273): 273ra13. 2015.

55. Oliveira G, Ruggiero E, Stanghellini MTL, Cieri N, D'Agostino M, Fronza R, et al. Tracking genetically engineered lymphocytes long-term reveals the dynamics of T cell immunological memory. Science translational medicine. 2015;7(317):317ra198-317ra198.

56. Marraco SAF, Soneson C, Cagnon L, Gannon PO, Allard M, Maillard SA, et al. Long-lasting stem cell–like memory CD8+ T cells with a naïve-like profile upon yellow fever vaccination. Science translational medicine. 2015;7(282):282ra48-ra48.

57. Geginat J, Lanzavecchia A, Sallusto F. Proliferation and differentiation potential of human CD8+ memory T-cell subsets in response to antigen or homeostatic cytokines. Blood. 2003;101(11):4260-6.

58. Hamann D, Baars PA, Rep MH, Hooibrink B, Kerkhof-Garde SR, Klein MR, et al. Phenotypic and functional separation of memory and effector human CD8+ T cells. The Journal of experimental medicine. 1997;186(9):1407-18.

59. Brenchley JM, Karandikar NJ, Betts MR, Ambrozak DR, Hill BJ, Crotty LE, et al. Expression of CD57 defines replicative senescence and antigen-induced apoptotic death of CD8+ T cells. Blood, The Journal of the American Society of Hematology. 2003;101(7):2711-20.

60. Koch S, Larbi A, Derhovanessian E, Özcelik D, Naumova E, Pawelec G. Multiparameter flow cytometric analysis of CD4 and CD8 T cell subsets in young and old people. Immunity & Ageing. 2008;5(1):1-12.

61. Verma K, Ogonek J, Varanasi PR, Luther S, Bünting I, Thomay K, et al. Human CD8+ CD57-TEMRA cells: Too young to be called" old". PloS one. 2017;12(5):e0177405.

62. Cohen AD, Garfall AL, Stadtmauer EA, Melenhorst JJ, Lacey SF, Lancaster E, et al. B cell maturation antigen–specific CAR T cells are clinically active in multiple myeloma. The Journal of clinical investigation. 2019;129(6):2210-21.

63. Fraietta JA, Lacey SF, Orlando EJ, Pruteanu-Malinici I, Gohil M, Lundh S, et al. Determinants of response and resistance to CD19 chimeric antigen receptor (CAR) T cell therapy of chronic lymphocytic leukemia. Nature medicine. 2018;24(5):563-71.

64. Garfall AL, Dancy EK, Cohen AD, Hwang W-T, Fraietta JA, Davis MM, et al. T-cell phenotypes associated with effective CAR T-cell therapy in postinduction vs relapsed multiple myeloma. Blood advances. 2019;3(19):2812-5.

65. Lécuroux C, Girault I, Urrutia A, Doisne J-M, Deveau C, Goujard C, et al. Identification of a particular HIV-specific CD8+ T-cell subset with a CD27+ CD45RO−/RA+ phenotype and memory characteristics after initiation of HAART during

acute primary HIV infection. Blood, The Journal of the American Society of Hematology. 2009;113(14):3209-17.

66. Precopio ML, Betts MR, Parrino J, Price DA, Gostick E, Ambrozak DR, et al. Immunization with vaccinia virus induces polyfunctional and phenotypically distinctive CD8+ T cell responses. The Journal of experimental medicine. 2007;204(6):1405-16.

67. Carrasco J, Godelaine D, Van Pel A, Boon T, van der Bruggen P. CD45RA on human CD8 T cells is sensitive to the time elapsed since the last antigenic stimulation. Blood. 2006;108(9):2897-905.

68. Yang Y, Kohler ME, Chien CD, Sauter CT, Jacoby E, Yan C, et al. TCR engagement negatively affects CD8 but not CD4 CAR T cell expansion and leukemic clearance. Science translational medicine. 2017;9(417).

69. Turtle CJ, Hanafi L-A, Berger C, Gooley TA, Cherian S, Hudecek M, et al. CD19 CAR–T cells of defined CD4+: CD8+ composition in adult B cell ALL patients. The Journal of clinical investigation. 2016;126(6):2123-38.

70. Turtle CJ, Hanafi L-A, Berger C, Hudecek M, Pender B, Robinson E, et al. Immunotherapy of non-Hodgkin's lymphoma with a defined ratio of CD8+ and CD4+ CD19-specific chimeric antigen receptor–modified T cells. Science translational medicine. 2016;8(355):355ra116-355ra116.

71. Hintzen R, De Jong R, Lens S, Brouwer M, Baars P, Van Lier R. Regulation of CD27 expression on subsets of mature T-lymphocytes. The Journal of Immunology. 1993;151(5):2426-35.

72. Larbi A, Fulop T. From "truly naïve" to "exhausted senescent" T cells: when markers predict functionality. Cytometry Part A. 2014;85(1):25-35.

73. Bromley SK, Thomas SY, Luster AD. Chemokine receptor CCR7 guides T cell exit from peripheral tissues and entry into afferent lymphatics. Nature immunology. 2005;6(9):895-901.

74. Kueberuwa G, Gornall H, Alcantar-Orozco EM, Bouvier D, Kapacee ZA, Hawkins RE, et al. CCR7+ selected gene-modified T cells maintain a central memory phenotype and display enhanced persistence in peripheral blood in vivo. Journal for Immunotherapy of Cancer. 2017;5(1):1-14.

75. Watson HA, Durairaj RRP, Ohme J, Alatsatianos M, Almutairi H, Mohammed RN, et al. L-selectin enhanced T cells improve the efficacy of cancer immunotherapy. Frontiers in Immunology. 2019;10:1321.

76. Le Gallo M, Poissonnier A, Blanco P, Legembre P. CD95/Fas, non-apoptotic signaling pathways, and kinases. Frontiers in immunology. 2017;8:1216.

77. Caccamo N, Joosten SA, Ottenhoff TH, Dieli F. Atypical human effector/memory CD4+ T cells with a naive-like phenotype. Frontiers in immunology. 2018;9:2832.

78. Gupta S, Gollapudi S. CD95-mediated apoptosis in naive, central and effector memory subsets of CD4+ and CD8+ T cells in aged humans. Experimental gerontology. 2008;43(4):266-74.

79. Paulsen M, Valentin S, Mathew B, Adam-Klages S, Bertsch U, Lavrik I, et al. Modulation of CD4+ T-cell activation by CD95 co-stimulation. Cell Death & Differentiation. 2011;18(4):619-31.

80. Groom JR, Luster AD. CXCR3 in T cell function. Experimental cell research. 2011;317(5):620-31.

81. Kared H, Martelli S, Ng TP, Pender SL, Larbi A. CD57 in human natural killer cells and T-lymphocytes. Cancer Immunology, Immunotherapy. 2016;65(4):441-52.

82. Kasakovski D, Xu L, Li Y. T cell senescence and CAR-T cell exhaustion in hematological malignancies. Journal of hematology & oncology. 2018;11(1):91.

Chapter VI

Implications of SARS-CoV-2 Mutations for Genomic RNA Structure and Host microRNA Targeting

The bulk of the data from the following manuscript was produced during the New Zealand lockdown period and was performed as a result of the skills gained in miRNA analysis prior to and during my PhD. The purpose of the work was to determine if SARS-CoV-2 had the potential to be recognised by the host gene-control and immune system of miRNA. Performed entirely in silico, the study shows a number of miRNA target sites filtered to low free-energy binding and represent only those targeted by miRNA with confirmed expression in target cells (e.g. airway epithelia). Importantly, a number of these SARS-CoV-2 binding sites have been lost by conserved mutations, including the C3037U mutation that has been independently mutated >40 times. The C3037U mutation is in linkage disequilibrium with both P232L (RdRp) and G614D (S) mutations, highlighting a possible cluster of functional changes that may impact on SARS-CoV-2 fitness and transmission.

Author contributions:

A.R. and A.M. wrote the paper and supervised the study. A.R. performed the bioinformatics analysis, prepared the figures and tables.

International Journal of
Molecular Sciences

MDPI

Article

Implications of SARS-CoV-2 Mutations for Genomic RNA Structure and Host microRNA Targeting

Ali Hosseini Rad SM * and Alexander D. McLellan *

Department of Microbiology and Immunology, University of Otago, Dunedin 9010, Otago, New Zealand
* Correspondence: a.hosseini.rad@postgrad.otago.ac.nz (A.H.R.S.); alex.mclellan@otago.ac.nz (A.D.M.)

Received: 15 May 2020; Accepted: 2 July 2020; Published: 7 July 2020

Abstract: The SARS-CoV-2 virus is a recently-emerged zoonotic pathogen already well adapted to transmission and replication in humans. Although the mutation rate is limited, recently introduced mutations in SARS-CoV-2 have the potential to alter viral fitness. In addition to amino acid changes, mutations could affect RNA secondary structure critical to viral life cycle, or interfere with sequences targeted by host miRNAs. We have analysed subsets of genomes from SARS-CoV-2 isolates from around the globe and show that several mutations introduce changes in Watson–Crick pairing, with resultant changes in predicted secondary structure. Filtering to targets matching miRNAs expressed in SARS-CoV-2-permissive host cells, we identified ten separate target sequences in the SARS-CoV-2 genome; three of these targets have been lost through conserved mutations. A genomic site targeted by the highly abundant miR-197-5p, overexpressed in patients with cardiovascular disease, is lost by a conserved mutation. Our results are compatible with a model that SARS-CoV-2 replication within the human host is constrained by host miRNA defences. The impact of these and further mutations on secondary structures, miRNA targets or potential splice sites offers a new context in which to view future SARS-CoV-2 evolution, and a potential platform for engineering conditional attenuation to vaccine development, as well as providing a better understanding of viral tropism and pathogenesis.

Keywords: SARS-CoV-2; RNA secondary structure; conserved mutation; miRNA

1. Introduction

The SARS-CoV-2 virus has rapidly emerged as a zoonotic pathogen with broad cellular tropism in human or zoonotic-host cells. Host selection pressure on the SARS-CoV-2 virus will have a major impact on the long-term conservation of mutations that enhance viral fitness. Of these selection pressures, the cellular-based adaptive and innate immune systems place constraints on viral fitness. Intracellular detection and anti-viral pathways within infected cells are a critical frontline to control virus replication. The success of the pathogenic SARS coronaviruses is proposed to be due to their ability to suppress intracellular anti-viral pathways [1]. For example, interference with dsRNA detection and the interferon response is enabled through the activity of several non-structural proteins (Nsp). In addition, the sequestration of genomic viral RNA into double membrane vesicles, and dsRNA cleavage by Nsp15, is inferred from the closely related SARS viruses, and likely acts to prevent intracellular detection of the virus [1]. In addition to encoded mechanisms of immune avoidance, the paucity of CpG runs in the SARS-CoV-2 genome with unexpectedly low GC-content at codon position three points to major selection pressure being placed on structural features of the genome [2].

As a recently-emerged zoonotic pathogen, it might be expected that bat-adaptations will not be optimal for infection and replication in human cells. However, extensive mutation and strain-radiation has not yet been observed [3]. The mutation rate in SARS-CoV-2 is reduced by the -proof-reading 3′–5′ exonuclease Nsp14 in the RNA-dependent RNA polymerase (RdRp) complex. The observed mutation

rate may be lower than the actual mutation rate, since deleterious mutations have likely been lost through natural selection. The short time frame of SARS-CoV-2 evolution, coupled to a low mutation rate is consistent with a founder effect for geographical bias in mutation patterns [3,4].

A common primary focus of mutational analysis of emerging viruses is the alteration in amino acid sequence of viral proteins that may provide enhanced or new functions for virus replication, immune avoidance, or spread. For instance, the non-synonymous A23403G mutation in the S gene may enhance viral infectivity through decreased S1 shedding and increased S trimer stability [5]. However, synonymous mutations can critically impact nucleic acid secondary structure and sub-translational events including genome replication and packaging, and virus maturation [6,7], as well as translation and polypeptide folding [8,9]. In addition, the RNA secondary structures of SARS-CoV-2 genes have been proposed to be druggable targets [10–12]. Because little is known of the influence of SARS-CoV-2 mutations on the RNA secondary structure, and its possible implications for inhibition by host miRNA, we have modelled the impact of common mutations of the SARS-CoV-2 RNA structure and the susceptibility of the genome to interference from host miRNA.

The incident presence of host miRNA targets within the SARS-CoV-2 genome may be pivotal for host selection pressures to further shape further viral evolution. Viruses not only alter host miRNA expression, but may also produce miRNAs to promote their infectivity [13–16]. On the other hand, the host targets viral transcripts for inhibition of translation, or mRNA destruction, through a miRNA-mediated defence system. Since miRNAs are divergent between species [17], it would be expected that bat-adapted SARS-CoV-2 will undergo selection pressure derived from human miRNA interference [13–15,18,19]. While perfect matches of miRNA to target viral sequences result in miRNA-induced silencing complex (miRISC)-mediate destruction of viral RNA, imperfect matches interfere with translation [20].

A growing body of evidence suggests that human miRNAs act as a critical host defence against coronaviruses. An interaction between human coronavirus OC43 nucleocapsid and miR-9 can enhance the type I interferon response necessary to clear viral infection [21]. Several host miRNAs (miR-574-5p, −214, −17, −98, −223, and −148a) bind to SARS-CoV encoded transcripts such as S, E, M, N, and ORF1a [22,23]. However, SARS-CoV escapes from miRNA-mediated defence through the manipulation of host miRNA machinery [22,23]. Additionally, SARS-CoV and SARS-CoV-2 express short RNAs that resemble miRNAs and could impact upon host house-keeping or immune defence processes [24–26]. More recently, several studies have proposed that host miRNAs bind SARS-CoV-2 transcripts [24,26,27]. However, the relevance of host miRNAs for inhibition of viral replication is relevant only if the identified miRNAs are expressed in target host cells.

Both DNA viruses, and 'cytoplasmically-confined' RNA viruses, use the host RNA splicing-machinery to generate new viral transcripts, or to modify the host transcriptome in favour of their own replication [28–32]. It has been suggested that the fused leader sequence in 5′ end of the mouse hepatitis virus (betacoronavirus) mRNAs is the result of a non-canonical splicing process [33]. Moreover, deep RNA sequencing has identified several unknown SARS-CoV-2 viral RNAs, possibly the result of non-canonical splicing events [34]. Therefore, our study has additionally identified and mapped mRNA splice sites within the SARS-CoV-2 genome.

No selective advantage of the identified sequence alterations in SARS-CoV-2 should be inferred by their inclusion here. However, the potential of these mutations to impact upon RNA structure and miRNA recognition provides a basis for ongoing monitoring of viral evolution at these sites in the SARS-CoV-2 genome.

The interplay of viral genome sequences and host miRNA is translatable for clinical outcomes. For example, the inclusion of host miRNA binding sites into the ORF of conserved viral regions essential for the viral life cycle is a feasible mechanism for the attenuation of live vaccines [35–38].

2. Results

2.1. Identification of SARS-Cov-2 Recurrence Mutations

A total of 65 SARS-CoV-2 patient isolate sequences were collected from NCBI and GISAID databases and aligned against SARS-CoV-2 reference sequence NC_045512.2 (Table S1). The mutations present in multiple sequences and in at least in three different countries were categorized as 'conserved mutations' (Table 1) [39].

Table 1. Conserved mutations in SARS-CoV-2 genome.

Gene	Mutation	Amino Acid Change
5′ UTR	C to U—nt241	-
Nsp1	C to U—nt313	No (L16)
Nsp2	C to U—nt1059	T85I
	G to A—nt1397	V198I
	Deletion 1606–1609	D268 deletion
Nsp3	C to U—nt3037	No (F106)
Nsp4	C to U—nt8782	No (S76)
	C to U—9802	No (A416)
	G to U—9803	No (L417)
Nsp6	G to U—nt11083	L37F
Nsp12	C to U—nt14408	P232L
	C to U—nt14805	No (Y455)
Nsp13	U to C—nt17247	No (R337)
S	A to G—nt23403	D614G
	C to U—nt24034	No (N824)
ORF3a	G to U—nt25563	Q57H
	G to U—nt26144	G251V
ORF8	C to U—nt27964	S24L
	U to C- nt28144	L84S
N	C to U—nt28311	P13L
	U to C—nt28688	No (L139)
	GGG to AAC—nt28881-28884	R203K and G204R
3′ UTR	G to U—nt29742	-

Greater than 50% of the observed mutations in our analysis were synonymous mutations (Figure 1, Table S2). Similar data was obtained from Observable notebook on all sequencing data available up to 12 June 2020 (Figure 1, Table S2). Recently, Li et al. suggested that SARS-CoV-2 is under purifying selection, with dN/dS < 1 [40]; similar results were observed in our study and others [40,41].

Most of these mutations are substitutions of C/G to U. The high A/U content (U = 32.1%; A = 29.9%; G = 19.6%; C = 18.4%) and enrichment of codons in pyrimidines is likely due to APOBEC editing of viral RNA and the fact that the proof-reading Nsp14 does not remove U (the product of cytosine deamination) [42]. Two mutations at 241 and 29742, are in the 5′ and 3′ untranslated regions (UTRs). Nine mutations are synonymous mutations, including 313, 9802, 9803, 14,805, 17,247, and 28,686, while the others are non-synonymous (Table 1). Interestingly, the C27964U (S24L in ORF8) exists only

in 97 USA sequences, with the earliest isolated on March 9th (MT325581.1), after USA underwent lockdown [43] (Figure S1).

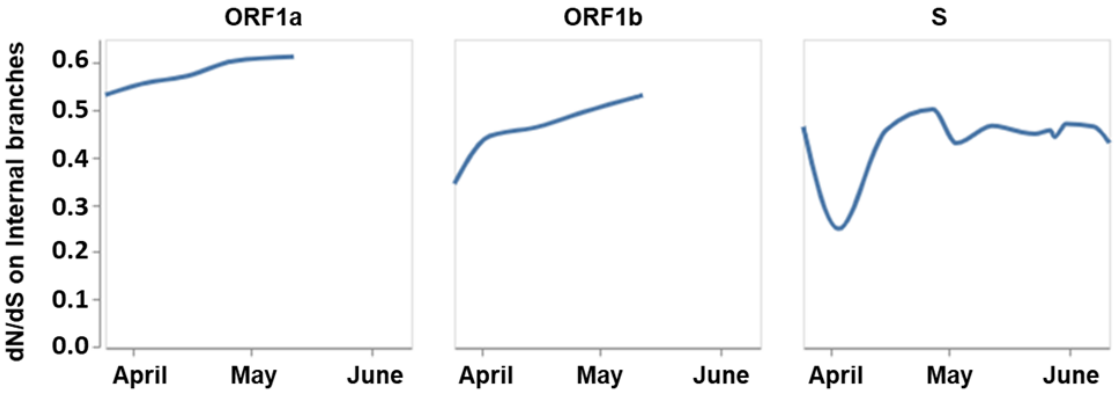

Figure 1. The ratio of SARS-CoV-2 nonsynonymous to synonymous mutations obtained from the Observable notebook (sequencing data available up to June 12, 2020).

2.2. *RNA Secondary Structure*

Among all the mutations, only two mutations were predicted to have an impact on the secondary structure of viral RNAs. First, a conserved mutation 1059 in Nsp2 changed the secondary structure of Nsp2 dramatically (Figure 2A). We performed local RNA secondary structure analysis on 500 bp flanking the mutation region (250 bp upstream and 250 bp downstream of mutation site), as global folding predictions for large mRNA have been shown to be unreliable [44].

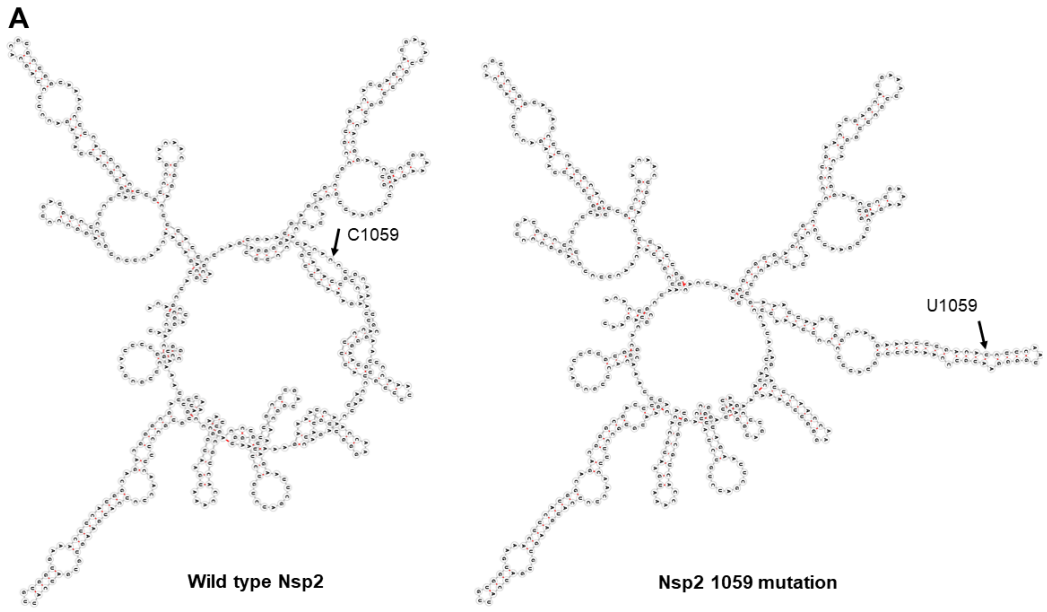

Figure 2. *Cont.*

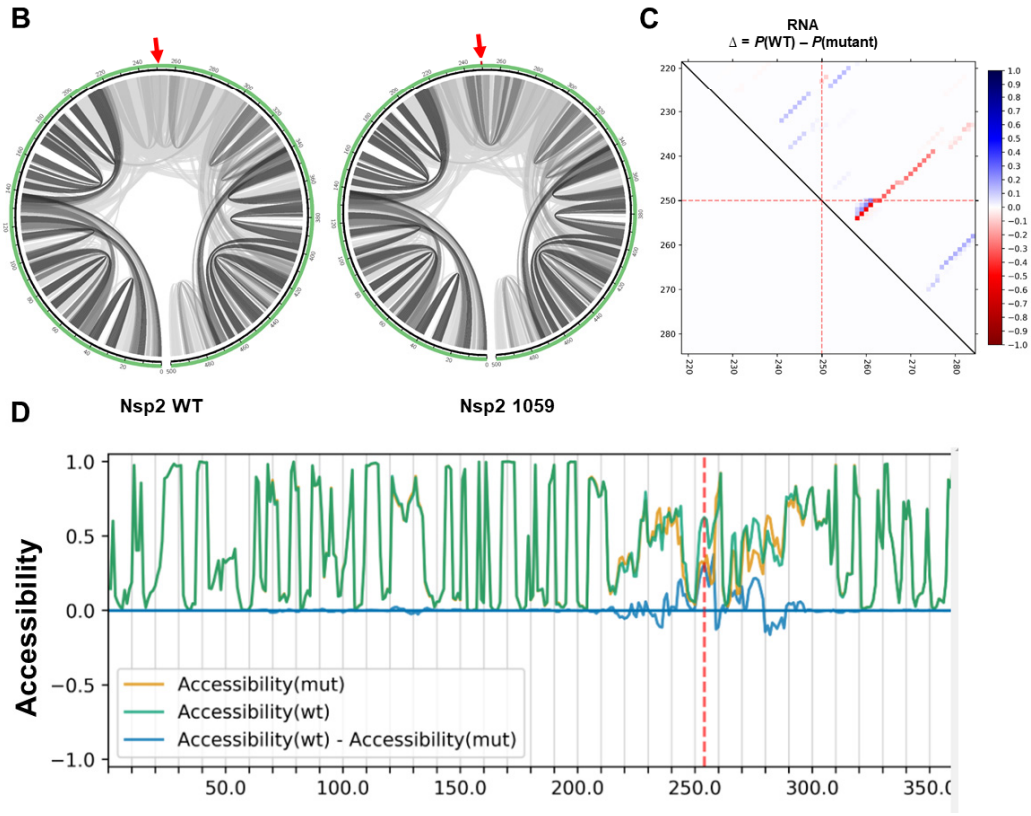

Figure 2. The impact of C1059U mutation on local RNA secondary structure of Nsp2. (**A**) RNA secondary structures of Nsp2 wild type (MFE structure: −146.10 kcal/mol—centroid structure: −132.30 kcal/mol) and 1059 mutation (MFE structure: −147.20 kcal/mol—centroid structure: −137.80 kcal/mol) using RNAfold tool. (**B**) The base pair probabilities by circular plots with higher base pairing potential is reflected in darker hues of grey lines and the mutated position highlighted by red arrow (MutaRNA). (**C**) The dot plot shows the differences of the base pairing probabilities of 1059 mutation vs. wild type RNA, Pr(bp in WT)—Pr(bp in mut). The base pairs weakened by the 1059 mutation are in blue, while higher base pair probability in the mutant is depicted in red. The mutated position is highlighted by red dotted lines (P values based on RNAsnp are as follows: mode-1 = 0.2617, mode-2 = 0.3344). (**D**) The accessibility profiles of wild type (green line) and the mutation (yellow line) and their differences provide an assessment of the mutation effect on the RNA single-strandedness, which may relate to its interaction potential with other RNAs or proteins. Accessibility is measured in terms of local single-position unpaired probabilities and is plotted as WT—Mut, whereby a negative value indicates increased accessibility caused by the mutation [45]. The mutated position is highlighted by a red line.

Next, the effects of mutations on base pair probabilities of local folding of Nsp2 RNA were investigated. As shown in Figure 2B, the 1059 mutation increased the Watson–Crick base pair probability in flanking regions, resulting in a more stable predicted RNA secondary structure (Figure 2C). The 1059 mutation had no effect on RNA accessibility which is a consideration for RNA-RNA and RNA-protein interactions (Figure 2D).

Mutation 29742 occurs in a conserved region within 3′ UTR known as the coronavirus 3′ stem-loop II-like motif (s2m). This mutation alters the global RNA secondary structure of the 3′ UTR (Figure 3A). An increase in stability of s2m in the mutated sequence was observed in both MFE (−6.10 kcal/mol vs. −11.70 kcal/mol) and centroid (−0.47 kcal/mol vs. −11.40 kcal/mol) structures. It is well known that s2m is present in most coronaviruses and plays a vital role in viral replication and invasion [46–48]. Mutations in this region have been shown to increase the stability of 3′ UTR and its interaction with 5′ UTR [47].

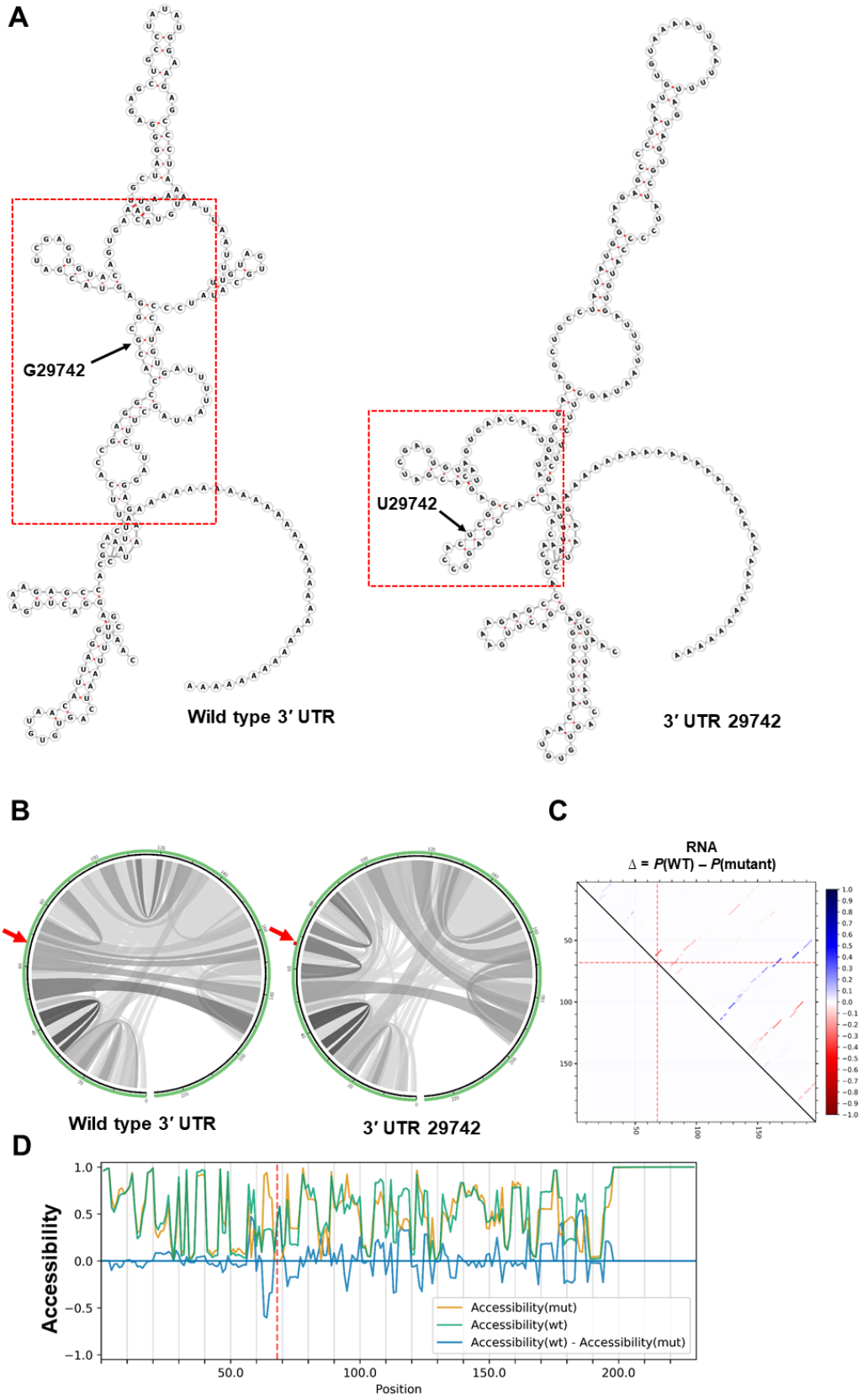

Figure 3. The impact of G29742U mutation on the 3′ UTR. (**A**) The RNA secondary structures of wild type 3′ UTR (MFE structure: −36.90 kcal/mol—centroid structure: −30.50 kcal/mol) and 29,742 mutation (MFE structure: −40.30 kcal/mol—centroid structure: −30.30 kcal/mol) using RNAfold tool. Note the

change in predicted secondary structure of 3′ UTR RNA through the 29742 mutation. The s2m regions are highlighted by red rectangles. (**B**) The base pair probabilities of global fold of Nsp2 RNA demonstrated by circular plots, with higher base pairing potential reflected in darker hues of graduated grey lines. The original and mutated nucleotides are highlighted by red arrows (MutaRNA). (**C**) The dot plot shows the differences of the base pairing probabilities of the 29,742 mutation vs. wild type RNA, Pr(bp in WT)—Pr(bp in mut). The base pairs weakened by the mutation are in blue while higher base pair probability in the mutant is depicted in red. The mutated position is highlighted by red dotted lines (P values based on RNAsnp are as follows: mode-1 = 0.6204, mode-2 = 0.6638). (**D**) The accessibility profiles of wild type (green line) and mutation (yellow line) and their differences provide an assessment of the effect of the mutation on the RNA single-strandedness. Accessibility is measured in terms of local single-position unpaired probabilities and is plotted as WT—Mut, whereby a negative value indicates increased accessibility caused by the mutation [45]. The mutated position is highlighted by a red line.

Analysing base pairing probability, the G29742U mutation slightly decreased base pair probabilities in the global folding of RNA (Figure 3B). But the same mutation slightly increased the number of strong base pair probabilities downstream of the mutation in the s2m region 29795-29865 (Figure 2C) and may contribute to the stronger thermodynamic structure predicted in mutated s2m (see above). Several SARS-CoV-2 encoded genes bind to the host proteins involved in biological processes, such as protein trafficking, translation, transcription, and ubiquitination regulation [49,50]. In addition, s2m interacts with viral and host proteins such as the polypyrimidine tract-binding protein (PTB), to regulate viral replication and transcription [47,48]. Interestingly, the G29742U mutation (underlined) removed a c-Myc binding site (GCC AC<u>G</u> CGG A) within s2m, but increased the RNA accessibility of this region (Figure 3D).

It should be noted that both 1059 and 29,746 mutations exist in the regions that are highly sensitive to nucleotide changes based on the RNAsnp mode-3 and RaSE programs (Tables S3–S6). Collectively, these results suggest that 1059 and 29,742 yield more stable RNA structures around the mutation sites. However, noting the limitations of prediction software, the relationship of changes in RNA secondary structure of Nsp2 and 3′ UTR to viral replication or infectivity must be tested in adequate experimental assays.

2.3. Potential Interaction of SARS-CoV-2 Transcripts and Human miRNAs

Using databases and published data, we filtered our considered miRNA to those with documented expression in SARS-CoV-2 target cells, and additionally focused on miRNAs that have been reported as components of the anti-viral miRNA-mediated defence system. Using independent programmes, we identified ten human miRNAs with potential binding sites across the SARS-CoV-2 genome (Figure 4 and Figures S3–S17).

As shown in Figure 5, a total of eight mutations were detected in six miRNA binding sites of which four are conserved mutations (3037, 9802, 9803 and 24034).

Out of eight mutations, two mutations are G↔A, while six mutations are G/C→U, likely the result of host RNA editing mechanisms [51]. We hypothesised that some mutations may affect the miRNA binding sites and therefore impact on miRNA-mediated defence, since miRNA-mRNA interactions are sensitive to the GC loss (see above). We also mapped the critical positions in which nucleotide substitutions will negatively affect miRNA binding to its target (Figure 5, asterisks).

MiR-197-5p is upregulated in patients with cardiovascular disease and has been proposed as a biomarker for the prediction of cardiovascular events [52–54]. It is well established that patients with cardiovascular disease are overrepresented in symptomatic COVID-19 cohorts and have a higher mortality rate [55]. The C3037U conserved, but synonymous, mutation within Nsp3 sequence abolished the miR-197-5p target sequence, as the C3037 nucleotide is among the sensitive nucleotides (Figure 5, Table S7). This mutation was introduced in early January 2020 (Figure S2), and is frequently linked to dominant D614G mutation [56]. Interestingly an analysis carried out by van Dorp et al. showed that

C3037U mutation is a homoplasy that has independently emerged three times in global lineages and has a positive association with clade expansion [4].

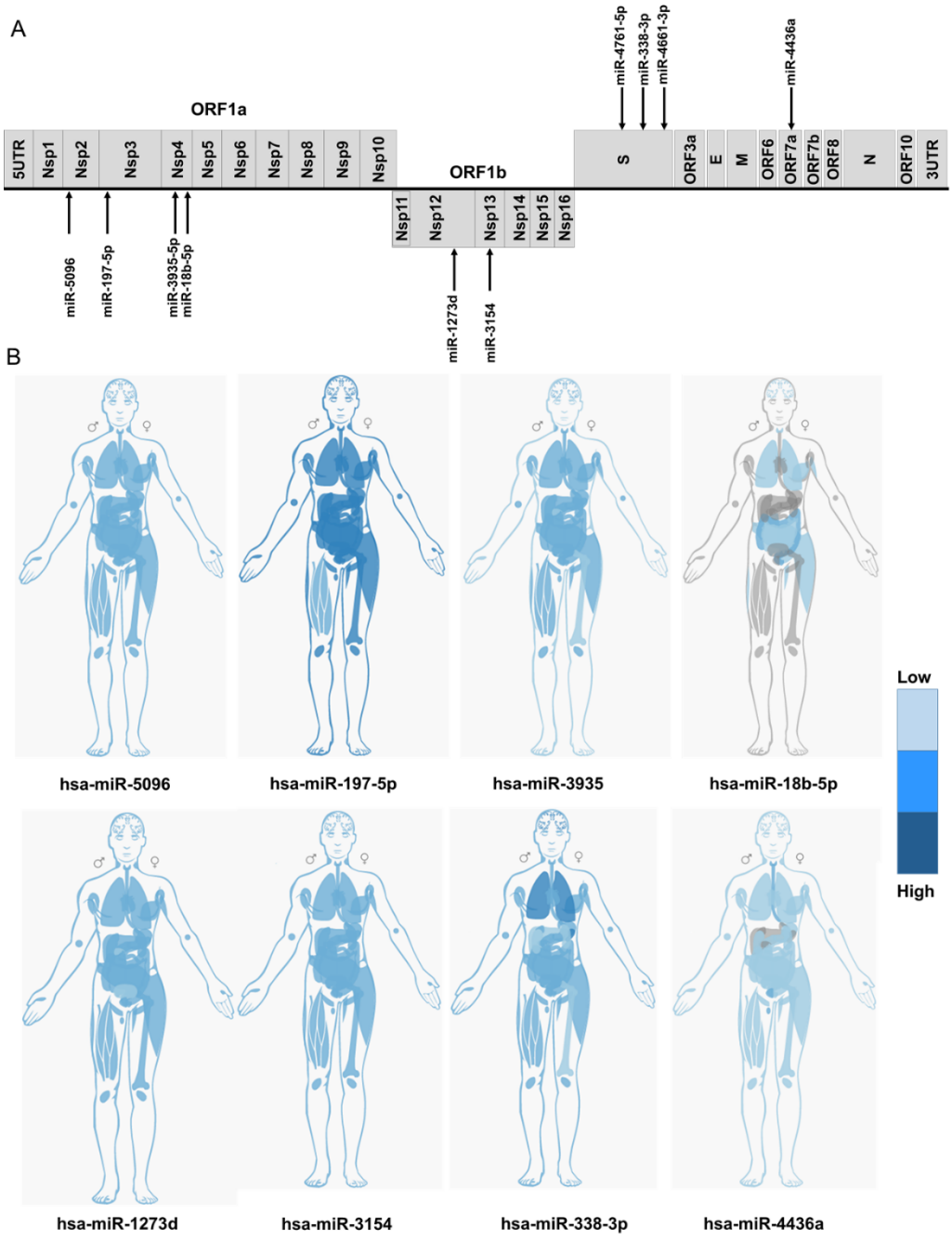

Figure 4. (**A**) Identification of host miRNA targeting different regions of SARS-CoV-2 genome. (**B**) The relative expression level of candidate miRNA in different human tissues. Data was obtained from the IMOTA database. Darker blue indicates the higher expression. Grey colour shows undetectable expression in those tissues. The plotted presentations of miRNA expression in different human tissues obtained from TissueAtlas and TISSUES databases are available in the supplementary figure file.

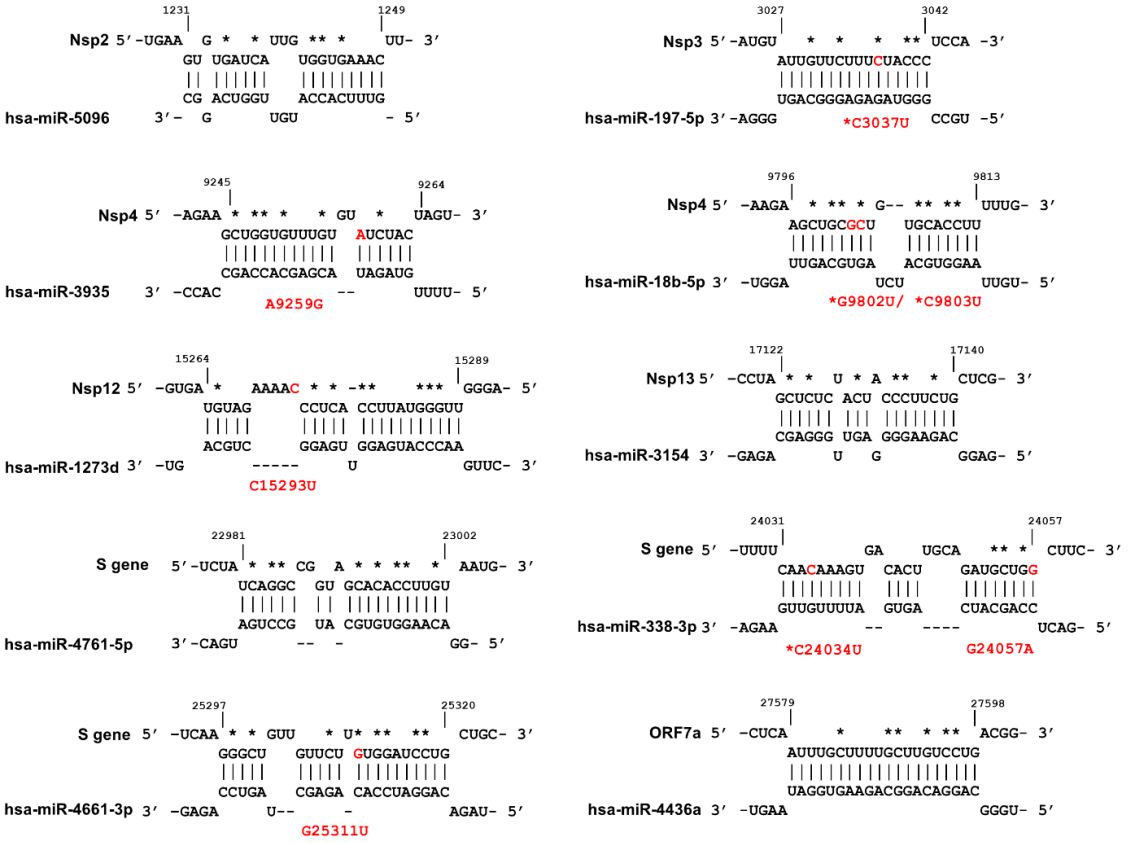

Figure 5. Prediction of host miRNAs binding sites within different regions of SARS-CoV-2 genome. The mutations that occur in miRNA binding sites are indicated in red, and the designations of the mutations are shown in red font. Conserved mutations are indicated with red asterisks while the nucleotide substitutions that result in significant effect on MBS are shown with black asterisks. The figure was produced using IntaRNA tool.

Three mutations within Nsp4 occur in target sequences of miR-3935 and miR-18b-5p. Both miRNAs are expressed in SAR-CoV-2 target cells (Figure 4B and Figures S7–S10). Nsp4 A9259G is present in a sequence obtained from Vietnam (GISAID: EPI_ISL_416429). Two recurring synonymous mutations, G9802U and G9803U, disrupt the miR-18b binding site of Nsp4. The miR-18b miRNA was reported to be downregulated in viral infections such as HBV and Ebola [57,58] while its expression in patients with cardiovascular disease is upregulated [59–61].

We identified three miRNAs with perfectly matched complementary sequences within the S-gene: miR-338-3p, miR-4661-3p, and miR-4761-5p. As shown in Figure 5, two of these sites were altered by recently identified mutations in the S-gene. In particular, the miR-338-3p miRNA is expressed at high levels in SARS-CoV-2 target cells (Figure 4B, and Figures S14 and S15). The sequences carrying recurrent mutations C24034U and G24057A (EPI_ISL_429691) were predicted to have lost the miR-338-3p binding sites, although these mutations did not decrease the binding energy of miR-338-3p to S (Table S7). The miR-338-3p miRNA acts as a tumour suppressor in liver, lung, and gastric cancers [62–64]. The expression level of miR-338-3p declines during HBV infection [65,66] and miR-338-3p has a recognition site within the Vaccinia virus genome [67].

Lastly, G25311U in a patient sample isolated in India (MT396242.1) removed the miR-4661-3p binding site within the S gene (Figure 5, Table S7).

In addition to the sites mentioned here, we identified an additional four host miRNAs with perfect complementarity within the receptor binding domain (RBD) region of S gene (Figure 6). These miRNAs are not expressed by SARS-CoV-2 target cells (data not shown). However, because these miRNA target

sequences exist within the critical ACE-2 targeting region, they may be relevant to miRNA-mediated virus attenuation technology. For example, viral replication can be attenuated in a species-specific and tissue-specific manner by host miRNA machinery, which controls viral tropism, replication, and pathogenesis [35–38].

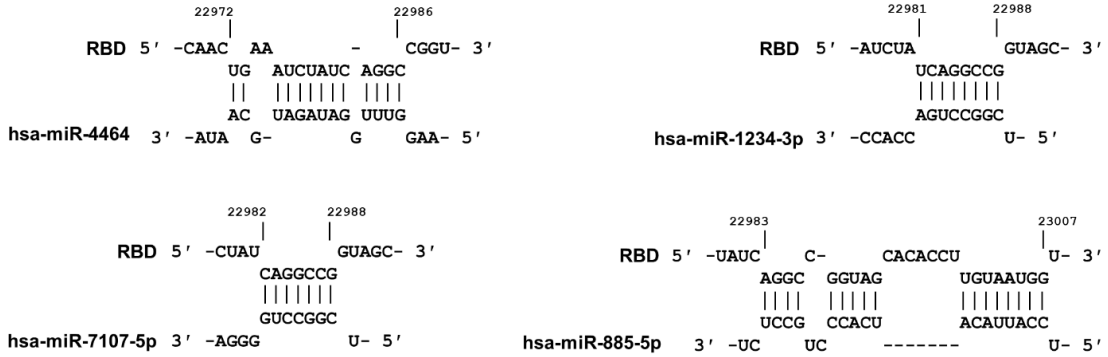

Figure 6. Identification of four miRNAs with ability to bind to the RBD within the S gene. Although not expressed in target cells, these potential miRNAs are included due to their potential use in miRNA-mediated attenuation of the SARS-CoV-2 [37,38].

2.4. Possible Impact of Mutations on Cryptic Splice Sites

Atypical cytoplasmic RNA splicing has been proposed to contribute to non-canonical viral transcripts, even for viruses that classically replicate in the cytoplasm [28–33]. Moreover, deep RNA sequencing has identified several previously unidentified SARS-CoV-2 viral RNAs that may be the result of non-canonical splicing events, or alternative transcriptional start sites [34]. We used RegRNA2 [68], HSF [69], and NIPU [70,71] tools to identify the putative splice sites and motifs within the SARS-CoV-2 genome. Our computational prediction identified several 5′ donor and 3′ acceptor splice sites, as well as splice enhancer/inhibitor motifs [72] (Table S8). However, none of the conserved mutations introduced, or deleted, any potential splice sites.

3. Discussion

At present there are nearly 200 mutations identified within global SARS-CoV-2 isolates. These mutations are mostly limited to point mutations, with little evidence for recombination events mediating the simultaneous transfer of multiple mutations. Although mutations may be due to RdRP/Nsp12 infidelity, the predominance of C → U and G → A mutations is consistent with base-editing defence (e.g., APOBEC/ADAR) [42,73]. The Nsp14 exonuclease-based proof-reader is a critical counter-defence against host base-editor attack on the coronavirus genome [1]. It is also possible that the position of mutations within the genome could reflect accessibility of host base-editors to the SARS-CoV-2 genome upon uncoating, or during genome translation [42].

In our study, we filtered mutations to common/conserved events according to published sources [39]. There is little evidence that the existing mutations in SARS-CoV-2 have an impact on transmission, replication, or viral load, but our study has flagged potential sites that could impact on viral fitness. It remains to be seen if these mutations be maintained in human populations over time. Carriage of SARS-CoV-2 mutations through rapid expansion into naive populations throughout the world can be due to neutral founder effect, or from fitness gains. However, the ratio of non-synonymous to synonymous mutations is consistent with an emerging virus undergoing purifying selection (see Figure 1 and ref. [40]).

Our study identified a potential binding site for miR-197-5p lost by the Nsp3 synonymous C3037U mutation. miR-197-5p is overexpressed in patients with cardiovascular disease – a patient group that demonstrates an increased susceptibility to SARS-CoV-2 infection. miR-197-5p was previously reported

to act in defence against hepatitis viruses, such as HBV, HCV, HAV, and Enterovirus 71 [74–76] and was highly elevated in serum of patients with H7N9 [77]. It is possible that a loss of miR-197-5p-mediated defence against SARS-CoV-2 is relevant to the increased mortality noted in this patient group [55]. van Dorp et al. showed that the Nsp3 C3037U mutation was significantly ($p = 0.027$) associated with 'transmission' – as determined by the relative frequency of homoplasies between sister clades [4]. The C3037U is linked to the A23403G (G614D) mutation [4,56], which may enhance viral infectivity through structural changes in the S protein [5]. Our studies provide further context to monitor the linkage of the C3037U and A23403G sites. However, further investigations into the interactions of miR-197-5p expression, the C3037U mutation, and COVID-19 disease severity in this cardiovascular patients are required.

It has been shown that folding energy and stability of the mRNA secondary structure influences polypeptide translation and folding. Stable RNA structures act as gauges during translation and reduce the speed of translation to avoid "ribosomal traffic jams" to allow proper folding of newly translated peptides [8]. Therefore, both the sequence and secondary structure of viral mRNA is subject to selection pressure for optimal translation in eukaryotes [9].

Recently, several studies have shown that RNA editing affects the specificity and strength of miRNA binding to its target, and tumour cells may exploit this mechanism to escape from miRNA recognition [78,79]. Three mutations within Nsp4 were predicted to affect miR-3935 and miR-18b-5p targeting. The expression of miR-3935 and miR-18b is altered upon viral infection [57,80–82]. The expression level of miR-3935 upregulates during H1N1, Crimean-Congo haemorrhagic fever virus, Coxsackievirus A16, and Enterovirus 71 infection [80–82]. The miR-18b was reported to be downregulated during HBV and Ebola virus infections [57,58]. Similar to what was observed for miR-197-5p, both miR-18b and miR-3935 are upregulated in patients with cardiovascular disease [59,60,83]. It should be noted that the effect of total free energy of binding on miRNA function is highly dependent on physiological temperature. For instance, if a mutation increases the ΔG of binding, the effect of mutation will be exacerbated at higher host temperature (e.g., related to the euthermia of the host species, or febrile temperature elevation).

We noted that filtered miRNAs (except miR-338-3p) belong to the GC-rich class of miRNA within their binding region (avg. GC content = 56%). The content of miRNA seed sequence plays critical roles in miRNA function, biogenesis, and ability to downregulate target genes. MiRNAs with higher GC content form relatively more stable duplexes with their target and preferentially originate from canonical pathways of miRNA biogenesis, correlating with greater target suppression [84]. In general, stress-responsive miRNAs have a higher GC content that might enhance miRNA-target duplex stability to activate the stress response [85,86]. Interestingly, the stability of interactions between miRNA and its targets correlates with body temperature: at higher body temperature miRNA-mRNA duplexes with lower GC contents are less functional [85,87]. It should be noted that both 3′ and 5′ ends of miRNAs are responsible for stable and specific interaction between miRNA and its target, particularly if the target region is in a coding region [88,89].

It is not yet clear if anti-viral miRNAs have evolved as host defence against viral infection, or are simply critical gene regulatory elements that assume an additional role for targeting viral transcripts—particularly when the human cellular defence machinery is confronted by an emerging zoonotic virus [13,18,19]. The possibility of including host miRNA binding sites into the genome of live-attenuated viruses offers a further checkpoint for the further attenuation of live vaccines, in a host-cell specific manner. For example, the identification of miRNA target sites in viral pathogens opens up opportunities for further study of viral host cell-tropism, or to create cell-specific or species-specific viral vaccines [35–38]. Finally, miRNA sites within the coding sequence of viral genes may be critical for ribosomal stalling, leading to the production of pioneer translation products (PTP). Enhanced production of PTP peptides may be critical for MHC-I loading for boosting the anti-viral CTL response [89–92].

4. Methods

4.1. Sequence Alignment

The SARS-CoV-2 virus reference sequence was downloaded from NCBI (NC_045512.2) along with 65 sequences up to May 26, 2020 from NCBI or GISAD databases. We included a range of countries with available sequences up to 26 May 2020. In the case of the USA, 16 sequences from 13 states were included. Clustal Omega (using mBed algorithm for guide tree) and Geneious alignment tools were used to perform multiple sequence alignment. The following parameters were used for Geneious alignment: sensitivity; highest/slow, fine tuning; iterate up to five times. Iterative fine tuning involves initial reads to map the consensus sequence, followed by repeated mapping to the consensus sequence. The results are then converted back to mappings relative to the original reference sequence and the process is repeated until the results stabilise, or for a maximum of five iterations.

4.2. Mutational Analysis

Mutations with occurrence in multiple sequences originating from different countries were categorized as 'conserved'. Cumulative plots of the average behaviour of each codon in alignment analysis for insertions/deletions (indels), synonymous (syn), and non-synonymous (nonsyn) substitutions, observed/potential syn and nonsyn mutations, and the ratio of syn to nonsyn substitutions (ds/dn) were calculated using SNAP v2.1.1 for all pairwise comparisons [93]. Natural selection analysis of SARS-CoV-2 sequences in GISAD up to 12th June 2020 was obtained from Observable (https://observablehq.com/).

For mapping the host-spot substitutions which lead to significant change on base pair probabilities of global folding, mode-3 (which is a combination of mode-1/2) of RNAsnp was used. The following parameters were considered using RNAsnp mode-3: folding window—selected size of flanking regions on either side of mutation; 200 nt, *p*-value threshold to filter substitutions that are predicted using mode-2; 0.1, *p*-value threshold to filter substitutions that are predicted using mode-1; 0.05, minimum length of flanking regions on either side of the substitution; 200 nt.

4.3. RNA Secondary Structure and Base Pair Probability Analysis

We used well-accepted methods to predict the RNA secondary structure in both wild type and mutated sequences. Minimum free energy (MFE) structures [94] and centroid structures [95] were calculated by RNAfold program to predict RNA secondary structures. To evaluate the impact of mutations on RNA secondary structure and base pair probability, we utilized RNAfold, RNAalifold [96], MutaRNA [71,97], and RNAsnp [98] programs.

The following parameters were used in RNAsnp program: mode-1 (designed to predict the effect of SNPs on short RNA sequences < 1000 bp); folding window (the size of flanking regions on either side of mutation) of 200 nt; minimum length of the sequence interval was 50; cut-off for the base pair probabilities was 0.01. Regardless of the length of sequence, the p values were calculated and presented with both modes ($p < 0.2$ considered significant). MutaRNA was used to calculate the effect of mutations on local folding with a window size of 200 nt and maximal base pair span of 150 nt.

RNAsnp mode-3 and RaSE [71] tools were used to predict the role of each single nucleotide and their substitutions in RNA secondary structure. RaSE program uses EDeN to determine the role of each nucleotide in the RNA secondary structure by assigning a score for each nucleotide based on RNAplfold base pair probabilities. The outputs are: (i) which substitution in each nucleotide has the most effect on RNA structure and (ii) similar to RNAsnp filters, the most significant substitutions. Default parameters were used in the RaSE structure graph, RNAplfold, and EDeN.

4.4. Potential miRNA Binding Site Analysis

For identifying potential miRNA binding sites, the SARS-COV-2 genome was screened with RegRNA2 (filtered to human miRNAs, score ≥ 170, free energy ≤ −25) and miRDB (custom prediction tool) [99]. We excluded miRNAs not expressed in SARS-CoV-2 target cells such as lung, oesophagus,

kidney, and small intestine [100,101]. The expression levels of miRNA in target cells were determined by TissueAtlas [102], IMOTA [103], TISSUES [104], or using published data. The impact of mutations on miRNA binding was visualized by RegRNA2.0, miRDB, IntaRNA (one interaction per RNA pair, minimum 7 base pairs in seed, no seed with GU end, no lonely base pairs) [105] and CopomuS (no A:U, G:U base pairs, no lonely base pairs, no helix ends, IntaRNA parameters: no GU at helix ends, min. 7 base pairs in seed) [71], and RNAup (avoid isolated base pairs, length of the unstructured region; 4nt, maximal length of the region of interaction; 25nt). We used IntaRNA to illustrate miRNA binding to its target.

Wild type and mutated sequences were analysed by RegRNA2.0 and miRDB to determine if mutations result in a loss of miRNA binding prediction. In addition, the total free energy of binding (ΔG) was calculated with IntaRNA and RNAup. If WT ΔG < Mut ΔG, the mutation was assumed to reduce the strength of miRNA binding to the target sequence.

4.5. Potential Splice Site Analysis

Potential splice donor/acceptor splice sites, exon splicing enhancer (ESE), exon splicing silencer (ESS), intron splicing enhancer (ISE), and intron splicing silencer (ISS) motifs were predicted using RegRNA2.0 [68], HSF [69], and NIPU [70,71] tools.

Supplementary Materials: The following are available online at http://www.mdpi.com/1422-0067/21/13/4807/s1.

Author Contributions: A.H.R.S. and A.D.M. conceived of the study and wrote the paper. A.H.R.S. performed the data analysis and produced the figures. All authors have read and agreed to the published version of the manuscript.

Funding: This research received no external funding.

Conflicts of Interest: The authors declare no conflict of interest.

References

1. Totura, A.L.; Baric, R.S. SARS coronavirus pathogenesis: Host innate immune responses and viral antagonism of interferon. *Curr. Opin. Virol.* **2012**, *2*, 264–275. [CrossRef] [PubMed]
2. Tort, F.L.; Castells, M.; Cristina, J. A comprehensive analysis of genome composition and codon usage patterns of emerging coronaviruses. *Virus Res.* **2020**, *283*, 197976. [CrossRef] [PubMed]
3. MacLean, O.A.; Orton, R.J.; Singer, J.B.; Robertson, D.L. No evidence for distinct types in the evolution of SARS-CoV-2. *Virus Evol.* **2020**, *6*, veaa034. [CrossRef]
4. van Dorp, L.; Richard, D.; Tan, C.C.; Shaw, L.P.; Acman, M.; Balloux, F. No evidence for increased transmissibility from recurrent mutations in SARS-CoV-2. *bioRxiv* **2020**.
5. Zhang, L.; Jackson, C.B.; Mou, H.; Ojha, A.; Rangarajan, E.S.; Izard, T.; Farzan, M.; Choe, H. The D614G mutation in the SARS-CoV-2 spike protein reduces S1 shedding and increases infectivity. *bioRxiv* **2020**. [CrossRef]
6. Kusov, Y.; Tan, J.; Alvarez, E.; Enjuanes, L.; Hilgenfeld, R. A G-quadruplex-binding macrodomain within the "SARS-unique domain" is essential for the activity of the SARS-coronavirus replication–transcription complex. *Virology* **2015**, *484*, 313–322. [CrossRef]
7. Chen, C.-Y.; Chang, C.-K.; Chang, Y.-W.; Sue, S.-C.; Bai, H.-I.; Riang, L.; Hsiao, C.-D.; Huang, T.-H. Structure of the SARS coronavirus nucleocapsid protein RNA-binding dimerization domain suggests a mechanism for helical packaging of viral RNA. *J. Mol. Biol.* **2007**, *368*, 1075–1086. [CrossRef]
8. Faure, G.; Ogurtsov, A.Y.; Shabalina, S.A.; Koonin, E.V. Role of mRNA structure in the control of protein folding. *Nucleic Acids Res.* **2016**, *44*, 10898–10911. [CrossRef]
9. Peeri, M.; Tuller, T. High-resolution modeling of the selection on local mRNA folding strength in coding sequences across the tree of life. *Genome Biol.* **2020**, *21*, 1–20. [CrossRef]
10. Rangan, R.; Watkins, A.M.; Kladwang, W.; Das, R. De novo 3D models of SARS-CoV-2 RNA elements and small-molecule-binding RNAs to guide drug discovery. *bioRxiv* **2020**. [CrossRef]
11. Rangan, R.; Zheludev, I.N.; Das, R. RNA genome conservation and secondary structure in SARS-CoV-2 and SARS-related viruses. *bioRxiv* **2020**. [CrossRef]

12. Andrews, R.J.; Peterson, J.M.; Haniff, H.F.; Chen, J.; Williams, C.; Greffe, M.; Disney, M.D.; Moss, W.N. An in silico map of the SARS-CoV-2 RNA Structurome. *bioRxiv* **2020**. [CrossRef]
13. Cullen, B.R. Five questions about viruses and microRNAs. *PLoS Pathog.* **2010**, *6*. [CrossRef] [PubMed]
14. Leon-Icaza, S.A.; Zeng, M.; Rosas-Taraco, A.G. microRNAs in viral acute respiratory infections: Immune regulation, biomarkers, therapy, and vaccines. *ExRNA* **2019**, *1*, 1. [CrossRef]
15. Pfeffer, S.; Voinnet, O. Viruses, microRNAs and cancer. *Oncogene* **2006**, *25*, 6211–6219. [CrossRef]
16. Kincaid, R.P.; Burke, J.M.; Sullivan, C.S. RNA virus microRNA that mimics a B-cell oncomiR. *Proc. Natl. Acad. Sci. USA* **2012**, *109*, 3077–3082. [CrossRef]
17. Ha, M.; Pang, M.; Agarwal, V.; Chen, Z.J. Interspecies regulation of microRNAs and their targets. *Biochim. Biophys. Acta (BBA) Gene Regul. Mech.* **2008**, *1779*, 735–742. [CrossRef]
18. Cullen, B.R. Viruses and microRNAs. *Nat. Genet.* **2006**, *38*, S25–S30. [CrossRef]
19. Mahajan, V.S.; Drake, A.; Chen, J. Virus-specific host miRNAs: Antiviral defenses or promoters of persistent infection? *Trends Immunol.* **2009**, *30*, 1–7. [CrossRef]
20. Linsen, S.E.; Tops, B.B.; Cuppen, E. miRNAs: Small changes, widespread effects. *Cell Res.* **2008**, *18*, 1157–1159. [CrossRef]
21. Lai, F.W.; Stephenson, K.B.; Mahony, J.; Lichty, B.D. Human coronavirus OC43 nucleocapsid protein binds microRNA 9 and potentiates NF-κB activation. *J. Virol.* **2014**, *88*, 54–65. [CrossRef] [PubMed]
22. Mallick, B.; Ghosh, Z.; Chakrabarti, J. MicroRNome analysis unravels the molecular basis of SARS infection in bronchoalveolar stem cells. *PLoS ONE* **2009**, *4*. [CrossRef] [PubMed]
23. Rakhmetullina, A.; Ivashchenko, A.; Akimniyazova, A.; Aisina, D.; Pyrkova, A. The miRNA Complexes Against Coronaviruses COVID-19, SARS-CoV, And MERS-CoV. *Preprint* **2020**. [CrossRef]
24. Ivashchenko, A.; Rakhmetullina, A.; Aisina, D. How miRNAs can protect humans from coronaviruses COVID-19, SARS-CoV, and MERS-CoV. *Preprint* **2020**. [CrossRef]
25. Morales, L.; Oliveros, J.C.; Fernandez-Delgado, R.; Robert tenOever, B.; Enjuanes, L.; Sola, I. SARS-CoV-encoded small RNAs contribute to infection-associated lung pathology. *Cell Host Microbe* **2017**, *21*, 344–355. [CrossRef]
26. Demirci, M.D.S.; Adan, A. Computational analysis of microRNA-mediated interactions in SARS-CoV-2 infection. *Peerj* **2020**, *8*, e9369. [CrossRef]
27. Liu, Z.; Wang, J.; Xu, Y.; Guo, M.; Mi, K.; Xu, R.; Pei, Y.; Zhang, Q.; Luan, X.; Hu, Z. Implications of the virus-encoded miRNA and host miRNA in the pathogenicity of SARS-CoV-2. *arXiv* **2020**, arXiv:2004.04874.
28. Dubois, J.; Terrier, O.; Rosa-Calatrava, M. Influenza viruses and mRNA splicing: Doing more with less. *MBio* **2014**, *5*, e00070-14. [CrossRef]
29. Hardy, W.R.; Sandri-Goldin, R. Herpes simplex virus inhibits host cell splicing, and regulatory protein ICP27 is required for this effect. *J. Virol.* **1994**, *68*, 7790–7799. [CrossRef]
30. Purcell, D.; Martin, M.A. Alternative splicing of human immunodeficiency virus type 1 mRNA modulates viral protein expression, replication, and infectivity. *J. Virol.* **1993**, *67*, 6365–6378. [CrossRef]
31. Schneider, P.A.; Schneemann, A.; Lipkin, W.I. RNA splicing in Borna disease virus, a nonsegmented, negative-strand RNA virus. *J. Virol.* **1994**, *68*, 5007–5012. [CrossRef] [PubMed]
32. Liu, Y.-C.; Kuo, R.-L.; Lin, J.-Y.; Huang, P.-N.; Huang, Y.; Liu, H.; Arnold, J.J.; Chen, S.-J.; Wang, R.Y.-L.; Cameron, C.E. Cytoplasmic viral RNA-dependent RNA polymerase disrupts the intracellular splicing machinery by entering the nucleus and interfering with Prp8. *PLoS Pathog.* **2014**, *10*, e1004119. [CrossRef] [PubMed]
33. Lai, M.; Baric, R.S.; Brayton, P.R.; Stohlman, S.A. Characterization of leader RNA sequences on the virion and mRNAs of mouse hepatitis virus, a cytoplasmic RNA virus. *Proc. Natl. Acad. Sci. USA* **1984**, *81*, 3626–3630. [CrossRef] [PubMed]
34. Kim, D.; Lee, J.-Y.; Yang, J.-S.; Kim, J.W.; Kim, V.N.; Chang, H. The architecture of SARS-CoV-2 transcriptome. *Cell* **2020**, *181*, 914–921.e10. [CrossRef]
35. Barnes, D.; Kunitomi, M.; Vignuzzi, M.; Saksela, K.; Andino, R. Harnessing endogenous miRNAs to control virus tissue tropism as a strategy for developing attenuated virus vaccines. *Cell Host Microbe* **2008**, *4*, 239–248. [CrossRef]
36. Kelly, E.J.; Hadac, E.M.; Greiner, S.; Russell, S.J. Engineering microRNA responsiveness to decrease virus pathogenicity. *Nat. Med.* **2008**, *14*, 1278–1283. [CrossRef]

37. Langlois, R.A.; Albrecht, R.A.; Kimble, B.; Sutton, T.; Shapiro, J.S.; Finch, C.; Angel, M.; Chua, M.A.; Gonzalez-Reiche, A.S.; Xu, K. MicroRNA-based strategy to mitigate the risk of gain-of-function influenza studies. *Nat. Biotechnol.* **2013**, *31*, 844–847. [CrossRef]
38. Perez, J.T.; Pham, A.M.; Lorini, M.H.; Chua, M.A.; Steel, J. MicroRNA-mediated species-specific attenuation of influenza A virus. *Nat. Biotechnol.* **2009**, *27*, 572–576. [CrossRef]
39. Pachetti, M.; Marini, B.; Benedetti, F.; Giudici, F.; Mauro, E.; Storici, P.; Masciovecchio, C.; Angeletti, S.; Ciccozzi, M.; Gallo, R.C. Emerging SARS-CoV-2 mutation hot spots include a novel RNA-dependent-RNA polymerase variant. *J. Transl. Med.* **2020**, *18*, 179. [CrossRef]
40. Li, X.; Giorgi, E.E.; Marichannegowda, M.H.; Foley, B.; Xiao, C.; Kong, X.-P.; Chen, Y.; Gnanakaran, S.; Korber, B.; Gao, F. Emergence of SARS-CoV-2 through recombination and strong purifying selection. *Sci. Adv.* **2020**, *6*, eabb9153. [CrossRef]
41. MacLean, O.A.; Lytras, S.; Singer, J.B.; Weaver, S.; Pond, S.L.K.; Robertson, D.L. Evidence of significant natural selection in the evolution of SARS-CoV-2 in bats, not humans. *bioRxiv* **2020**. [CrossRef]
42. Khrustalev, V.V.; Giri, R.; Khrustaleva, T.A.; Kapuganti, S.K.; Stojarov, A.N.; Poboinev, V.V. Translation-associated mutational U-pressure in the first ORF of SARS-CoV-2 and other coronaviruses. *bioRxiv* **2020**. [CrossRef]
43. Farkas, C.; Fuentes-Villalobos, F.; Garrido, J.L.; Haigh, J.J.; Barría, M.I. Insights on early mutational events in SARS-CoV-2 virus reveal founder effects across geographical regions. *bioRxiv* **2020**, *8*, e9255.
44. Lange, S.J.; Maticzka, D.; Möhl, M.; Gagnon, J.N.; Brown, C.M.; Backofen, R. Global or local? Predicting secondary structure and accessibility in mRNAs. *Nucleic Acids Res.* **2012**, *40*, 5215–5226. [CrossRef]
45. Bernhart, S.H.; Mückstein, U.; Hofacker, I.L. RNA Accessibility in cubic time. *Algorithms Mol. Biol.* **2011**, *6*, 3. [CrossRef] [PubMed]
46. Robertson, M.P.; Igel, H.; Baertsch, R.; Haussler, D.; Ares, M., Jr.; Scott, W.G. The structure of a rigorously conserved RNA element within the SARS virus genome. *PLoS Biol.* **2004**, *3*, e5. [CrossRef]
47. Li, L.; Kang, H.; Liu, P.; Makkinje, N.; Williamson, S.T.; Leibowitz, J.L.; Giedroc, D.P. Structural lability in stem–loop 1 drives a 5′ UTR–3′ UTR interaction in coronavirus replication. *J. Mol. Biol.* **2008**, *377*, 790–803. [CrossRef] [PubMed]
48. Yang, D.; Leibowitz, J.L. The structure and functions of coronavirus genomic 3′ and 5′ ends. *Virus Res.* **2015**, *206*, 120–133. [CrossRef]
49. Gordon, D.E.; Jang, G.M.; Bouhaddou, M.; Xu, J.; Obernier, K.; O'meara, M.J.; Guo, J.Z.; Swaney, D.L.; Tummino, T.A.; Huttenhain, R. A SARS-CoV-2-human protein-protein interaction map reveals drug targets and potential drug-repurposing. *bioRxiv* **2020**. [CrossRef]
50. Khan, M.A.-A.-K.; Islam, A.B. SARS-CoV-2 proteins exploit host's genetic and epigenetic mediators for the annexation of key host signaling pathways that confers its immune evasion and disease pathophysiology. *bioRxiv* **2020**. [CrossRef]
51. Kleinman, C.L.; Adoue, V.; Majewski, J. RNA editing of protein sequences: A rare event in human transcriptomes. *Rna* **2012**, *18*, 1586–1596. [CrossRef] [PubMed]
52. Schulte, C.; Molz, S.; Appelbaum, S.; Karakas, M.; Ojeda, F.; Lau, D.M.; Hartmann, T.; Lackner, K.J.; Westermann, D.; Schnabel, R.B. miRNA-197 and miRNA-223 predict cardiovascular death in a cohort of patients with symptomatic coronary artery disease. *PLoS ONE* **2015**, *10*. [CrossRef]
53. Liu, W.; Zheng, J.; Dong, J.; Bai, R.; Song, D.; Ma, X.; Zhao, L.; Yao, Y.; Zhang, H.; Liu, T. Association of miR-197-5p, a circulating biomarker for heart failure, with myocardial fibrosis and adverse cardiovascular events among patients with stage C or D heart failure. *Cardiology* **2018**, *141*, 212–225. [CrossRef] [PubMed]
54. Gupta, S.K.; Bang, C.; Thum, T. Circulating microRNAs as biomarkers and potential paracrine mediators of cardiovascular disease. *Circ. Cardiovasc. Genet.* **2010**, *3*, 484–488. [CrossRef]
55. Xu, Z.; Shi, L.; Wang, Y.; Zhang, J.; Huang, L.; Zhang, C.; Liu, S.; Zhao, P.; Liu, H.; Zhu, L. Pathological findings of COVID-19 associated with acute respiratory distress syndrome. *Lancet Respir. Med.* **2020**, *8*, 420–422. [CrossRef]
56. Korber, B.; Fischer, W.M.; Gnanakaran, S.; Yoon, H.; Theiler, J.; Abfalterer, W.; Hengartner, N.; Giorgi, E.E.; Bhattacharya, T.; Foley, B.; et al. Tracking changes in SARS-CoV-2 Spike: evidence that D614G increases infectivity of the COVID-19 virus. *Cell* **2020**, *20*, 30820–308025. [CrossRef]

57. Yang, Z.; Li, J.; Feng, G.; Wang, Y.; Yang, G.; Liu, Y.; Zhang, S.; Feng, J.; Zhang, X. Hepatitis B virus X protein enhances hepatocarcinogenesis by depressing the targeting of NUSAP1 mRNA by miR-18b. *Cancer Biol. Med.* **2019**, *16*, 276. [CrossRef] [PubMed]
58. Duy, J.; Koehler, J.W.; Honko, A.N.; Schoepp, R.J.; Wauquier, N.; Gonzalez, J.-P.; Pitt, M.L.; Mucker, E.M.; Johnson, J.C.; O'Hearn, A. Circulating microRNA profiles of Ebola virus infection. *Sci. Rep.* **2016**, *6*, 24496. [CrossRef]
59. Condorelli, G.; Latronico, M.V.; Dorn, G.W. microRNAs in heart disease: Putative novel therapeutic targets? *Eur. Heart J.* **2010**, *31*, 649–658. [CrossRef]
60. Luo, P.; Zhang, W. MicroRNA-18b* induces apoptosis in cardiomyocytes through targeting Topoisomerase 1 (TOP1). *Int. J. Clin. Exp. Med.* **2017**, *10*, 6742–6748.
61. Tijsen, A.J.; Creemers, E.E.; Moerland, P.D.; de Windt, L.J.; van der Wal, A.C.; Kok, W.E.; Pinto, Y.M. MiR423-5p as a circulating biomarker for heart failure. *Circ. Res.* **2010**, *106*, 1035. [CrossRef] [PubMed]
62. Fu, X.; Tan, D.; Hou, Z.; Hu, Z.; Liu, G.; Ouyang, Y.; Liu, F. The effect of miR-338-3p on HBx deletion-mutant (HBx-d382) mediated liver-cell proliferation through CyclinD1 regulation. *PLoS ONE* **2012**, *7*, e43204. [CrossRef] [PubMed]
63. Liang, Y.; Xu, X.; Wang, T.; Li, Y.; You, W.; Fu, J.; Liu, Y.; Jin, S.; Ji, Q.; Zhao, W. The EGFR/miR-338-3p/EYA2 axis controls breast tumor growth and lung metastasis. *Cell Death Dis.* **2017**, *8*, e2928. [CrossRef] [PubMed]
64. Li, P.; Chen, X.; Su, L.; Li, C.; Zhi, Q.; Yu, B.; Sheng, H.; Wang, J.; Feng, R.; Cai, Q. Epigenetic silencing of miR-338-3p contributes to tumorigenicity in gastric cancer by targeting SSX2IP. *PLoS ONE* **2013**, *8*. [CrossRef] [PubMed]
65. Winther, T.N.; Bang-Berthelsen, C.H.; Heiberg, I.L.; Pociot, F.; Hogh, B. Differential plasma microRNA profiles in HBeAg positive and HBeAg negative children with chronic hepatitis B. *PLoS ONE* **2013**, *8*. [CrossRef] [PubMed]
66. Yu, K.; Shi, G.; Li, N. The function of MicroRNA in hepatitis B virus-related liver diseases: From Dim to Bright. *Ann. Hepatol.* **2015**, *14*, 450–456. [CrossRef]
67. Hasan, M.; McLean, E.; Bagasra, O. A computational analysis to construct a potential post-Exposure therapy against pox epidemic using miRNAs in silico. *J. Bioterror Biodef* **2016**, *7*, 2. [CrossRef]
68. Chang, T.-H.; Huang, H.-Y.; Hsu, J.B.-K.; Weng, S.-L.; Horng, J.-T.; Huang, H.-D. An enhanced computational platform for investigating the roles of regulatory RNA and for identifying functional RNA motifs. *Proc. BMC Bioinf.* **2013**, *14*, 1–8. [CrossRef]
69. Desmet, F.-O.; Hamroun, D.; Lalande, M.; Collod-Béroud, G.; Claustres, M.; Béroud, C. Human Splicing Finder: An online bioinformatics tool to predict splicing signals. *Nucleic Acids Res.* **2009**, *37*, e67. [CrossRef]
70. Hiller, M.; Zhang, Z.; Backofen, R.; Stamm, S. Pre-mRNA secondary structures influence exon recognition. *PLoS Genet.* **2007**, *3*, e204. [CrossRef]
71. Raden, M.; Ali, S.M.; Alkhnbashi, O.S.; Busch, A.; Costa, F.; Davis, J.A.; Eggenhofer, F.; Gelhausen, R.; Georg, J.; Heyne, S. Freiburg RNA tools: A central online resource for RNA-focused research and teaching. *Nucleic Acids Res.* **2018**, *46*, W25–W29. [CrossRef]
72. Sironi, M.; Menozzi, G.; Riva, L.; Cagliani, R.; Comi, G.P.; Bresolin, N.; Giorda, R.; Pozzoli, U. Silencer elements as possible inhibitors of pseudoexon splicing. *Nucleic Acids Res.* **2004**, *32*, 1783–1791. [CrossRef]
73. Xia, X. Extreme genomic CpG deficiency in SARS-CoV-2 and evasion of host antiviral defense. *Mol. Biol. Evol.* **2020**. [CrossRef]
74. Chen, L.; Li, C.; Peng, Z.; Zhao, J.; Gong, G.; Tan, D. miR-197 expression in peripheral blood mononuclear cells from hepatitis B virus-infected patients. *Gut Liver* **2013**, *7*, 335. [CrossRef]
75. Tang, W.-F.; Huang, R.-T.; Chien, K.-Y.; Huang, J.-Y.; Lau, K.-S.; Jheng, J.-R.; Chiu, C.-H.; Wu, T.-Y.; Chen, C.-Y.; Horng, J.-T. Host microRNA miR-197 plays a negative regulatory role in the enterovirus 71 infectious cycle by targeting the RAN protein. *J. Virol.* **2016**, *90*, 1424–1438. [CrossRef]
76. Wang, H.; Su, X.; Yang, M.; Chen, T.; Hou, J.; Li, N.; Cao, X. Reciprocal control of miR-197 and IL-6/STAT3 pathway reveals miR-197 as potential therapeutic target for hepatocellular carcinoma. *Oncoimmunology* **2015**, *4*, e1031440. [CrossRef]
77. Peng, F.; Loo, J.F.C.; Kong, S.K.; Li, B.; Gu, D. Identification of serum MicroRNAs as diagnostic biomarkers for influenza H7N9 infection. *Virology Reports* **2017**, *7*, 1–8. [CrossRef]
78. Nishikura, K. Functions and regulation of RNA editing by ADAR deaminases. *Ann. Rev. Biochem.* **2010**, *79*, 321–349. [CrossRef]

79. Zhang, L.; Yang, C.-S.; Varelas, X.; Monti, S. Altered RNA editing in 3′ UTR perturbs microRNA-mediated regulation of oncogenes and tumor-suppressors. *Sci. Rep.* **2016**, *6*, 1–13. [CrossRef]
80. Lim, J.; Byun, J.; Guk, K.; Hwang, S.G.; Bae, P.K.; Jung, J.; Kang, T.; Lim, E.-K. Highly Sensitive in Vitro Diagnostic System of Pandemic Influenza A (H1N1) Virus Infection with Specific MicroRNA as a Biomarker. *ACS Omega* **2019**, *4*, 14560–14568. [CrossRef]
81. Zhu, Z.; Qi, Y.; Fan, H.; Cui, L.; Shi, Z. Systematic identification and bioinformatic analysis of microRNAs in response to infections of coxsackievirus A16 and enterovirus 71. *BioMed Res. Int.* **2016**, *2016*. [CrossRef]
82. Arslan, S.; Engin, A.; Aydemir, E.I.; Sahin, N.O.; Bayyurt, B.; Sari, I.; Cosgun, Y.; Bakir, M. Identification of potential microRNA markers related to Crimean-Congo hemorrhagic fever disease. *J. Cell. Biochem.* **2019**, *120*, 15506–15517. [CrossRef]
83. Dong, D.-L.; Yang, B.-F. Role of microRNAs in cardiac hypertrophy, myocardial fibrosis and heart failure. *Acta Pharm. Sin. B* **2011**, *1*, 1–7. [CrossRef]
84. Wang, X. Composition of seed sequence is a major determinant of microRNA targeting patterns. *Bioinformatics* **2014**, *30*, 1377–1383. [CrossRef]
85. Carmel, I.; Shomron, N.; Heifetz, Y. Does base-pairing strength play a role in microRNA repression? *Rna* **2012**, *18*, 1947–1956. [CrossRef]
86. Rolle, K.; Piwecka, M.; Belter, A.; Wawrzyniak, D.; Jeleniewicz, J.; Barciszewska, M.Z.; Barciszewski, J. The sequence and structure determine the function of mature human miRNAs. *PLoS ONE* **2016**, *11*. [CrossRef]
87. O'shea, T.J.; Cryan, P.M.; Cunningham, A.A.; Fooks, A.R.; Hayman, D.T.; Luis, A.D.; Peel, A.J.; Plowright, R.K.; Wood, J.L. Bat flight and zoonotic viruses. *Emerg. Infect. Dis.* **2014**, *20*, 741. [CrossRef]
88. Broughton, J.P.; Lovci, M.T.; Huang, J.L.; Yeo, G.W.; Pasquinelli, A.E. Pairing beyond the seed supports microRNA targeting specificity. *Mol. Cell* **2016**, *64*, 320–333. [CrossRef]
89. Zhang, K.; Zhang, X.; Cai, Z.; Zhou, J.; Cao, R.; Zhao, Y.; Chen, Z.; Wang, D.; Ruan, W.; Zhao, Q. A novel class of microRNA-recognition elements that function only within open reading frames. *Nat. Struct. Mol. Biol.* **2018**, *25*, 1019–1027. [CrossRef]
90. Apcher, S.; Daskalogianni, C.; Lejeune, F.; Manoury, B.; Imhoos, G.; Heslop, L.; Fåhraeus, R. Major source of antigenic peptides for the MHC class I pathway is produced during the pioneer round of mRNA translation. *Proc. Natl. Acad. Sci. USA* **2011**, *108*, 11572–11577. [CrossRef]
91. Granados, D.P.; Yahyaoui, W.; Laumont, C.M.; Daouda, T.; Muratore-Schroeder, T.L.; Côté, C.; Laverdure, J.-P.; Lemieux, S.; Thibault, P.; Perreault, C. MHC I–associated peptides preferentially derive from transcripts bearing miRNA response elements. *Blood J. Am. Soc. Hematol.* **2012**, *119*, e181–e191. [CrossRef] [PubMed]
92. Wei, J.; Yewdell, J.W. Flu DRiPs in MHC Class I Immunosurveillance. *Virol. Sin.* **2019**, *34*, 162–167. [CrossRef]
93. Korber, B. Computational analysis of HIV molecular sequences. *HIV Signat. Seq. Var. Anal.* **2000**, *55*, 55–72.
94. Zuker, M.; Stiegler, P. Optimal computer folding of large RNA sequences using thermodynamics and auxiliary information. *Nucleic Acids Res.* **1981**, *9*, 133–148. [CrossRef] [PubMed]
95. Ding, Y.; Chan, C.Y.; Lawrence, C.E. RNA secondary structure prediction by centroids in a Boltzmann weighted ensemble. *Rna* **2005**, *11*, 1157–1166. [CrossRef] [PubMed]
96. Bernhart, S.H.; Hofacker, I.L.; Will, S.; Gruber, A.R.; Stadler, P.F. RNAalifold: Improved consensus structure prediction for RNA alignments. *BMC Bioinf.* **2008**, *9*, 474. [CrossRef]
97. Sharma, Y.; Miladi, M.; Dukare, S.; Boulay, K.; Caudron-Herger, M.; Groß, M.; Backofen, R.; Diederichs, S. A pan-cancer analysis of synonymous mutations. *Nat. Commun.* **2019**, *10*, 1–14.
98. Sabarinathan, R.; Tafer, H.; Seemann, S.E.; Hofacker, I.L.; Stadler, P.F.; Gorodkin, J. RNA snp: Efficient detection of local RNA secondary structure changes induced by SNP s. *Hum. Mutat.* **2013**, *34*, 546–556. [CrossRef] [PubMed]
99. Chen, Y.; Wang, X. miRDB: An online database for prediction of functional microRNA targets. *Nucleic Acids Res.* **2020**, *48*, D127–D131. [CrossRef]
100. Muus, C.; Luecken, M.D.; Eraslan, G.; Waghray, A.; Heimberg, G.; Sikkema, L.; Kobayashi, Y.; Vaishnav, E.D.; Subramanian, A.; Smilie, C. Integrated analyses of single-cell atlases reveal age, gender, and smoking status associations with cell type-specific expression of mediators of SARS-CoV-2 viral entry and highlights inflammatory programs in putative target cells. *bioRxiv* **2020**. [CrossRef]
101. Puelles, V.G.; Lütgehetmann, M.; Lindenmeyer, M.T.; Sperhake, J.P.; Wong, M.N.; Allweiss, L.; Chilla, S.; Heinemann, A.; Wanner, N.; Liu, S.; et al. Multiorgan and Renal Tropism of SARS-CoV-2. *N. Engl. J. Med.* **2020**. [CrossRef] [PubMed]

102. Ludwig, N.; Leidinger, P.; Becker, K.; Backes, C.; Fehlmann, T.; Pallasch, C.; Rheinheimer, S.; Meder, B.; Stähler, C.; Meese, E. Distribution of miRNA expression across human tissues. *Nucleic Acids Res.* **2016**, *44*, 3865–3877. [CrossRef] [PubMed]
103. Palmieri, V.; Backes, C.; Ludwig, N.; Fehlmann, T.; Kern, F.; Meese, E.; Keller, A. IMOTA: An interactive multi-omics tissue atlas for the analysis of human miRNA–target interactions. *Nucleic Acids Res.* **2018**, *46*, D770–D775. [CrossRef]
104. Santos, A.; Tsafou, K.; Stolte, C.; Pletscher-Frankild, S.; O'Donoghue, S.I.; Jensen, L.J. Comprehensive comparison of large-scale tissue expression datasets. *PeerJ* **2015**, *3*, e1054. [CrossRef] [PubMed]
105. Mann, M.; Wright, P.R.; Backofen, R. IntaRNA 2.0: Enhanced and customizable prediction of RNA–RNA interactions. *Nucleic Acids Res.* **2017**, *45*, W435–W439. [CrossRef]

Chapter VII:

Discussion

CAR T cell therapy has revolutionized cancer treatment, but has also provided an opportunity for treating chronic viral infections such as HIV, HBV, and HCV (1, 2). Despite the profound outcomes in the treatment of hematological malignancies, CAR T cell therapy for solid tumours has not been successful. Hostile condition of TME, low tumour infiltration, lack of persistence, and absence of memory CAR T cell formation are the main obstacles ahead of CAR T cell therapy for solid tumours. This study aimed to improve Her2-CAR T cell persistence and T_M development.

Mitochondria play a central role in both T cell survival and T_M development. Interaction of CD95:CD95L initiates AICD, which leads to depolarization of the mitochondria outer membrane resulting in downstream events in apoptosis (3). On the other hand, the mitochondrial transition from fission to fusion is an essential step in T_M development (4, 5). Facilitating mitochondrial fusion in T cells enhances T_M differentiation (4, 5).

Recently, several studies suggested that AICD induced by the CD95 pathway is the main reason for CAR T cell low persistency *in vivo*, and blockage of this signaling enhanced CAR T cell survival (6-9). For instance, inhibition of CD95 or CD95L via RNAi increases the CD171-CAR T cell persistence (7). Interestingly, expanding CAR T cells under 46 ng/mL of CD95L enhanced T_M differentiation (10).

To enhance persistence and memory, we selected Mcl-1 to overexpress in CAR T cells. Mcl-1 blocks the AICD by binding and sequestering Bak and Bax at OMM (11). Mcl-1 also inhibits the mitochondrial fission by directly binding to Drp-1 (12). Mcl-1S that localizes at IMM promotes mitochondrial fusion through interacting with OPA-1, MFN1, and MFN2. Mcl-1S is required for the formation of typical IMM structures, OXPHOS metabolism, and arrangements of ETC and ATPase complexes (12-15).

We also decided to downregulate TCAIM to enhance the mitochondrial fusion and thereby improve CAR T cell memory differentiation. The TCAIM protein localises exclusively to mitochondria, and only a few studies have been carried out on the TCAIM gene or protein. TCAIM is highly expressed in T_N, T_{reg}, while its expression is being downregulated in T_M cells (16). T cells upregulating TCAIM have decreased proliferation, lower mitochondrial membrane potential ($\Delta\Psi m$), and reduced number of T_N and T_M phenotypes (17-19).

We decided to downregulate TCAIM in our Her2-CAR T cells using a miRNA. Among all potential miRNA, we chose miR429 because it also targets MFF and TET-2 (Figure 5.3). MFF enhances mitochondrial fission by recruiting Drp1 at OMM (20), and the downregulation of MFF by miR27 increased the mitochondrial fusion in human cells (21). Downregulation of TET-2 has been associated with long-term CAR T cell persistence and complete remission (22, 23). Further studies showed that inhibition of TET-2 improves the CAR T cell therapy via epigenetic changes that encourage T_M differentiation (23, 24).

Mcl-1 has been classified as oncogene due to its contribution to stopping apoptosis and enhancing tumour cell survival (13, 25). Overexpressing Mcl-1 (or any GOI) raises concerns about developing cancerous CAR T cells. Therefore, our first aim was to induce the endogenous level of Mcl-1. We tested eight small activating RNA (saRNA) targeting different regions of the Mcl-1 promoter, but none of them was able to induce Mcl-1. Further, we noticed an uncharacterized lncRNA (LOC107985203) is transcribing from the opposite direction of the Mcl-1 promoter. Often the antisense (AS) transcripts have a negative role in the regulation of a gene (26). Using gain-of-function and loss-of-function experiments, we verified LOC107985203 lncRNA (named mcl1-AS1) expresses from Mcl-1 promoter and negatively modulates Mcl-1 expression (27). However, due to the late manifestation of gene regulation (at 48 - 72 hours) that was seen following mcl1-AS1 inhibition, it was not applicable for us to use this strategy to Mcl-1 expression.

The next strategy was the controlled expression of Mcl-1 using the Tet-On system. Tet-On system is the most commonly used drug inducible system (28). The most significant weakness of this system is high background expression in the absence of doxycycline (28). We used several approaches to improve the Tet-On system, including gene replacement, codon-optimisation of rt-TA, using G72V-rtTA, removing cryptic splice sites within rt-TA, creating an autoregulatory Tet-On system, and manipulating regulatory elements in TCE minimal promoter (29). As we have shown in chapter III, our final optimised construct showed high inducibility and a very low background expression compared to the original construct (29). However, due to the low transfection efficiency of SB system in primary T cells and lack of aAPC at the time for expansion of T cells, we decided to create an inducible LV system. This system had several drawbacks. The lack of inducibility in low doxycycline concentration and low transduction efficiency

were the major weaknesses (Figure 5.2). Therefore, we decided to use a constitutive system to see the effects of Mcl-1 and miR429 overexpression in CAR T cells. We decided to address the safety concerns later since we still did not know that Mcl-1 and miR429 upregulation will benefit the CAR T cell therapy.

The primary step to express a GOI in a constitutive system is the promoter choice. Promoters vary in terms of lengths, strength, TF binding sites, their effect on LV titer and transduction. Hence in a series of experiments, we tested the strength of four commonly used promoters, EF-1, CMV, RPBSA, and hPGK, in running short and long transcripts. EF-1 showed to be the best promoter in running short and long RNA in T cells. As a result, we chose EF-1 to run the GFP-P2A-Her2CAR and hPGK to transcribe Mcl-1 or miR429.

To the best of our knowledge, this is the first report of the downregulation of TCAIM, TET-2, and MFF by miR429. Overexpressing miR429 increased the susceptibility of CAR T cells to AICD (Figure 5.7), probably due to the Bcl-2 downregulation by miR429 (30). Her2-CAR T cells upregulating miR429 had ~2.8-5% lower phenotypes similar to T_{reg} and T_{EMRA} cells in both $CD4^+$ and $CD8^+$ CAR T cells. Also, T_{SCM} had 2.5%, and T_{CM} had 5.6% more in $CD4^+$ Her2CAR T cells (Figure 5.9 and 5.10). It is well-known that miRNA targets are cell- and context-dependent. Usually, genes have multiple isoforms with distinct 3′UTR due to alternative splicing or alternative polyadenylation (31, 32). Consequently, overexpression of a miRNA does not always result in target inhibition. For example, miR429 downregulates ZEB1 and ZEB2 in CD4 T cells, whereas in CD8 T cells, it only inhibits ZEB2. Interestingly, TCAIM has six different variants with unique 3′ UTR. Thus, miR429 may downregulate TCAIM only in CD4, not CD8 T cells. However, the expression of these variants has not been shown in CD4 or CD8 T cells.

As noted before in the introduction, Mcl-1 has a central role in the mitochondrial dynamic. Expression of Mcl-1 is vital for FAO and OXPHOS metabolism, formation of crista, assembly of ETC, and ATPase complexes, and mitochondrial fusion (12-14). Overexpression of Mcl-1 in T cells promotes $CD8^+$ T_M development and survival in viral infection (33, 34). Mcl-1 also is necessary for maintaining stemness in human pluripotent stem cells, and depletion of Mcl-1 promotes stem cell differentiation (35).

In line with previous reports, overexpression of Mcl-1 enhanced the T_M development in Her2-CAR T cells (Figure 5.10). In this study, both CD^+ and $CD8^+$ CAR T cells overexpressed Mcl-1 showed an increase in phenotypes similar to T_{SCM} and T_{CM} numbers (Figure 5.10). Expansion of CAR T cells under 46 ng/mL of CD95L enhanced the number of T_{SCM} and augmented T_{CM} development. These results confirm the previous report that CD95L treatment enhances T_{SCM} development (10, 36). Single-cell serial transfer of T_M subsets showed that T_{CM} and T_{SCM} were able to reconstitute the murine immune system, while an infusion of 100-fold T_{EM} cells in mice failed to rebuild the host immune system (37, 38). In another study, the T_{SCM} number was unchanged for decades, whereas the population of T_{CM} and T_{EM} were reduced by 10 to 100 fold, respectively (39). T_{SCM} number was constant in patients receiving engineered T cells decades after ACT (40, 41). Remarkably, vaccination with yellow fever created $CD8^+$ T_{SCM} cells that remained unchanged after 25 years (42).

Several differentiation models have been proposed for the development of T_M subsets from T_N cells (Figure 6.1) (43, 44). The high frequency of T_{EM} cells at day-10 following an increase in the number of T_{CM} at day-21 suggests that Mcl-1 overexpression promotes phenotypes similar to T_{CM} differentiation via the $T_N \rightarrow T_{EEF} \rightarrow T_{EM} \rightarrow T_{CM}$ route. However, cell tracking experiments must be done to verify this theory. Although our study cannot provide a mechanism for the Mcl-1 role in memory CAR T cell development, an increase in mitochondrial mass and mtDNA suggest that Mcl-1 probably enhance the mitochondrial fusion. It should be noted that T_M subsets identified in this study are more likely intermediate phenotypes that resemble different T_M subsets, rather than distinct populations.

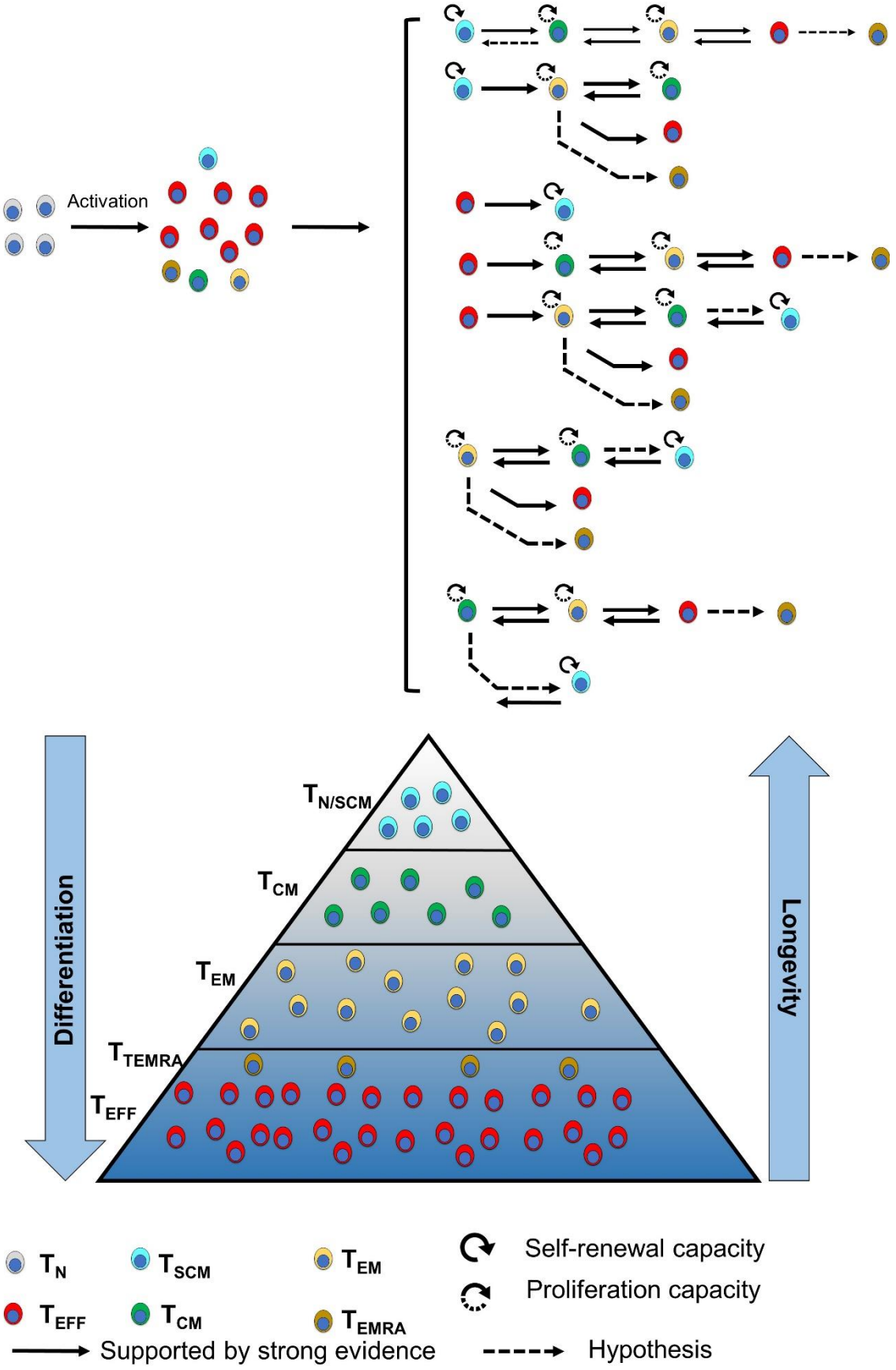
Activation
Differentiation
Longevity
$T_{N/SCM}$
T_{CM}
T_{EM}
T_{TEMRA}
T_{EFF}
T_N
T_{SCM}
T_{EM}
T_{EFF}
T_{CM}
T_{EMRA}
Self-renewal capacity
Proliferation capacity
Supported by strong evidence
Hypothesis

Figure 6.1. Multiple paths for T_N development to T_M subsets after antigen encounter. T_N to T_M development starts simultaneously with T_{EFF} development. In addition, T_M cells have been shown to develop from T_{EFF} cells. T_M subsets have differences in proliferation and multipotency capacity.

Several CAR T cell clinical trials revealed parameters associated with successful therapy, such as the presence of T_{SCM} CAR T cells ($CD45RO^-CD27^+$) or a CD4:CD8 ratio higher than 1 at the time of infusion. Strikingly, overexpression of Mcl-1 increased the number of $CD45RO^-CD27^+$ CAR T cells and CD4:CD8 ratio (Figure 5.12). The rise in CD4 T cells after Mcl-1 overexpression could be due to the selective survival of CD4 T cells over CD8 T cells. However, this has not been reported yet that the anti-apoptotic function of Mcl-1 is only restricted in CD4 T cells and not CD8 T cells. On the contrary, studies have shown that Mcl-1 protects both CD4 and CD8 T cells against AICD (45-47). Another theory is overexpression of Mcl-1 promotes CD8 to CD4 conversion. Recently, CD8 ↔ CD4 conversions have been shown to occur due to the high plasticity of T cells (48-51). This process is similar to the transdifferentiation in which cells from a lineage can be converted to another lineage (52). Thus, forced expression of Mcl-1 may enhance T_M development and CD8 to CD4 conversion.

Future direction

1. Imaging and metabolically analysis of CAR T cells in order to reveal Mcl-1 contribution in mitochondrial fusion. We will swap the GFP in our construct with GFP-targeted mitochondria for confocal imaging to observe the fusion process. Also, using the Seahorse XF kit, we will investigate the metabolism of CAR T cells.

2. Following transduction, we will separate $CD4^+$ and $CD8^+$ CAR T cells (FACS cell sorting) and observe if the increase in $CD4^+$ cells is the result of the $CD8^+$ conversion to $CD4^+$ T cells. Another approach is to transduce CD4 and CD8 T cells with different markers (e.g., GFP and RFP) if the cross-differentiation only happens in a mixed culture.

3. Besides IL-2 and IFN-γ cytokines, expanding the composition of cytokines, and surface markers analysed (e.g. 4-1BB and CD40L) would give further insights into the

phenotypic differences in T cells induced by miRNA and mitochondrial remodelling in our culture system.

4. We will sort different T_M subsets at day-21 and challenge them with antigen to see if T_{SCM} and T_{CM} cells possess polyfunctional properties such as cytotoxicity activity and IL-2, IFN-γ, Perforin, and TNF-α production.

5. For *in vivo* assays, our laboratory has already developed an NSG mice model using the MCF-7 breast cancer cell line. *In vivo* studies will be carried out to see if Mcl-1 overexpression improves survival and reduces the tumour size. We are also interested in following the longevity of the T_{SCM} population in healthy NSG mice.

6. Lastly, if the *in vitro* and *in vivo* studies provided substantial evidence that Mcl-1 overexpression enhances CAR T cell function, controlled expression or using death-switches must be considered in the CAR T cells. In our laboratory, two lab members are investigating the approaches to improve the safety of the CAR T cell therapy.

References

1. Maldini CR, Claiborne DT, Okawa K, Chen T, Dopkin DL, Shan X, et al. Dual CD4-based CAR T cells with distinct costimulatory domains mitigate HIV pathogenesis in vivo. Nature Medicine. 2020:1-12.
2. Strati P, Nastoupil LJ, Fayad LE, Samaniego F, Adkins S, Neelapu SS. Safety of CAR T-cell therapy in patients with B-cell lymphoma and chronic hepatitis B or C virus infection. Blood, The Journal of the American Society of Hematology. 2019;133(26):2800-2.
3. Hadji A, Ceppi P, Murmann AE, Brockway S, Pattanayak A, Bhinder B, et al. Death induced by CD95 or CD95 ligand elimination. Cell reports. 2014;7(1):208-22.
4. Desdín-Micó G, Soto-Heredero G, Mittelbrunn M. Mitochondrial activity in T cells. Mitochondrion. 2018;41:51-7.
5. Lanna A, Dustin ML. Mitochondrial fusion fuels T cell memory. Cell research. 2016;26(9):969-70.

6. Yamamoto TN, Lee P-H, Vodnala SK, Gurusamy D, Kishton RJ, Yu Z, et al. T cells genetically engineered to overcome death signaling enhance adoptive cancer immunotherapy. The Journal of clinical investigation. 2019;129(4).
7. Künkele A, Johnson AJ, Rolczynski LS, Chang CA, Hoglund V, Kelly-Spratt KS, et al. Functional tuning of CARs reveals signaling threshold above which CD8+ CTL antitumor potency is attenuated due to cell Fas–FasL-dependent AICD. Cancer immunology research. 2015;3(4):368-79.
8. Tschumi BO, Dumauthioz N, Marti B, Zhang L, Schneider P, Mach J-P, et al. CART cells are prone to Fas-and DR5-mediated cell death. Journal for immunotherapy of cancer. 2018;6(1):71.
9. He B, Wang L, Neuber B, Schmitt A, Kneisel N, Hoeger T, et al. Blockade of CD95/CD95L Death Signaling Enhances CAR T Cell Persistence and Antitumor Efficacy. American Society of Hematology Washington, DC; 2019.
10. Klebanoff CA, Scott CD, Leonardi AJ, Yamamoto TN, Cruz AC, Ouyang C, et al. Memory T cell–driven differentiation of naive cells impairs adoptive immunotherapy. The Journal of clinical investigation. 2016;126(1):318-34.
11. Thomas LW, Lam C, Edwards SW. Mcl-1; the molecular regulation of protein function. FEBS letters. 2010;584(14):2981-9.
12. Morciano G, Giorgi C, Balestra D, Marchi S, Perrone D, Pinotti M, et al. Mcl-1 involvement in mitochondrial dynamics is associated with apoptotic cell death. Molecular biology of the cell. 2016;27(1):20-34.
13. Perciavalle RM, Opferman JT. Delving deeper: MCL-1's contributions to normal and cancer biology. Trends in cell biology. 2013;23(1):22-9.
14. Perciavalle RM, Stewart DP, Koss B, Lynch J, Milasta S, Bathina M, et al. Anti-apoptotic MCL-1 localizes to the mitochondrial matrix and couples mitochondrial fusion to respiration. Nature cell biology. 2012;14(6):575-83.
15. Escudero S, Zaganjor E, Lee S, Mill CP, Morgan AM, Crawford EB, et al. Dynamic regulation of long-chain fatty acid oxidation by a noncanonical interaction between the MCL-1 BH3 helix and VLCAD. Molecular cell. 2018;69(5):729-43. e7.
16. Sawitzki B, Bushell A, Steger U, Jones N, Risch K, Siepert A, et al. Identification of gene markers for the prediction of allograft rejection or permanent acceptance. American Journal of Transplantation. 2007;7(5):1091-102.

17. Keeren K, Friedrich M, Gebuhr I, Philipp S, Sabat R, Sterry W, et al. Expression of tolerance associated gene-1, a mitochondrial protein inhibiting T cell activation, can be used to predict response to immune modulating therapies. The Journal of Immunology. 2009;183(6):4077-87.
18. Vogel SZ, Schlickeiser S, Jürchott K, Akyuez L, Schumann J, Appelt C, et al. TCAIM decreases T cell priming capacity of dendritic cells by inhibiting TLR-induced Ca2+ influx and IL-2 production. The Journal of Immunology. 2015;194(7):3136-46.
19. Panov I, Schlickeiser S, Vogel S, Schumann J, Schliesser U, Gossen M, et al. Transcriptional control of tolerance associated gene TCAIM is CREB, NFATc1 and C/EBPβ dependent resulting in generation of tolerogenic dendritic cells (P2152). Am Assoc Immnol; 2013.
20. Youle RJ, Van Der Bliek AM. Mitochondrial fission, fusion, and stress. Science. 2012;337(6098):1062-5.
21. Tak H, Kim J, Jayabalan AK, Lee H, Kang H, Cho D-H, et al. miR-27 regulates mitochondrial networks by directly targeting the mitochondrial fission factor. Experimental & molecular medicine. 2014;46(11):e123-e.
22. Fraietta JA, Lacey SF, Orlando EJ, Pruteanu-Malinici I, Gohil M, Lundh S, et al. Determinants of response and resistance to CD19 chimeric antigen receptor (CAR) T cell therapy of chronic lymphocytic leukemia. Nature medicine. 2018;24(5):563-71.
23. Fraietta JA, Nobles CL, Sammons MA, Lundh S, Carty SA, Reich TJ, et al. Disruption of TET2 promotes the therapeutic efficacy of CD19-targeted T cells. Nature. 2018;558(7709):307-12.
24. Ladle BH, Li K-P, Phillips MJ, Pucsek AB, Haile A, Powell JD, et al. De novo DNA methylation by DNA methyltransferase 3a controls early effector CD8+ T-cell fate decisions following activation. Proceedings of the National Academy of Sciences. 2016;113(38):10631-6.
25. Shore GC, Warr MR. Unique biology of Mcl-1: therapeutic opportunities in cancer. Current molecular medicine. 2008;8(2):138-47.

26. Lin S, Zhang L, Luo W, Zhang X. Characteristics of antisense transcript promoters and the regulation of their activity. International journal of molecular sciences. 2016;17(1):9.
27. Sm AHR, Tan GMY, Poudel A, He K, McLellan AD. Regulation of Human Mcl-1 by a Divergently-Expressed Antisense Transcript. Gene. 2020:145016.
28. T Das A, Tenenbaum L, Berkhout B. Tet-on systems for doxycycline-inducible gene expression. Current gene therapy. 2016;16(3):156-67.
29. Rad SAH, Poudel A, Tan GMY, McLellan AD. Optimisation of Tet-On inducible systems for Sleeping Beauty-based chimeric antigen receptor (CAR) applications. Scientific Reports. 2020;10(1):1-12.
30. Wang Y, Li M, Zang W, Ma Y, Wang N, Li P, et al. MiR-429 up-regulation induces apoptosis and suppresses invasion by targeting Bcl-2 and SP-1 in esophageal carcinoma. Cellular oncology. 2013;36(5):385-94.
31. Sandberg R, Neilson JR, Sarma A, Sharp PA, Burge CB. Proliferating cells express mRNAs with shortened 3'untranslated regions and fewer microRNA target sites. Science. 2008;320(5883):1643-7.
32. Tamaddon M, Shokri G, Rad SMAH, Rad I, Razavi ÀE, Kouhkan F. involved microRNAs in alternative polyadenylation intervene in breast cancer via regulation of cleavage factor "CFIm25". Scientific reports. 2020;10(1):1-11.
33. Gui J, Hu Z, Tsai C-Y, Ma T, Song Y, Morales A, et al. MCL1 enhances the survival of CD8+ memory T Cells after viral infection. Journal of virology. 2015;89(4):2405-14.
34. Kim EH, Neldner B, Gui J, Craig RW, Suresh M. Mcl-1 regulates effector and memory CD8 T-cell differentiation during acute viral infection. Virology. 2016;490:75-82.
35. Rasmussen ML, Kline LA, Park KP, Ortolano NA, Romero-Morales AI, Anthony CC, et al. A non-apoptotic function of MCL-1 in promoting pluripotency and modulating mitochondrial dynamics in stem cells. Stem cell reports. 2018;10(3):684-92.
36. Guégan JP, Legembre P. Nonapoptotic functions of fas/CD 95 in the immune response. The FEBS Journal. 2018;285(5):809-27.

37. Gattinoni L, Speiser DE, Lichterfeld M, Bonini C. T memory stem cells in health and disease. Nature medicine. 2017;23(1):18-27.
38. Buchholz VR, Flossdorf M, Hensel I, Kretschmer L, Weissbrich B, Gräf P, et al. Disparate individual fates compose robust CD8+ T cell immunity. Science. 2013;340(6132):630-5.
39. Lugli E, Dominguez MH, Gattinoni L, Chattopadhyay PK, Bolton DL, Song K, et al. Superior T memory stem cell persistence supports long-lived T cell memory. The Journal of clinical investigation. 2013;123(2).
40. Biasco L, Scala S, Basso Ricci L, Dionisio F, Baricordi C, Calabria A, et al. In vivo tracking of T cells in humans unveils decade-long survival and activity of genetically modified T memory stem cells. Sci Transl Med 7 (273): 273ra13. 2015.
41. Oliveira G, Ruggiero E, Stanghellini MTL, Cieri N, D'Agostino M, Fronza R, et al. Tracking genetically engineered lymphocytes long-term reveals the dynamics of T cell immunological memory. Science translational medicine. 2015;7(317):317ra198-317ra198.
42. Marraco SAF, Soneson C, Cagnon L, Gannon PO, Allard M, Maillard SA, et al. Long-lasting stem cell–like memory CD8+ T cells with a naïve-like profile upon yellow fever vaccination. Science translational medicine. 2015;7(282):282ra48-ra48.
43. Golubovskaya V, Wu L. Different subsets of T cells, memory, effector functions, and CAR-T immunotherapy. Cancers. 2016;8(3):36.
44. Ho LP, San Yit P, Ng LH, Linn YC, Zhao Y, Sun L, et al. The road to memory: an early rest for the long journey. The Journal of Immunology. 2013;191(11):5603-14.
45. Tripathi P, Koss B, Opferman J, Hildeman D. Mcl-1 antagonizes Bax/Bak to promote effector CD4+ and CD8+ T-cell responses. Cell Death & Differentiation. 2013;20(8):998-1007.
46. Dzhagalov I, Dunkle A, He Y-W. The anti-apoptotic Bcl-2 family member Mcl-1 promotes T lymphocyte survival at multiple stages. The Journal of Immunology. 2008;181(1):521-8.
47. Opferman JT, Letai A, Beard C, Sorcinelli MD, Ong CC, Korsmeyer SJ. Development and maintenance of B and T lymphocytes requires antiapoptotic MCL-1. Nature. 2003;426(6967):671-6.

48. Liu H, Xu Y, Xiang J, Long L, Green S, Yang Z, et al. Targeting alpha-fetoprotein (AFP)–MHC complex with CAR T-cell therapy for liver cancer. Clinical cancer research. 2017;23(2):478-88.
49. Robins E, Zheng M, Ni Q, Liu S, Liang C, Zhang B, et al. Conversion of effector CD4+ T cells to a CD8+ MHC II-recognizing lineage. Cellular & Molecular Immunology. 2020:1-12.
50. Lui JB, McGinn LS, Chen Z. Gut microbiota amplifies host-intrinsic conversion from the CD8 T cell lineage to CD4 T cells for induction of mucosal immune tolerance. Gut microbes. 2016;7(1):40-7.
51. Guzman MP, Chen Z. Conversion of the CD8 lineage to CD4 T cells. Oncotarget. 2015;6(25):20748.
52. Jopling C, Boue S, Belmonte JCI. Dedifferentiation, transdifferentiation and reprogramming: three routes to regeneration. Nature reviews Molecular cell biology. 2011;12(2):79-89.